

Signal Enhancement Strategies in Classical Electrochemiluminescence Techniques for Modern Biosensing

Dissertation zur Erlangung des Doktorgrades der Naturwissenschaften

(Dr. rer. nat.)

der Fakultät Chemie und Pharmazie

der Universität Regensburg

Deutschland



vorgelegt von

Michael Mayer

aus Rosenheim

im Jahr 2018

Die vorgelegte Dissertation entstand in der Zeit von März 2015 bis November 2018 am Institut für Analytische Chemie, Chemo- und Biosensorik der Universität Regensburg.

Die Arbeit wurde angeleitet von Prof. Dr. Antje J. Bäumner.

Promotionsgesuch eingereicht am: 26.10.2018

Kolloquiumstermin: 19.12.2018

Prüfungsausschuss

Vorsitzender: Prof. Dr. Oliver Tepner

Erstgutachterin: Prof. Dr. Antje J. Bäumner

Zweitgutachter: PD Dr. Axel Duerkop

Drittprüferin: PD Dr. Miriam Breunig

Acknowledgements

Zuerst möchte ich mich bei meiner Betreuerin Prof. Dr. Antje J. Baeumner für die Möglichkeit meine Promotion in Ihrer Gruppe zu machen und für Ihr immer offenes Ohr bei Fragen und die tolle Unterstützung bedanken. Dann möchte ich mich ebenso bei PD Dr. Axel Duerkop bedanken, der mir auch immer bei Fragen beistand und viele gute Diskussionen und Tipps für meine Arbeit beisteuerte. Weiterhin gilt mein Dank PD Dr. Miriam Breunig und Prof. Dr. Oliver Tepner für die Übernahme der Rollen der Drittprüferin und des Vorsitzenden in meiner Promotionsprüfung.

Bei „meinem Labor“ möchte ich mich zuerst bei Andrei und anschließend bei Christian bedanken. Dazu möchte ich auch Matthias und Arne, Simone, Meike und Franziska danken. Anschließend danke ich auch allen anderen Kollegen unserer Arbeitsgruppe und allen anderen der Nachbararbeitsgruppen. Es war immer eine angenehme Atmosphäre vorhanden und gab viele lustige Momente. Und ein besonderes Dankeschön gilt auch Nicole für die Hilfsbereitschaft. Weiterhin bedanke ich mich bei meinen Kooperationspartnern – besonders Michael für das super Projekt und Maximilian für die große Hilfe. Dann danke ich meinen Studenten für die kompetente Hilfe während Eurer Arbeiten und Praktika oder WHKs – Christine, Jiří, Florian, Simone, Marion und Thomas. Zuletzt bedanke ich mich bei der Feinmechanischen Werkstatt unserer Fakultät für die super Ausführung der vielen Projekte. Weiterhin möchte ich mich bei meinen Freunden in Regensburg, besonders bei Peter, Lydia, Andrea, Matthias, Carola und Anton bedanken. Danke Euch für die vielen gemeinsamen Erlebnisse. Genauso bedanke ich mich bei meinen Heimatfreunden, Markus, Stephan, Anja, Schorsch, Max und Regina – es war immer eine super Zeit an den Wochenenden.

Zuletzt möchte ich mich ganz besonders bei meiner Familie, allen voran meinen Eltern Inge und Peter bedanken – danke für Eure immerwährende Unterstützung und alles andere. Genauso will ich mich bei meiner Oma Rosi und meinen Onkeln Rupert und Paul besonders bedanken.

Declaration of Collaborations

Most of the experimental and theoretical results presented in this thesis was done exclusively by the author. Though, partly, results were received together with other researchers. In accordance with § 8 Abs. 1 Satz 2 Ziff. 7 of the “Ordnung zum Erwerb des akademischen Grades eines Doktors der Naturwissenschaften (Dr. rer. nat.) an der Universität Regensburg vom 18. Juni 2009“, this paragraph states these collaborations.

ABC Spotlight on Analytics 4.0 (Chapter 1)

The literature search and writing of the editorial manuscript was done by Antje J. Baeumner and the author. The author wrote the first draft of the manuscript and Antje J. Baeumner revised the manuscript. Antje J. Baeumner is corresponding author.

Trends: Sensors and Analytical Chemistry for the Internet of Things (IoT) (Chapter 2)

The literature search and writing of the review article was done by the author and Antje J. Baeumner. Andrei Georgescu initially contributed with a literature search and strategic thoughts. The author wrote the first draft of the article and Antje J. Baeumner revised the article. Antje J. Baeumner is corresponding author.

PAMAM dendrimers: A multifunctional nanomaterial for ECL biosensors (Chapter 3)

Sudeshna Chandra, the author and Antje J. Baeumner planned the experiments. Most of the experimental work was done by Sudeshna Chandra and some experiments by the author. Sudeshna Chandra did the data evaluation and wrote the initial draft of the manuscript. The author revised the manuscript together with Antje J. Baeumner. Antje J. Baeumner is corresponding author.

Electrochemiluminescence Bioassays with a Water-Soluble Luminol Derivative Can Outperform Fluorescence Assay (Chapter 4)

The author did most of the experimental work (all ECL measurements, the luminol derivative liposome syntheses, the ECL/EC/solubility/emission characterization of the luminol derivative and luminol derivative liposomes, the surfactant and matrix effects study, the assay optimization, the data evaluation of these experiments and part of the luminol liposome syntheses). Shigehiko Takegami did most of the luminol liposome syntheses and their characterization with data evaluation. Michael Neumeier did the

luminol derivative synthesis and its full characterization with NMR and IR Spectroscopy and data evaluation. Simone Rink supported the luminol derivative liposome DNA bioassays and ECL measurements of these assays. Axel Jacobi von Wangelin supported the synthesis validation. Silja Schulte did the first luminol derivative synthesis, Moritz Vollmer optimized that synthesis. Axel G. Griesbeck supported the synthesis design. Axel Duerkop and Antje J. Baeumner did the project administration. The author wrote most of the manuscript. Michael Neumeier wrote the luminol derivative synthesis and NMR/IR characterization part of the manuscript. The author, Michael Neumeier, Axel Jacobi von Wangelin, Axel G. Griesbeck, Axel Duerkop and Antje J. Baeumner revised the manuscript. Antje J. Baeumner is corresponding author.

Surfactant Interactions with Luminol and m-Carboxy Luminol Electrochemiluminescence (Chapter 5)

Michael Mayer, Axel Duerkop and Antje J. Baeumner planned most of the experiments. The author did most of the experimental work and wrote the manuscript. Florian Gerstl, Thomas Köwer and Simone Rink helped with the ECL measurements. Maximilian Hahn discussed the surfactant adsorption models on electrodes and provided expertise. Maximilian Hahn revised the surfactant adsorption part of the manuscript. The author, Axel Duerkop and Antje J. Baeumner revised the manuscript. Antje J. Baeumner is corresponding author.

Microfabrication strategies for ECL detection (chapter 6)

The author did most of the experimental work and wrote this chapter. Andrei Georgescu contributed initially with expertise, microfluidic and interfacing design strategies and CAD modeling. The mechanical workshop of the faculty of chemistry built several microfluidic parts which were used in this project. Christine Unger, Marion Vogl and Florian Gerstl contributed with ECL measurements on ITO and LSG electrodes. Jiří Houšť helped with bonding tests of PMMA with PET. Christian Griesche contributed with discussions to microfluidic design strategic ideas. Michael Mayer, Andrei Georgescu, Antje J. Baeumner, Axel Duerkop and Thomas Hirsch discussed strategic decisions. Antje J. Baeumner was project administrator.

Contents

Summary	1
Zusammenfassung	4
Introduction and structure of the work.....	7
References	12
Chapter 1: ABC Spotlight on Analytics 4.0	15
1. ABC Spotlight on Analytics 4.0.....	16
2. References:	21
Chapter 2: Trends: Sensors and Analytical Chemistry for the Internet of Things (IoT) 22	
1. Introduction	23
2. Sensor solutions for the point-of-care and <i>in vivo</i> detection.....	26
2.1 Appliances/accessories	29
2.2 Bandages, patches, tattoos.....	30
2.3 Contact lenses	34
2.4 <i>In vivo</i> sensing	36
2.5 Sensing enhancement through microfluidic strategies	40
2.6 Progress needed for IoAT in wearable point-of-care biosensors	42
2.7 Safety and security considerations	47
3. Sensor solutions for agriculture, food and environmental sensing	48
3.1 Global climate and large-scale agriculture monitoring	51
3.2 Local environmental and urban area monitoring	52
3.3 Local agriculture monitoring.....	56
3.4 Livestock monitoring.....	57
3.5 Sensing for processed and packaged food	58

4. Lab-based solutions for the IoAT	61
4.1 Mass spectrometry for the IoAT	62
4.2 Next generation DNA sequencing (NGS) for the IoAT	65
5. Existing commercial technologies for the IoAT	68
5.1 Business and IT sector initiatives can drive innovations in analytical chemistry	69
6. Key requirements and challenges towards a successful integration of Analytical chemistry with the IoT to generate the IoAT	72
7. References	75

Chapter 3: PAMAM dendrimers: A multifunctional nanomaterial for ECL biosensors

.....	103
1. Introduction	104
2. Assay Principles.....	105
3. Materials and Methods	106
4. Results and Discussion.....	107
5. Conclusion.....	112
6. References	113
7. Supplementary Information	115

Chapter 4: Electrochemiluminescence Bioassays with a Water-Soluble Luminol

Derivative Can Outperform Fluorescence Assays	118
1. Introduction	119
2. Results and Discussion.....	120
3. Conclusion.....	125
4. References	126
5. Supplementary Information	129
5.1 Abbreviations.....	129
5.2 Experimental Procedures.....	129

5.2.1 Materials	129
5.2.2 Buffers and reaction mixes.....	130
5.2.3 <i>m</i> -Carboxy luminol synthesis.....	131
5.2.4 Detailed procedures for the synthesis of <i>m</i> -carboxy luminol.....	131
5.2.5 Selected NMR spectra of isolated products.....	136
5.2.6 Liposome synthesis.....	140
5.2.7 ECL measurements	140
5.2.8 Liposome characterization	142
5.2.9 Surfactant study	143
5.2.10 Sandwich hybridization assay	143
5.2.11 Optimization of sandwich assay protocol steps.....	145
5.2.12 Effect of matrices	147
5.3 Results and Discussion	147
5.3.1 Luminol derivatives comparison.....	147
5.3.2 Luminol liposomes.....	149
5.3.3 <i>m</i> -Carboxy luminol ECL.....	151
5.3.4 <i>m</i> -Carboxy luminol liposomes	153
5.3.5 Surfactants as lysis and ECL enhancing agents.....	155
5.3.6 Optimization of sandwich assay protocol steps.....	156
5.3.7 Effect of matrices	157
5.4 References	158

Chapter 5: Surfactant Interactions with Luminol and *m*-Carboxy Luminol

Electrochemiluminescence	162
1. Introduction	163
2. Experimental part	167
2.1 Materials	167
2.2 Buffers and reaction mixtures	167
2.3 ECL measurements	167

2.4 ITO electrode hydrophilisation	168
2.5 LSG electrodes	168
2.6 Resistivity measurements	169
2.7 CL measurements	169
2.8 Contact angle measurements	169
2.9 CV measurements.....	169
2.10 Emission Scans	170
2.11 Liposome lysis study	170
3. Results and Discussion.....	171
3.1 Correlation with basic surfactant parameters.....	171
3.2 Electrochemiluminescence effects.....	173
3.3 Surfactant effects on the underlying electrochemical reactions of ECL.....	177
3.4 Investigation toward a correlation between surfactant effects on EC, CL and ECL.....	180
4. Conclusion.....	181
5. References	182
6. Supporting Information	186
6.1 Luminol and surfactant molecules.....	186
6.2 Electrode area determination.....	188
6.3 ECL with chosen surfactants for luminol and <i>m</i> -carboxy luminol ECL on different electrodes	188
6.3.1 <i>Remarks and settings</i>	188
6.3.2 <i>Discussion</i>	189
6.3.3 <i>Surfactant adsorption behavior on the employed electrode surfaces</i>	198
6.4 Surfactant's ECL signal effects with respect to their cmc.....	201
6.5 Luminol and <i>m</i> -carboxy luminol ECL with CTAB and CTAC.....	203
6.6 HLB correlation to quenching/ enhancement with ECL signal or EC current ..	204
6.7 Luminescence emission scans	205

6.7.1 Luminol ECL	205
6.7.2 <i>m</i> -Carboxy luminol ECL.....	207
6.8 Cyclic voltammetry measurements	209
6.8.1 CV on Gold WEs.....	209
6.9 CV on ITO WEs	211
6.9.1 Luminol.....	211
6.9.2 <i>m</i> -Carboxy luminol	211
6.10 Total charge transfer for different surfactants on various electrodes for both luminol species and background currents.....	212
6.11 Effect of buffer presence	219
6.12 Electrode surface area calculation.....	220
6.13 Chemiluminescence comparative measurements	221
6.14 Comparison of maximum absolute ECL signals on different electrodes	223
6.15 Contact angle measurements.....	224
6.16 Surfactant effect on liposome lysis.....	225
6.17 References	227
Chapter 6: Microfabrication strategies for ECL detection.....	229
1. Introduction	231
1.1 Strategic route for ECL miniaturization in this project	232
1.2 Fluidic design strategies.....	234
2. Materials & Methods.....	238
2.1 Materials	238
2.2 Photolithography of ITO foils.....	239
2.3 Silica-mesochannels (SMC) modification of ITO electrodes.....	240
2.4 ECL and electrochemical measurements.....	240
2.5 Hot embossing of PMMA.....	241
2.6 Thermal bonding of ITO@PET on PMMA (optimized procedure)	242

3. Results.....	244
3.1 Electrochemical implications towards materials choice and fabrication strategies.....	244
3.2 Development of thermal bonding of PET with PMMA	245
3.3 Electrochemical tests with $[\text{Ru}(\text{bpy})_3]^{2+}$ -ECL solutions on microfluidic ITO electrodes	247
3.4 ITO modifications.....	249
3.4.1 SMC modified ITO electrodes.	250
3.5 $[\text{Ru}(\text{bpy})_3]^{2+}$ -ECL characterization and luminol on LSG electrodes.	252
4. Conclusions	256
5. References	258
Chapter 7: Conclusions and perspectives	260
References	266
Curriculum Vitae	269
Presentations.....	271
Publications	272
Eidesstattliche Erklärung.....	273

Summary

With the ascent of IT, and since Ashton has invented the term Internet of Things (IoT) in 1999, this future idea of connected machines that can do tasks and perform decision-control cycles without human input has become more and more attractive and is today an established future scenario. Obviously, in an IoT, “sensors for everything” are one crucial corner stone of its existence and Analytical chemistry can and must deliver them. While many challenges towards a functioning IoT remain, we are on the verge of its beginning. This can be also seen with “Analytics 4.0” in research and on the market, tending to more IT-connected, portable, easier-controllable and integrated solutions. The entrance of mobility in the health sector or Point-of-Care (POC) diagnostics trends are alike influencing biosensing. Whether in mobile solutions or lab- and clinical environments, versatile, powerful and easy-to-adapt detection strategies like Electrochemiluminescence (ECL) are an attractive option.

Investigation and optimization of ECL strategies

The ECL molecules $[\text{Ru}(\text{bpy})_3]^{2+}$ and luminol represent the most prominent and most abundantly investigated luminophores for ECL since Bard’s accomplishment to make ECL a well-known technique. Because both are also two of the most efficient ECL emitters that can be well-handled in bioanalysis, and are available on the market, they are still today frequently used in research and also commercial applications. To cope with current benchmarks of sensitive detection, however a combination with a certain signal enhancement strategy is recommended. Several different routes can here be employed and one option is dendrimers. PAMAM dendrimers can function as ECL coreactant in $[\text{Ru}(\text{bpy})_3]^{2+}$ -ECL via their amino groups and at the same time expose primary amino groups as possible bioconjugation elements. Exploring this multifunctionality of the dendrimers was investigated here. This was done on a model system employing PAMAM dendrimers with $[\text{Ru}(\text{bpy})_3]^{2+}$ -ECL together with biotin/streptavidin as biorecognition element and analyte, respectively. The dendrimer’s bi-functionality was successfully proven and a joint-role of a biorecognition element and a possible reporter function suggests an optimum application in homogeneous assays. A different toolset for ECL signal enhancement is offered by

liposomes. Numerous signaling molecules can be encapsulated inside the inner cavity of these synthetic vesicles, while they provide protection from the environment and connection-functionality to probes via lipids and surface groups on the outside. That application was here explored, together with a newly synthesized luminol derivative obtained by a simple synthesis route from commercial starting materials and exhibiting a four times increased ECL efficiency versus standard luminol. That was necessary as a liposome enhancement was denied for the standard luminol through its poor aqueous solubility. The new *m*-carboxy luminol considerably improved this feature which allowed its own encapsulation in liposomes. The superior signal generation with this dual system was proven in a model sandwich hybridization assay which yielded a 150-times better detection performance than the equal fluorescence-based assay while being almost zero affected through matrices like serum, soil or river water. As such the good performance of luminol ECL together with liposomes for highly sensitive detection applications was demonstrated. A further necessary element with liposomal amplification, are surfactants to set free the signaling molecules. However, this case depicts only one example of a multitude of applications of surfactants in bioassays and biochemical methods. Hence, surfactants are commonly present solution constituents which also have to be considered in general with ECL because they can influence the ECL signals positively or negatively. This was further investigated for luminol ECL by exploring the effect of 13 different surfactants on the luminol ECL efficiency on four different electrode materials. A deeper understanding of the distinct effects was obtained by looking into ECL emission behavior, electrochemical effects, the surfaces and Chemiluminescence effects. After all, the revelation of a complicated mechanism that involves many contributing factors and as such directs signal quenching or enhancement is an important finding for assay design. In this way, the selection of a suitable surfactant is possible to exploit maximum reachable signal efficiencies.

Miniaturization of ECL assays

A combination of signal enhancement tools like a better ECL molecule derivative, dendrimers, liposomes or surfactants has proven to boost the ECL performance considerably. A further means of signal enhancement is offered via miniaturization, which also makes the detection method better suited towards common application as liquid handling and easier automation are on hand. This can be used for single ECL assays or combinations of different ECL reagents in one system for multi-detection.

Different strategies for the miniaturization of an ECL readout-capable system were investigated, taking requirements for $[\text{Ru}(\text{bpy})_3]^{2+}$ and luminol as ECL reporters into account. This includes materials, electrochemical demands and simple design. Here, ITO electrodes – while advantageous for luminol ECL could not convince with their performance in $[\text{Ru}(\text{bpy})_3]^{2+}$ -ECL. Alternatively, laser scribed graphene electrodes have shown to be promising candidates for a future miniaturized system encompassing both, luminol and $[\text{Ru}(\text{bpy})_3]^{2+}$ as ECL systems. Ultimately, the different signal amplifying strategies, investigated in this work that can be applied standalone or combined, offer a great toolset for state-of-the-art ECL detection applications in research and also for possible commercial applications.

Zusammenfassung

Mit dem Aufstieg der Internettechnologie und seit Ashton 1999 den Begriff Internet of Things (IoT) prägte, ist diese Zukunftsidee von vernetzten Maschinen, die Aufgaben und Entscheidungs- und Kontrollzyklen ohne menschliches Zutun ausführen können, immer attraktiver geworden und heute ein etabliertes Zukunftsszenario. Für die dienliche Existenz eines IoT sind „Sensoren für alles“ ein entscheidender Grundpfeiler, welche die analytische Chemie liefern kann und muss. Während viele Herausforderungen für ein funktionierendes IoT bestehen bleiben, stehen wir kurz vor dem Beginn. Dies zeigt sich auch in der „Analytik 4.0“ sowohl in der Forschung als auch auf dem freien Markt, die zu mehr IT-vernetzten, portablen, einfacher steuerbaren und integrierten Lösungen neigt. Der Einstieg in die Mobilität im Gesundheitssektor oder Point-of-Care (POC) - Diagnosetrends beeinflussen gleichermaßen die Biosensorik. Ob in mobilen Lösungen oder Labor- und klinischen Umgebungen - vielseitige, leistungsstarke und einfach zu adaptierende Detektionsstrategien wie Elektrochemilumineszenz (ECL) sind eine attraktive Option.

Untersuchung und Optimierung von ECL-Strategien

Die ECL-Moleküle $[\text{Ru}(\text{bpy})_3]^{2+}$ und Luminol repräsentieren die bekanntesten und am häufigsten verwendeten Luminophore für ECL, seit der Pionierleistung von Bard ECL zu einer wohlbekannten Technik zu machen. Da beide zwei der effizientesten ECL-Emitter sind, die in der Bioanalytik gut gehandhabt werden können und kommerziell erhältlich sind, finden sie auch heute häufig in der Forschung und in kommerziellen Anwendungen Verwendung. Um zeitgemäßen Anforderungen für sensitive Nachweise zu entsprechen, ist jedoch eine Kombination mit verschiedenen Signalverbesserungsstrategien zu empfehlen. Hierzu können mehrere verschiedene Ansätze verwendet werden, wobei Dendrimere eine der Optionen darstellen. Polyamidoamin (PAMAM)-Dendrimere können mittels ihrer Aminogruppen als ECL-Coreactant in $[\text{Ru}(\text{bpy})_3]^{2+}$ -ECL fungieren und enthalten ebenso funktionelle primäre Aminogruppen, die eine Biokonjugation der Dendrimere ermöglichen. Für ein tieferes Verständnis dieser Multifunktionalität, wurden Dendrimere hier in ihrer Rolle als ECL-Coreactant parallel zu ihrer Funktion als Bioerkennungselements genutzt. Dies wurde an einem Modellsystem, mit PAMAM-Dendrimeren und $[\text{Ru}(\text{bpy})_3]^{2+}$ -ECL zusammen mit

Biotin/Streptavidin als Bioerkennungselement bzw. Analyt untersucht. Die Nutzung der Bi-funktionalität der Dendrimere wurde erfolgreich gezeigt und ihre universelle Rolle als Bioerkennungselement und mögliche Reporterfunktionalität suggeriert eine optimale Anwendung in homogenen Assayformaten. Liposome stellen ein weiteres Werkzeug zur ECL-Signalverstärkung dar. Zahlreiche Signalmoleküle können dabei innerhalb des inneren Hohlraums dieser synthetischen Vesikel verkapselt werden, während diese Schutz vor der Umwelt und über Lipide, mit deren vielseitigen funktionellen Oberflächengruppen auf der Außenseite, eine einfache Kopplung zu Sonden ermöglichen. Diese Anwendung wurde hier zusammen mit einem neu synthetisierten Luminolderivat untersucht, das mittels eines einfachen Synthesewegs aus kommerziellen Ausgangsmaterialien erhalten wurde und eine vierfach höhere ECL-Effizienz als Standard-Luminol zeigte. Dies wurde notwendig, da eine Liposom-basierte Signalverstärkung mit Standard-Luminol aufgrund dessen schlechten Wasserlöslichkeit verwehrt wurde. Das neue *m*-Carboxy-Luminol verbesserte dieses Merkmal beträchtlich, was dessen eigene Verkapselung in Liposome ermöglichte. Die herausragende Eignung zur Signalerzeugung dieses dualen Systems wurde in einem Modell-Sandwich-Hybridisierungsassay nachgewiesen, der eine 150-fach bessere Detektionsleistung als der gleiche fluoreszenzbasierte Assay ergab, während ein möglicher Einfluß durch Matrizen wie Serum, Boden oder Flusswasser vernachlässigbar blieb. Anhand dieses Assays wurde die überragende Leistung von Luminol ECL kombiniert mit Liposomen für hochempfindliche Detektionsanwendungen offensichtlich. Ein weiteres notwendiges Element bei Liposom-basierter Verstärkung sind Tenside, zur kontrollierten Freisetzung der Signalmoleküle. Diese Nutzung von Tensiden stellt jedoch nur ein Beispiel aus einer Vielzahl an Anwendungen in Bioassays und biochemischen Verfahren dar. Daher sind Tenside üblicherweise vorhandene Lösungsbestandteile, die im Allgemeinen auch in der ECL berücksichtigt werden müssen, da sie die ECL-Signalintensität positiv oder negativ beeinflussen können. Dies wurde für Luminol-ECL untersucht, indem die Wirkung von 13 verschiedenen Tensiden auf die Luminol-ECL-Effizienz an vier verschiedenen Elektrodenmaterialien erforscht wurde. Ein tieferes Verständnis der verschiedenen Effekte wurde durch Untersuchungen des ECL-Emissionsverhaltens, der elektrochemischen Effekte, der Oberflächen und der Chemilumineszenzeffekte erworben. Dabei stellt die Entdeckung eines komplizierten Mechanismus, zu dem viele Faktoren beitragen und welcher die

Signallöschung oder -verstärkung lenkt, einen wichtigen Befund für das Design neuer Assays dar. Auf diese Weise ist die Auswahl eines geeigneten Tensids möglich, um entweder die maximal erreichbare Signaleffizienz zu erhalten oder, falls dies nicht notwendig ist, die Wahl des bestgeeigneten Tensids auszunutzen.

Miniaturisierung von ECL Assays

Eine Kombination mit Signalverstärkungswerkzeugen wie beispielsweise einem verbesserten Derivats eines ECL Moleküls, Dendrimeren, Liposomen oder Tensiden kann die ECL-Leistung erheblich steigern. Eine weitere Möglichkeit zur Signalverbesserung bietet hier Miniaturisierung, die die Detektionsmethode auch hinsichtlich der allgemeinen Anwendung verbessert, da eine gesteuerte Handhabung von Flüssigkeiten und eine einfachere Automatisierung zur Verfügung stehen. Dies kann in einzelnen ECL-Assays oder bei Kombinationen von verschiedenen ECL-Reagenzien in einem System zur Mehrfachdetektion genutzt werden. Unterschiedliche Strategien zur Miniaturisierung eines Systems, das mit ECL-Detektion genutzt werden kann, wurden hier untersucht, wobei Anforderungen für $[\text{Ru}(\text{bpy})_3]^{2+}$ und Luminol als ECL-Reporter berücksichtigt wurden. Dies beinhaltet Materialien, elektrochemische Anforderungen und einfaches Design. Hier konnten ITO-Elektroden - obwohl vorteilhaft für Luminol ECL - mit ihrer Leistung für $[\text{Ru}(\text{bpy})_3]^{2+}$ -ECL nicht überzeugen. Alternativ haben sich laser-scribed-Graphen Elektroden als vielversprechende Kandidaten für ein zukünftiges miniaturisiertes System erwiesen, das sowohl zur ECL Detektion von Luminol als auch $[\text{Ru}(\text{bpy})_3]^{2+}$ geeignet ist. Letztendlich bieten die verschiedenen Signalverstärkungsstrategien, die in dieser Arbeit untersucht wurden und die einzeln oder kombiniert angewendet werden können, einen umfassenden Werkzeugsatz für moderne ECL-Detektionsanwendungen in der Forschung und auch für zukünftige kommerzielle Anwendungen.

Introduction and structure of the work

The focus of this thesis lies in the advancement of Electrochemiluminescence (ECL) coupled with different signal amplification tools as sensitive detection technique towards application in modern biosensing with special considerations on highly sensitive applications and miniaturized, mobile solutions for possible implementation in growing Point-of-Care (POC) and Internet-of-Things (IoT)-directed biosensing solutions.

More than ever, analytical chemistry and biosensing are transitioning into everyday tools for the common person, leaving an allocation as peripheries of chemistry and biochemical sciences and proceeding towards key elements and crucial toolsets of a growing and evolving IoT. Despite of today's situation where we are still a fair step away from a functioning overall network, we are on the edge of realization and roll-outs of smaller and larger IoT-shaped networks and information hives with an exponential growth. **Chapter 1** in this thesis, gives a short glance in and overview of this large topic and trends while in **Chapter 2** existing analytical and biosensing solutions are addressed that depict examples how analytical chemistry can be- and will become a helpful tool for everybody. This chapter also outlines in-depth existing challenges (e.g. true long-term stability of sensors), and required advancements (e.g. joint IT-communication protocols), towards a successful evolution of sensing and biosensing in this setting. One large area of such an "IoT horizon" deals with evolving challenges to face existent and emerging worldwide health risks,¹ how to shape the fields of modern healthcare, with developing point-of-care (POC) diagnostics and finally the area of highly personalized medicine. This joint venture of health risks, sensing requirements, (bio)sensing solutions and the all-embracing framework of an upcoming IoT profoundly impacts the future direction of biosensor development.

Broken down to the actual methods and tools that are necessary and useful for such applications, the choice of a versatile detection method is one crucial decision. With respect to that, complying core requirements here are condensed under the terms of "miniaturization& portability", "suitability for mass production& cost reduction", "simple construction", "reliability", "automation& layman usability", "sustainability" and "ruggedness". Parts or all of that are required, while the method should ideally exhibit outstanding reachable sensitivities to make it versatile and ready to cope with

given needs. Also, the transition of purely scientific thoughts to show and exhaust “what is possible”, “what is new” and “what can be realized in the lab” towards realization of true marketable products, that can cope with given requirements of POC or mobile sensing is becoming more and more important. One factor of these application-set requirements, “miniaturization and integration” plays a key role in realizing small-enough devices with little weight. These should either adhere to the current and future wearables realm or be embedded in a size-restricted application setting and be true lab-on-chip (LOC) devices. In detail, this means that not only a single element of the systems can be small while the remaining parts are typical benchtop instruments. Here, the whole analytical process from sample introduction to results analysis must be miniaturized. Addressing that, has been disregarded often² and is still observed in current biosensing research³ while recent works also recognize this issue and lead by example by showing true whole sensor devices that can integrate the overall analytical process.^{4,5} In this work, a detection method suitable for such sensing systems is investigated.

Electrochemiluminescence (ECL) as detection technique has proven over the years of its success since A.J. Bard paved its way,⁶ that it is more than a niche application but a powerful method perfectly suited for highly sensitive detection demands (See **chapter 4** and e.g. Hu et al.⁷). Through its intrinsic light generation at an electrode as the analytical signal, the required instrumentation can be designed miniaturized and simple. The optimally flat electrodes can be easily downscaled and patterned freely,^{8,9} are available on thin, flexible substrates (e.g. ITO on PET foil) and certain electrode types can be simply scaled-up to meet industrial high throughput fabrication processes e.g. screen-printing. The second part of the detection system simply requires to capture the light emission which can be implemented as easily. What has been shown a lot recently, are solutions using smartphone-camera based readouts,^{10,11} off-the-shelf CCD/CMOS chips, photodiodes and such systems¹² that can be readily used for sensitive ECL emission detection. At the same time, the surrounding instrumentation to power and control the two elements of electrochemistry (potentiostat) and optical detection can as well be broken down to very small formats.¹³⁻¹⁵ Finally, ECL’s nature of a luminescence process, eliminates the need of other light sources, which allows for direct detection of the absolute amount of light present, without an urgency for filter or monochromator systems when the system is simply enclosed from ambient light.

Also compared with chemiluminescence (CL) based signal generation, which omits the electrochemical side, in several applications ECL can play out different advantages which are briefly discussed. The total spatial control regarding the signal generation (in ECL) is important in flow systems, whereas reactants in CL could drift-off and broaden the detection zone. An absolute time control over the luminescence initiation (beneficial in cases the employed assay needs lysis or incubation steps prior to detection, and luminescence termination are additionally helpful. In ECL all necessary reagents can readily be included prior to the start of luminescence and no residual emission is persistent after stopping the potential. Also, in multi detection setups ("microtiter plate-alike design") no need to account for residual emissive stray light from neighboring spots is advantageous. Finally, a generally more stable signal (for coreactant ECL) versus CL, the possibility to use the electrochemical signal (current or better, transferred charge) as second analytical signal in a multimodal approach (e.g. correction for luminescence quenching or enhancement in amperometric readout¹⁶) and the possibility to directly modify the electrode (e.g. SAM's,¹⁷ pyrenebutyric acid,^{9,18} silanes¹⁹) with probes to capture the analyte directly at the detection spot are further amenities. The necessary additional electrochemical instrumentation in ECL vs. CL doesn't depict a major drawback as these components can all be readily miniaturized. Also, in CL, the employed instrumentation has to cover the critical timing of luminescence initiation and simultaneous initiation of signal capturing in a reproducible way. Thus, along all and especially optical detection methods, luminescence techniques like ECL lend themselves well for sensitive and versatile - but facile sensor designs. This also qualifies ECL for different routes, be it in POC applications, mobile field solutions or powerful benchtop routine assay applications.

The selection of very classical ECL luminophores (luminol, Tris(2,2'-bipyridyl)ruthenium(II) chloride ($[\text{Ru}(\text{bpy})_3]^{2+}$) and their derivatives) employed within this research project was driven by several arguments. Both ECL systems were handled, operating them in their (oxidative-reductive) coreactant-ECL pathways (luminol- H_2O_2 , $[\text{Ru}(\text{bpy})_3]^{2+}$ -tertiary amine)²⁰ and applying earlier findings^{21,22} on optimized signal efficiencies. This route enables their application in aqueous environments while maintaining moderate environmental conditions (pH, temperature) with their standard forms being commercially available. Within these boundaries, both candidates are amongst the most efficient, existent ECL emitters. The option to focus on two different

species which follow the same constraints, while their emission wavelengths are far separated, allows for the design of multi-sensing solutions e.g. applying both reporters in one shared medium at the same time (concept shown in earlier master project²²) or with a two-in-one signal readout. Besides that, two different ECL probes offer different advantages for varying assay applications. While recent ECL research is mostly focused on different and newer types of materials, e.g. quantum dots²³ or other compounds,²⁴ $[\text{Ru}(\text{bpy})_3]^{2+}$ still represents the benchmark for commercially available ECL applications²⁵ and luminol is commercially applied on a large scale in CL assays.²⁶⁻²⁸ There are several, grand, unexploited prospects that the classical luminophores comprise, while the ready use in commercial ECL assay kits indicates the market relevance and possible transition towards upcoming POC and diagnostics applications.

While ECL itself is a powerful and sensitive detection technique, signal enhancement strategies beyond single-probe approaches cannot be neglected to truly unleash the full power of detection capabilities. In this regard, different combinations of ECL reagents and signal enhancement tools can be used, which all have different advantages. The combination of $[\text{Ru}(\text{bpy})_3]^{2+}$ as ECL reagent together with PAMAM dendrimers, which is presented in **chapter 3**, highlights one possible route for ECL signal enhancement. Here, four different PAMAM dendrimers encompassing between 5-16 terminal amino groups were compared for their performance in $[\text{Ru}(\text{bpy})_3]^{2+}$ - ECL. Additionally, the possibility to combine the function of a biorecognition element for the analyte and at the same time the role of the ECL coreactant in a single entity, i.e. the dendrimer is shown. This bi-functionality was investigated with the model system biotin/streptavidin in a homogeneous format while it suggested that the presence of $[\text{Ru}(\text{bpy})_3]^{2+}$ in the vicinity of dendrimers at the electrode surface is beneficial towards stabilizing these assemblies and for a signal enhancement nature. A very different approach is shown in **chapter 4**, with the combination of a new luminol derivative with liposomes as signal enhancement means. Here, the novel synthesis of *m*-carboxy luminol created a superior ECL probe. This new molecule was analyzed towards its ECL properties where its superiority compared to standard luminol, mediated by its good water solubility was shown. This also enabled its inclusion into liposomes as multiplexing probe. These were investigated for different parameters like their stability, synthesis reproducibility and their performance under changed conditions with *m*-carboxy luminol as encapsulant. The liposomes were then employed in a heterogeneous DNA sandwich hybridization

assay for performance comparison to the same assay employing fluorescence detection with minor optimization. Here, the superiority of this concept for highly sensitive detection demands also with respect to the presence of complex, environmental matrices (e.g. soil) was proved.

Besides the combination with dendrimers or liposomes as small-polymer- or biochemical macrostructure probes for signal enhancement also the addition of surfactants can alter the ECL signal extent dramatically. This is an important, but double-edged feature which can either strongly limit the performance of the applied system but also be used for signal enhancement. For this reason, it is important to understand the underlying mechanistical aspects which drive the signal influencing nature of the respective surfactants. In **chapter 5**, the influence of several different surfactants on the ECL of the luminol-H₂O₂ system was investigated for two different luminol variants and on four different electrode materials. The choice of different, charged and uncharged surfactant types as well as of gold, ITO, hydrophilized ITO and laser scribed graphene electrodes allowed to acquire a broad picture of the ambiguous surfactant effects on the employed luminol system. The underlying signal enhancing and reducing mechanisms were investigated by looking into the ECL properties, the electrochemical properties, the electrode surfaces, CL behavior and finally by comparing these with the respective surfactant properties. As such, possible influencing factors were critically assessed and suggestions for a symbiotic mechanism presented. With the frequent presence and requirement of surfactants in different bioassays, this created library of surfactant effects on the luminol-H₂O₂ ECL system can be beneficial in intelligent assay design.

Besides signal enhancement means via combination with probes or surfactants, in **chapter 6**, conceptual and assay design considerations for a possible joint-venture of both ECL reagents, luminol and Ru(bpy)₃²⁺ with respect to a miniaturized and versatile ECL detection system are presented. The use of microfluidic technology can lead to further signal enhancement effects can further prepare the ECL detection method for a possible mobile application. Here, the capability towards a function with both ECL systems is discussed, addressing electrode material choice, electrode performance and limitations. A new direct thermal bonding method between the polymers PMMA and PET is presented and the suitability of the resulting microfluidic system for luminol and

$\text{Ru}(\text{bpy})_3^{2+}$ ECL is assessed. Finally, an alternative carbon based electrode material is characterized for its general ECL capability towards microfluidic use.

References

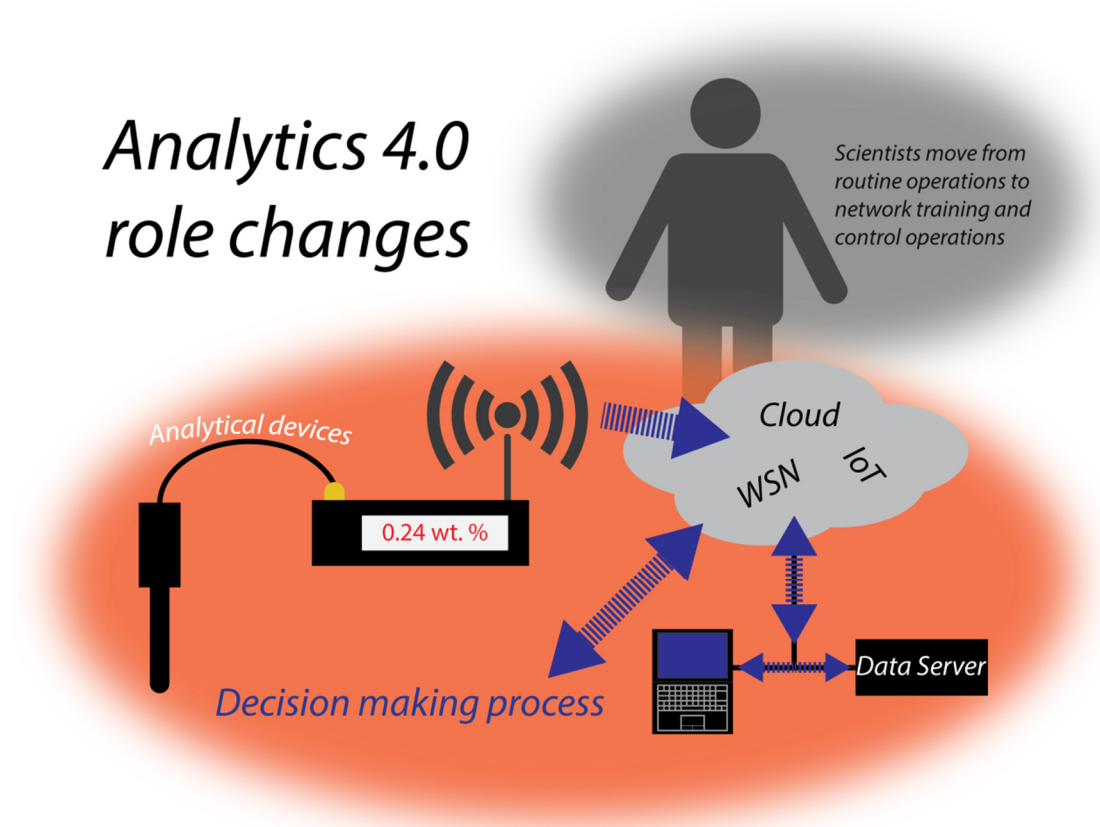
- (1) Munster, V. J.; Bausch, D. G.; de Wit, E.; Fischer, R.; Kobinger, G.; Muñoz-Fontela, C.; Olson, S. H.; Seifert, S. N.; Sprecher, A.; Ntoumi, F.; Massaquoi, M.; Mombouli, J.-V. Outbreaks in a Rapidly Changing Central Africa — Lessons from Ebola. *N. Engl. J. Med.* **2018**. doi: 10.1056/NEJMp1807691.
- (2) Mohammed, M. I.; Haswell, S.; Gibson, I. Lab-on-a-chip or Chip-in-a-lab: Challenges of Commercialization Lost in Translation. *Procedia Technology* **2015**, *20*, 54-59. doi: 10.1016/j.protcy.2015.07.010.
- (3) Balakrishnan, S. R.; Hashim, U.; Gopinath, S. C. B.; Poopalan, P.; Ramayya, H. R.; Iqbal Omar, M.; Haarindraprasad, R.; Veeradasan, P. A Point-of-Care Immunosensor for Human Chorionic Gonadotropin in Clinical Urine Samples Using a Cuneated Polysilicon Nanogap Lab-on-Chip. *PLoS One* **2015**, *10*, e0137891. doi: 10.1371/journal.pone.0137891.
- (4) Zór, K.; Heiskanen, A.; Caviglia, C.; Vergani, M.; Landini, E.; Shah, F.; Carminati, M.; Martínez-Serrano, A.; Moreno, T. R.; Kokaia, M.; Benayahu, D.; Keresztes, Z.; Papkovsky, D.; Wollenberger, U.; Svendsen, W. E.; Dimaki, M.; Ferrari, G.; Raiteri, R.; Sampietro, M.; Dufva, M., et al. A compact multifunctional microfluidic platform for exploring cellular dynamics in real-time using electrochemical detection. *RSC Advances* **2014**, *4*, 63761-63771. doi: 10.1039/c4ra12632g.
- (5) Nascetti, A.; Mirasoli, M.; Marchegiani, E.; Zangheri, M.; Costantini, F.; Porchetta, A.; Iannascoli, L.; Lovecchio, N.; Caputo, D.; de Cesare, G.; Pirrotta, S.; Roda, A. Integrated chemiluminescence-based lab-on-chip for detection of life markers in extraterrestrial environments. *Biosens. Bioelectron.* **2018**. doi: 10.1016/j.bios.2018.08.056.
- (6) Tokel, N. E.; Bard, A. J. Electrogenerated chemiluminescence. IX. Electrochemistry and emission from systems containing tris(2,2'-bipyridine)ruthenium(II) dichloride. *J. Am. Chem. Soc.* **1972**, *94*, 2862-2863. doi: 10.1021/ja00763a056.
- (7) Hu, G. B.; Xiong, C. Y.; Liang, W. B.; Zeng, X. S.; Xu, H. L.; Yang, Y.; Yao, L. Y.; Yuan, R.; Xiao, D. R. Highly Stable Mesoporous Luminescence-Functionalized MOF with Excellent Electrochemiluminescence Property for Ultrasensitive Immunosensor Construction. *ACS Appl. Mater. Interfaces* **2018**, *10*, 15913-15919. doi: 10.1021/acsami.8b05038.
- (8) See chapter 6, photolithography of ITO electrodes with benchtop chemistry.

- (9) Fenzl, C.; Nayak, P.; Hirsch, T.; Wolfbeis, O. S.; Alshareef, H. N.; Baeumner, A. J. Laser-Scribed Graphene Electrodes for Aptamer-Based Biosensing. *ACS Sens.* **2017**, *2*, 616-620. doi: 10.1021/acssensors.7b00066.
- (10) Gao, W. Y.; Muzyka, K.; Ma, X. G.; Lou, B. H.; Xu, G. B. A single-electrode electrochemical system for multiplex electrochemiluminescence analysis based on a resistance induced potential difference. *Chem. Sci.* **2018**, *9*, 3911-3916. doi: 10.1039/c8sc00410b.
- (11) Doeven, E. H.; Barbante, G. J.; Harsant, A. J.; Donnelly, P. S.; Connell, T. U.; Hogan, C. F.; Francis, P. S. Mobile phone-based electrochemiluminescence sensing exploiting the 'USB On-The-Go' protocol. *Sens. Actuators, B* **2015**, *216*, 608-613. doi: 10.1016/j.snb.2015.04.087.
- (12) Roda, A.; Mirasoli, M.; Michelini, E.; Di Fusco, M.; Zangheri, M.; Cevenini, L.; Roda, B.; Simoni, P. Progress in chemical luminescence-based biosensors: A critical review. *Biosens. Bioelectron.* **2016**, *76*, 164-179. doi: 10.1016/j.bios.2015.06.017.
- (13) Ghodsevali, E.; Morneau-Gamache, S.; Mathault, J.; Landari, H.; Boisselier, É.; Boukadoum, M.; Gosselin, B.; Miled, A. Miniaturized FDDA and CMOS Based Potentiostat for Bio-Applications. *Sensors (Basel)* **2017**, *17*. doi: 10.3390/s17040810.
- (14) Bezuidenhout, P.; Smith, S.; Joubert, T.-H. A Low-Cost Inkjet-Printed Paper-Based Potentiostat †. *Appl. Sci.* **2018**, *8*. doi: 10.3390/app8060968.
- (15) Wojciechowski, J. R.; Shriver-Lake, L. C.; Yamaguchi, M. Y.; Füreder, E.; Pieler, R.; Schamesberger, M.; Winder, C.; Prall, H. J.; Sonnleitner, M.; Ligler, F. S. Organic Photodiodes for Biosensor Miniaturization. *Anal. Chem.* **2009**, *81*, 3455-3461. doi: 10.1021/ac8027323.
- (16) Qiu, H.; Yin, X.-B.; Yan, J.; Zhao, X.; Yang, X.; Wang, E. Simultaneous electrochemical and electrochemiluminescence detection for microchip and conventional capillary electrophoresis. *ELECTROPHORESIS* **2005**, *26*, 687-693. doi: 10.1002/elps.200410015.
- (17) Kang, C. H.; Choi, Y.-B.; Kim, H.-H.; Choi, H. N.; Lee, W.-Y. Electrogenated Chemiluminescence Sensor Based on a Self-Assembled Monolayer of Ruthenium(II)-bis(2,2'-bipyridyl)(aminopropyl imidazole) on Gold Deposited Screen Printed Electrode. *Electroanalysis* **2011**, *23*, 2131-2138. doi: 10.1002/elan.201100214.
- (18) Tsuwaki, M.; Kasahara, T.; Edura, T.; Oshima, J.; Kunisawa, E.; Ishimatsu, R.; Matsunami, S.; Imato, T.; Adachi, C.; Shoji, S.; Mizuno, J. Fabrication of a Portable Electrochemiluminescence-induced Fluorescence Detection Chip with Microfluidic Excitation Source for Point-of-care Diagnostics. *IEEJ Transactions on Sensors and Micromachines* **2015**, *135*, 230-235. doi: 10.1541/ieejsmas.135.230.
- (19) Zhang, Y.; Liu, W.; Ge, S.; Yan, M.; Wang, S.; Yu, J.; Li, N.; Song, X. Multiplexed sandwich immunoassays using flow-injection electrochemiluminescence with designed substrate spatial-resolved technique for detection of tumor markers. *Biosens. Bioelectron.* **2013**, *41*, 684-690. doi: 10.1016/j.bios.2012.09.044.

- (20) Miao, W. Electrogenated chemiluminescence and its biorelated applications. *Chem. Rev.* **2008**, *108*, 2506-2553. doi: 10.1021/cr068083a.
- (21) Kirschbaum-Harriman, S.; Duerkop, A.; Baeumner, A. J. Improving ruthenium-based ECL through nonionic surfactants and tertiary amines *Analyst* **2017**, *142*, 2648-2653. doi: 10.1039/C7AN00197E.
- (22) Mayer, M. *Luminol and ruthenium electrochemiluminescence for a dual ECL detection approach*. Master thesis, Regensburg, **2015**.
- (23) Pan, Q. X.; Wang, J. Y.; Cheng, Y. Z.; Li, W. J.; Wang, X. D. Determination of Hydrogen Peroxide by Electrochemiluminescence Using a Chitosan-graphene Composite Film Doped Cadmium-Tellurium Quantum Dot Modified Glassy Carbon Electrode. *Anal. Lett.* **2018**, *51*, 1373-1383. doi: 10.1080/00032719.2017.1374964.
- (24) Carrara, S.; Aliprandi, A.; Hogan, C. F.; De Cola, L. Aggregation-Induced Electrochemiluminescence of Platinum(II) Complexes. *J. Am. Chem. Soc.* **2017**, *139*, 14605-14610. doi: 10.1021/jacs.7b07710.
- (25) Roche Diagnostics, "Die ECL-Technologie", can be found under <https://www.roche.de/diagnostics/systeme/gesamtkonzepte/electrochemiluminescence.html#Die-ECL-Technologie> **2018**.
- (26) Ortho Clinical Diagnostics, "VITROS® MicroWell Technology", can be found under <https://www.orthoclinicaldiagnostics.com/en-hk/home/products/vitros-microwell-technology> **2018**.
- (27) Elabscience, "CLIA Kits", can be found under https://www.elabscience.com/Products-clia_kits-108.html, **2018**.
- (28) Rodriguez-Orozco, A. R.; Ruiz-Reyes, H.; Medina-Serriteno, N. Recent Applications of Chemiluminescence Assays in Clinical Immunology. *Mini-Rev. Med. Chem.* **2010**, *10*, 1393-1400. doi: 10.2174/138955710793564142.

Chapter 1: ABC Spotlight on Analytics 4.0

Graphical Abstract



This chapter has been published.

Michael Mayer, Antje J. Baeumner, *Anal. Bioanal. Chem.*, **2018**, 410 (21), 5095-5097,

DOI: 10.1007/s00216-018-1191-7

Author contributions:

AJB and MM did the scientific literature search. MM wrote the first draft of the manuscript. AJB revised the manuscript. AJB is corresponding author.

1. ABC Spotlight on Analytics 4.0

Analytical Chemistry plays a key role in our daily life albeit often not realized by the layman, and is a crucial contributor to areas such as food safety, health care, production processes, environmental monitoring, forensics and life sciences research.

With an ever evolving Internet of things (IoT), i.e. the increasing automation and networking within and of industrial processes, businesses and our homes, it is obvious that analytical chemistry will become an integral part of the IoT and will contribute by providing analytical data for decision-making processes just as it does off-line in today's analytical facilities. Analytics 4.0 describes technologies ready for automation, and for connection to IT and computing technologies to realize data transmission, interpretation, learning and self-evolution. It is associated with a dramatic decentralization of data generation expanding from centralized labs to individuals, to remote sensing locations and to the cloud. Analytics 4.0 is thus the evolution analytical chemistry is undergoing as it becomes an inevitable part of the IoT.

Today, the chemical industry plays a leading role in Analytics 4.0's advancements by integrating analytical chemistry directly into process lines (termed "Process Analytical Technology", PAT) and hence stepping away from the traditional use of separate, external sensors in the decision making process. Gouveia et al. have shown the suitability of different spectroscopic methods and their importance as PAT elements either applied in quality monitoring of a chemical synthesis process routine, or in the design of process layouts for a scale-up from batch to continuous production lines.¹ Hence, automated analytical chemical technology is embedded in the overall process control. It is coupled to up- or downstream decision making steps and hence directly influences the outcome of the whole process in real-time, as opposed to being a disconnected, passive sensing element that requires human interaction to cause a reaction. Furthermore, Gouveia and colleagues illustrate how such an integrated small-scale solution provides understanding needed for translation to large-scale productions.

Analytics 4.0 will often rely on multi-sensing solutions to obtain required reliability in an automated system. This may be achieved by connecting and networking analytical

devices of the same type at different locations, or by incorporating different analytical (detection) methods for orthogonal verification of results. Obtaining the same answer through independent methods has a long tradition in analytical chemistry. In automated situations as envisioned in the IoT this need is even greater and research for orthogonal detection strategies for the same analyte are in high demand. Uteschil et al. have for example presented the combination of a TOF-IMS together with laser-induced fluorescence detection ² hence, spectroscopic and mass-based data are obtained during the same analysis. The authors demonstrate that this combination delivers not only more precise molecular information from IMS (i.e. the specific drift times) but also optical parameters such as fluorescence lifetimes or emission maxima, thus gathering simultaneous in-depth information on the analytes. Many of the exquisite hyphenated, complex technologies developed over the last decades, or traditional combinations of microbiological and biochemical methods, or verifications of molecular biological results through immunological staining fall into the same orthogonal detection approach strategy. Developing these technologies toward Analytics 4.0 performance is an important grand future task and highly desirable for multidimensional analysis.

In this day and age high-throughput screening (HTS) is a highly automated process with semi-automated data processing and minimal user interaction in the pharmaceutical industry. Further progress can link combinatorial syntheses with HTS, which is more an IT and engineering task than an analytical challenge. At the same time though, the development of new screening procedures, alternatives to the ubiquitous microtiter plate format, is desirable as many analytical answers cannot be obtained in such a format, and as applications outside of centralized facilities would also benefit from screening strategies. Jagannadh et al.³ demonstrated a microscopy method with the potential to screen large entities of cells in a short timeframe and with reasonably priced equipment e.g. for blood cell counting in a point-of-care (POC) diagnostics setting. Combined with chemometric techniques e.g. PCA and other algorithms, with neuronal networks and with deep learning strategies this can become a more interaction-independent tool.

Portable sensors may be the one analytical technology that the layperson can directly associate with as it relates to interconnected, automated Analytics 4.0. Many people voluntarily wear accessories that incorporate sensors, whether these are simple step counters, pulse monitors or temperature sensors. Wearable glucose sensors, EKG

monitors, smartphones with interactive health monitoring apps have entered our daily life and find acceptance with the users. Smart phones, smart homes, smart cars are at the forefront of making our lives “more convenient”. Thus, it is foreseeable that the (bio)chemical sensors that are part of the Trillion Sensor Vision will drive the development of Analytics 4.0. In fact, where possible, today’s portable (bio)analytical sensors published describe their potential for wireless data transmission, which is a mandatory necessity for Analytics 4.0. Also, in most scenarios, data acquisition via cell phone is suggested. Chen et al. have presented recently a smartphone add-on for the optical readout of colorimetric assays exemplary shown with an ELISA for zearalenone, which is a fungal toxin relevant in food safety testing.⁴ Also, Gao et al. have built a smart wristband multiple sensor-array for multiple physiological parameter monitoring based on sweat analysis.⁵ Their device is able to monitor levels of lactate, glucose, Na⁺, K⁺, and temperature via enzyme- or ion selective electrodes or microwires with at least 5 weeks of long-term stability. Data are sent via a Bluetooth module to a smartphone for readout and logging. Furthermore, Sharma et al. have presented an amperometric, microneedle based *in-vivo* glucose monitoring device, with state-of-the art performance also during a short clinical testing phase in humans.⁶ Such multi-analyte *ex-vivo* and *in-vivo* sensing applications will define the progress of portable sensing, and are an important cornerstone of the future Analytics 4.0.

One of the greatest challenges for wearable, *in-vivo* or *in-situ* sensors may be the integration of sample preparation and analyte pre-concentration steps with the detection module, all to be located in a simple device that does not require user interaction and can be used long-term. Hence, this is an area of intensive research and great needs. Much success has been seen through the development of lab-on-a-chip systems. While not wearable, these tend to be portable devices in which analytical operations are miniaturized. For example, Furutani et al. recently demonstrated a portable system for highly complex bioanalytical challenges. The size of a suitcase, it incorporates a real-time PCR system for on-site pathogen detection.⁷ Microfluidic-based liquid handling and integrated system design allows processing from sampling to result-output. Their system compares well to a conventional PCR setup exemplary shown for *E. coli* detection.

In the present day, rapid, portable and low-cost detection of analytes based on DNA or RNA information remains challenging due to complex sample preparation, expensive

amplification and detection assay requirements. Yet, nucleic acid-based sensing is of great interest also for Analytics 4.0 as observable phenotypes and many diseases are associated with specific genomic information. Next generation sequencing (NGS) has thus the potential to become the routine technology for nucleic acid testing in the lab, in screening applications but also for the point-of-care setting. Considering sufficient computing power, wireless data transmission and cloud technology, large databases will be created as source for automated data analysis.

Connectivity, data readout, storage, sharing and logging are as important to Analytics 4.0 as these are integral elements of the IoT. Connection between devices is highlighted in the review by Lopez-Barbosa *et al.* on the future of point-of-care disease detection emphasizing in fact the role of the IoT.⁸ The unfolding independence of user-operation and the evolution of standalone analytical devices (not only automatically reporting results but also being integrated in decision-making routines with closed loop sensing and feedback control systems) will prepare Analytics 4.0 for the IoT. Stenzel has written an exciting article on sensor systems onboard of the International Space Station (ISS).⁹ Here, the onboard sensor system is a complete wireless sensor network (WSN), connecting and coupling all single sensing elements together to one large, intercommunicating entity. Being a small-scale version, expansion to different application areas (such as smart homes, environmental monitoring, healthcare, industrial processes) is highly projectable. While no (bio)chemical techniques and sensors are included yet onboard the ISS-own WSN (rather microscale sensors for temperature, humidity, pressure or light), the architecture can be a blue-print for the integration with any aforementioned Analytics 4.0 sensor or system and those off-line sensors used already on-board for ISS-based experiments.

Such multi-orthogonal, autonomously reacting, large sensor networks can be realized, as long as interfaces, communication protocols and data formats are standardized. Also, low and sustainable energy consumption is a mandatory requirement for WSNs and any portable sensor approaches. Here, low-power communication and MEMS devices, and a photovoltaic energy harvesting system avoid batteries and improve the independence of the networked system on the ISS. Obviously, benchtop measurement devices will profit equally from all of these described developments and added connectivity will boost interoperability, automation, user independence, processing and many more features.

Analytics 4.0 is a step toward an Internet of Analytical Things, in which networked analytical labs communicate with distributed sensors, provide information, which drives automated decision making. Application areas include health care, smart homes, food and agricultural systems, environmental monitoring and industrial processes. It will be a highly relevant, important, and in fact necessary resource for the goal of solving ubiquitous challenges in our societies. It should be noted though that with a “trillion sensor vision”, with the integration of Analytics 4.0 into the IoT, and with the desired unlimited analytical possibilities come great responsibilities related to cybersecurity, data privacy and a fair evolution. Making these aspects part of our scientific communications is our responsibility.

2. References:

- (1) Gouveia, F. F.; Rahbek, J. P.; Mortensen, A. R.; Pedersen, M. T.; Felizardo, P. M.; Bro, R.; Mealy, M. J. Using PAT to accelerate the transition to continuous API manufacturing. *Anal. Bioanal. Chem.* **2017**, *409*, 821-832. doi: 10.1007/s00216-016-9834-z.
- (2) Uteschil, F.; Kuklya, A.; Kerpen, K.; Marks, R.; Telgheder, U. Time-of-flight ion mobility spectrometry in combination with laser-induced fluorescence detection system. *Anal. Bioanal. Chem.* **2017**, *409*, 6279-6286. doi: 10.1007/s00216-017-0584-3.
- (3) Jagannadh, V. K.; Bhat, B. P.; Nirupa Julius, L. A.; Gorthi, S. S. High-throughput miniaturized microfluidic microscopy with radially parallelized channel geometry. *Anal. Bioanal. Chem.* **2016**, *408*, 1909-1916. doi: 10.1007/s00216-015-9301-2.
- (4) Chen, Y.; Fu, Q.; Li, D.; Xie, J.; Ke, D.; Song, Q.; Tang, Y.; Wang, H. A smartphone colorimetric reader integrated with an ambient light sensor and a 3D printed attachment for on-site detection of zearalenone. *Anal. Bioanal. Chem.* **2017**, *409*, 6567-6574. doi: 10.1007/s00216-017-0605-2.
- (5) Gao, W.; Emaminejad, S.; Nyein, H. Y. Y.; Challa, S.; Chen, K.; Peck, A.; Fahad, H. M.; Ota, H.; Shiraki, H.; Kiriya, D.; Lien, D. H.; Brooks, G. A.; Davis, R. W.; Javey, A. Fully integrated wearable sensor arrays for multiplexed in situ perspiration analysis. *Nature* **2016**, *529*, 509-514. doi: 10.1038/nature16521.
- (6) Sharma, S.; Huang, Z.; Rogers, M.; Boutelle, M.; Cass, A. E. Evaluation of a minimally invasive glucose biosensor for continuous tissue monitoring. *Anal. Bioanal. Chem.* **2016**, *408*, 8427-8435. doi: 10.1007/s00216-016-9961-6.
- (7) Furutani, S.; Naruishi, N.; Hagihara, Y.; Nagai, H. Development of an on-site rapid real-time polymerase chain reaction system and the characterization of suitable DNA polymerases for TaqMan probe technology. *Anal. Bioanal. Chem.* **2016**, *408*, 5641-5649. doi: 10.1007/s00216-016-9668-8.
- (8) Lopez-Barbosa, N.; Gamarra, J. D.; Osma, J. F. The future point-of-care detection of disease and its data capture and handling. *Anal. Bioanal. Chem.* **2016**, *408*, 2827-2837. doi: 10.1007/s00216-015-9249-2.
- (9) Stenzel, C. Deployment of precise and robust sensors on board ISS-for scientific experiments and for operation of the station. *Anal. Bioanal. Chem.* **2016**, *408*, 6517-6536. doi: 10.1007/s00216-016-9789-0.

Chapter 2: Trends: Sensors and Analytical Chemistry for the Internet of Things (IoT)

Abstract

The Internet of Things (IoT) is a megatrend that cuts across all scientific and engineering disciplines and establishes an integrating technical evolution to improve production efficiencies and daily human life. Linked machines and sensors use decision-making routines to work toward a common product or solution. Expanding this technical revolution into the value chain of complex areas such as agriculture, food production, and healthcare requires the implementation and connection of sophisticated analytical methods. Today, wearable sensors, monitors and point-of-care diagnostic tests are part of our daily life and improve patients' medical progression or athletes' monitoring capabilities that are already beyond imagination. Wireless data collection and transmission via Bluetooth or smartphones have set the foundation to connect remote sensors and distributed analytical chemical services with centralized labs, cloud storage and cloud computing. Thus, analytical chemists will become critical influencers in the progressing IoT due to their innovations and IoT's need to implement analytical expertise into decision-making machine structures. Here, we critically review those analytical and chemo/biosensor technologies that are used in an IoT setting and those that are IoT-ready. We identify predominant technologies including physical, bio- or chemosensors, mass spectrometry and Next Generation Sequencing that can provide the type of information needed for future machine-based decision-making. Finally, we highlight requirements, existing and future challenges and provide possible solutions important towards the vision of a seamless integration into a global analytical concept.

Parts of this chapter are intended for publication.

Author contributions:

MM wrote the first draft of the manuscript. AJB revised the manuscript. AJB is corresponding author.

1. Introduction

Since its origination in 1999 through Kevin Ashton¹ and since the invention of the first to-the-web-connected device in 1990,² the Internet of things (IoT) sees major attention today not only by all internet technology-affiliated communities but also by the general industry and science. Its original development was enabled by the hyperexponential growth of computer and internet technology since the mid-1990's. Today, health technology and even insurance companies seem to make the first baby steps and indeed profit from wearable health tracking^{3,4} in a basic manner, from step counting and pulse monitoring to ECG control.³ General mobility benefits from connected driving^{5,6} and cars evolving to driver-less means of transportation⁷ albeit still plagued with an abundance of remaining problems.⁸ Also smart homes developed over the last years into invisible servants for all kinds of imaginable home tasks.⁹ The longest history of connected and self-operating devices has been observed in industrial and automated process control and regulation. Analytical examples are sophisticated IoT integrations from lab-scaled demo-units such as "LeyLab"¹⁰ to industrial-scale processes commonly contained in the field of process analytical technology (PAT).^{11,12} Yet, the here partly used sophisticated physical sensors cover only a small portion of required information and significantly more advances in integrating other types of sensors with the IoT is needed, especially as performance requirements are driven by the desired application areas.

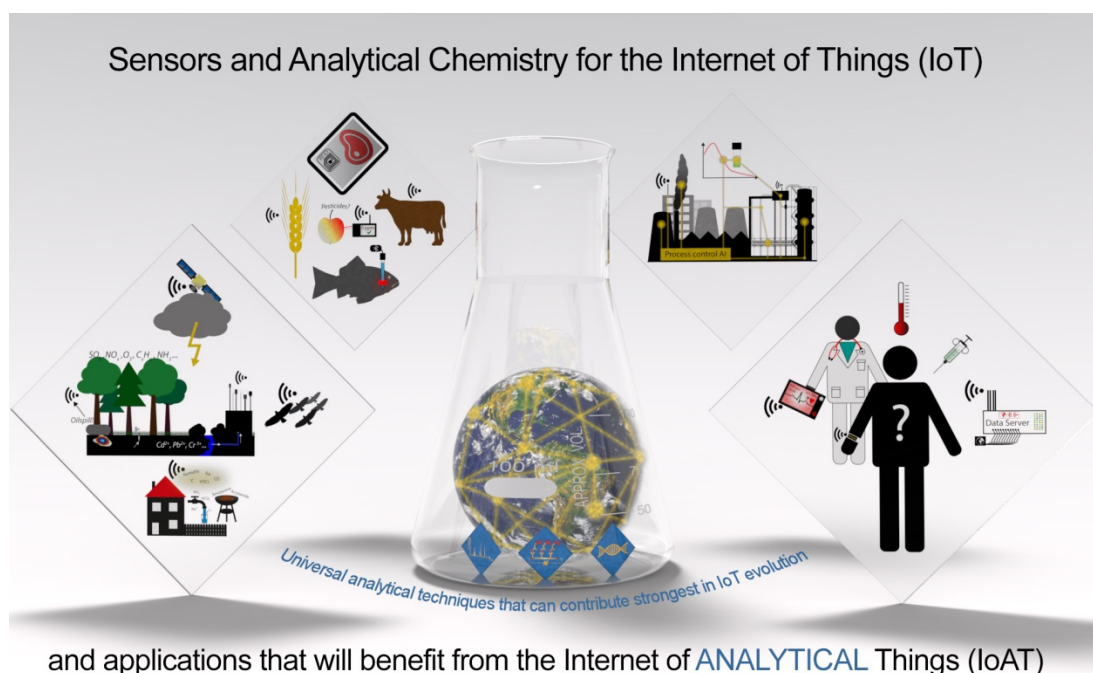


Figure 1. Analytical chemistry and sensors for the Internet of Analytical Things (IoAT)

Thus, analytical chemistry will be necessary to provide data for the IoT when it addresses complex challenges related to health, environment, climate, food and water on the local and global, on the individual and the population scale. Questions that must be asked are for example: Which technologies lend themselves to answer challenges of global health and disease monitoring, of safe food and water, of optimized industrial processes, of food fraud, of a clean and safe environment that can be integrated in an IoT fashion and not only function in a local, individual manner? Do we need the entire breadth of analytical chemistry or can we initially choose just a few technologies to succeed in logistical integration as an IoT network? Can we generate an Internet of Analytical Things, IoAT for the IoT?

Typically, the lower the required limit of detection and the more difficult the specific identification in a given matrix, the more sophisticated sensing platforms are required. Simple examples are blood glucose and pregnancy hormone detection that are routinely done in point-of-care over-the-counter testing kits whereas sophisticated analyses reach high-throughput, or single-analyte detection limits using FACS,¹³ microscopy imaging,¹⁴ mass spectrometry¹⁵ and next generation sequencing.¹⁶

We suggest three technologies to stand out to provide an initial answer of the questions posed: (1) Point-of-care sensors are developed today encompassing WHO's "ASSURED" principle¹⁷ or targeting implantable *in vivo* sensing, and therefore lend themselves for in-field and on-site monitoring of individuals and remote locations, which we describe through body, food and environmental sensors. (2) Mass spectrometry and its hyphenated platforms integrated with chromatography develops into a technology that can provide qualitative and quantitative, structural and composition-related information on an ever-growing number of molecules.¹⁸⁻²² It requires mostly lab infrastructure but that does not have to be a drawback for IoT integration. (3) In the future, next generation sequencing (NGS) may make all molecular biological and microbiological assays obsolete and provide an answer to all questions that can be based on genomic answers.²³⁻²⁵

At the end of the article we propose future requirements and developments needed to provide a seamless integration to an overall, global analytical concept providing "an answer to everything". Futuristic planning of smart cities such as Quayside, Toronto, may provide stimulus to nudge analytical chemists toward an IoAT so that analytical data can assist in driving decisions continuously. In such a smart city, driverless shuttle buses, monitoring and steering of public activity, robots for transport (i.e. delivery) and basic infrastructure support (e.g. waste management), modularity of buildings, self-sustaining energy supply and ubiquitous sensing come here together.²⁶

It should be pointed out that this review does not focus on the interface between cloud computing and sensors, such as different architectures for communication to e.g. wireless sensor networks, machine to machine communication and software aspects research as this has been discussed in more detail elsewhere²⁷⁻²⁹. We focus instead on those critical common considerations relevant to analytical chemistry.

2. Sensor solutions for the point-of-care and *in vivo* detection

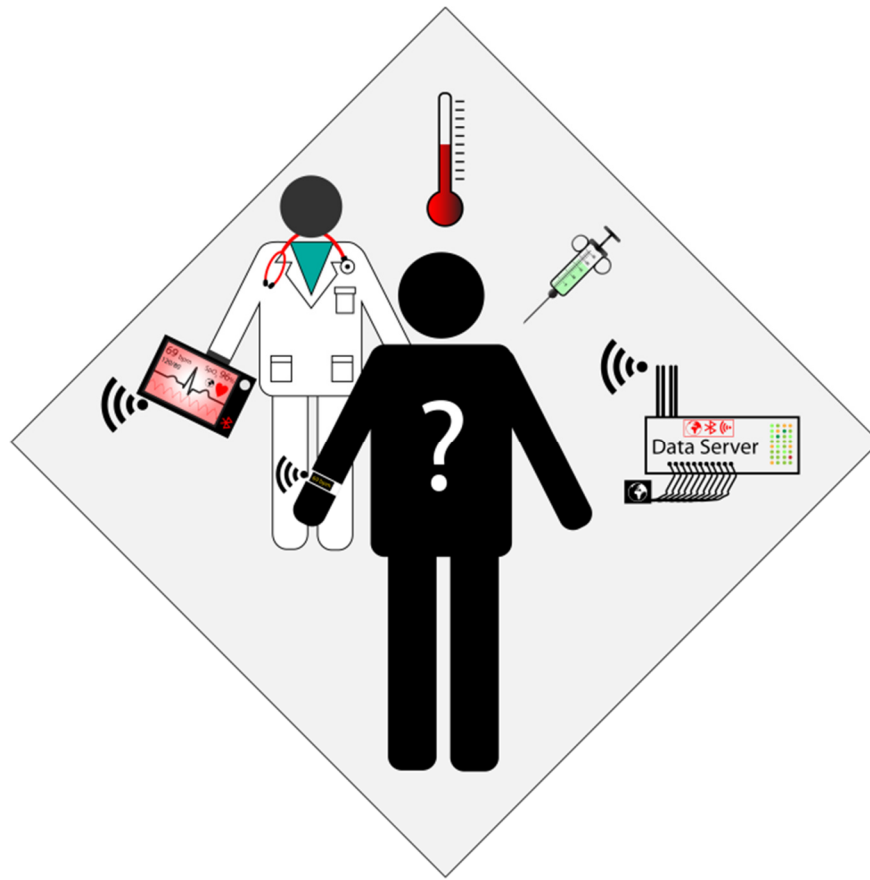


Figure 2. Sensor solutions for the point-of care and *in vivo* detection.

With the progress of consumer products developed in recent years, body sensors or wearables may be the easiest to envision in an IoAT (Fig. 2). Patient data are sent to health centers triggering individual diagnoses and population-wide analyses; a person's health status causes responses by the IoT-house or car; a disease can be controlled before it becomes an epidemic. Prevention, early diagnosis, immediate help, lower costs, availability in all areas, also the most remote rural countryside are keywords we associate with these principles. The next step, i.e. from wearable to IoAT seems simple – connect the single devices to a network -- as advances in recent years relating to miniaturization, connectivity and power supplies have led to sophisticated devices needed.³⁰⁻³² The stumbling blocks, i.e. the common analytical challenges, relate to the fact that autonomous/remote/lay-person applications are required and that long-term use is favored.³³ *The common challenges are:* How to prevent electrode fouling,^{33,34} electrode drift, optical transducer blockage, probe degradation in those complex

matrices of interest? We present here a few excellent examples that address these challenges and have found relevant solutions resulting in sensors ready for the IoAT. Table 1 provides an overview of sensor solutions and components addressing major challenges in the point-of-care.

Category	Keyword	Sensing principle	Analyte	Ref number
Appliances/accessories	Mouth guard	EC	Uric acid	32
	Eye glasses, ring, gloves	EC	Lactate, K ⁺ organophosphates	35, 36, 37
	Face mask	EC, flow sensor	breath	39
	Contact lens	EC,		31, 61-63
Bandages, patches tattoos	Bandage, wristband	Impedance, EC, resistance cells/optical	Cortisol, Na ⁺ , K ⁺ , glucose, lactate	30, 42, 50, 53
	patch	EC, optical, colorimetric,	ECG, lactate, blood oxygen level, Cl ⁻ , glucose, pH, skin-melanoma, T	43, 47, 48, 51, 52, 54, 55, 56, 112
	Tattoo	EC, colorimetric	Ethanol, pH, signaling chemicals	49, 56, 58, 60
	Components	Electrodes, connectors, electronics		44, 46, 113

<i>In-vivo</i> sensing	In-vivo (animal)	EC, optical, optofluidic, FET	Glucose, lactate, paracetamol, ATP, glutamate, doxorubicin, oxygen,	67-73, 80-81, 82, 84, 86
	In-vivo (human)	EC, optical, motion	Glucose, cardiac implant, pH, T	59, 74, 75, 77-78, 79, 85
	Foreign body reactions, bio-barriers and sensing element stability	-	Bioactive coatings, membranes, biodegradables, probe stability, implantable sensor elements	83, 94-111
Microfluidic strategies	Sample prep and amplification	EC, microneedles, optofluidics	Influenza virus, bacterial strains, glucose, alcohol, nerve agents	118, 121-128, 130
Power supplies	Batteries, body energy harvesting	-	-	131-144, 149-154

Table 1. Sensor solutions for POC& in-vivo sensing.

2.1 Appliances/accessories

Kim et al. presented a mouth guard integrated biosensing system to monitor uric acid levels in saliva with wireless data transmission that is only the size of a 2-cent coin.³² Uric acid is an important marker for diseases (hyperuricemia, gout, renal syndrome) and an indicator for type II diabetes.

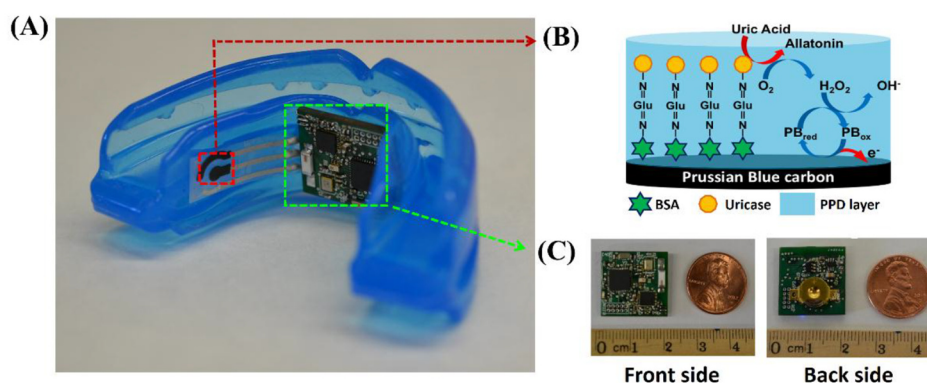


Figure 3. (A) Photograph of the mouthguard biosensor integrated with wireless amperometric circuit board. (B) Reagent layer of the chemically modified printed Prussian-Blue carbon working electrode containing uricase for SUA biosensor. (C) Photograph of the wireless amperometric circuit board: front side (left) and back side (right). Reprinted with permission from ref ³². Copyright© 2015. Elsevier.

A screen-printed, enzyme-modified electrode is integrated with miniaturized electronics and a bluetooth transmitter for wireless data broadcast. The latter requires less energy and has a longer range compared to RFID based modules.

The use of a mouth guard is highly attractive similar to nose-pieces of eye glasses, rings and gloves demonstrated by the Wang group recently shown for the detection of lactate and potassium in sweat or hazardous substances like organophosphates.³⁵⁻³⁷ Reasonably large sensors or multiple sensors can be integrated in such an accessory that is or can be used daily for several hours, can be charged during normal “off times”. As with other voluntary wearables, it depends on the consumer’s reliance of using it, requires attention of care or regular switching of sensing units.³² Kim et al. tested their

sensor stability for 2 hours, but realistic applications ready for the market must at least have 8 hours of continuous usability (e.g. during sleep). Recently, Liang and colleagues, went one step further and showed their mouthguard-integrated oral drug delivery module, designed via 3D-printing and proved the applicability of their concept in a human study.³⁸

The 2001 accepted patent (US 6718982 B2) from Smith, Fasching and Howard, details a face mask with an incorporated respiratory flow sensor.³⁹ This opens up interesting possibilities to incorporate gas and breath sensing into such an accessory. Sensors as described above integrated into mouth guards and eye glass pieces can also be integrated into a face mask and assist in breath analysis, detection of pathogens such as influenza or seasonal viruses or bacterial infections and even emerging infectious diseases. Especially in those regions of the world, where wearing a face mask is part of the socially accepted or requested habit when people are affected by flu-like symptoms,⁴⁰ this will be a valuable approach for comprehensive monitoring not only of an individual but a population as a whole in order to identify outbreaks during typical “flu seasons”. Here, connectivity could be easily established due to the quite large size of a face mask and if used in a densely populated urban area, grids of sensors with large range communicating with each other can be established as also proposed by Güder et al.⁴¹

2.2 Bandages, patches, tattoos

A significant effort in wearable sensor research focuses on patches, bandages or tattoos that are worn directly on the skin and provide both sensing as well as data transmission possibilities in a non-invasive mode (no microneedles used). Predominantly electrochemical, enzyme-based or potentiometric sensors are being developed to identify specific analytes. For example, Munje et al. designed a biosensor for sweat diagnosis based on impedance measurements of the electrical double layer in reaction to antibody –analyte interaction at the semiconductor-liquid interface.⁴² Cortisol as a marker for physically induced stress – a relevant parameter for everyday use in sports or at the workplace was detected. The antibody afforded high specificity, but unfortunately also limited it to only single-use. AC voltage performed better than DC voltage as the latter caused damage to biomolecules and had significantly higher power

consumption. An alternative Cortisol sensing platform as polymeric wearable patch with a nanoporous membrane layer and a transistor, using the concentration dependent source-drain current as analytical signal, has been presented by Parlak and coworkers.⁴³ Overall, the flexible substrates, the small size and the highly specific biosensing suggests these sensor design to be an ideal technology for IoAT as long as power supply, regulation and transmission units will be integrated with the sensor. Here, important elements for skin-wearable sensing have been introduced by the group of Lu: electronics for RF transmission,⁴⁴ a transparent ITO/Cu mixed material⁴⁵ for control applications or displays, or graphene-based tattoo-like materials directly for biosignal monitoring.⁴⁶

All-integrated wearable biosensors patches include the hybrid biosensing system from Imani et al., comprised of an amperometric and a bipolar ECG electrochemical sensor, monitoring lactate levels and the ECG signal. The device is worn directly on the skin and enables wireless signal readout.⁴⁷ It is especially noteworthy as orthogonal approaches are used to monitor health conditions hence increasing the reliability of measured data in contrast to the stand-alone pulse oximetry device but which allows for variable placing on the body.⁴⁸ Kim et al. have demonstrated that a biosensor tattoo can detect ethanol by combining iontophoresis of pilocarpine to induce sample collection (sweat) with enzymatic amperometric detection and wireless data transmission⁴⁹ and Sonner et al. present a sweat stimulation device, helpful for continuous monitoring under rest when sweat production is limited.⁵⁰ Exemplary for a multiple biosensing approach, Gao et al.³⁰ have shown a whole sensor array for the detection of Na⁺, K⁺, lactate and glucose and additional temperature measurement as analytical signal and for signal compensation of the other sensing moieties.

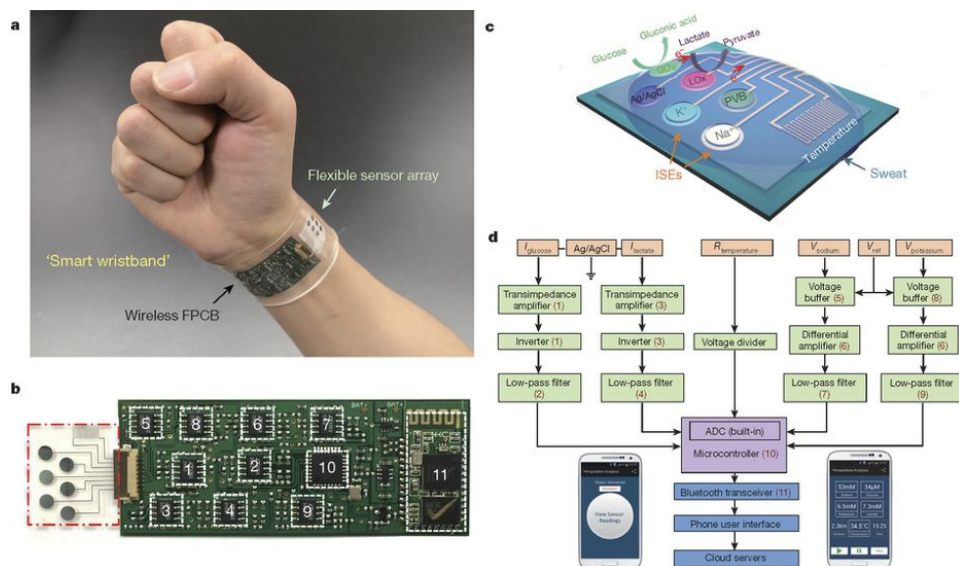


Figure 4. a, Photograph of a wearable FISA on a subject's wrist, integrating the multiplexed sweat sensor array and the wireless FPCB. (All photographs in this paper were taken by the authors.) b, Photograph of a flattened FISA. The red dashed box indicates the location of the sensor array and the white dashed boxes indicate the locations of the integrated circuit components. c, Schematic of the sensor array (including glucose, lactate, sodium, potassium and temperature sensors) for multiplexed perspiration analysis. GOx and LOx, glucose oxidase and lactate oxidase. d, System-level block diagram of the FISA showing the signal transduction (orange) (with potential V , current I and resistance R outputs), conditioning (green), processing (purple) and wireless transmission (blue) paths from sensors to the custom-developed mobile application (numbers in parentheses indicate the corresponding labelled components in b). ADC, analogue-to-digital converter. The inset images show the home page (left) and the real-time data display page (right) of the mobile application. Reprinted with permission from ref ³⁰. Copyright © 2016, Springer Nature.

The authors use a combination of enzymatic amperometric detection of glucose and lactate, ion-selective electrodes for ion sensing and resistivity-temperature sensing. Different coatings of the sensing elements (e.g. chitosan or PEDOT:PSS) provide robustness. All sensors, together with circuit components, A/D-converter, and further processing units with wireless data transmission via Bluetooth to a smartphone app. The whole sensor array with all elements and a Li-Ion battery was designed as wristband on a PET support with an additional rayon fabric as skin-contacting and sweat sampling element. Longtime storage was tested over 4 weeks with no obvious

change in efficiency and the longest continuous measuring application tested was over 90 minutes. Alternatively, a colorimetric approach for sweat chloride, glucose, lactate and pH sensing has been presented by Koh et al.⁵¹ They used a PDMS basis to integrate their capillary and sweat pressure driven microfluidic system leading to chromogenic reactions indicating the analyte abundance. Finally, NFC technology was integrated to facilitate e.g. smartphone-camera based signal readout. In addition, a good overview of the current state of the art for sweat sensor devices is given by Choi et al.⁵² Other wearable sensors include the skin-melanoma sensor by Ciui et al. which is presented as a bandage with wireless readout,⁵³ a sensor monitoring personal UV exposure⁵⁴ and a heart-monitoring sensor which is self-powered.⁵⁵ Finally, Zhu et al. have recently presented their capability to directly 3D-print and add via robotics, electrodes, connectors and electronic components for all sensing components on moving surfaces, shown on a freely moving human hand with at least 2h stability on the hand and being fully removable.⁵⁶ This example shows the capability to provide on-body sensing without the crucial need for support materials. An important contribution towards the long-term applicability, stability of printed electrochemical devices, has been made recently by Bandodkar et al. who presented their printed electrochemical devices with the capability of magnetical self-healing, irrespective of environmental conditions.⁵⁷ This is a promising solution for long-term stable wearable on-skin or textile and similar devices.

Tatoos can also be applied to fingernails as demonstrated by Kim et al. for pH determination taking advantage of the simplicity of visual detection and recording with a cell phone camera.⁵⁸ A PVC membrane containing different pH sensitive dyes was immobilized on tattoo transfer paper and placed onto fingernails. In order to obtain a broad dynamic range, different nails with different indicator dyes were used and provided sensing between pH 3 to 10, and multiple reversible usability (7-times).

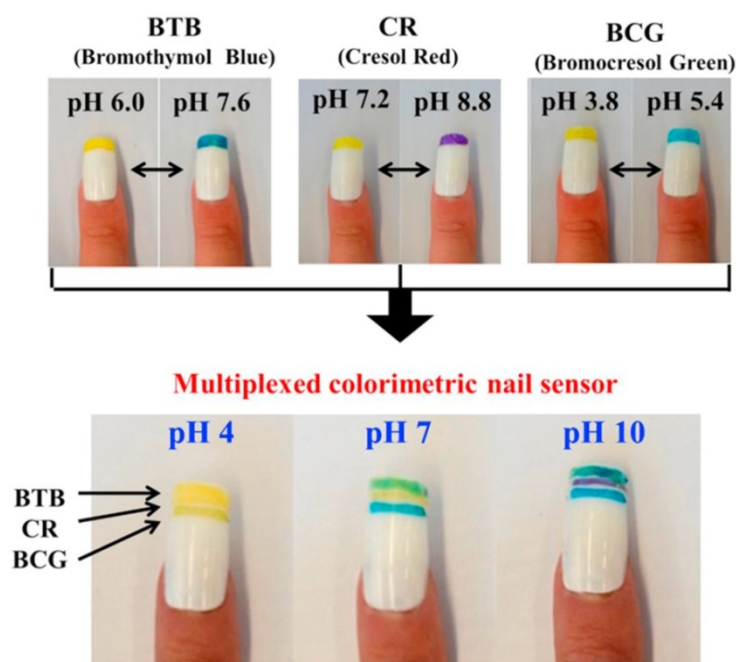


Figure 5. Colorimetric response and application pH ranges of BTB, CR, And BCG dye loaded nail sensors (top) and multiplexed colorimetric response at pH 4, 7, and 10(bottom). Reprinted with permission from ref⁵⁸. Copyright © 2016, Elsevier.

An *in-vivo* application via a patch is presented by Tseng et al. with an on-tooth mounted (2mmx2mm) RFID sensor made of functional materials like porous silk of PNIPAM hydrogels monitoring the oral cavity (pH and temperature) as well as food intake.⁵⁹ Going a step further, Liu et al. developed a 3-D-printable living tattoo made from a patch with genetically engineered, living bacterial cells as active material for sensing.⁶⁰

2.3 Contact lenses

Contact lenses are attractive wearables as similar to glasses the user wears it to serve daily needs and tends to forget about their presence after initial insertion and adjustment. Thus, data collection takes place without hampering any daily activities. Yao and later Liao et al. demonstrate a contact lens integrated amperometric glucose biosensor for detection in tear fluid with wireless transmission.^{31,61} Their fully developed system⁶¹ contains an enzymatic glucose biosensor, detecting physiologically relevant glucose levels in tear fluid, together with a potentiostat, a readout unit and a capacitor driven power supply to enable wireless RF-power transmission without the need for batteries or other energy storage units. Transmittance currently is limited to a distance of 15 cm and unfortunately, the authors don't state the performance of their

system for long-term use and no data on electrode fouling or sensor drift are available which obviously must match the wearing time of the contact lenses.

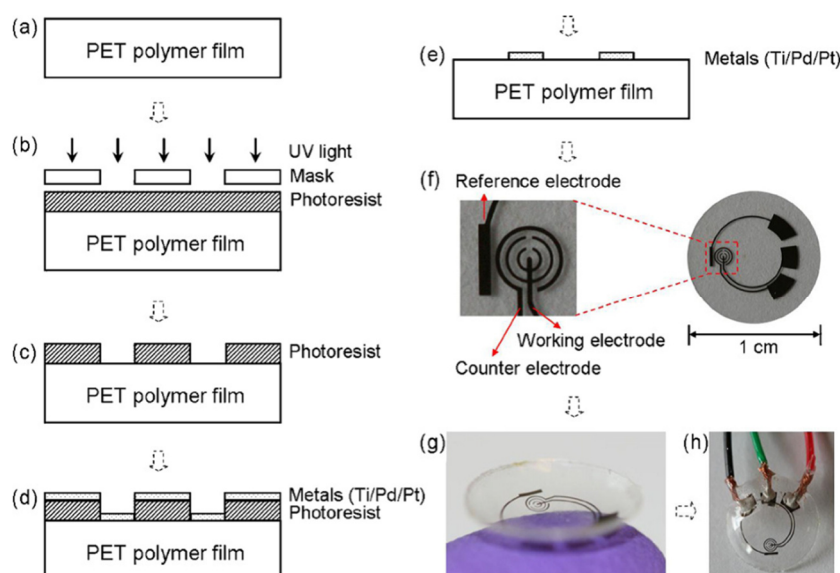


Figure 6. The sensor fabrication process and results: (a) a clean PET substrate is prepared; (b) the substrate is covered by photoresist and exposed to UV light through a mask; (c) the photoresist is developed; (d) thin metal films are evaporated on the sample; (e) after lift-off the metal pattern remains on the surface. After this step, the sensor is cut out of the polymer substrate and heat molded to the contact lens shape and functionalized with enzymes; (f) images of a sensor after it has been cut out of the substrate; (g) image of a completed sensor after molding held on a finger; (h) the sensor may be hardwired for testing. Reprinted with permission from ref ³¹. Copyright © 2011, Elsevier.

Park et al. have shown a different strategy through an inductively wirelessly powered, all-integrated glucose sensing contact lens.⁶² Their approach is different, as the glucose level is directly shown in situ through an embedded LED. This makes their system independent of larger circuits and transmission elements to retain better optical compliance with the eye-vision through the lens.

Typically, contact lenses, glasses, mouth guards and similar accessories are not worn 24/7, so continuous online-monitoring is not possible, which suggests that for these applications, patches or tattoos are more appropriate. If these are combined with systems that trigger an action, the next step toward an IoAT is done. Examples here are

Google's glucose sensor,⁶³ and the concept suggested by Pesl et al.⁶⁴ comprising a real-time insulin bolus calculator and through this giving personalized advice for diabetes patients.

2.4 *In vivo* sensing

The ideal "wearable" biosensor can be an *in-vivo* implanted probe with the sensing element directly exposed to the required biological fluid or tissue and the whole unit being fully incorporated inside the human body. As these sensors are accompanied by an invasive integration process, the realization is complicated and adds to technical issues with those due to medical regulations slowing innovation significantly.^{65,66} Implantable sensors developed are exciting examples of technical innovation though. In recent years various approaches for continuous glucose or lactate monitoring, monitoring of glucose and paracetamol have been shown⁶⁷ or those for single, remote monitoring of ATP or glutamate⁶⁸ or those associated with neurodevices.⁶⁹⁻⁷³ *In-vivo* experiments were done on animal models of rats, rabbits or pigs or the respective tissue models throughout. A few human-implanted trial studies are conducted as well.^{74,75} Medical regulatory approval complying with the European AIMD directive⁷⁶ and public market availability is rare (see: section 6, Senseonics, Inc.). While medical regulatory institutions approved devices such as cardiac implantable electronics (i.e. pacemakers et al.), airway-stimulatory units or neurodevices, no classical biosensors has been approved yet.^{77,78} It may be noted that an older approach for continuous glucose monitoring from the company Medtronic plc⁷⁹ is not a classical *in-vivo* approach as it is connected to an outside monitoring, pumping and supply feed unit.

Expanding the electrochemical sensing approaches to nucleic acids, Arroyo-Currás et al. have published their concept of integrated DNA electrodes for *in vivo* sensing of small molecules (e.g. doxorubicin) in point-of-care applications in rats.⁸⁰ A DNA-probe (aptamer) immobilized on an electrode and modified with a redox marker, will undergo conformational changes upon hybridization with the complementary chemical structure. This change will alter the electrode surface and result in a current change that is directly correlated to the concentration of the sample molecules. Furthermore, the same group has modified their method for a calibration-free sensing principle by using the target concentration dependent lifetime changes of the exponential current

decay with chronoamperometry, enabling even better compliance with demands of *in-vivo* sensing.⁸¹

Also, a dual sensing approach for glucose and lactate has been shown in a piglet model⁸² and a subcutaneous biochip platform, capable of measuring temperature, pH and 5 additional bioelectrodes for further analytes (e.g. suggested: ATP, glutamate or drugs) was presented by Cavallini et al.⁸³ While the latter is not yet comprised of the actual additional sensors, the biochip sets the foundation and its biocompatibility was tested via 30-day *in-vivo* mouse implants, with good host recoveries after that certain time,⁸³ suggesting a compatibility for long-time implants. Thus, the biochip is a good example of a platform capable of bearing multiple *in-vivo* sensing modalities. Taking it one step further, combinations of sensing and medication release elements have been shown as e.g. for glucose sensing combined with NO release, implanted in pigs.⁸⁴

Also some optical approaches have been demonstrated for *in-vivo* sensing. Chien et al. have shown an implanted optical oxygen sensor in an *in-vivo* rat model e.g. for postoperative tissue regeneration studies.⁸⁵ Furthermore, an optofluidic approach for optical stimulation of neural regions and microfluidic drug delivery, for “wireless pharmacology and optogenetics” has been shown by Noh et al.⁸⁶ Their system uses soft microfabricated LEDs with a wireless RF power supply to improve classical fiber-based systems and make the unit independent.

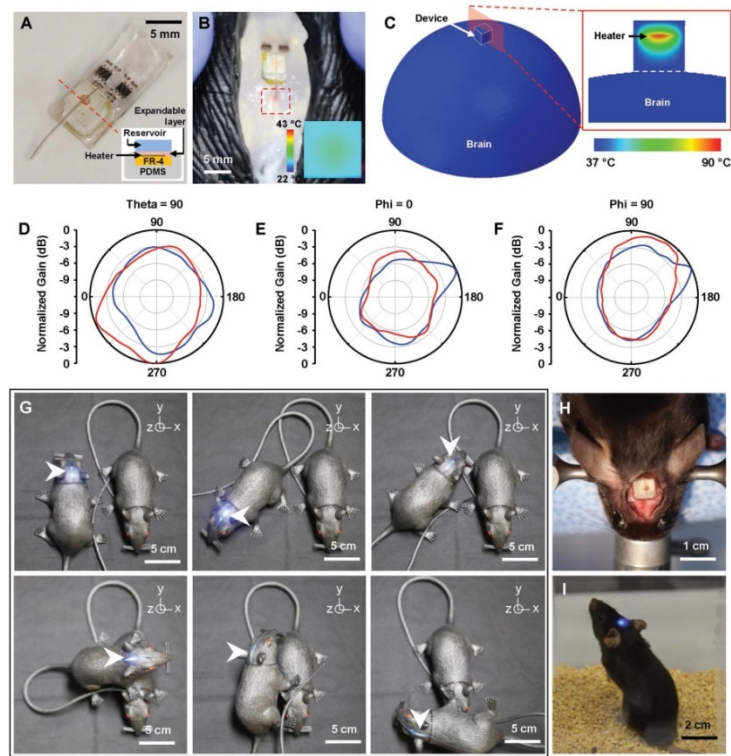


Figure 7. Feasibility study of fully implantable, battery-free, wireless optofluidic systems for operation in freely moving animals. A) Optical image of a wireless optofluidic device encapsulated with 2 mm thick PDMS for thermally safe operation of the heater on brain tissue. The inset shows the crosssectional image of the device, defined by the red dotted line. B) Wireless delivery of red dye into the phantom brain (0.6% agarose gel) in the rat model. The red dotted box indicates the infused dye. IR image in the inset shows surface temperature of the heater's PDMS encapsulant (≈ 30 °C) in ambient environment at room temperature when the heater temperature reaches ≈ 100 °C during fluid delivery, verifying rapid heat dissipation through the PDMS encapsulant. C) FEA modeling of temperature distribution at the surface of the 3D model simulating the device operated on the brain surface (left) and that at the cross-section cut by the red plane (right). D–F) Normalized angular radiation pattern of two-channel antennas in optofluidic systems. Cross-sectional view at D) $\theta = 90^\circ$, where polar angle θ is the angle measured from the zenith direction of the antenna plane, E) $\phi = 0^\circ$, where azimuthal angle ϕ is the angle measured from the orthogonal projection onto the antenna plane from the direction toward the antenna input, and F) $\phi = 90^\circ$. G) Pictures of a model rat implanted with a wireless optofluidic system, demonstrating wireless operation at various angles. H) Optical image showing full implantation of an optofluidic device into a mouse's head. I) Optical image of a freely behaving mouse with an optofluidic device implanted under the skin, on the skull. Reprinted with permission from ref ⁸⁶. Copyright © 2018, Wiley-VCH.

Other optical methods show promise as well. Li et al. and also others presented a nanomaterial technology that can be used for miniaturized, self-powered photodetection systems,⁸⁷⁻⁹⁰ Zobenica demonstrated a more sophisticated opto-electrochemical combination with a footprint of only 15x15 μm^2 .⁹¹ Combination with a nano-sized light sources for illumination might also be possible.⁹² Even eye-implanted, optoelectronics for soft retinal implants⁹³ could be envisioned not only for an eye function supporting mode but also for further sensing applications.

A key factor for successful *in-vivo* sensing is knowledge and control over body reactions to the implant. Size, shape and material of the implants, but also the extent of tissue trauma generated during implantation have major effects on a successful implant.^{94,95} Exemplary from continuous glucose sensing, Wang et al. have shown the possible effects caused by sizes of implants, sizes of needles for implantation and tissue trauma through model implants in rats.⁹⁴ Using histological evaluations, the sizes of generated foreign body capsules and inflammation factors were determined. Former can lead to a reduction of the biosensor functionality, commonly referred to the biofouling effect. Coating with hydrogels (e.g. PLGA/PVA containing dexamethasone)⁹⁶ can limit foreign body reaction (FBR) and thus sustain sensor performance. Furthermore, the rate of initial tissue trauma (caused by size of implantation needles) was found to control the rate of acute inflammation reactions while sensor size was mainly responsible for extents of chronic inflammation and FBR.⁹⁴ Following the authors conclusion, the results stress the importance of (1) miniaturization of the biosensors – “the smaller the better” as well as (2) a need for bioactive, immune suppressive coatings for long-time body acceptance of the foreign elements. Other coating materials could be silicone, or polyurethane.⁹⁷ Furthermore, investigations focus on different materials and techniques used as biofluid-barriers⁹⁸ of implantable devices or biodegradable silicon-based encapsulation layers and electrical interfaces,⁹⁹ e.g. for temporary *in-vivo* sensors, biodegradable conducting inks¹⁰⁰ or degradable supercapacitors for energy storage¹⁰¹.

Protecting the sensor is equally important. In the case of enzyme sensors, enzyme molecule stability is often achieved through the use of protective membrane layers. In the case of DNA-sensors, DNA probe stability must be assured,¹⁰² for which various approaches have been suggested, such as creating different DNA nanostructures¹⁰³⁻¹⁰⁵ – origami-like¹⁰⁶ or else,¹⁰⁷ by chemically end-sealing the DNA probes^{108,109} or using

locked nucleic acids (LNA's)¹¹⁰ as probes. Further probe designs for electrochemical-DNA-based biosensing have been shown by Zhang et al.¹¹¹

Also allergic potential or skin irritations especially upon medium and long-term use are of immediate concern. An overview of requirements with transdermal patches has been published by Pastore et al.¹¹² which must be matched with materials needed for sensing and wireless data transmission. Miyamoto et al. have shown an interesting approach of directly skin-worn electronics as nanomeshes, that are stable for at least one week constant wearing and according to the authors are better skin-compatible and reduce itching or similar effects due to their breathability.¹¹³

Finally, patient safety is a most important issue for *in-vivo* sensors, as invasive methods are needed for implantation and health effects caused by the implant have to be avoided.¹¹⁴ Automated insertion or extraction devices for implantable biosensors have been addressed as a patent recently.¹¹⁵ Wireless solutions for control and data transfer to the IoAT are mandatory which ties research for in vivo sensing direction to research towards wireless integratable potentiostats¹¹⁶ or data transfer systems.¹¹⁷

2.5 Sensing enhancement through microfluidic strategies

In point-of-care sensing, DNA-based detection systems play an important role.^{118,119} However, the inherent need of sample preparation, i.e. obtaining access to intracellular nucleic acid molecules and often amplifying those through a molecular biological reaction, currently prevents their application as a wearable device. Hsieh et al. have shown a promising solution.¹²⁰ The authors used the concept of before mentioned *in-vivo* aptamer electrode⁸⁰ in a lab-on-a-chip together with microfluidic sample preparation and DNA amplification steps and demonstrated almost on-line detection of pathogens (influenza virus from throat swabs or bacterial strains from mouse blood).

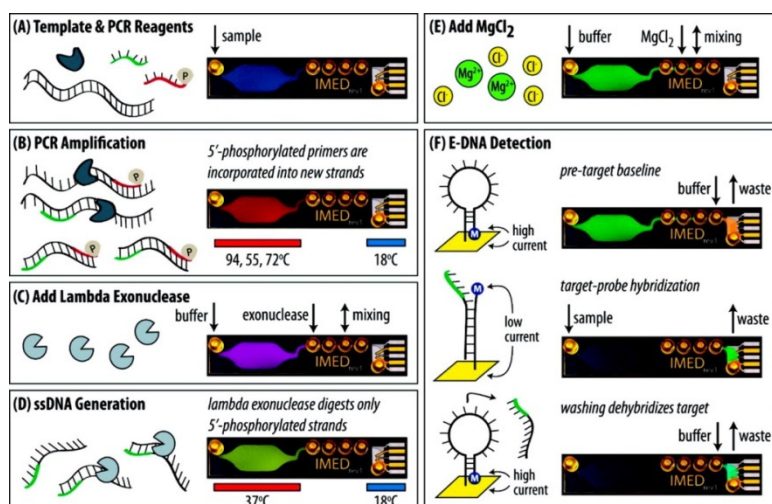


Figure 8. IMED assay overview. (A) Template DNA is added to a PCR reagent mixture containing phosphorylated reverse primers and (B) PCR amplified. (C) Lambda exonuclease is mixed with the product and (D) digests the phosphorylated strands. (E) $MgCl_2$ is added to optimize hybridization conditions. (F) Before introducing the sample, baseline sensor redox current is measured. Next, the single-stranded DNA product hybridizes with the E-DNA probe, modulating the redox current signal. Finally, the E-DNA probe is regenerated to verify target hybridization. Reprinted with permission from ref ¹²¹. Copyright © 2009, American Chemical Society.

Clearly, this concept is still far from use as a wearable or *in vivo* sensor, but it points the way toward body-integrated DNA sensors, from which especially pathogen detection at the point-of-need would benefit.

In general, microfluidic approaches (in polymers or in paper) are promising as they enable more sophisticated on-skin testing. An interesting sampling approach was shown by Ranamukhaarachchi et al. where a hollow microneedle draws minute accurate sample volumes using optofluidics. It could be employed for wearable, therapeutic drug monitoring in the future.¹²² Other, less sophisticated approaches use capillary-driven sweat flow.¹²³ The concept of microneedles is an *in-situ* sensing approach but lends itself as well for sampling by implanted *in vivo* sensors for future developments. Current examples include the detection of alcohol,¹²⁴ nerve agents,¹²⁵ generally enzyme-linked assays¹²⁶ and classical glucose monitoring or combined with transdermal drug delivery.^{127,128}

2.6 Progress needed for IoAT in wearable point-of-care biosensors

The many examples of sophisticated biosensors integrated for wearable detection demonstrates that analytical chemistry is ready for the IoAT. Sensing is feasible, signal readout and transmission has been accomplished via RF or Bluetooth or cell-phone recordings, and wireless transmission can easily be integrated. In fact, Kang et al.¹²⁹ just demonstrated immense progress in the miniaturization of inductors, which removes limits in generation of ultra-small wireless communication systems as possible bottleneck.

Aside from the development of (bio)sensors for more and more difficult analytes, attention is needed to provide sufficient power for this level of sensing and its associated data transmission. Batteries are not an ideal solution due to a need for frequent changes, waste generation, additional weight and wearability issues related to safety albeit LOC device development pushes this area forward as well.¹³⁰ Solar-power is only possible under sufficient light-conditions and wouldn't allow for 24/7 monitoring. Hence, much effort is undertaken on the improvement and adaptation of rechargeable batteries¹³¹ or as Zamarayeva and colleagues have shown, with their combination of safe & stretchable batteries and solar cells for recharging.¹³² Also new power-generation solutions such as via nanogenerators through small mechanical movements (blinking eyes,¹³³ muscle movements^{134,135}), power enhancement strategies¹³⁶ and even *in-vivo* generators^{137,138} are of great interest to amend the power-production strategy of wearable sensors.

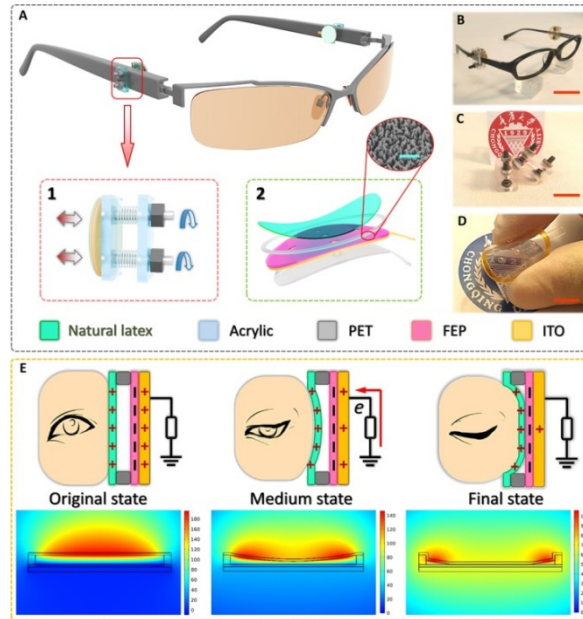


Figure 9. Structure, and working mechanism of the msTENG. (A) Schematic structure of a pair of ordinary glasses mounted with msTENG. Bottom left: Structure of the fixing device for convenient adjustment. Bottom right: Schematic diagram of the msTENG. Inset: An SEM image of FEP nanowires. Scale bar, 5 μm. (B) Photograph of an ordinary glasses mounted with an as-fabricated msTENG. Scale bar, 2 cm. (C and D) Photographs of the simple fixator (C) and the flexible and transparent msTENG (D). Scale bars, 1 cm. (E) Schematics of the operating principle of msTENG. Top: Charge behavior when the eye is at different states during the blinking process. Bottom: Potential simulation by COMSOL to elucidate the working principle. Reprinted with permission from ref ¹³³. Copyright © 2017, AAAS.

In fact, Wang et al. demonstrated a triboelectric generator¹³⁹ harvesting energy through a skin-like structure by employing a cell layer with physiological saline as transduction and electrode layer together with a silicone rubber layer as triboelectric element. The device can withstand a very high amount of strain of 600%, which makes it very versatile. Furthermore, Fan et al. have investigated the different dynamics of wearable energy harvesting devices (in solar or thermoelectric working modes),¹⁴⁰ providing deeper insights and allowing for better design of future models. Other solutions have been presented by Wen et al. with a composite textile-based solar-cell, nanogenerator and supercapacitor combination¹⁴¹ or Lui et al., with a very low power consuming wearable device and microwave-based, 2m range wireless power transmission to the sensor¹⁴² or Sanni et al. from the same group using induction and ultrasonic transmission for deep tissue implanted devices.¹⁴³ Both variants are interesting for applications requiring low-frequency read-out and those with low-power

requiring sensing systems. They provide the possibility to have an easily exchangeable battery system decoupled from the sensing element. In a very different approach, Pang et al. developed a textile integrated biobattery using *Pseudomonas aeruginosa* as catalysts which can produce up to $6.4 \mu\text{W}/\text{cm}^2$ usable energy.¹⁴⁴ This might be a small value compared to the energy storage of today's Li-ion battery cells,¹⁴⁵ however, power delivery is permanently available. Though health concerns with *Pseudomonas* species may arise¹⁴⁶ with direct contact to the skin, the idea of microbial fuel cells¹⁴⁴ as self-sustaining and robust system is an interesting alternative as energy source for body-wearable sensors and much research is being done in this area including genetic engineering of better microbial systems.^{147,148} A further overview of possible energy harvesting mechanisms is discussed by Shaikh et al. in their review.¹⁴⁹

Misra et al. have presented recent advances regarding the area of energy harvest, storage, low power consumption sensing and transmitting elements,¹⁵⁰ emphasizing the importance of low-power consumption strategies also for data processing and on-sensor controls.¹⁵¹ The power consumption of today's low energy Bluetooth solutions is in the range of microwatts (e.g. $33 \mu\text{W}$, 120 second supply intervals)¹⁵² and also the power supply of wearable power supply systems mostly lies in the low microwatt regime^{135,137} up to greater power values,¹⁵³ aside from yet still rare exceptions as shown by Wang et al.¹⁵⁴ Thus, the provision of power and the demands are approximately on the same level but still not sufficient in all cases, requiring further advances and fit-to-application technology choices.

As the true power of IoAT comes into play when thousands, millions of sensors are connected, standardized communication protocols and methods are needed, a collective basis should be found and few methods established for successful future market-ready products (to avoid situations such as the USB standards in cell phone charging we face today). This will ensure that new generations of sensors can easily be connected to the network and data analyses can expand from individuals to entire populations. Data sets must be presented in normed formats a seemingly simple request that yet at this point is far from being reached albeit attempts by groups of scientists such as the Allotrope Foundation.¹⁵⁵ Similarly, special considerations regarding the design and layout of sensors have to be kept in mind with implications on their performance as highlighted by Sohbaty and Toumazou exemplary for ISFET CMOS sensors.¹⁵⁶ The same is true for data transmission. Jackets with radiation-protecting

pouches must be avoided increasing people's exposure to electric smog. Hertleer et al.¹⁵⁷ describe instead a foam-based, clothing-integrated antenna for signal transduction. Also the placement of sensing patches on the body must be carefully studied. Murphy et al. showed that heart beating can affect miniaturized, body-integrated antennas and detune with time¹⁵⁸ Thus, antennas have to be placed carefully or interference independent transmission bandwidths must be chosen.

The obvious next step is for sensing data to trigger action without the need of human decision making. Good examples are the combination of glucose sensors with insulin dispense units,¹⁵⁹ pacemakers,⁷⁷ antibiotics release devices,¹⁶⁰ warning and alert routines,¹⁶¹ preclinical diagnosis-to-cure pathways,¹⁶² and will expand to the integration with smart-home applications for sports or preventative medical nutrition plans and many more. In Table 2 challenges inherent to analytical methods designed for automatic and remote sensing are listed together with proposed solutions where already available.

Category	Challenges	Possible solutions	Refs.
Long-term stability	Fragility of biorecognition element, fouling, aging, replacement cycles for <i>in-vivo</i> sensors	Bioactive coatings, preventing fouling, membranes	163-175
Calibration	Sensor drift	Calibration-free sensors, self-calibration (orthogonal approaches), AI-based control	176-178
Multi-element sensors	Same, uniform calibration over all distributed sensing elements	Network-linked matching and algorithm-based compensation	-
Portable solutions	Robust energy supply	Body energy harvesting or batteries	-
Wireless connection	Unified communication standards (WiFi, RFID, Bluetooth)	Implementation of interoperability and agreed-upon standards	-
Wireless protocols	NFC& range, Bluetooth& power consumption and multiplexing	Choice for each application, improvement of capabilities	-
Substrate/sensor material choice	Geometrical compatibility, flexibility, stretchability, curvature resistance, stress-strain withstanding to prevent high-noise ratios and bad sensing element/analyte matrix contacts	Flexible polymers as e.g. Ecoflex silicone or parylene	179,180
Bio-compatibility	Immune and FBR reactions, allergic potential, skin irritation	Choice of materials and design, e.g. nanomeshes	112,113
Common influencing factors	Seasoning, shelf-life, environmental conditions	Guarantee stability, sensor concept design with stable components	-
Personal variations	Food preferences, age, body status	Training on large test groups with AI based matching	-

Table 2. Challenges and areas requiring progress in wearables & POC sensing.

2.7 Safety and security considerations

Safety and security considerations will not be addressed in this article as these expand into important and broad discussions of individual rights, protection of personal information, cybercrime etc. Possible malicious use¹⁸¹ is easily foreseeable and a rise throughout the next years in cybercrime activities is already predicted.¹⁸² However, it should be pointed out that extensive research is done towards the protection of infrastructure elements¹⁸³⁻¹⁸⁶ and towards IoT-based systems.¹⁸⁷

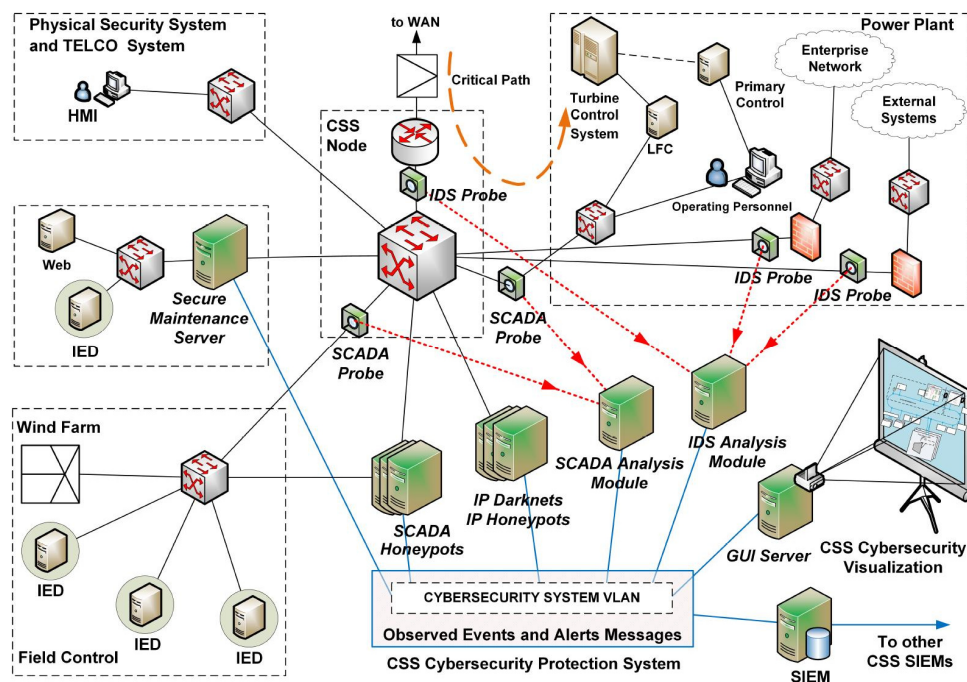


Figure 10. Power grid control system and the designed cybersecurity protection system. Reprinted with permission from ref ¹⁸⁶. Copyright © 2017, Elsevier.

As a solution for the herein described body sensors or wearables, investigations towards safe authentication protocols for body sensor networks have been done by Wu et al.¹⁸⁸ Also for implantable medical devices, these considerations are especially important.¹⁸⁹

While today most people seem to be physically linked to their cell phone, direct exposure of the human body to unknown doses of electromagnetic fields and irradiation caused by the wireless transmission techniques in very close proximity to the body or even inside the body must be considered by the scientific community for the IoAT. Here, Lecoutere et al. have introduced a possibility to monitor the individual exposures¹⁹⁰ and deduce possible health effects from that data in a later step.

3. Sensor solutions for agriculture, food and environmental sensing

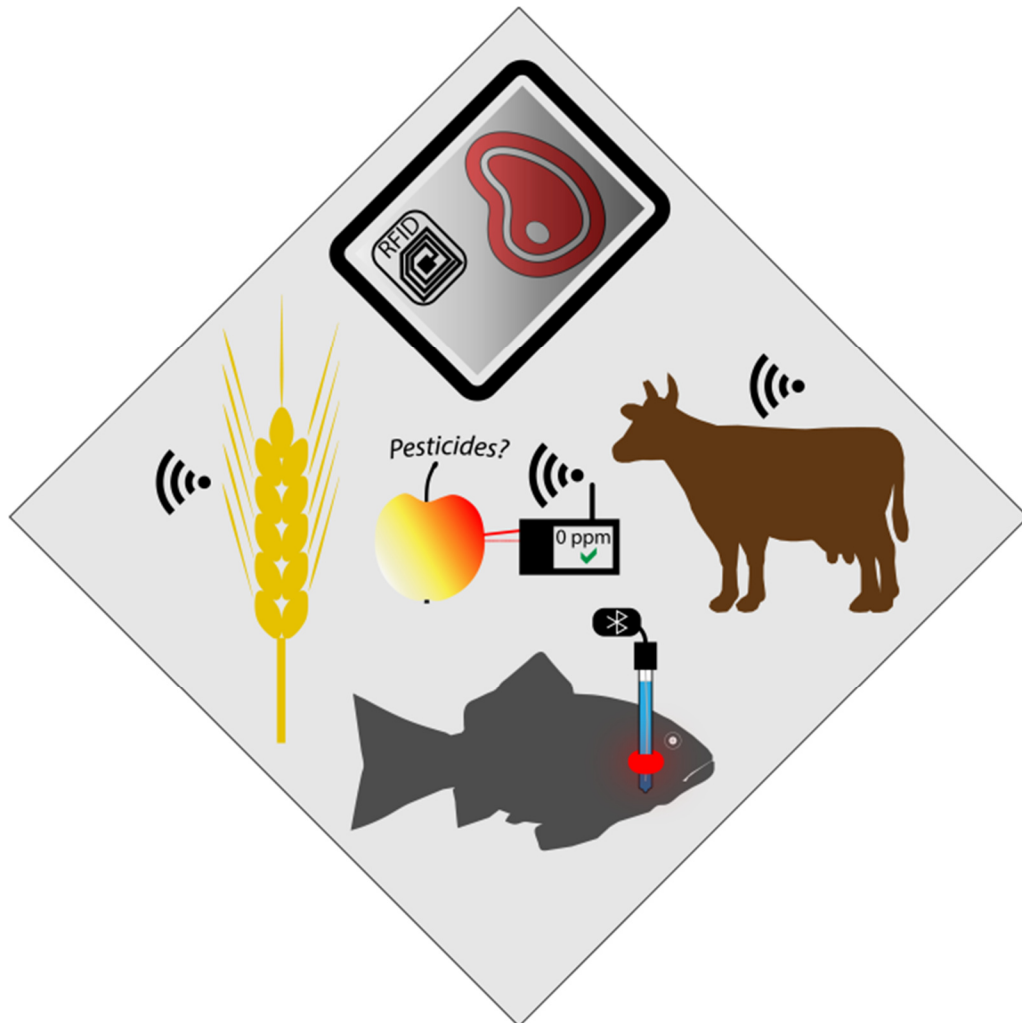


Figure 11. Sensor applications in agriculture and food sensing.



Figure 12. Sensor needs for environmental sensing.

Sensor systems, requirements and solutions to deal with analytical challenges surrounding agriculture, food and the environment are met with similar technological requirements, complexities and challenges and are more often than not intertwined especially when considering the IoAT. Sensing from farm-to-fork, for personalized food, ensuring food safety, protecting crop from pests and dramatic climate events play hand-in-hand and require sensing capabilities at all stages of the supply chain similar to the just-in-time principle of industrial production. We present here only a few examples of this vast research field (Table 4). The first examples of environmental monitoring require label-free techniques for long-term online sensing capabilities, whereas the last examples of packaged food sensing can be solved by single-use sensors and with an endpoint result (e.g. food is not fresh). In contrast to the point-of-care and *in vivo* sensors, power supply demands are mostly not an issue here, yet ruggedness and functionality over a large range of scales are major challenges. Hence, the inexpensive

and rugged chemo/physicosensors used in environmental settings are typically accompanied by computational techniques to ensure selectivity and accuracy. Information related to regional monitoring and towards foresighted predictions is generated in environmental monitoring,¹⁹¹⁻¹⁹⁴ for soil quality determination in agriculture¹⁹⁵ and predictive pollution locating¹⁹⁶. Kelly et al. demonstrated that the same can be used on a small scale, e.g. for home-monitoring in single houses or living environments.¹⁹⁷ While their platform contains only simple sensors for temperatures and light intensity, it can be expanded towards other analytes (gas sensing, etc.) for smart home monitoring and control. Further insights into suitable hardware programming for signal processing, data formatting for transmission or an interface for data review - all intended for a wireless building monitoring solution are shown by Jang et al.¹⁹⁸

Category	Keyword	Sensing principle	Analyte	Refs.
Global climate and agriculture	Climate	Birds, GPS, ISFET	Humidity, pH, pressure	199-204
Local environmental and urban monitoring	Gas sensing, Mobile& stationary	EC, optical (drones)	T, humidity, BTX gas, H ₂ S, H ₂ , NO _x , NH ₃ , CO, microbial analysis, water flow, contaminants	197,205-216
Local agriculture	Precision farming, soil sensing, harvest size	EC, optical (drones)	Cl ⁻ , image-based, water-transport,	217-226
Livestock monitoring	Wearables, in-vivo	EC, acoustic, probes	Cholesterol, herd monitoring/grazing, T, estrus cycle	227-232
Processed & packaged food	Freshness,	Optical, EC, FET, MOX	T, humidity, cadaverine, biogenic amines, gas, Ethanol	233-246

Table 3. Environmental and Food sensing solutions.

3.1 Global climate and large-scale agriculture monitoring

Agriculture relies on regional and global climate conditions and the natural ecosystem, hence large-scale environmental monitoring is an invaluable tool for modern agriculture. New sensor concepts can augment traditional and modern climate prediction strategies and expand much beyond even drones to taking advantage of naturally occurring globetrotters. Mandel et al. and later Gumus et al.^{199,200} have presented different sensors related to bird research.

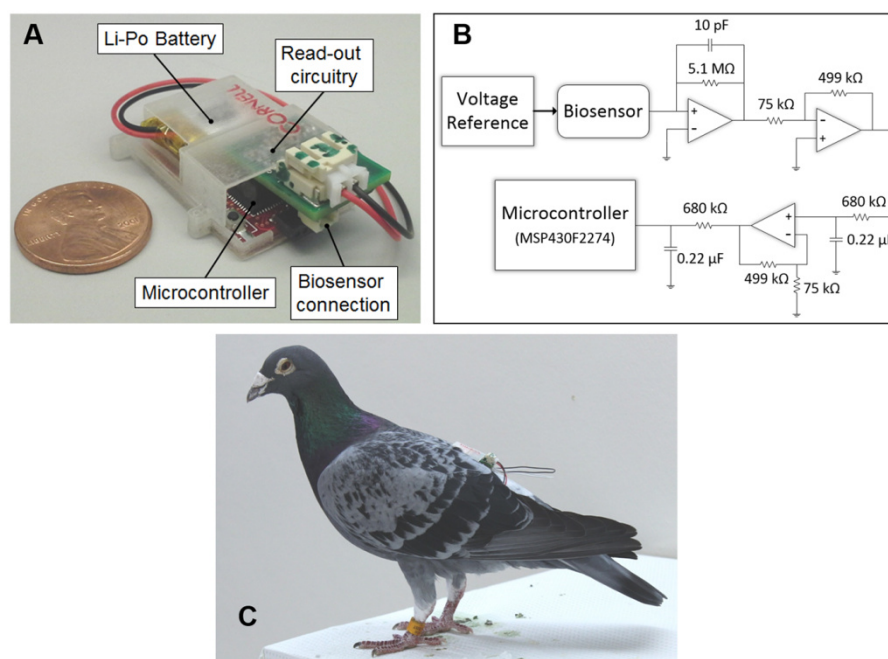


Figure 13. A) The system consists of microcontroller, read-out circuitry, high capacity lithium polymer battery, and needle-type uric acid biosensor. B) Two-electrode potentiostat system for driving the biosensor and collecting the data. C) A pigeon with Lab-on-a-Bird system installed. The entire system weighs approximately 6.5 g, which is well under 4% of an average pigeon's weight and allows for long-term tag-attachment without limiting their motion. Reprinted with permission from ref ²⁰⁰. Copyright © 2015 Public Library of Science under the creative commons CC-BY license.

A first version represented GPS modules mounted on birds¹⁹⁹ to study their migratory paths to then inventing a "lab-on-a-bird"²⁰⁰ monitoring physiological conditions during the birds' flight. Although these sensors are not used for climate monitoring, this concept is a promising avenue for regional or global climate data acquisition combined

with already existing wearable sensors for e.g. monitoring atmospheric pressure, adapted from wearable body position detection²⁰¹ or sensors capable of monitoring humidity, adapted from a gum-strain sensor²⁰² or small scale humidity responsive materials.²⁰³ If these are combined to a yet-fictional “bird-sensor-networks” with wireless communication and automated transmission to distributed ground stations, a live forecast could be possible – birds replacing drones. Then, even better conclusions about local or larger weather changes can be drawn. Also farming can benefit through even more precise and in-time weather forecasts considering the weather’s very different but intense regional implications. A further good example of a new class of global sensor networks for environmental monitoring with a large impact on whole ecosystem processes is the pH sensing device presented by Johnson et al.²⁰⁴ Their self-calibrating, pressure tolerant - and therefore depth adapting pH monitoring ISFET sensor could be used for a very sensitive, global ocean pH monitoring network from surface to large depths, drawing important data for water ecology and ocean-life insights.

3.2 Local environmental and urban area monitoring

For local-scale environmental monitoring, stationary and hence more traditional bio/chemo/physico sensors are easily applicable. In general, for atmospheric or gas sensing humidity/temperature effects and cross-sensitivities to other gases are major challenges. As chemoresistor-based gas sensors share a relative unspecific response characteristic²⁰⁵ various approaches have been suggested to address selectivity.²⁰⁵⁻²⁰⁷ In computational approaches a neural network of sensors can be trained on gas mixtures (see Chiesa et al discussed below) and result in highly selective sensor responses. Otherwise, specific single sensors can be used, such as the miniaturized toxic gas sensing platform with wireless (NFC) powering and data collection by Ishihara et al. They sense electrophilic gaseous molecules with a combination of wrapped SWCNTs and metallic-supramolecular polymers through conductivity changes.²⁰⁹ Im et al. have shown a potentiometric approach for BTX gas sensing for on-field usage.²⁰⁸ Fahad et al. presented a room temperature, multi gas sensing platform on the basis of a modified nanoscale-silicon field-effect transistor.²¹⁰

Chiesa et al. have published 2012 their results on an ammonia gas sensor system, allowing for area monitoring of urban pollution on the scale of a small city.²⁰⁵ They use

a carbon-nanotube based chemresistor gas sensor to monitor ammonia in environmentally relevant concentrations to supervise urban pollution arising from vehicle emissions. The inherent inability to be specific toward just one analyte was overcome by using a fuzzy logic-based algorithm that trained a neural network system and was able to distinguish analyte from interfering signals (NO_x and ozone). Ceramic was chosen as substrate for a rugged system, being stable under outdoor conditions resulting in overall low manufacturing and operational costs.²⁰⁵ This combination of a chemosensor with data interpretation using machine learning like algorithms points toward future IoAT applicability, i.e. sensors connected wirelessly linked to a central data analysis unit. Furthermore, data analysis units on each single sensor can be combined, sensors communicate with each other yielding a very detailed mapping of urban air pollution on a short timescale. These results can then be used to trigger automatic alarm systems at a specific rate or to actively regulate traffic flow with new automated driving settings or implement bans on driving when public health is endangered. A similar study was conducted in city parts of Cambridge, UK, with an electrochemical sensor network for CO, NO and NO_2 .²¹¹

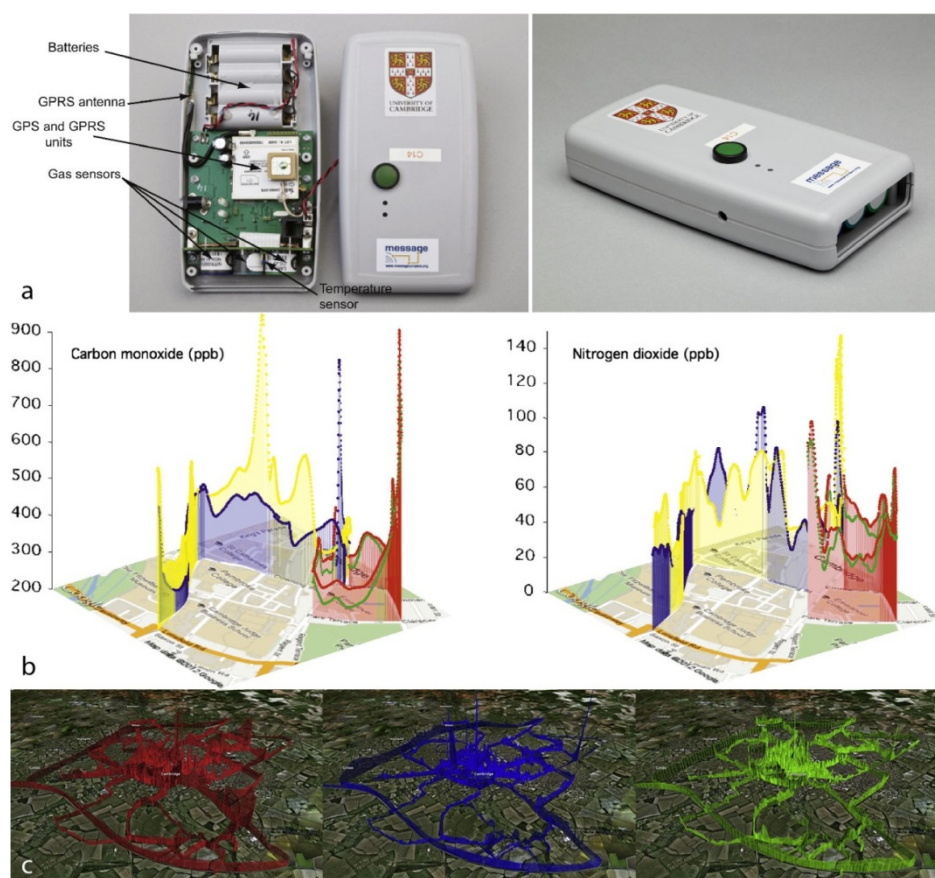


Figure 14 (a-c). a) Mobile sensor unit incorporating three electrochemical sensors (for CO, NO and NO₂ in this case). Various components (GPS/GPRS, batteries etc.) are identified in the left panel. For clarity, the unit is shown without its protective wire mesh, which, during operation, is located in front of the sensors. b) Selected CO and NO₂ measurements from two sensor nodes in parts of central Cambridge superposed on a road map (map data© 2012 Google). Data from periods during which volunteers walked together are shown in red and green, and those from when they walked apart are shown in yellow and blue. NO₂ data not corrected for interference with O₃ (see Section 3.3 in corresponding reference). c) 3D plots (left to right respectively) of CO, NO and NO₂ mixing ratios giving overviews of measurements obtained during a large, mobile sensor deployment. The peak heights correspond to mixing ratio, with maximum values of 7 ppm, 4.5 ppm and 840 ppb for CO, NO and NO₂ respectively (map data© 2012 Google and© 2012 Infoterra Ltd & Bluesky. Reprinted with permission from ref ²¹¹. Copyright © 2013, Elsevier.

A comprehensive overview of sensing in urban area environments for smart cities, was presented by Hancke et al.²¹² Broday et al. have also highlighted remaining issues and necessary improvements towards a densely stacked, accurate pollution prediction in urban environments.²¹³ Capolupo et al. have presented a drone-based approach, together with predictive modeling to evaluate contamination of soils.²¹⁶ Finally, approaches like those from IBM, receiving a patent for a drone-based microbial analysis system for area monitoring towards possible contamination²¹⁴ or a system for hydrological evaluation of surface water flows presented by Tauro et al.²¹⁵ underline the possibilities for sensing from a hazmat or natural disaster protection perspective.

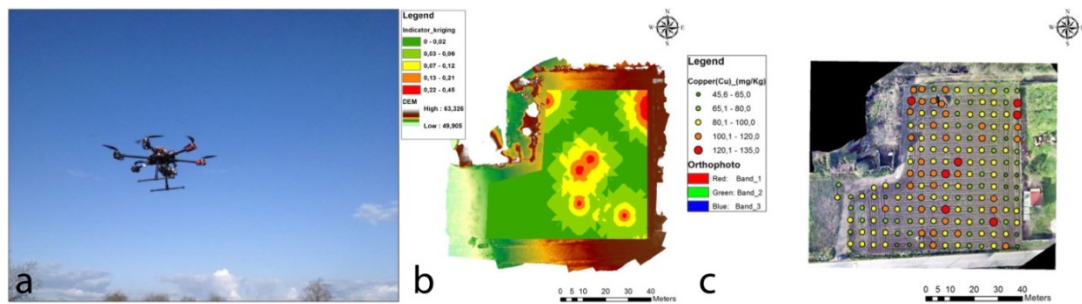


Figure 15 (a-c). a) The drone Tarot FY690s equipped with all hardware components and software tools. b) Map of copper concentration interpolated with Indicator Kriging. c) Copper concentration classes (in mg/kg) over the obtained orthophoto map. Reprinted with permission from ref ²¹⁶. Copyright © 2015, Elsevier.

3.3 Local agriculture monitoring

Precision farming refers to the high-resolution spatial monitoring of soil, crop and plant needs^{247,248} as well as harvest yield prediction. Here, mainly “above ground sensing” is used and efforts are made for connected, wireless networks of sensors in the farming area, reviewed nicely by Ohja et al.²¹⁷ Next steps are IoT-like machine systems, driverless tractors^{218,219} and research towards intelligent farming robot swarms.²²⁰



Figure 16. Precision farming in modern agriculture, exemplary in harvest and fertilization control and monitoring. Reprinted with permission from CLAAS. Copyright © CLAAS.

In-soil sensing is of equal importance for crop production, which is addressed by Harris et al. through a sensor system to be distributed in soil.²²¹ Screen-printed potentiometric electrodes are used in distributed networks to obtain a spatially resolved chloride monitoring. This enables the measurement and automated supervision of soil salinity for irrigation cultures, as their sensors transmit information wirelessly and are extended into a network. While the authors tested only distances of sensors of maximally 30 cm –expansion to larger area networks can easily be achieved, and is now already suitable for greenhouse applications. Furthermore, expanding from chloride ion monitoring to other essential soil nutrient ions²⁴⁹ like nitrate, ammonium, phosphate or potassium, a detailed picture of soil nutrient availability and distribution can be drawn. It is just a matter of time until the “above ground” and the “in-soil” sensing systems are combined for precision agriculture enabled through the IoAT. Also drone supported monitoring solutions gain in importance such as for crop quality and needs evaluation,^{222,223} early-stage highly resolved treatment necessity detection²²⁴ or harvest size prediction.²²⁵

A third line of research studies investigates plant sensing to obtain information about climate and soil effects on the crop itself. Oren et al. developed graphene-based plant-

leaf “wearable” sensor films to monitor the water transport process and timescale²²⁶ and hence provide information for irrigation or nutrient needs on a single plant scale. Demands on such sensors are high with respect to energy supply (e.g. small, flexible photovoltaics²⁵⁰), ruggedness, small sizing, and the tolerance of weather, mechanical and plant-growth strains.

3.4 Livestock monitoring

Health and nutritional status of individual animals in the livestock could easily be monitored taking the examples of wearable and implantable sensors described in chapter 1. *In vivo* monitoring connected to a network through an IoAT can assist in the management of large production animals by maximizing health and minimizing antibiotic distribution just as precaution measure.²⁵¹⁻²⁵³. A relevant example is the concept of Takase et al. who developed a wireless biosensor system mounted on live fish to monitor their cholesterol concentration, which is an indicator for is immunity level and hence correlates directly to the physiological condition.²²⁷

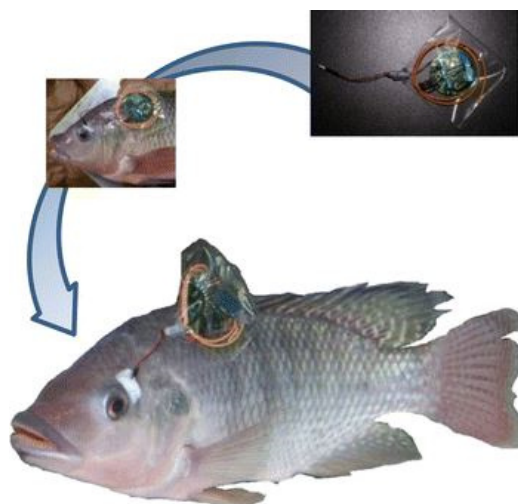


Figure 17. Picture of Nile tilapia (*O. niloticus*) with wireless monitoring system. Reprinted with permission from ref ²²⁷. Copyright © 2014, Springer Nature.

The sensor is a typical electrochemical enzyme electrode comprised of Nafion® protective layer and a chitosan layer containing enzymes and a mediator. The electrode is connected to a miniaturized potentiostat and a coiled wire for wireless transmission in the radio frequency band. The cholesterol concentration in a live fish was monitored for 48h continuously, which is a first step toward long-term and life-phase monitoring. Currently, more research, towards practical sensor solutions or suited calculation

algorithms (e.g. for grazing behavior)²²⁸ is done for monitoring²²⁹ and sensing with large herds of livestock²³⁰ or farm animals and WSN's²³¹ even in very remotely located, nomadic Mongolian farming.²³² Finally, this setting requires capabilities for very large sensing networks that incorporate many single entities.²⁵⁴

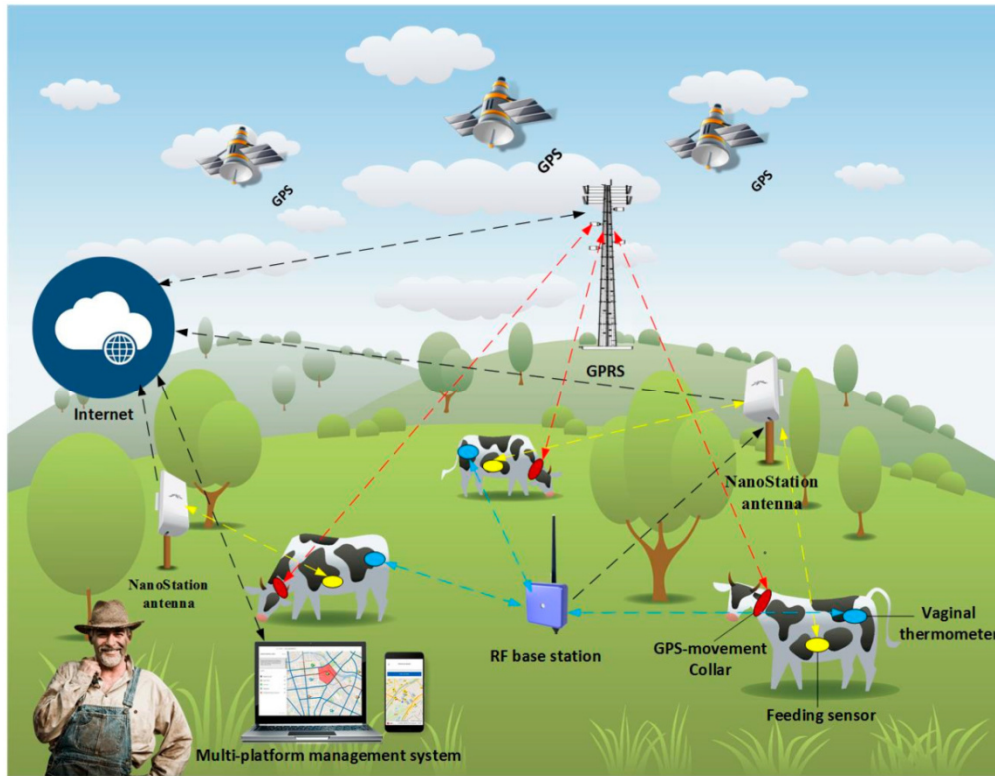


Figure 18. Infrastructure from the proposed system of a combination of multi-agent systems and wireless sensor networks for cattle monitoring. Reprinted with permission from ref ²³¹. Copyright © 2018, under the creative commons CC-BY 4.0 license.

3.5 Sensing for processed and packaged food

Sensing the freshness and safety of food prior and post processing, during storage and transport as well as prior to reaching the end-user requires highly controlled conditions. Temperature and humidity sensing is well-established and is a straightforward example for the IoAT. Not only larger container loads, but small crates of products and single-packages of processed food can be automatically assessed with respect to their freshness through integrated sensors. Le et al. for example used a wireless sensor (temperature and humidity) for freshness monitoring of packaged vegetables.²³³ They integrated two passive radio frequency identification (RFID) sensor tags so that no internal energy supply is needed. Instead, energy required for sending is provided by

the RFID reader wirelessly through an electromagnetic field with a range of 30 cm. Much research is undertaken currently to expand this concept to rather directly determine the freshness and or safety of the packaged food. Early work demonstrated optical detection principles in microtiter plates, then progressed to test strips and films which integratable in food packaging as simple sensor with visual read-out,²³⁴⁻²³⁶ or through monitoring camera set-ups.²³⁷ Similar approaches for reversible colorimetric amine, ammonia or other small molecule detection have been presented as well.²³⁸⁻²⁴⁰ Electrochemical miniaturized sensors include a nanosensor for food freshness detection by Yang et al.²⁴¹ Their sensor is a combination of a carbon nanotube field effect transistor grid with receptor nanodisc structures, being sensitive for cadaverine as food spoilage marker, i.e. binding of the biogenic amine results in an easily detectable conductance change. Liu et al. use chemoresistive sensors capable of the detection of biogenic amines as a sum parameter arising during meat or fish spoilage.²⁴² This sensor could be combined either with above described platform with RFID tags or another NFC based platform with smartphone readout, that has been published by the same group.²⁴³ The latter uses simple, already market-available NFC tags that are manipulated to include chemosensors for gas sensing. Other efforts to the development of amine sensing in food packaging have been made from the industrial side²⁵⁵ or shown in patents.²⁴⁴



Figure 19. Freshness indicator sensing spot on packaged meat showing the food status. Reprinted with permission from ref ²³⁶. Copyright © 2014, Elsevier.

Finally, in another approach, Abad et al. integrated a gas sensor into RFID tags for food packaging.²⁴⁵ They combined a physical (humidity, temperature and light) and one chemical gas sensor (MOX) together with memory and energy storage units on a flexible substrate (Kapton®). The authors focus in this publication on the fabrication methods and production of the tags and don't demonstrate actual food sensing yet. It is

possible though to imagine the expansion of their concept with other sensor technologies such as gas sensors described further above or Sharma's et al. "electronic nose" which is based on the combination of rotational spectroscopy with a wireless EF CMOS transmitter for human breath ethanol detection²⁴⁶ which could be modified to food freshness monitoring.

In Table 5, challenges inherent to analytical methods designed for sensing across the farm-to-fork value chain are listed together with possible solutions.

Category	Challenges	Possible solutions
Cost	Low profit margins	Inexpensive sensors, single-use
Ruggedness	Environmental & agricultural settings require ruggedness	Design of sensors in accordance to that
Supply& maintenance	Human efforts with large-scale distributed sensors	Inventory of reagents, low miniaturization needs, drones for maintenance

Table 5. Remaining challenges for Food& Environmental sensing.

4. Lab-based solutions for the IoAT

Obviously, the whole range of Analytical Chemistry can be used in order to provide data for the IoAT if a full-scale analytical laboratory is available. However, for the IoAT concept, choosing a few key technologies that can be fully automated and integrated into an IoT is a more desirable approach. We propose that mass spectrometry and next generation sequencing represent two key technologies that have the future potential to together provide analytical information on nearly any analyte of interest (as long as the sample can be brought to the devices). First steps are demonstrated in industrial process monitoring. Analytical techniques from sensors (e.g. ultrasonic sensing, conductometry, resonators, optical spectroscopy, photoacoustics) to MS are used in this field already¹² indicating that the development towards IoT is more focused on the IT side, artificial intelligence, and data treatment.. An interesting common challenge is the transfer of process data into a larger value chain. It should be noted that we are not reviewing latest developments in the detection capabilities of MS and NGS technologies. Instead, we focus on trends indicating their readiness for IoAT applications.

4.1 Mass spectrometry for the IoAT

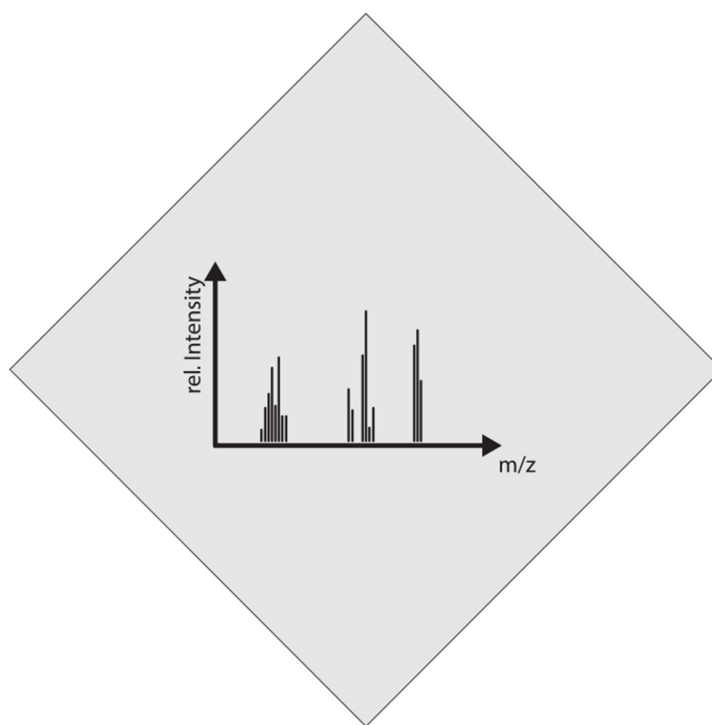


Figure 20. Mass Spectrometry for the IoAT.

Mass spectrometry and its combination in hyphenated technologies (LC/MS, GC/MS, ICP-MS etc.) is an immensely versatile detection technology. Current research efforts seek to ever expand the range of analytes, lower the limits of detection, increase its ability to cope with matrix effects (especially through combinations with separation technologies), and develop strategies for automated interpretation of spectra even in highly complex applications such as in proteomics, clinical biomarker research,^{256,257} geochemistry,²⁵⁸ and more recently for environmental samples^{259,260} and other applications.²⁶¹⁻²⁶⁴ In its full range and best capabilities it will remain a lab-based sophisticated detection technology for the foreseeable future, requiring thorough calibration with standards when used quantitatively and separation techniques when used with “real world samples”. Yet, portable solutions are under intense and creative investigations, which will better prepare MS-analysis for the IoAT, as costs will decrease, automation increase and hence make integration into a network of things feasible. For example, Frandsen et al. presented a “miniaturized” MS device already in 2007 weighing 10 kg²⁶⁵, 908 Devices Inc. demonstrated a 2 kg device in 2014. Wright et al. realized a truly miniaturized ion optics part for a triple-quadrupol MS in 2015 (albeit

the device still needs support parts, namely vacuum and turbomolecular pumps, a control pc and an electrospray emitter).²⁶⁶ The device could detect a sample analyte from food in relevant concentrations. Blakeman et al. have eliminated these needs by constructing a high pressure mass spectrometer (HPMS), not only allowing for atmospheric pressure ionization (API),²⁶⁷ but also mass analysis is performed at higher pressure.²⁶⁸ Therefore, no turbopumps for ionization are needed anymore, enabling even smaller sizes and weights. Such a portable MS device for a predetermined set of analytes, available in a spectral database or accessible via cloud integration, is perfect for mobile applications in emergency or defense application areas or even at home as introduced by Pulliam et al.²⁶⁹ and a step toward easier integration into an IoAT. More research is done towards miniaturization of parts of mass spectrometers e.g. microfluidic electrospray ion sources,²⁷⁰ ion traps,²⁷¹⁻²⁷³ or HPLC miniaturized devices,²⁷⁴ detection elements²⁷⁵ or applications, using miniaturized MS devices.²⁷⁶ For a more complete overview of further MS miniaturization approaches, the review from Syms and Wright from 2015 is recommended.²⁷⁷ Tian et al. have highlighted recently challenges related to the miniaturization of ion traps as mass analyzers including limited high voltages due to power consumption and supply, lower ion counts and resulting lower reachable sensitivities.²⁷⁸

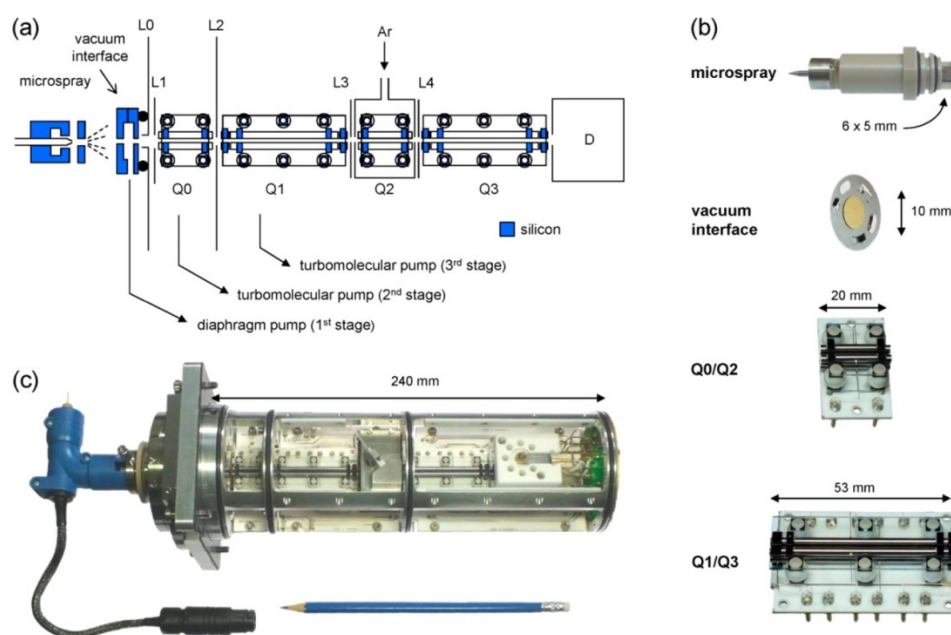


Figure 21. (a) Schematic of the miniaturized ion optics bench (not to scale). Q0 and Q2 are quadrupole ion guides, Q1 and Q3 are quadrupole mass filters, and L0–L4 are electrostatic elements. D is a multiplying detector. (b) Microengineered microspray, vacuum interface, quadrupole ion guide, and quadrupole mass filter. (c) Complete ion optics bench. Reprinted with permission from ref ²⁶⁶. Copyright © 2015, American Chemical Society.

Whether miniaturized or a full-lab based versions, for IoAT applicability, data connection and unit operation will be automated and network integrated, in part through access to online data banks. An example are the use of protein glycosylation levels for personalized medicine,²⁷⁹ using MS²⁸⁰ as a helpful technique. Together with a future IoT-based network, which includes personal glycomics data of different cancer patients, differences or similarities could easily be identified that help accelerating cancer diagnostics and treatment routines. Also a combination of portable and lab-based MS is a useful symbiosis as Zhang et al. have highlighted.²⁸¹ Other examples are tied into process control and include the work presented by Hamilton et al., who used a single quadrupole MS from Microsaic Systems plc for pharmaceutical process research intended for online analysis and quality control.²⁸² Bristow et al. used the same set-up for online measurements coupled into a flow system for organic syntheses.²⁸³

Challenges in the area of MS for IoAT application relate mainly to the need to provide solid, large and publicly available data bases so that automatic sample analysis can be done. Whether mobile and miniaturized MS are necessary for th IoAT or whether lab-based stations suffice will be decided in the future. The typically intense need for

sample preparation may keep reliable, sensitive and accurate MS in centralized labs for quite a while.

4.2 Next generation DNA sequencing (NGS) for the IoAT

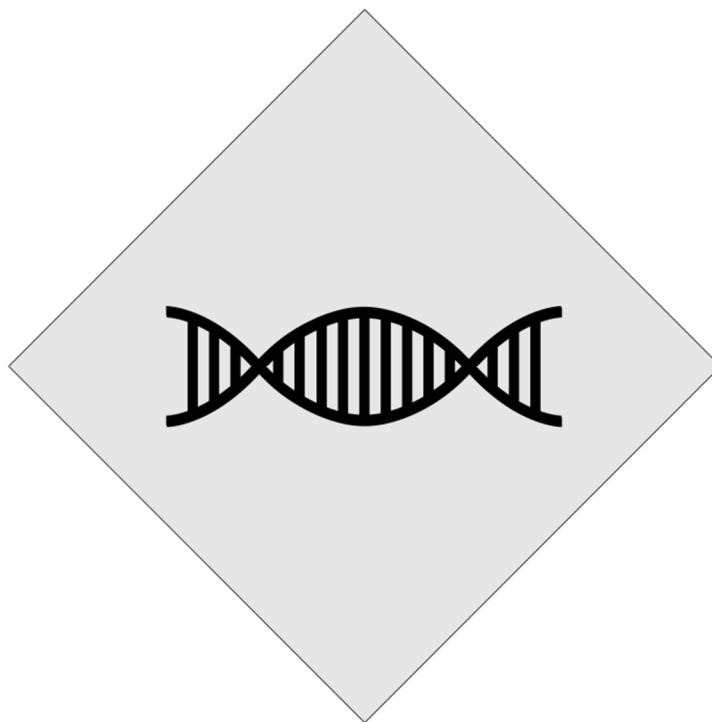


Figure 22. Next generation DNA sequencing for the IoAT.

Nucleic acids determine the genotype and to a large degree the phenotype of any living organism and therefore are an ideal target analyte. Much remains to be discovered about DNAs' and RNAs' many roles played in nature, but key to that discovery is the ability of quick and inexpensive sequencing, as nucleic acids are a unique class of molecules in that their information and actions is directly determined by their sequences. Thus, in the future, sequencing may be the key analytical tool to obtain relevant information on living organisms related to identity, health, nutritional status, age, protection, tracking& tracing and more.²⁸⁴⁻²⁸⁹ Next generation sequencing (NGS)²⁹⁰ has opened the doors for this possibility to become reality as it developed into a standard analytical tool focused on biochemical and clinical analysis with a foreseeable immense impact on therapy. Costs of whole genome sequencing is reduced from 5 digits amounts to below 1000\$,²⁹¹ and a plan to reach a cost scale of 100\$²⁹² is likely. The sequence-based information obtained through NGS requires big data analysis and

lends itself very well to automated, remote data-bank driven processing, which in turn makes it an ideal candidate for the IoAT. For example, Rothberg et al.²⁹³ introduced a semiconductor ion-chip for sequencing, consisting of more than 1 million single reaction wells and enabling a new level of high throughput sequencing. Sahm et al. described a method based on NGS to identify mutations in neurological tissue samples for neuropathology diagnostics and identification of possible targets for individual therapy.²⁹⁴ The high quality results obtained through NGS allowed decision making in therapy. In the future, linked to larger databases, NGS-based results can trigger automated pre-screening and therapeutics identification processes and hence speed-up and reduce costs of such personalized treatments.

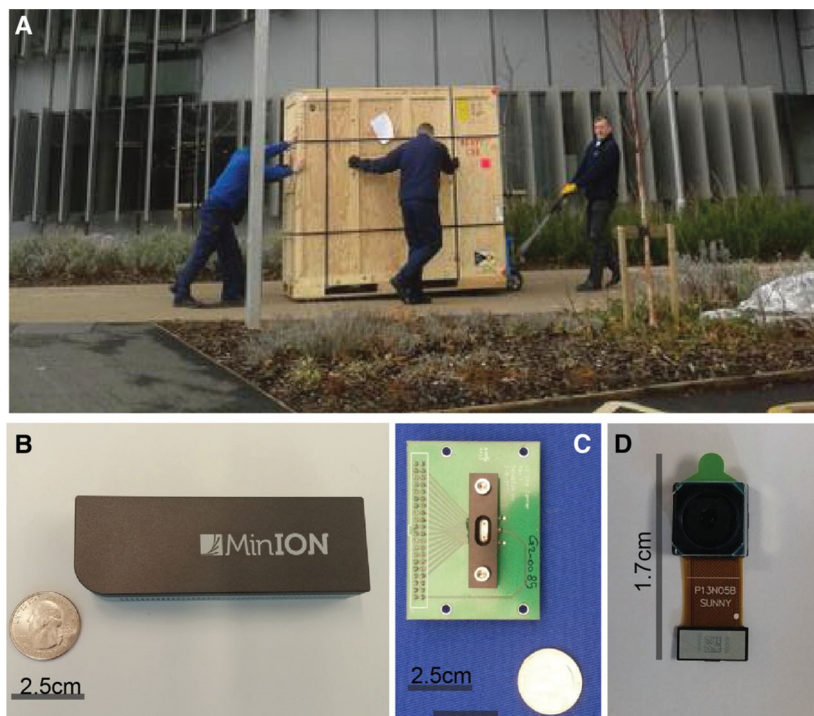


Figure 23. Sizes of sequencing platforms vs. sequencing sensors. For other differences, see Table 1. (A) Three men haul an 860-kg Pacific Biosciences RSII, a sequencing platform, to the University of Exeter (photo courtesy of @PsyEpigenetics). (B) MinION sequencing sensor. (C) An early prototype of a Genapsys flowcell. The company develops an iPad-size sequencer. (D) A commodity digital camera chip ready for cell phone integration. Can DNA sequencers be that small? Reprinted with permission from ref ²⁹⁵. Copyright © 2015, under the creative commons attribution-noncommercial 4.0 international license (CC-BY-NC).

Miniaturization and integration within automated work-flows is an important research component of NGS. For example, Lan et al. use droplet based microfluidics for selection

and barcoding of the genomes of their analyte cells which are then undertaken an Illumina sequencing step with pooled DNA.²⁹⁶ Much remains to be done as standard benchtop thermocycler for the PCR reaction and a standard microscope for evaluation of the dye-marked samples was used,²⁹⁶ but ample microfluidic-based PCR or thermocycling approaches,²⁹⁷ as well as droplet-based techniques²⁹⁸ have been described. Other examples use the microfluidic system²⁹⁹ “Fluidigm Access Array System” (Fluidigm Inc.), a benchtop device containing microfluidic elements for sample library preparations.³⁰⁰ Of great interest for NGS is a future perspective paper²⁹⁵ in which the translation of sequencing platforms from a room-sized dimension towards prototypes and lab variants of sequencing microdevices in the size of a small coin is well illustrated. Oxford Nanopore Technologies has brought a smartphone-sized, USB-connectable sequencing machine, the MinION, to the market with a starting kit with sequencing reagents for just 1000\$.³⁰¹ Similar models from other suppliers are also available ³⁰². Rapid, inexpensive, automated and miniaturized NGS is a desirable and feasible technology, perfect for the integration into the IoAT.

Future challenges that need to be overcome for NGS to become a true player in the IoAT relate to the miniaturization, lowering of costs and especially the structured generation of data and publicly available data bases. As data interpretation is more costly today than the actual sequences, progress in AI and algorithm-based data processing will assist in making NGS more applicable as human efforts will be dramatically reduced.

5. Existing commercial technologies for the IoAT

As the IoT is driving innovation especially in the engineering and IT fields, numerous companies have already demonstrated how analytical systems (beyond the physical sensors ubiquitous in automated industrial processes already) can be integrated. Products exist for all previously discussed application areas. For example, MC10, Inc. uses silicone sensor patches worn on the skin to deliver basic body monitoring data including ECG or pulse monitoring.³⁰³ AgaMatrix, Inc., presents an electrochemical glucose sensor as a connected solution with data presentation, sharing, monitoring and health report generation.³⁰⁴ Senseonics, Inc. have presented a 90 day-implantable continuous glucose monitoring biosensor³⁰⁵ complying with medical regulations in Europe³⁰⁶ and already in the assessment process at the FDA³⁰⁷ being at the moment the first approved device on the market. Basil Leaf Technologies LLC,³⁰⁸ evolved from Final Frontier Medical Devices which has won the Qualcomm Tricorder Xprize for the design of an artificial intelligence engine “DxtER” that combines emergency medical and patient derived data for diagnosis together with several non-invasive sensors for health data enquiry.³⁰⁹ Non-invasive monitoring of blood glucose, hemoglobin concentration and white blood cell count are in phase 1 clinical trials, and a urine dip-test connected with a mobile app for urine analysis and wearable digital stethoscope and breath sound analysis devices are available.³⁰⁸ Two Pore Guys, Inc. developed a molecular meter, which is a handheld device designed as an open system diagnosis and analysis platform.³¹⁰ Based on silicon nanopores, generating an electrical current, sensing can process various sample forms (e.g. saliva, blood, urine, soil, food) and detect e.g. DNA, RNA, proteins or small molecules. Their goal is to develop test stripes from existing assays and adapt them to the handheld readout platform.³¹⁰ MyDx, Inc. promotes a portable smartphone add-on-style chemical sensing device, using the electronic nose principle. The device is currently able to sense quality or contamination of cannabis and will soon be able to detect pesticides in food, air quality or metal or other contamination in drinking water according to the manufacturer.^{311,312} Upon connection of many end-user devices, a thorough area monitoring could be envisioned.

In the case of environmental monitoring, the widely available modern precision farming software solutions are a good example. For instance, Cropio³¹³ can display the on-field

gathered nutrient information of soils related to the exact GPS position and therefore suggest interactions, care actions and harvesting times. Another approach was presented by Bosch with their “Plantect™” system for plant disease prediction in greenhouse farming.³¹⁴ Software architecture has already been investigated to interconnect technologies from different suppliers and enable communication,³¹⁵ demonstrating that in general a basic consensus for interoperability is needed.³¹⁶ Farmer interaction to steer tractors or machines³¹⁷ or for decision making³¹⁸ can be minimized within such IoT setting. Ripe.io provides blockchain technology for the farm-to-fork concept and ties it directly into the IoT.³¹⁹

5.1 Business and IT sector initiatives can drive innovations in analytical chemistry

Innovation in analytical chemistry relevant to the IoT is in part driven by initiatives such as those of the Xprize Foundation or the Trillion Sensors Initiative.³²⁰ Where traditionally the chemical, pharmaceutical and food industries supported innovations in sensor and analytical chemistry developments, new partners and driving forces emerge today, as IT and analytical chemistry develop toward an IoAT. With this vision, predictions on the number of sensors to be employed go into the region of several dozen trillions of sensors during the next approximately 30 years.³²¹ Several projects have been launched and are under development, e.g. the “5 in 5” initiative from IBM³²² or the CeNSE project from HP.³²³ New solutions like Intel with context aware computing³²⁴ or Qualcomm, offering newly, designed-for-purpose hardware elements (e.g. systems on chips) for IoT sensors³²⁵ are on the forefront of innovations. Analytical chemists must also be aware of basic IT infrastructural development. Examples are, the implementation of the IPv6 standard, enabling sufficient IP addresses to be able to connect every single sensor or concepts like edge,³²⁶ mist or fog computing,³²⁷ saving bandwidths for the enormous data traffic that can be expected for a worldwide IoT network. Much research is done towards IoT-suited edge computing infrastructure, regarding context-aware and real-time data processing as shown by Ren et al.,³²⁸ network and architecture design considerations (e.g. P2P- or content distribution networks) as commented by Lopez et al.³²⁹ or how to smartly link edge and cloud computing under safety and security considerations.³³⁰ Of immediate interest to analytical chemists are developments such as the Movidius™ neural compute stick from Intel. It allows edge computing applications for a larger user-base, and enables neural

networking or deep learning applications with 100 Gflops computing power in the size of a USB stick for a prize lower than one hundred dollar. This is well suited for small, standalone sensor designs.³³¹ In fact, such components lower the technological hurdle for a broader base of researchers to apply neural computing design considerations to use it without too many development and programming into their sensor studies. In the future, IT innovations will drive innovation also in analytical chemistry such as enabled through neural networks, deep learning strategies, artificial intelligence, and social- or other predictive and incentive modeling. Successfully applied to environmental sensing improved “user experience” drives people to save drinking water.³³² On a larger scale, IBM’s Watson project³³³ helps in the analytical steps of data treatment, -analysis and results predictions and -usage. It thus links detection and decision-making steps and makes them user-independent. AI goes a step further and enables new routes for sensing and detection of analytes that would not be possible without its capabilities. Shaker et al. who develop a radar-based, noninvasive blood glucose detection device, using radar waves that allow measurements from outside, through the skin combined their technology with AI-based data evaluation, which could translate the several hundred wave features towards a certain glucose level.³³⁴ Mar et al. found that a trained artificial intelligence outperformed experienced dermatologists in reliable diagnosis of melanoma,³³⁵ Luechtefeld and his colleagues have just shown that advanced algorithms working from large chemical databases can predict a new chemical’s toxicity better than standard animal tests³³⁶ and Jo et al. used a deep learning approach for anthrax screening.³³⁷ Deep learning approaches can function well when trained for common pattern recognition tasks but much still needs to be done in AI development to reach a human emulating intelligence and thinking as Dehaene and colleagues just illustrated.³³⁸ Alternative current developments such as “Alexandria” or “Vicarious” will reduce the need for large training datasets.³³⁹ Other challenges and possible solutions are listed in Table 6.

Category	Challenges	Possible solutions
Cloud computing	Bandwidth with “a Trillion sensors”	Implement edge/mist/fog computing concepts.
Edge computing	Overlap of miniaturization requirements and required computing power	Improve miniaturized hardware performance or reduce calculation power requirements
AI & algorithm training	Overfitting of data, training on testing data, false matches and conclusions	Accuracy, question decision making, control, large enough training sets
AI & algorithm training	To which extent is AI capable of training itself to new frameworks?	“Self-training” capabilities would make AI and algorithms even more operator independent
AI & algorithms	Limited algorithm workspace in what it is trained for (boundaries)	Capability to make it work outside of narrow frames, more powerful AI
Unified protocols and data	Communication-, data processing and handling standards needed	“ISO-BUS” alike, joint data format like Allotrope

Table 6. Remaining challenges for IT infrastructure, -elements, AI & algorithms.

6. Key requirements and challenges towards a successful integration of Analytical chemistry with the IoT to generate the IoAT

The research discussed in this article provides a small overview of the substantial knowledge gained over the last years, it contains a roadmap of requirements and tasks necessary to synergistically and successfully merge analytical chemistry with the IoT concept. With respect to sensors and analytical chemistry, these tasks can be grouped into challenges related to (1) detection, (2) data processing and (3) engineering.

(1) Each analytical method that is used today for real-world applications must obviously provide highly reliable, accurate and clear answers to the questions posed. Finding a specific analyte or a group of analytes within a defined sample is likely the least challenging task. Identifying an unexpected analyte in a defined matrix or finding an unexpected analyte in an unexpected sample increases the degree of difficulty immensely. Analytical chemistry has been traditionally very good in providing accurate results even in the most complex testing scenarios. However, this detection success is typically paired with ever-increasing sophistication of the analytical method, training of the operator, and cost and time spent. This trajectory, i.e. addressing complex analytical challenges with highly sophisticated analytical methods, however, is not sustainable for an IoAT. Instead, strategies and requirements that have already been defined for the point-of-care diagnostic tests will likely be adopted by other analytical techniques as well to enable IoAT applications. This includes that sample preparation and detection must go hand-in-hand; orthogonal approaches must be developed to increase specificity and reliability in complex matrices; integrated controls must enable reliable single-point analyses (such as done in current homecare diagnostics), long-term stability and signal drifts must be addressed within the analytical system e.g via ratiometric measurements. Solutions for many of these challenges have been demonstrated in publications, patents or products as outlined in this article. We therefore don't think that these will pose an insurmountable hurdle in the development of sensors and analytical chemistry for the IoAT. However, they certainly must always be an integral part in the development of any method to be integrated into the IoT.

(2) Big data, transmission of data to centralized labs, access-free data bases are buzzwords when thinking about networking analytical devices and creating more information than achievable with separate devices. The biggest hurdle we face here may be the fact that we don't use a unified strategy for data recording, data presentation and data interpretation. To create the large databases that we dream of harnessing for curing diseases, finding sources of food safety concerns or predicting local agricultural production capabilities, we must use standardized protocols in generating and presenting data, sharing meta data, and have defined and standardized data processing strategies. Organizations such as IUPAC and national chemical societies have traditionally provided leadership, as have institutions such as the National Institute of Standards and Technology (NIST). The Allotrope Foundation is an example in the right direction, but for an IoAT these standards must be followed across different businesses and research fields, which in itself will be a difficult task for the future.

What we do with the data produced, will equally change in the future. Artificial intelligence, machine learning, neural networks, smart algorithms are part of the future of analytical chemistry as it advances to networked sensing systems that have significantly broader impact than our current locally focused analytical approaches.

(3) Engineering ingenuity and design will continue in their effort to integrate the analytical chemistry and sensor world with its surroundings. For many of the IoAT applications, small, inexpensive, rapid analytical methods are desirable. For others, integration into larger systems requires careful attention to interfaces, and for a few applications no demand for new engineering solution exists as those have been solved already such as for environmental pollution control stations and for some cell-phone based point-of-care diagnostics. Also with respect to costs, engineering design will play a major role. For the vast majority of analytical systems, lowering the costs per analysis is not only achieved through the assay components used, but also through the engineering design of transducers, packaging and interfaces.

Finally, sustainability will become an immensely important aspect for analytical chemistry with respect to waste produced, energy consumed and enabling on-demand local production. Already today the plastic waste produced by point-of-care devices in remote and resource-limited areas on the globe are a threat to the environment and new solutions are tepidly sought. For example, moving to recyclable plastic cartridges

isn't as simple as it sounds, as those severely and negatively affect storage capabilities in hot, humid climates. Therefore, new strategies for sustainable production, use and recycling must be developed especially when considering a trillion sensor world.

7. References

- (1) Schoenberger, C. R., "www.forbes.com, *Internet of Things first definition*," can be found under <https://www.forbes.com/forbes/2002/0318/155.html#5dc6bc4559d4>, **2002**.
- (2) Postscapes, "*Internet of Things (IoT) History*," can be found under <https://postscapes.com/internet-of-things-history/>, **2016**.
- (3) Martin, A., "*step-and-save-the-risks-of-using-fitness-tracker-to-save-on-your-insurance-premium*", can be found under <https://www.wareable.com/wearable-tech/step-and-save-the-risks-of-using-fitness-tracker-to-save-on-your-insurance-premium-1163>, **2015**.
- (4) Booton, J., "*You may be forced to wear a health tracker at work - MarketWatch*", can be found under <https://www.marketwatch.com/story/you-might-be-wearing-a-health-tracker-at-work-one-day-2015-03-11>, **2015**.
- (5) Wiesmüller, M., "*\"Drängeln erlaubt: Teilautomatisierte Lkw-Konvois bestehen Versuchsfahrt\" @ www.computerbild.de*," can be found under <http://www.computerbild.de/artikel/cb-News-Connected-Car-Truck-Platoon-Lkw-Konvoi-15361657.html>, **2016**.
- (6) AutoBild, "*Daimler-Truck auf Premieren-Geisterfahrt @ www.autobild.de*," can be found under <http://www.autobild.de/artikel/autonomer-lkw-test-in-baden-wuerttemberg-5971499.html>, **2015**.
- (7) Google, "*Google Self driving car*," can be found under <https://www.google.com/selfdrivingcar/>, **2016**.
- (8) King, D., "*Second Tesla Model S driver blames Autopilot failure for crash*," can be found under <http://www.autoblog.com/2016/05/16/second-tesla-model-s-driver-blames-autopilot-failure-for-crash/> **2016**.
- (9) Lobaccaro, G.; Carlucci, S.; Löfström, E. A Review of Systems and Technologies for Smart Homes and Smart Grids. *Energy* **2016**, 9, 1-33. doi: 10.3390/en9050348.
- (10) Fitzpatrick, D. E.; Battilocchio, C.; Ley, S. V. A Novel Internet-Based Reaction Monitoring, Control and Autonomous Self-Optimization Platform for Chemical Synthesis. *Org. Process Res. Dev.* **2016**, 20, 386-394. doi: 10.1021/acs.oprd.5b00313.
- (11) CAMO Software AS, "*Process Analytical Technology (PAT) and Quality by Design (QbD)*", can be found under <http://www.camo.com/services/process-analytical-technology.html>, **2016**.
- (12) Simon, L. L.; Pataki, H.; Marosi, G.; Meemken, F.; Hungerbühler, K.; Baiker, A.; Tummala, S.; Glennon, B.; Kuentz, M.; Steele, G.; Kramer, H. J. M.; Rydzak, J. W.;

- Chen, Z.; Morris, J.; Kjell, F.; Singh, R.; Gani, R.; Gernaey, K. V.; Louhi-Kultanen, M.; O'Reilly, J., et al. Assessment of recent process analytical technology (PAT) trends: A multi-author review. *Org. Process Res. Dev.* **2015**, *19*, 3-62. doi: 10.1021/op500261y.
- (13) Lee, J. H.; Lee, S. H.; Yim, S. S.; Kang, K. H.; Lee, S. Y.; Park, S. J.; Jeong, K. J. Quantified high-throughput screening of *Escherichia coli* producing poly(3-hydroxybutyrate) based on FACS. *Appl. Biochem. Biotechnol.* **2013**, *170*, 1767-1779. doi: 10.1007/s12010-013-0311-2.
 - (14) Zong, S. F.; Zong, J. Z.; Chen, C.; Jiang, X. Y.; Zhang, Y. Z.; Wang, Z. Y.; Cui, Y. P. Single molecule localization imaging of exosomes using blinking silicon quantum dots. *Nanotechnology* **2018**, *29*. doi: 10.1088/1361-6528/aaa375.
 - (15) Naik, A. K.; Hanay, M. S.; Hiebert, W. K.; Feng, X. L.; Roukes, M. L. Towards single-molecule nanomechanical mass spectrometry. *Nat. Nanotechnol.* **2009**, *4*, 445. doi: 10.1038/nnano.2009.152.
 - (16) Vacca, D.; Cancila, V.; Gulino, A.; Lo Bosco, G.; Belmonte, B.; Di Napoli, A.; Florena, A. M.; Tripodo, C.; Arancio, W. Real-time detection of BRAF V600E mutation from archival hairy cell leukemia FFPE tissue by nanopore sequencing. *Mol. Biol. Rep.* **2018**, *45*, 1-7. doi: 10.1007/s11033-017-4133-0.
 - (17) Mabey, D.; Peeling, R. W.; Ustianowski, A.; Perkins, M. D. Diagnostics for the developing world. *Nat. Rev. Microbiol.* **2004**, *2*, 231-240. doi: 10.1038/nrmicro841.
 - (18) Holčápek, M.; Jirásko, R.; Lída, M. Recent developments in liquid chromatography-mass spectrometry and related techniques. *J. Chromatogr. A* **2012**, *1259*, 3-15. doi: <https://doi.org/10.1016/j.chroma.2012.08.072>.
 - (19) Tsednee, M.; Huang, Y.-C.; Chen, Y.-R.; Yeh, K.-C. Identification of metal species by ESI-MS/MS through release of free metals from the corresponding metal-ligand complexes. *Sci. Rep.* **2016**, *6*, 26785. doi: 10.1038/srep26785.
 - (20) Albert, A.; Shelley, J. T.; Engelhard, C. Plasma-based ambient desorption/ionization mass spectrometry: state-of-the-art in qualitative and quantitative analysis. *Anal. Bioanal. Chem.* **2014**, *406*, 6111-6127. doi: 10.1007/s00216-014-7989-z.
 - (21) Sun, N.; Walch, A. Qualitative and quantitative mass spectrometry imaging of drugs and metabolites in tissue at therapeutic levels. *Histochem. Cell Biol.* **2013**, *140*, 93-104. doi: 10.1007/s00418-013-1127-4.
 - (22) Liu, S.; Wang, Y. S. Mass spectrometry for the assessment of the occurrence and biological consequences of DNA adducts. *Chem. Soc. Rev.* **2015**, *44*, 7829-7854. doi: 10.1039/c5cs00316d.
 - (23) Didelot, X.; Bowden, R.; Wilson, D. J.; Peto, T. E. A.; Crook, D. W. Transforming clinical microbiology with bacterial genome sequencing. *Nat. Rev. Genet.* **2012**, *13*, 601-612. doi: 10.1038/nrg3226.
 - (24) Meldrum, C.; Doyle, M. A.; Tothill, R. W. Next-Generation Sequencing for Cancer Diagnostics: a Practical Perspective. *Clin. Biochem. Rev. (Ultimo, Aust.)* **2011**, *32*, 177-195.

- (25) Deurenberg, R. H.; Bathoorn, E.; Chlebowicz, M. A.; Couto, N.; Ferdous, M.; García-Cobos, S.; Kooistra-Smid, A. M. D.; Raangs, E. C.; Rosema, S.; Veloo, A. C. M.; Zhou, K.; Friedrich, A. W.; Rossen, J. W. A. Application of next generation sequencing in clinical microbiology and infection prevention. *J. Biotechnol.* **2017**, *243*, 16-24. doi: <https://doi.org/10.1016/j.jbiotec.2016.12.022>.
- (26) Woyke, E., "A smarter smart city", can be found under <https://www.technologyreview.com/s/610249/a-smarter-smart-city/#comments>, **2018**.
- (27) Piyare, R.; Lee, S. R. Towards Internet of Things (IOTS): Integration of Wireless Sensor Network to Cloud Services for Data Collection and Sharing. *International journal of Computer Networks & Communications* **2013**, *5*, 59-72. doi: 10.5121/ijcnc.2013.5505.
- (28) Ngu, A. H.; Gutierrez, M.; Metsis, V.; Nepal, S.; Sheng, Q. Z. IoT Middleware: A Survey on Issues and Enabling Technologies. *IEEE Internet Things J.* **2017**, *4*, 1-20. doi: 10.1109/jiot.2016.2615180.
- (29) Razzaque, M. A.; Milojevic-Jevric, M.; Palade, A.; Clarke, S. Middleware for Internet of Things: A Survey. *IEEE Internet Things J.* **2016**, *3*, 70-95. doi: 10.1109/jiot.2015.2498900.
- (30) Gao, W.; Emaminejad, S.; Nyein, H. Y. Y.; Challa, S.; Chen, K.; Peck, A.; Fahad, H. M.; Ota, H.; Shiraki, H.; Kiriya, D.; Lien, D.-H.; Brooks, G. A.; Davis, R. W.; Javey, A. Fully integrated wearable sensor arrays for multiplexed in situ perspiration analysis. *Nature* **2016**, *529*, 509-514. doi: 10.1038/nature16521.
- (31) Yao, H.; Shum, A. J.; Cowan, M.; Lähdesmäki, I.; Parviz, B. A. A contact lens with embedded sensor for monitoring tear glucose level. *Biosens. Bioelectron.* **2011**, *26*, 3290-3296. doi: 10.1016/j.bios.2010.12.042.
- (32) Kim, J.; Imani, S.; de Araujo, W. R.; Warchall, J.; Valdés-Ramírez, G.; Paixão, T. R. L. C.; Mercier, P. P.; Wang, J. Wearable salivary uric acid mouthguard biosensor with integrated wireless electronics. *Biosens. Bioelectron.* **2015**, *74*, 1061-1068. doi: 10.1016/j.bios.2015.07.039.
- (33) Hu, Y.; Liang, B.; Fang, L.; Ma, G.; Yang, G.; Zhu, Q.; Chen, S.; Ye, X. Antifouling Zwitterionic Coating via Electrochemically Mediated Atom Transfer Radical Polymerization on Enzyme-Based Glucose Sensors for Long-Time Stability in 37 degrees C Serum. *Langmuir* **2016**, *32*, 11763-11770. doi: 10.1021/acs.langmuir.6b03016.
- (34) Bucur, B. Technological Barriers in the Use of Electrochemical Microsensors and Microbiosensors for in vivo Analysis of Neurological Relevant Substances. *Curr. Neuropharmacol.* **2012**, *10*, 197-211. doi: 10.2174/157015912803217350.
- (35) Mishra, R. K.; Hubble, L. J.; Martin, A.; Kumar, R.; Barfidokht, A.; Kim, J.; Musameh, M. M.; Kyratzis, I. L.; Wang, J. Wearable Flexible and Stretchable Glove Biosensor for On-Site Detection of Organophosphorus Chemical Threats. *ACS Sens.* **2017**, *2*, 553-561. doi: 10.1021/acssensors.7b00051.

- (36) Sempionatto, J. R.; Nakagawa, T.; Pavinatto, A.; Mensah, S. T.; Imani, S.; Mercier, P.; Wang, J. Eyeglasses based wireless electrolyte and metabolite sensor platform. *Lab Chip* **2017**, *17*, 1834-1842. doi: 10.1039/c7lc00192d.
- (37) Sempionatto, J. R.; Mishra, R. K.; Martin, A.; Tang, G.; Nakagawa, T.; Lu, X.; Campbell, A. S.; Lyu, K. M.; Wang, J. Wearable Ring-Based Sensing Platform for Detecting Chemical Threats. *ACS Sens.* **2017**, *2*, 1531-1538. doi: 10.1021/acssensors.7b00603.
- (38) Liang, K.; Carmone, S.; Brambilla, D.; Leroux, J.-C. 3D printing of a wearable personalized oral delivery device: A first-in-human study. *Sci. Adv.* **2018**, *4*, eaat2544. doi: 10.1126/sciadv.aat2544.
- (39) Smith, M. A.; Fasching, R., T.; Howard, C. P., *Face mask incorporating respiratory flow sensor*. US 6,718,982 B2, April 13, 2004.
- (40) Caseel, B., "Why do Japanese people wear surgical masks? It's not always for health reasons", can be found under <https://japantoday.com/category/features/lifestyle/why-do-japanese-people-wear-surgical-masks-its-not-always-for-health-reasons>, **2014**.
- (41) Güder, F.; Ainla, A.; Redston, J.; Mosadegh, B.; Glavan, A.; Martin, T. J.; Whitesides, G. M. Paper-Based Electrical Respiration Sensor. *Angew. Chem. Int. Ed.* **2016**, *55*, 5727-5732. doi: 10.1002/anie.201511805.
- (42) Munje, R. D.; Muthukumar, S.; Panneer Selvam, A.; Prasad, S. Flexible nanoporous tunable electrical double layer biosensors for sweat diagnostics. *Sci. Rep.* **2015**, *5*, 14586. doi: 10.1038/srep14586.
- (43) Parlak, O.; Keene, S. T.; Marais, A.; Curto, V. F.; Salleo, A. Molecularly selective nanoporous membrane-based wearable organic electrochemical device for noninvasive cortisol sensing. *Sci. Adv.* **2018**, *4*, eaar2904. doi: 10.1126/sciadv.aar2904.
- (44) Chang, H. Y.; Yogeesh, M. N.; Ghosh, R.; Rai, A.; Sanne, A.; Yang, S.; Lu, N.; Banerjee, S. K.; Akinwande, D. Large-Area Monolayer MoS₂ for Flexible Low-Power RF Nanoelectronics in the GHz Regime. *Adv. Mater.* **2016**, *28*, 1818-1823. doi: 10.1002/adma.201504309.
- (45) Song, J.-K.; Son, D.; Kim, J.; Yoo, Y. J.; Lee, G. J.; Wang, L.; Choi, M. K.; Yang, J.; Lee, M.; Do, K.; Koo, J. H.; Lu, N.; Kim, J. H.; Hyeon, T.; Song, Y. M.; Kim, D.-H. Wearable Force Touch Sensor Array Using a Flexible and Transparent Electrode. *Adv. Funct. Mater.* **2017**, *27*, 1605286. doi: 10.1002/adfm.201605286.
- (46) Kabiri Ameri, S.; Ho, R.; Jang, H.; Tao, L.; Wang, Y.; Wang, L.; Schnyer, D. M.; Akinwande, D.; Lu, N. Graphene Electronic Tattoo Sensors. *ACS nano* **2017**, *11*, 7634-7641. doi: 10.1021/acsnano.7b02182.
- (47) Imani, S.; Bandodkar, A. J.; Mohan, A. M. V.; Kumar, R.; Yu, S.; Wang, J.; Mercier, P. P. A wearable chemical–electrophysiological hybrid biosensing system for real-time health and fitness monitoring. *Nat. Commun.* **2016**, *7*, 1-7. doi: 10.1038/ncomms11650.

- (48) Kim, J.; Gutruf, P.; Chiarelli, A. M.; Heo, S. Y.; Cho, K.; Xie, Z.; Banks, A.; Han, S.; Jang, K. I.; Lee, J. W.; Lee, K. T.; Feng, X.; Huang, Y.; Fabiani, M.; Gratton, G.; Paik, U.; Rogers, J. A. Miniaturized Battery-Free Wireless Systems for Wearable Pulse Oximetry. *Adv Funct Mater* **2017**, *27*. doi: 10.1002/adfm.201604373.
- (49) Kim, J.; Jeerapan, I.; Imani, S.; Cho, T. N.; Bandodkar, A.; Cinti, S.; Mercier, P. P.; Wang, J. Noninvasive Alcohol Monitoring Using a Wearable Tattoo-Based Iontophoretic-Biosensing System. *ACS Sens.* **2016**, *1*, 1011-1019. doi: 10.1021/acssensors.6b00356.
- (50) Sonner, Z.; Wilder, E.; Gaillard, T.; Kasting, G.; Heikenfeld, J. Integrated sudomotor axon reflex sweat stimulation for continuous sweat analyte analysis with individuals at rest. *Lab Chip* **2017**, *17*, 2550-2560. doi: 10.1039/c7lc00364a.
- (51) Koh, A.; Kang, D.; Xue, Y.; Lee, S.; Pielak, R. M.; Kim, J.; Hwang, T.; Min, S.; Banks, A.; Bastien, P.; Manco, M. C.; Wang, L.; Ammann, K. R.; Jang, K.-I.; Won, P.; Han, S.; Ghaffari, R.; Paik, U.; Slepian, M. J.; Balooch, G., et al. A soft, wearable microfluidic device for the capture, storage, and colorimetric sensing of sweat. *Sci. Transl. Med.* **2016**, *8*, 366ra165. doi: 10.1126/scitranslmed.aaf2593.
- (52) Choi, J.; Ghaffari, R.; Baker, L. B.; Rogers, J. A. Skin-interfaced systems for sweat collection and analytics. *Sci. Adv.* **2018**, *4*, eaar3921. doi: 10.1126/sciadv.aar3921.
- (53) Ciui, B.; Martin, A.; Mishra, R. K.; Brunetti, B.; Nakagawa, T.; Dawkins, T. J.; Lyu, M.; Cristea, C.; Sandulescu, R.; Wang, J. Wearable Wireless Tyrosinase Bandage and Microneedle Sensors: Toward Melanoma Screening. *Adv. Healthcare Mater.* **2018**. doi: 10.1002/adhm.201701264.
- (54) Shi, Y.; Manco, M.; Moyal, D.; Huppert, G.; Araki, H.; Banks, A.; Joshi, H.; McKenzie, R.; Seewald, A.; Griffin, G.; Sen-Gupta, E.; Wright, D.; Bastien, P.; Valceschini, F.; Seite, S.; Wright, J. A.; Ghaffari, R.; Rogers, J.; Balooch, G.; Pielak, R. M. Soft, stretchable, epidermal sensor with integrated electronics and photochemistry for measuring personal UV exposures. *PLoS One* **2018**, *13*, e0190233. doi: 10.1371/journal.pone.0190233.
- (55) Lee, S. P.; Ha, G.; Wright, D. E.; Ma, Y.; Sen-Gupta, E.; Haubrich, N. R.; Branche, P. C.; Li, W.; Huppert, G. L.; Johnson, M.; Mutlu, H. B.; Li, K.; Sheth, N.; Wright, J. A.; Huang, Y.; Mansour, M.; Rogers, J. A.; Ghaffari, R. Highly flexible, wearable, and disposable cardiac biosensors for remote and ambulatory monitoring. *npj Digital Medicine* **2018**, *1*. doi: 10.1038/s41746-017-0009-x.
- (56) Zhu, Z.; Guo, S. Z.; Hirdler, T.; Eide, C.; Fan, X.; Tolar, J.; McAlpine, M. C. 3D Printed Functional and Biological Materials on Moving Freeform Surfaces. *Adv. Mater.* **2018**, *30*, e1707495. doi: 10.1002/adma.201707495.
- (57) Bandodkar, A. J.; López, C. S.; Vinu Mohan, A. M.; Yin, L.; Kumar, R.; Wang, J. All-printed magnetically self-healing electrochemical devices. *Sci. Adv.* **2016**, *2*, e1601465. doi: 10.1126/sciadv.1601465.
- (58) Kim, J.; Cho, T. N.; Valdés-Ramírez, G.; Wang, J. A wearable fingernail chemical sensing platform: PH sensing at your fingertips. *Talanta* **2016**, *150*, 622-628. doi: 10.1016/j.talanta.2015.12.083.

- (59) Tseng, P.; Napier, B.; Garbarini, L.; Kaplan, D. L.; Omenetto, F. G. Functional, RF-Trilayer Sensors for Tooth-Mounted, Wireless Monitoring of the Oral Cavity and Food Consumption. *Adv. Mater.* **2018**, *30*, e1703257. doi: 10.1002/adma.201703257.
- (60) Liu, X.; Yuk, H.; Lin, S.; Parada German, A.; Tang, T.-C.; Tham, E.; de la Fuente-Nunez, C.; Lu Timothy, K.; Zhao, X. 3D Printing of Living Responsive Materials and Devices. *Adv. Mater.* **2017**, *30*, 1704821. doi: 10.1002/adma.201704821.
- (61) Liao, Y.-t.; Yao, H.; Lingley, A.; Parviz, B.; Otis, B. P. A 3- μ W CMOS Glucose Sensor for Wireless Contact-Lens Tear Glucose Monitoring. *IEEE J. Solid-State Circuits* **2012**, *47*, 335-344. doi: 10.1109/JSSC.2011.2170633.
- (62) Park, J.; Kim, J.; Kim, S.-Y.; Cheong, W. H.; Jang, J.; Park, Y.-G.; Na, K.; Kim, Y.-T.; Heo, J. H.; Lee, C. Y.; Lee, J. H.; Bien, F.; Park, J.-U. Soft, smart contact lenses with integrations of wireless circuits, glucose sensors, and displays. *Sci. Adv.* **2018**, *4*, eaap9841. doi: 10.1126/sciadv.aap9841.
- (63) Otis, B.; Parviz, B., "introducing-our-smart-contact-lens @ googleblog," can be found under <https://blog.google/topics/alphabet/introducing-our-smart-contact-lens/>, **2014**.
- (64) Pesl, P.; Herrero, P.; Reddy, M.; Xenou, M.; Oliver, N.; Johnston, D.; Toumazou, C.; Georgiou, P. An Advanced Bolus Calculator for Type 1 Diabetes: System Architecture and Usability Results. *IEEE J. Biomed. Health Inform.* **2016**, *20*, 11-17. doi: 10.1109/jbhi.2015.2464088.
- (65) Bergsland, J.; Elle, O. J.; Fosse, E. Barriers to medical device innovation. *Med. Devices: Evidence Res.* **2014**, *7*, 205-209. doi: 10.2147/mder.s43369.
- (66) Kramer, D. B.; Xu, S.; Kesselheim, A. S. Regulation of Medical Devices in the United States and European Union. *N. Engl. J. Med.* **2012**, *366*, 848-855. doi: 10.1056/NEJMhle1113918.
- (67) Baj-Rossi, C.; Cavallini, A.; Kiliç, E. G.; Stradolini, F.; Rezzonica Jost, T.; Proietti, M.; De Micheli, G.; Dehollain, C.; Carrara, S. In-Vivo Validation of Fully Implantable Multi-Panel Devices for Remote Monitoring of Metabolism. *IEEE Trans. Biomed. Circuits Syst.* **2016**, *10*, 955-962. doi: 10.1109/tbcas.2016.2584239.
- (68) Carrara, S.; Bolomey, L.; Boero, C.; Cavallini, A.; Meurville, E.; Micheli, G. D.; Rezzonico, T.; Proietti, M.; Grassi, F., *Single-metabolite Bio-Nano-Sensors and system for remote monitoring in animal models*. 2011 IEEE SENSORS Proceedings, **2011**, pp. 716-719. doi: 10.1109/icsens.2011.6126962.
- (69) Poscia, A.; Messeri, D.; Moscone, D.; Ricci, F.; Valgimigli, F. A novel continuous subcutaneous lactate monitoring system. *Biosens. Bioelectron.* **2005**, *20*, 2244-2250. doi: <https://doi.org/10.1016/j.bios.2004.10.031>.
- (70) Yu, B.; Long, N.; Moussy, Y.; Moussy, F. A long-term flexible minimally-invasive implantable glucose biosensor based on an epoxy-enhanced polyurethane membrane. *Biosens. Bioelectron.* **2006**, *21*, 2275-2282. doi: <https://doi.org/10.1016/j.bios.2005.11.002>.

- (71) Gough, D. A.; Kumosa, L. S.; Routh, T. L.; Lin, J. T.; Lucisano, J. Y. Function of an implanted tissue glucose sensor for more than 1 year in animals. *Sci. Transl. Med.* **2010**, *2*, 42ra53. doi: 10.1126/scitranslmed.3001148.
- (72) Lewitus, D. Y.; Smith, K. L.; Landers, J.; Neimark, A. V.; Kohn, J. Bioactive agarose carbon-nanotube composites are capable of manipulating brain-implant interface. *J. Appl. Polym. Sci.* **2014**, *131*, 40297. doi: 10.1002/app.40297.
- (73) Zong, X.; Zhu, R. ZnO nanorod-based FET biosensor for continuous glucose monitoring. *Sens. Actuators, B* **2018**, *255*, 2448-2453. doi: 10.1016/j.snb.2017.09.037.
- (74) Lucisano, J. Y.; Routh, T. L.; Lin, J. T.; Gough, D. A. Glucose Monitoring in Individuals With Diabetes Using a Long-Term Implanted Sensor/Telemetry System and Model. *IEEE Trans. Biomed. Eng.* **2017**, *64*, 1982-1993. doi: 10.1109/tbme.2016.2619333.
- (75) Kropff, J.; Choudhary, P.; Neupane, S.; Barnard, K.; Bain, S. C.; Kapitza, C.; Forst, T.; Link, M.; Dehennis, A.; DeVries, J. H. Accuracy and Longevity of an Implantable Continuous Glucose Sensor in the PRECISE Study: A 180-Day, Prospective, Multicenter, Pivotal Trial. *Diabetes Care* **2017**, *40*, 63. doi: 10.2337/dc16-1525.
- (76) European Commission, "'Active implantable medical devices" (AIMD) directive - Directive 90/385/EEC," can be found under https://ec.europa.eu/growth/single-market/european-standards/harmonised-standards/implantable-medical-devices_de, **2018**.
- (77) Rome, B. N.; Kramer, D. B.; Kesselheim, A. S. FDA approval of cardiac implantable electronic devices via original and supplement premarket approval pathways, 1979-2012. *JAMA* **2014**, *311*, 385-391. doi: 10.1001/jama.2013.284986.
- (78) Proffitt, A. Epilepsy neurodevice approved. *Nat. Biotechnol.* **2014**, *32*, 301-301. doi: 10.1038/nbt0414-301.
- (79) Sachedina, N.; Pickup, J. C. Performance assessment of the Medtronic-MiniMed Continuous Glucose Monitoring System and its use for measurement of glycaemic control in Type 1 diabetic subjects. *Diabetic Med.* **2003**, *20*, 1012-1015. doi: 10.1046/j.1464-5491.2003.01037.x.
- (80) Arroyo-Currás, N.; Somerson, J.; Vieira, P. A.; Ploense, K. L.; Kippin, T. E.; Plaxco, K. W. Real-time measurement of small molecules directly in awake, ambulatory animals. *Proc. Natl. Acad. Sci. U.S.A.* **2017**, *114*, 645. doi: 10.1073/pnas.1613458114.
- (81) Arroyo-Currás, N.; Dauphin-Ducharme, P.; Ortega, G.; Ploense, K. L.; Kippin, T. E.; Plaxco, K. W. Subsecond-Resolved Molecular Measurements in the Living Body Using Chronoamperometrically Interrogated Aptamer-Based Sensors. *ACS Sens.* **2017**. doi: 10.1021/acssensors.7b00787.
- (82) Karunwi, O.; Alam, F.; Guiseppi-Elie, A., *Biofabrication and Evaluation, in vitro and in vivo, of a Dual Responsive Glucose and Lactate Implantable Biosensor in a Piglet Trauma Model*. Paper presented at the Graduate Research and Discovery Symposium (GRADS), **2015**.

- (83) Cavallini, A.; Jost, T. R.; Ghoreishizadeh, S. S.; Olivo, J.; Beeck, M. O. d.; Gorissen, B.; Grassi, F.; Micheli, G. D.; Carrara, S. A Subcutaneous Biochip for Remote Monitoring of Human Metabolism: Packaging and Biocompatibility Assessment. *IEEE Sensors J.* **2015**, *15*, 417-424. doi: 10.1109/jsen.2014.2339638.
- (84) Soto, R. J.; Privett, B. J.; Schoenfisch, M. H. In vivo analytical performance of nitric oxide-releasing glucose biosensors. *Anal. Chem.* **2014**, *86*, 7141-7149. doi: 10.1021/ac5017425.
- (85) Chien, J. S.; Mohammed, M.; Eldik, H.; Ibrahim, M.; Nichols, S.; Wisniewski, N.; Klitzman, B. Abstract 41: Implantable Oxygen Biosensor Reveals Post-Occlusion Tissue Reactive Hyperoxia. *Plast. Reconstr. Surg. Glob. Open.* **2017**, *5*, 32-33. doi: 10.1097/01.GOX.0000516562.54306.4f.
- (86) Noh, K. N.; Park, S. I.; Qazi, R.; Zou, Z.; Mickle, A. D.; Grajales-Reyes, J. G.; Jang, K. I.; Gereau, R. W. t.; Xiao, J.; Rogers, J. A.; Jeong, J. W. Miniaturized, Battery-Free Optofluidic Systems with Potential for Wireless Pharmacology and Optogenetics. *Small* **2018**, *14*. doi: 10.1002/sml.201702479.
- (87) Li, X.; Li, X.; Cheng, J.; Yuan, D.; Ni, W.; Guan, Q.; Gao, L.; Wang, B. Fiber-shaped solid-state supercapacitors based on molybdenum disulfide nanosheets for a self-powered photodetecting system. *Nano Energy* **2016**, *21*, 228-237. doi: <https://doi.org/10.1016/j.nanoen.2016.01.011>.
- (88) Ballard, Z. S.; Ozcan, A., in *Mobile Health* (Eds.: Rehg, J.; Murphy, S.; Kumar, S.), Springer, Cham, **2017**, pp. 313-342. doi: 10.1007/978-3-319-51394-2.
- (89) Guo, J.; Niu, M.; Yang, C. Highly flexible and stretchable optical strain sensing for human motion detection. *Optica* **2017**, *4*, 1285-1288. doi: 10.1364/optica.4.001285.
- (90) Sheykhi, S.; Mosca, L.; Anzenbacher, P. Toward wearable sensors: optical sensor for detection of ammonium nitrate-based explosives, ANFO and ANNM. *Chem. Commun.* **2017**, *53*, 5196-5199. doi: 10.1039/c7cc01949a.
- (91) Zobenica, Z.; van der Heijden, R. W.; Petruzzella, M.; Pagliano, F.; Leijssen, R.; Xia, T.; Midolo, L.; Cotrufo, M.; Cho, Y.; van Otten, F. W. M.; Verhagen, E.; Fiore, A. Integrated nano-opto-electro-mechanical sensor for spectrometry and nanometrology. *Nat. Commun.* **2017**, *8*, 2216. doi: 10.1038/s41467-017-02392-5.
- (92) Choi, M. K.; Yang, J.; Kim, D. C.; Dai, Z.; Kim, J.; Seung, H.; Kale, V. S.; Sung, S. J.; Park, C. R.; Lu, N.; Hyeon, T.; Kim, D. H. Extremely Vivid, Highly Transparent, and Ultrathin Quantum Dot Light-Emitting Diodes. *Adv. Mater.* **2018**, *30*. doi: 10.1002/adma.201703279.
- (93) Choi, C.; Choi, M. K.; Liu, S.; Kim, M. S.; Park, O. K.; Im, C.; Kim, J.; Qin, X.; Lee, G. J.; Cho, K. W.; Kim, M.; Joh, E.; Lee, J.; Son, D.; Kwon, S. H.; Jeon, N. L.; Song, Y. M.; Lu, N.; Kim, D. H. Human eye-inspired soft optoelectronic device using high-density MoS₂-graphene curved image sensor array. *Nat. Commun.* **2017**, *8*, 1664. doi: 10.1038/s41467-017-01824-6.
- (94) Wang, Y.; Vaddiraju, S.; Gu, B.; Papadimitrakopoulos, F.; Burgess, D. J. Foreign Body Reaction to Implantable Biosensors: Effects of Tissue Trauma and Implant Size. *J. Diabetes Sci. Technol.* **2015**, *9*, 966-977. doi: 10.1177/1932296815601869.

- (95) Nichols, S. P.; Koh, A.; Storm, W. L.; Shin, J. H.; Schoenfisch, M. H. Biocompatible materials for continuous glucose monitoring devices. *Chem Rev* **2013**, *113*, 2528-2549. doi: 10.1021/cr300387j.
- (96) Wang, Y.; Papadimitrakopoulos, F.; Burgess, D. J. Polymeric "smart" coatings to prevent foreign body response to implantable biosensors. *J. Controlled Release* **2013**, *169*, 341-347. doi: <https://doi.org/10.1016/j.jconrel.2012.12.028>.
- (97) Baj-Rossi, C.; Cavallini, A.; Rezzonico Jost, T.; Proietti, M.; Grassi, F.; De Micheli, G.; Carrara, S., *Biocompatible Packagings for Fully Implantable Multi-Panel Devices for Remote Monitoring of Metabolism*. Paper presented at the Biomedical Circuits and Systems Conference (BiOCAS 2015), Atlanta, Georgia, 2015 **2015**. doi: 10.1109/BioCAS.2015.7348398.
- (98) Lee, Y. K.; Yu, K. J.; Kim, Y.; Yoon, Y.; Xie, Z.; Song, E.; Luan, H.; Feng, X.; Huang, Y.; Rogers, J. A. Kinetics and Chemistry of Hydrolysis of Ultrathin, Thermally Grown Layers of Silicon Oxide as Biofluid Barriers in Flexible Electronic Systems. *ACS Appl. Mater. Interfaces* **2017**, *9*, 42633-42638. doi: 10.1021/acsami.7b15302.
- (99) Lee, Y. K.; Yu, K. J.; Song, E.; Barati Farimani, A.; Vitale, F.; Xie, Z.; Yoon, Y.; Kim, Y.; Richardson, A.; Luan, H.; Wu, Y.; Xie, X.; Lucas, T. H.; Crawford, K.; Mei, Y.; Feng, X.; Huang, Y.; Litt, B.; Aluru, N. R.; Yin, L., et al. Dissolution of Monocrystalline Silicon Nanomembranes and Their Use as Encapsulation Layers and Electrical Interfaces in Water-Soluble Electronics. *ACS nano* **2017**, *11*, 12562-12572. doi: 10.1021/acsnano.7b06697.
- (100) Lee, Y. K.; Kim, J.; Kim, Y.; Kwak, J. W.; Yoon, Y.; Rogers, J. A. Room Temperature Electrochemical Sintering of Zn Microparticles and Its Use in Printable Conducting Inks for Bioresorbable Electronics. *Adv. Mater.* **2017**, *29*. doi: 10.1002/adma.201702665.
- (101) Lee, G.; Kang, S.-K.; Won, S. M.; Gutruf, P.; Jeong, Y. R.; Koo, J.; Lee, S.-S.; Rogers, J. A.; Ha, J. S. Fully Biodegradable Microsupercapacitor for Power Storage in Transient Electronics. *Adv. Energy Mater.* **2017**, *7*, 1700157. doi: 10.1002/aenm.201700157.
- (102) Surana, S.; Bhatia, D.; Krishnan, Y. A method to study in vivo stability of DNA nanostructures. *Methods* **2013**, *64*, 94-100. doi: 10.1016/j.ymeth.2013.04.002.
- (103) Bujold, K. E.; Fakhoury, J.; Edwardson, T. G. W.; Carneiro, K. M. M.; Briard, J. N.; Godin, A. G.; Amrein, L.; Hamblin, G. D.; Panasci, L. C.; Wiseman, P. W.; Sleiman, H. F. Sequence-responsive unzipping DNA cubes with tunable cellular uptake profiles. *Chem. Sci.* **2014**, *5*, 2449-2455. doi: 10.1039/c4sc00646a.
- (104) Keum, J. W.; Bermudez, H. Enhanced resistance of DNA nanostructures to enzymatic digestion. *Chem. Commun.* **2009**, 7036-7038. doi: 10.1039/b917661f.
- (105) McLaughlin, C. K.; Hamblin, G. D.; Hänni, K. D.; Conway, J. W.; Nayak, M. K.; Carneiro, K. M. M.; Bazzi, H. S.; Sleiman, H. F. Three-dimensional organization of block copolymers on "DNA-minimal" scaffolds. *J. Am. Chem. Soc.* **2012**, *134*, 4280-4286. doi: 10.1021/ja210313p.

- (106) Mei, Q.; Wei, X.; Su, F.; Liu, Y.; Youngbull, C.; Johnson, R.; Lindsay, S.; Yan, H.; Meldrum, D. Stability of DNA origami nanoarrays in cell lysate. *Nano Lett.* **2011**, *11*, 1477-1482. doi: 10.1021/nl1040836.
- (107) Walsh, A. S.; Yin, H.; Erben, C. M.; Wood, M. J. A.; Turberfield, A. J.; Al, W. E. T. DNA Cage Delivery to Mammalian Cells. *ACS nano* **2011**, *5*, 5427-5432. doi: 10.1021/nn2005574.
- (108) Conway, J. W.; McLaughlin, C. K.; Castor, K. J.; Sleiman, H. DNA nanostructure serum stability: greater than the sum of its parts. *Chem. Commun.* **2013**, *49*, 1172-1174. doi: 10.1039/c2cc37556g.
- (109) Plochowietz, A.; El-Sagheer, A. H.; Brown, T.; Kapanidis, A. N. Stable End-Sealed DNA as Robust Nano-rulers for In Vivo Single-Molecule Fluorescence. *Chem. Sci.* **2016**, *7*, 4418. doi: 10.1039/C6SC00639F.
- (110) Shi, H.; He, X.; Cui, W.; Wang, K.; Deng, K.; Li, D.; Xu, F. Locked nucleic acid/DNA chimeric aptamer probe for tumor diagnosis with improved serum stability and extended imaging window in vivo. *Anal. Chim. Acta* **2014**, *812*, 138-144. doi: 10.1016/j.aca.2013.12.023.
- (111) Zhang, Z.; Tao, C. Rational design of a mismatched aptamer-DNA duplex probe to improve the analytical performance of electrochemical aptamer sensors. *Electrochim. Acta* **2016**, *209*, 479-485. doi: 10.1016/j.electacta.2016.05.107.
- (112) Pastore, M. N.; Kalia, Y. N.; Horstmann, M.; Roberts, M. S. Transdermal patches: history, development and pharmacology. *Br. J. Pharmacol.* **2015**, *172*, 2179-2209. doi: 10.1111/bph.13059.
- (113) Miyamoto, A.; Lee, S.; Cooray, N. F.; Lee, S.; Mori, M.; Matsuhisa, N.; Jin, H.; Yoda, L.; Yokota, T.; Itoh, A.; Sekino, M.; Kawasaki, H.; Ebihara, T.; Amagai, M.; Someya, T. Inflammation-free, gas-permeable, lightweight, stretchable on-skin electronics with nanomeshes. *Nat. Nanotechnol.* **2017**, *12*, 907. doi: 10.1038/nnano.2017.125.
- (114) Maisel, W. H. Semper Fidelis — Consumer Protection for Patients with Implanted Medical Devices. *N. Engl. J. Med.* **2008**, *358*, 985-987. doi: 10.1056/NEJMp0800495.
- (115) Papadimitrakopoulos, F.; Costa, A.; Jain, F.; Vaddiraju, S., *Automated insertion and extraction of an implanted biosensor* U.S. Patent Application Publication US 2017/0027608 A1, Feb. 2, 2017.
- (116) Kotanen, C. N.; Guiseppi-Elie, A. Characterization of a Wireless Potentiostat for Integration With a Novel Implantable Biotransducer. *IEEE Sensors J.* **2014**, *14*, 768-776. doi: 10.1109/JSEN.2013.2288059.
- (117) Kilinc, E. G.; Baj-Rossi, C.; Ghoreishizadeh, S.; Riario, S.; Stradolini, F.; Boero, C.; Micheli, G. D.; Maloberti, F.; Carrara, S.; Dehollain, C. A System for Wireless Power Transfer and Data Communication of Long-Term Bio-Monitoring. *IEEE Sensors J.* **2015**, *15*, 6559-6569. doi: 10.1109/jsen.2015.2462362.
- (118) Su, W.; Gao, X.; Jiang, L.; Qin, J. Microfluidic platform towards point-of-care diagnostics in infectious diseases. *J. Chromatogr. A* **2015**, *1377*, 13-26. doi: https://doi.org/10.1016/j.chroma.2014.12.041.

- (119) Hartman, M. R.; Ruiz, R. C. H.; Hamada, S.; Xu, C. Y.; Yancey, K. G.; Yu, Y.; Han, W.; Luo, D. Point-of-care nucleic acid detection using nanotechnology. *Nanoscale* **2013**, *5*, 10141-10154. doi: 10.1039/c3nr04015a.
- (120) Hsieh, K.; Ferguson, B. S.; Eisenstein, M.; Plaxco, K. W.; Soh, H. T. Integrated electrochemical microsystems for genetic detection of pathogens at the point of care. *Acc. Chem. Res.* **2015**, *48*, 911-920. doi: 10.1021/ar500456w.
- (121) Ferguson, B. S.; Buchsbaum, S. F.; Swensen, J. S.; Hsieh, K.; Lou, X.; Soh, H. T. Integrated Microfluidic Electrochemical DNA Sensor. *Anal. Chem.* **2009**, *81*, 6503-6508. doi: 10.1021/ac900923e.
- (122) Ranamukhaarachchi, S. A.; Padeste, C.; Dubner, M.; Hafeli, U. O.; Stoeber, B.; Cadarso, V. J. Integrated hollow microneedle-optofluidic biosensor for therapeutic drug monitoring in sub-nanoliter volumes. *Sci. Rep.* **2016**, *6*, 29075. doi: 10.1038/srep29075.
- (123) Curto, V. F.; Fay, C.; Coyle, S.; Byrne, R.; O'Toole, C.; Barry, C.; Hughes, S.; Moyna, N.; Diamond, D.; Benito-Lopez, F. Real-time sweat pH monitoring based on a wearable chemical barcode micro-fluidic platform incorporating ionic liquids. *Sens. Actuators, B* **2012**, *171-172*, 1327-1334. doi: <https://doi.org/10.1016/j.snb.2012.06.048>.
- (124) Mohan, A. M. V.; Windmiller, J. R.; Mishra, R. K.; Wang, J. Continuous minimally-invasive alcohol monitoring using microneedle sensor arrays. *Biosens. Bioelectron.* **2017**, *91*, 574-579. doi: <https://doi.org/10.1016/j.bios.2017.01.016>.
- (125) Mishra, R. K.; Vinu Mohan, A. M.; Soto, F.; Chrostowski, R.; Wang, J. A microneedle biosensor for minimally-invasive transdermal detection of nerve agents. *Analyst* **2017**, *142*, 918-924. doi: 10.1039/c6an02625g.
- (126) Sahan, A. R.; Celestino, P.; Urs, O. H.; Boris, S.; Victor, J. C. Design considerations of a hollow microneedle-optofluidic biosensing platform incorporating enzyme-linked assays. *J. Micromech. Microeng.* **2018**, *28*, 024002. doi: 10.1088/1361-6439/aa9c9c.
- (127) Lee, H.; Song, C.; Hong, Y. S.; Kim, M. S.; Cho, H. R.; Kang, T.; Shin, K.; Choi, S. H.; Hyeon, T.; Kim, D.-H. Wearable/disposable sweat-based glucose monitoring device with multistage transdermal drug delivery module. *Sci. Adv.* **2017**, *3*, e1601314. doi: 10.1126/sciadv.1601314.
- (128) Wang, H.; Pastorin, G.; Lee, C. Toward Self-Powered Wearable Adhesive Skin Patch with Bendable Microneedle Array for Transdermal Drug Delivery. *Adv. Sci. (Weinheim, Ger.)* **2016**, *3*, 1500441. doi: 10.1002/advs.201500441.
- (129) Kang, J.; Matsumoto, Y.; Li, X.; Jiang, J.; Xie, X.; Kawamoto, K.; Kenmoku, M.; Chu, J. H.; Liu, W.; Mao, J.; Ueno, K.; Banerjee, K. On-chip intercalated-graphene inductors for next-generation radio frequency electronics. *Nat. Electron.* **2018**, *1*, 46-51. doi: 10.1038/s41928-017-0010-z.
- (130) Xu, S.; Zhang, Y.; Jia, L.; Mathewson, K. E.; Jang, K. I.; Kim, J.; Fu, H.; Huang, X.; Chava, P.; Wang, R.; Bhole, S.; Wang, L.; Na, Y. J.; Guan, Y.; Flavin, M.; Han, Z.; Huang, Y.; Rogers, J. A. Soft microfluidic assemblies of sensors, circuits, and radios for the skin. *Science* **2014**, *344*, 70-74. doi: 10.1126/science.1250169.

- (131) He, Y.; Matthews, B.; Wang, J.; Song, L.; Wang, X.; Wu, G. Innovation and challenges in materials design for flexible rechargeable batteries: from 1D to 3D. *J. Mater. Chem. A* **2018**, *6*, 735-753. doi: 10.1039/C7TA09301B.
- (132) Zamarayeva, A. M.; Ostfeld, A. E.; Wang, M.; Duey, J. K.; Deckman, I.; Lechêne, B. P.; Davies, G.; Steingart, D. A.; Arias, A. C. Flexible and stretchable power sources for wearable electronics. *Sci. Adv.* **2017**, *3*, e1602051. doi: 10.1126/sciadv.1602051.
- (133) Pu, X.; Guo, H.; Chen, J.; Wang, X.; Xi, Y.; Hu, C.; Wang, Z. L. Eye motion triggered self-powered mechnosensational communication system using triboelectric nanogenerator. *Sci. Adv.* **2017**, *3*. doi: 10.1126/sciadv.1700694.
- (134) Chen, X. Y.; Wu, Y. L.; Shao, J. J.; Jiang, T.; Yu, A. F.; Xu, L.; Wang, Z. L. On-Skin Triboelectric Nanogenerator and Self-Powered Sensor with Ultrathin Thickness and High Stretchability. *Small* **2017**, *13*. doi: 10.1002/smll.201702929.
- (135) Liu, Z.; Zhang, S.; Jin, Y. M.; Ouyang, H.; Zou, Y.; Wang, X. X.; Xie, L. X.; Li, Z. Flexible piezoelectric nanogenerator in wearable self-powered active sensor for respiration and healthcare monitoring. *Semicond. Sci. Technol.* **2017**, *32*, 064004. doi: 10.1088/1361-6641/aa68d1.
- (136) Lee, J. W.; Cho, H. J.; Chun, J.; Kim, K. N.; Kim, S.; Ahn, C. W.; Kim, I. W.; Kim, J.-Y.; Kim, S.-W.; Yang, C.; Baik, J. M. Robust nanogenerators based on graft copolymers via control of dielectrics for remarkable output power enhancement. *Sci. Adv.* **2017**, *3*. doi: 10.1126/sciadv.1602902.
- (137) Yu, Y.; Sun, H.; Orbay, H.; Chen, F.; England, C. G.; Cai, W.; Wang, X. Biocompatibility and in vivo operation of implantable mesoporous PVDF-based nanogenerators. *Nano Energy* **2016**, *27*, 275-281. doi: 10.1016/j.nanoen.2016.07.015.
- (138) Song, K.; Han, J. H.; Yang, H. C.; Nam, K. I.; Lee, J. Generation of electrical power under human skin by subdermal solar cell arrays for implantable bioelectronic devices. *Biosens. Bioelectron.* **2017**, *92*, 364-371. doi: <https://doi.org/10.1016/j.bios.2016.10.095>.
- (139) Wang, X.; Yin, Y.; Yi, F.; Dai, K.; Niu, S.; Han, Y.; Zhang, Y.; You, Z. Bioinspired stretchable triboelectric nanogenerator as energy-harvesting skin for self-powered electronics. *Nano Energy* **2017**, *39*, 429-436. doi: <https://doi.org/10.1016/j.nanoen.2017.07.022>.
- (140) Fan, D.; Ruiz, L. L.; Gong, J.; Lach, J. EHDC: An Energy Harvesting Modeling and Profiling Platform for Body Sensor Networks. *IEEE J. Biomed. Health Inform.* **2018**, *22*, 33-39. doi: 10.1109/jbhi.2017.2733549.
- (141) Wen, Z.; Yeh, M.-H.; Guo, H.; Wang, J.; Zi, Y.; Xu, W.; Deng, J.; Zhu, L.; Wang, X.; Hu, C.; Zhu, L.; Sun, X.; Wang, Z. L. Self-powered textile for wearable electronics by hybridizing fiber-shaped nanogenerators, solar cells, and supercapacitors. *Sci. Adv.* **2016**, *2*. doi: 10.1126/sciadv.1600097.
- (142) Lui, K. W.; Murphy, O. H.; Toumazou, C. 32- μ W Wirelessly-Powered Sensor Platform With a 2-m Range. *IEEE Sensors J.* **2012**, *12*, 1919-1924. doi: 10.1109/jsen.2011.2181356.

- (143) Sanni, A.; Vilches, A.; Toumazou, C. Inductive and Ultrasonic Multi-Tier Interface for Low-Power, Deeply Implantable Medical Devices. *IEEE Trans. Biomed. Circuits Syst.* **2012**, *6*, 297-308. doi: 10.1109/tbcas.2011.2175390.
- (144) Pang, S.; Gao, Y.; Choi, S. Flexible and Stretchable Biobatteries: Monolithic Integration of Membrane-Free Microbial Fuel Cells in a Single Textile Layer. *Adv. Energy Mater.* **2017**, 1702261. doi: 10.1002/aenm.201702261.
- (145) Blomgren, G. E. The Development and Future of Lithium Ion Batteries. *J. Electrochem. Soc.* **2016**, *164*, A5019-A5025. doi: 10.1149/2.0251701jes.
- (146) Mena, C. D.; Gerba, C. P. Risk Assessment of *Pseudomonas aeruginosa* in Water. *Rev. Environ. Contam. Toxicol.* **2009**, *201*, 71-115. doi: 10.1007/978-1-4419-0032-6_3.
- (147) Baym, M.; Shaket, L.; Anzai, I. A.; Adesina, O.; Barstow, B. Rapid construction of a whole-genome transposon insertion collection for *Shewanella oneidensis* by Knockout Sudoku. *Nat. Commun.* **2016**, *7*, 13270. doi: 10.1038/ncomms13270.
- (148) Adesina, O.; Anzai, I. A.; Avalos, J. L.; Barstow, B. Embracing Biological Solutions to the Sustainable Energy Challenge. *Chem* **2017**, *2*, 20-51. doi: <https://doi.org/10.1016/j.chempr.2016.12.009>.
- (149) Shaikh, F. K.; Zeadally, S. Energy harvesting in wireless sensor networks: A comprehensive review. *Renewable Sustainable Energy Rev.* **2016**, *55*, 1041-1054. doi: 10.1016/j.rser.2015.11.010.
- (150) Misra, V.; Bozkurt, A.; Calhoun, B.; Jackson, T.; Jur, J. S.; Lach, J.; Lee, B.; Muth, J.; Ö, O.; Öztürk, M.; Troler-McKinstry, S.; Vashae, D.; Wentzloff, D.; Zhu, Y. Flexible Technologies for Self-Powered Wearable Health and Environmental Sensing. *Proc. IEEE* **2015**, *103*, 665-681. doi: 10.1109/jproc.2015.2412493.
- (151) Sarpeshkar, R. Universal Principles for Ultra Low Power and Energy Efficient Design. *IEEE Trans. Circuits Syst. II, Express Briefs* **2012**, *59*, 193-198. doi: 10.1109/tcsii.2012.2188451.
- (152) Dementyev, A.; Hodges, S.; Taylor, S.; Smith, J., *Power consumption analysis of Bluetooth Low Energy, ZigBee and ANT sensor nodes in a cyclic sleep scenario*. 2013 IEEE International Wireless Symposium (IWS), **2013**, pp. 1-4. doi: 10.1109/iee-iws.2013.6616827.
- (153) Lee, J. W.; Xu, R.; Lee, S.; Jang, K.-I.; Yang, Y.; Banks, A.; Yu, K. J.; Kim, J.; Xu, S.; Ma, S.; Jang, S. W.; Won, P.; Li, Y.; Kim, B. H.; Choe, J. Y.; Huh, S.; Kwon, Y. H.; Huang, Y.; Paik, U.; Rogers, J. A. Soft, thin skin-mounted power management systems and their use in wireless thermography. *Proc. Natl. Acad. Sci. U.S.A.* **2016**, 201605720. doi: 10.1073/pnas.1605720113.
- (154) Wang, H.; Wang, X.; Barfidokht, A.; Park, J.; Wang, J.; Mercier, P. P. A Battery-Powered Wireless Ion Sensing System Consuming 5.5 nW of Average Power. *IEEE J. Solid-State Circuits* **2018**, *53*, 2043-2053. doi: 10.1109/jssc.2018.2815657.
- (155) Allotrope Foundation, "*Allotrope - Rethinking Scientific Data*", can be found under <https://www.allotrope.org/>, **2018**.

- (156) Sohbaty, M.; Toumazou, C. Dimension and Shape Effects on the ISFET Performance. *IEEE Sensors J.* **2015**, *15*, 1670-1679. doi: 10.1109/jsen.2014.2365291.
- (157) Hertleer, C.; Langenhove, L. V.; Rogier, H.; Vallozzi, L., *Off-body Communication for Protective Clothing*. 2009 Sixth International Workshop on Wearable and Implantable Body Sensor Networks, **2009**, pp. 301-304. doi: 10.1109/bsn.2009.37.
- (158) Murphy, O. H.; Borghi, A.; Bahmanyar, M. R.; McLeod, C. N.; Navaratnarajah, M.; Yacoub, M.; Toumazou, C. RF communication with implantable wireless device: effects of beating heart on performance of miniature antenna. *Healthc. Technol. Lett.* **2014**, *1*, 51-55. doi: 10.1049/htl.2014.0066.
- (159) Medtronic, "*Continuous Glucose Monitoring*", can be found under <https://www.medtronicdiabetes.com/treatments/continuous-glucose-monitoring>, **2018**.
- (160) Zilberman, M.; Elsner, J. J. Antibiotic-eluting medical devices for various applications. *J. Controlled Release* **2008**, *130*, 202-215. doi: <https://doi.org/10.1016/j.jconrel.2008.05.020>.
- (161) Nelson, E. C.; Verhagen, T.; Noordzij, M. L. Health empowerment through activity trackers: An empirical smart wristband study. *Comput. Hum. Behav.* **2016**, *62*, 364-374. doi: 10.1016/j.chb.2016.03.065.
- (162) Day, C.-P.; Merlino, G.; Van Dyke, T. Preclinical Mouse Cancer Models: A Maze of Opportunities and Challenges. *Cell* **2015**, *163*, 39-53. doi: 10.1016/j.cell.2015.08.068.
- (163) Amano, Y.; Koto, A.; Matsuzaki, S.; Sakamoto, H.; Satomura, T.; Suye, S. I. Construction of a biointerface on a carbon nanotube surface for efficient electron transfer. *Mater. Lett.* **2016**, *174*, 184-187. doi: 10.1016/j.matlet.2016.03.113.
- (164) Kim, S. J.; Cho, K. W.; Cho, H. R.; Wang, L.; Park, S. Y.; Lee, S. E.; Hyeon, T.; Lu, N.; Choi, S. H.; Kim, D.-H. Stretchable and Transparent Biointerface Using Cell-Sheet-Graphene Hybrid for Electrophysiology and Therapy of Skeletal Muscle. *Adv. Funct. Mater.* **2016**, *26*, 3207-3217. doi: 10.1002/adfm.201504578.
- (165) Ou, K.-L.; Chu, J.-S.; Hosseinkhani, H.; Chiou, J.-F.; Yu, C.-H. Biomedical nanostructured coating for minimally invasive surgery devices applications: characterization, cell cytotoxicity evaluation and an animal study in rat. *Surg. Endosc.* **2014**, *28*, 2174-2188. doi: 10.1007/s00464-014-3450-9.
- (166) Alcaide, M.; Taylor, A.; Fjorback, M.; Zachar, V.; Pennisi, C. P. Boron-Doped Nanocrystalline Diamond Electrodes for Neural Interfaces: In vivo Biocompatibility Evaluation. *Front. Neurosci.* **2016**, *10*, 87. doi: 10.3389/fnins.2016.00087.
- (167) Jeong, J.; Bae, S. H.; Seo, J.-M.; Chung, H.; Kim, S. J. Long-term evaluation of a liquid crystal polymer (LCP)-based retinal prosthesis. *J. Neural Eng.* **2016**, *13*, 25004. doi: 10.1088/1741-2560/13/2/025004.
- (168) Knaack, G. L.; McHail, D. G.; Borda, G.; Koo, B. S.; Peixoto, N.; Cogan, S. F.; Dumas, T. C.; Pancrazio, J. J. In vivo Characterization of Amorphous Silicon Carbide as a Biomaterial for Chronic Neural Interfaces. *Front. Neurosci.* **2016**, *10*, 301. doi: 10.3389/FNINS.2016.00301.

- (169) Stauffer, O.; Weber, S.; Bengtson, C. P.; Bading, H.; Spatz, J. P.; Rustom, A. Functional fusion of living systems with synthetic electrode interfaces. *Beilstein J. Nanotechnol.* **2016**, *7*, 296-301. doi: 10.3762/bjnano.7.27.
- (170) Sun, K.-H.; Liu, Z.; Liu, C.; Yu, T.; Shang, T.; Huang, C.; Zhou, M.; Liu, C.; Ran, F.; Li, Y.; Shi, Y.; Pan, L. Evaluation of in vitro and in vivo biocompatibility of a myo-inositol hexakisphosphate gelated polyaniline hydrogel in a rat model. *Sci. Rep.* **2016**, *6*, 23931. doi: 10.1038/srep23931.
- (171) Rahimi, R.; Ochoa, M.; Parupudi, T.; Zhao, X.; Yazdi, I. K.; Dokmeci, M. R.; Tamayol, A.; Khademhosseini, A.; Ziaie, B. A low-cost flexible pH sensor array for wound assessment. *Sens. Actuators, B* **2016**, *229*, 609-617. doi: 10.1016/j.snb.2015.12.082.
- (172) Worley, B. V.; Schilly, K. M.; Schoenfish, M. H. Anti-Biofilm Efficacy of Dual-Action Nitric Oxide-Releasing Alkyl Chain Modified Poly(amidoamine) Dendrimers. *Mol. Pharmaceutics* **2015**, *12*, 1573-1583. doi: 10.1021/acs.molpharmaceut.5b00006.
- (173) Li, H.; Dauphin-Ducharme, P.; Arroyo-Curras, N.; Tran, C. H.; Vieira, P. A.; Li, S.; Shin, C.; Somerson, J.; Kippin, T. E.; Plaxco, K. W. A Biomimetic Phosphatidylcholine-Terminated Monolayer Greatly Improves the In Vivo Performance of Electrochemical Aptamer-Based Sensors. *Angew Chem Int Ed Engl* **2017**, *56*, 7492-7495. doi: 10.1002/anie.201700748.
- (174) Ahnood, A.; Fox, K. E.; Apollo, N. V.; Lohrmann, A.; Garrett, D. J.; Nayagam, D. A. X.; Karle, T.; Stacey, A.; Abberton, K. M.; Morrison, W. A.; Blakers, A.; Prawer, S. Diamond encapsulated photovoltaics for transdermal power delivery. *Biosens. Bioelectron.* **2016**, *77*, 589-597. doi: 10.1016/j.bios.2015.10.022.
- (175) Teo, A.; Mishra, A.; Park, I.; Kim, Y.-J.; Park, W.-T.; Yoon, Y. J. Polymeric Biomaterials for Medical Implants & Devices. *ACS Biomater. Sci. Eng.* **2016**, *2*, 454-472. doi: 10.1021/acsbomaterials.5b00429.
- (176) Cisternas, R.; Ballesteros, L.; Valenzuela, M. L.; Kahlert, H.; Scholz, F. Decreasing the time response of calibration-free pH sensors based on tungsten bronze nanocrystals. *J. Electroanal. Chem.* **2017**, *801*, 315-318. doi: 10.1016/j.jelechem.2017.08.005.
- (177) Li, H.; Dauphin-Ducharme, P.; Ortega, G.; Plaxco, K. W. Calibration-Free Electrochemical Biosensors Supporting Accurate Molecular Measurements Directly in Undiluted Whole Blood. *J. Am. Chem. Soc.* **2017**, *139*, 11207-11213. doi: 10.1021/jacs.7b05412.
- (178) Steinberg, M. D.; Kassal, P.; Steinberg, I. M. System Architectures in Wearable Electrochemical Sensors. *Electroanalysis* **2016**, *28*, 1149-1169. doi: 10.1002/elan.201600094.
- (179) Bandodkar, A. J.; Nunez-Flores, R.; Jia, W.; Wang, J. All-printed stretchable electrochemical devices. *Adv. Mater.* **2015**, *27*, 3060-3065. doi: 10.1002/adma.201500768.
- (180) Nawrocki, R. A.; Matsuhisa, N.; Yokota, T.; Someya, T. 300-nm Imperceptible, Ultraflexible, and Biocompatible e-Skin Fit with Tactile Sensors and Organic Transistors. *Adv. Electron. Mater.* **2016**, *2*, 1500452. doi: 10.1002/aelm.201500452.

- (181) Williams-Grut, O., "*Hackers once stole a casino's high-roller database through a thermometer in the lobby fish tank*", can be found under <https://www.businessinsider.de/hackers-stole-a-casinos-database-through-a-thermometer-in-the-lobby-fish-tank-2018-4?r=UK&IR=T>, **2018**.
- (182) Morgan, S., "*2017 Cybercrime Report*", can be found under <https://cybersecurityventures.com/2015-wp/wp-content/uploads/2017/10/2017-Cybercrime-Report.pdf>, **2017**.
- (183) Khalil, Y. F. A novel probabilistically timed dynamic model for physical security attack scenarios on critical infrastructures. *Process Saf. Environ. Prot.* **2016**, *102*, 473-484. doi: 10.1016/j.psep.2016.05.001.
- (184) Chen, P. Y.; Cheng, S. M.; Chen, K. C. Smart Attacks in Smart Grid Communication Networks. *IEEE Commun. Mag.* **2012**, *50*, 24-29. doi: 10.1109/mcom.2012.6257523.
- (185) Panguluri, S.; Phillips, W.; Cusimano, J. Protecting water and wastewater infrastructure from cyber attacks. *Front. Earth Sci.* **2011**, *5*, 406-413. doi: 10.1007/s11707-011-0199-5.
- (186) Jarmakiewicz, J.; Parobczak, K.; Maślanka, K. Cybersecurity protection for power grid control infrastructures. *Int. J. Crit. Infrastruct. Prot.* **2017**, *18*, 20-33. doi: 10.1016/j.ijcip.2017.07.002.
- (187) Khanduzi, R.; Peyghami, M. R.; Sangaiah, A. K. Data envelopment analysis and interdiction median problem with fortification for enabling IoT technologies to relieve potential attacks. *Future Gener. Comput. Syst.* **2018**, *79*, 928-940. doi: 10.1016/j.future.2017.08.056.
- (188) Wu, L.; Zhang, Y.; Li, L.; Shen, J. Efficient and Anonymous Authentication Scheme for Wireless Body Area Networks. *J. Med. Syst.* **2016**, *40*, 134. doi: 10.1007/s10916-016-0491-8.
- (189) Halperin, D.; Heydt-Benjamin, T. S.; Fu, K.; Kohno, T.; Maisel, W. H. Security and Privacy for Implantable Medical Devices. *IEEE Pervasive Computing* **2008**, *7*, 30-39. doi: 10.1109/mpvr.2008.16.
- (190) Lecoutere, J.; Thielens, A.; Agneessens, S.; Rogier, H.; Joseph, W.; Puers, R. Wireless Fidelity Electromagnetic Field Exposure Monitoring With Wearable Body Sensor Networks. *IEEE Trans. Biomed. Circuits Syst.* **2016**, *10*, 779-786. doi: 10.1109/tbcas.2015.2487264.
- (191) Schaefer, K.; Einax, J. W. Source Apportionment and Geostatistics: An Outstanding Combination for Describing Metals Distribution in Soil. *Clean: Soil, Air, Water* **2016**, *44*, 877-884. doi: 10.1002/clen.201400459.
- (192) Baborowski, M.; Einax, J. W. Flood-event based metal distribution patterns in water as approach for source apportionment of pollution on catchment scale: Examples from the River Elbe. *J. Hydrol. (Amsterdam, Neth.)* **2016**, *535*, 429-437. doi: 10.1016/j.jhydrol.2016.01.077.
- (193) Pourjabbar, A.; Sârbu, C.; Kostarelos, K.; Einax, J. W.; Büchel, G. Fuzzy hierarchical cross-clustering of data from abandoned mine site contaminated with heavy metals. *Comput. Geosci.* **2014**, *72*, 122-133. doi: 10.1016/j.cageo.2014.07.004.

- (194) Möller, S.; Einax, J. W. Metals in sediments — spatial investigation of Saale River applying chemometric tools. *Microchem. J.* **2013**, *110*, 233-238. doi: 10.1016/j.microc.2013.03.017.
- (195) Kötschau, A.; Büchel, G.; Einax, J. W.; Meißner, R.; von Tümpling, W.; Merten, D. Element pattern recognition and classification in sunflowers (*Helianthus annuus*) grown on contaminated and non-contaminated soil. *Microchem. J.* **2014**, *114*, 164-174. doi: 10.1016/j.microc.2013.12.006.
- (196) Aitkenhead, M. J.; Coull, M. C.; Dawson, L. A. Predicting Sample Source Location from Soil Analysis Using Neural Networks. *Environ. Forensics* **2014**, *15*, 281-292. doi: 10.1080/15275922.2014.930764.
- (197) Kelly, S. D. T.; Suryadevara, N. K.; Mukhopadhyay, S. C. Towards the Implementation of IoT for Environmental Condition Monitoring in Homes. *IEEE Sensors J.* **2013**, *13*, 3846-3853. doi: 10.1109/jsen.2013.2263379.
- (198) Jang, W.-S.; Healy, W. M.; Skibniewski, M. J. Wireless sensor networks as part of a web-based building environmental monitoring system. *Automat. Constr.* **2008**, *17*, 729-736. doi: 10.1016/j.autcon.2008.02.001.
- (199) Mandel, J. T.; Bohrer, G.; Winkler, D. W.; Barber, D. R.; Houston, C. S.; Bildstein, K. L. Migration path annotation: of migration-flight response cross -continental to environmental study conditions. *Ecol. Appl.* **2011**, *21*, 2258-2268. doi: 10.1890/10-1651.1.
- (200) Gumus, A.; Lee, S.; Ahsan, S. S.; Karlsson, K.; Gabrielson, R.; Guglielmo, C. G.; Winkler, D. W.; Erickson, D. Lab-on-a-bird: Biophysical monitoring of flying birds. *PLoS One* **2015**, *10*, 1-10. doi: 10.1371/journal.pone.0123947.
- (201) Massé, F.; Bourke, A. K.; Chardonens, J.; Paraschiv-Ionescu, A.; Aminian, K. Suitability of commercial barometric pressure sensors to distinguish sitting and standing activities for wearable monitoring. *Med. Eng. Phys.* **2014**, *36*, 739-744. doi: 10.1016/j.medengphy.2014.01.001.
- (202) Darabi, M. A.; Khosrozadeh, A.; Wang, Q.; Xing, M. Gum Sensor: A Stretchable, Wearable, and Foldable Sensor Based on Carbon Nanotube/Chewing Gum Membrane. *ACS Appl. Mater. Interfaces* **2015**, *7*, 26195-26205. doi: 10.1021/acsami.5b08276.
- (203) Wang, Z.; Song, C.; Yin, H.; Zhang, J. Capacitive humidity sensors based on zinc oxide nanorods grown on silicon nanowires arrays at room temperature. *Sens. Actuators, A* **2015**, *235*, 234-239. doi: 10.1016/j.sna.2015.10.020.
- (204) Johnson, K. S.; Jannasch, H. W.; Coletti, L. J.; Elrod, V. A.; Martz, T. R.; Takeshita, Y.; Carlson, R. J.; Connery, J. G. Deep-Sea DuraFET: A Pressure Tolerant pH Sensor Designed for Global Sensor Networks. *Anal. Chem.* **2016**, *88*, 3249-3256. doi: 10.1021/acs.analchem.5b04653.
- (205) Chiesa, M.; Rigoni, F.; Paderno, M.; Borghetti, P.; Gagliotti, G.; Bertoni, M.; Ballarin Denti, A.; Schiavina, L.; Goldoni, A.; Sangaletti, L. Development of low-cost ammonia gas sensors and data analysis algorithms to implement a monitoring grid

- of urban environmental pollutants. *J. Environ. Monit.* **2012**, *14*, 1565. doi: 10.1039/c2em30102d.
- (206) Penza, M.; Rossi, R.; Alvisi, M.; Serra, E. Metal-modified and vertically aligned carbon nanotube sensors array for landfill gas monitoring applications. *Nanotechnology* **2010**, *21*, 105501. doi: 10.1088/0957-4484/21/10/105501.
- (207) Bourgeois, W.; Romain, A.-C.; Nicolas, J.; Stuetz, R. M. The use of sensor arrays for environmental monitoring: interests and limitations. *J. Environ. Monit.* **2003**, *5*, 852. doi: 10.1039/b307905h.
- (208) Im, J.; Sterner, S. E.; Swager, M. T. Integrated Gas Sensing System of SWCNT and Cellulose Polymer Concentrator for Benzene, Toluene, and Xylenes. *Sensors (Basel)* **2016**, *16*. doi: 10.3390/s16020183.
- (209) Ishihara, S.; Azzarelli, J. M.; Krikorian, M.; Swager, T. M. Ultratrace Detection of Toxic Chemicals: Triggered Disassembly of Supramolecular Nanotube Wrappers. *J. Am. Chem. Soc.* **2016**, *138*, 8221-8227. doi: 10.1021/jacs.6b03869.
- (210) Fahad, H. M.; Shiraki, H.; Amani, M.; Zhang, C.; Hebbbar, V. S.; Gao, W.; Ota, H.; Hettick, M.; Kiriya, D.; Chen, Y.-Z.; Chueh, Y.-L.; Javey, A. Room temperature multiplexed gas sensing using chemical-sensitive 3.5-nm-thin silicon transistors. *Sci. Adv.* **2017**, *3*. doi: 10.1126/sciadv.1602557.
- (211) Mead, M. I.; Popoola, O. A. M.; Stewart, G. B.; Landshoff, P.; Calleja, M.; Hayes, M.; Baldovi, J. J.; McLeod, M. W.; Hodgson, T. F.; Dicks, J.; Lewis, A.; Cohen, J.; Baron, R.; Saffell, J. R.; Jones, R. L. The use of electrochemical sensors for monitoring urban air quality in low-cost, high-density networks. *Atmos. Environ.* **2013**, *70*, 186-203. doi: 10.1016/j.atmosenv.2012.11.060.
- (212) Hancke, G. P.; Silva, B. d. C. E.; Hancke, G. P., Jr. The role of advanced sensing in smart cities. *Sensors (Basel)* **2012**, *13*, 393-425. doi: 10.3390/s130100393.
- (213) Broday, D. M.; Citi-Sense Project, C. Wireless Distributed Environmental Sensor Networks for Air Pollution Measurement The Promise and the Current Reality. *Sensors (Basel)* **2017**, *17*. doi: 10.3390/s17102263.
- (214) Kozloski, J. R.; Lynar, T. M.; Pickover, C. A.; Wagner, J. M., *Drone-based microbial analysis system*. U.S. Patent US 9,447,448 B1, Sept. 20, 2016.
- (215) Tauro, F.; Petroselli, A.; Arcangeletti, E. Assessment of drone-based surface flow observations. *Hydrol. Processes* **2015**, *30*, 1114-1130. doi: 10.1002/hyp.10698.
- (216) Capolupo, A.; Pindozi, S.; Okello, C.; Fiorentino, N.; Boccia, L. Photogrammetry for environmental monitoring: The use of drones and hydrological models for detection of soil contaminated by copper. *Sci. Total Environ.* **2015**, *514*, 298-306. doi: 10.1016/j.scitotenv.2015.01.109.
- (217) Ojha, T.; Misra, S.; Singh, N. Wireless sensor networks for agriculture : The state-of-the-art in practice and future challenges. *Comput. Electron. Agric.* **2015**, *118*, 66-84. doi: 10.1016/j.compag.2015.08.011.
- (218) Hest, D., "new-driverless-tractor-grain-cart-systems-coming-year @ farmindustrynews.com", can be found under

<http://www.farministrynews.com/precision-guidance/new-driverless-tractor-grain-cart-systems-coming-year>, **2012**.

- (219) Reinards, M.; Kormann, G.; Scheff, U., in *Handbook of Driver Assistance Systems: Basic Information, Components and Systems for Active Safety and Comfort* (Eds.: Winner, H.; Hakuli, S.; Lotz, F.; Singer, C.), Springer International Publishing, Cham, **2014**, pp. 1-19. doi: 10.1007/978-3-319-09840-1_54-1.
- (220) Blender, T.; Buchner, T.; Fernandez, B.; Pichlmaier, B.; Schlegel, C., *Managing a Mobile Agricultural Robot Swarm for a seeding task*. IECON 2016 - 42nd Annual Conference of the IEEE Industrial Electronics Society, **2016**, pp. 6879-6886. doi: 10.1109/iecon.2016.7793638.
- (221) Harris, N.; Cranny, A.; Rivers, M.; Smettem, K.; Barrett-Lennard, E. G. Application of Distributed Wireless Chloride Sensors to Environmental Monitoring : Initial Results. *IEEE Trans. Instrum. Meas.* **2016**, *65*, 736-743. doi: 10.1109/TIM.2015.2490838.
- (222) Saha, A. K.; Saha, J.; Ray, R.; Sircar, S.; Dutta, S.; Chattopadhyay, S. P.; Saha, H. N., *IOT-based drone for improvement of crop quality in agricultural field*. 2018 IEEE 8th Annual Computing and Communication Workshop and Conference (CCWC), **2018**, pp. 612-615. doi: 10.1109/ccwc.2018.8301662.
- (223) Gabriel, J. L.; Zarco-Tejada, P. J.; López-Herrera, P. J.; Pérez-Martín, E.; Alonso-Ayuso, M.; Quemada, M. Airborne and ground level sensors for monitoring nitrogen status in a maize crop. *Biosyst. Eng.* **2017**, *160*, 124-133. doi: <https://doi.org/10.1016/j.biosystemseng.2017.06.003>.
- (224) López-Granados, F.; Torres-Sánchez, J.; De Castro, A.-I.; Serrano-Pérez, A.; Mesas-Carrascosa, F.-J.; Peña, J.-M. Object-based early monitoring of a grass weed in a grass crop using high resolution UAV imagery. *Agron. Sustain. Dev.* **2016**, *36*, 67. doi: 10.1007/s13593-016-0405-7.
- (225) Reinecke, M.; Prinsloo, T., *The influence of drone monitoring on crop health and harvest size*. 2017 1st International Conference on Next Generation Computing Applications (NextComp), **2017**, pp. 5-10. doi: 10.1109/nextcomp.2017.8016168.
- (226) Oren, S.; Ceylan, H.; Schnable, P. S.; Dong, L. High-Resolution Patterning and Transferring of Graphene-Based Nanomaterials onto Tape toward Roll-to-Roll Production of Tape-Based Wearable Sensors. *Adv. Mater. Technol.* **2017**, *2*, 1700223. doi: 10.1002/admt.201700223.
- (227) Takase, M.; Murata, M.; Hibi, K.; Huifeng, R.; Endo, H. Development of mediator-type biosensor to wirelessly monitor whole cholesterol concentration in fish. *Fish Physiol. Biochem.* **2014**, *40*, 385-394. doi: 10.1007/s10695-013-9851-1.
- (228) Chelotti, J. O.; Vanrell, S. R.; Milone, D. H.; Utsumi, S. A.; Galli, J. R.; Rufiner, H. L.; Giovanini, L. L. A real-time algorithm for acoustic monitoring of ingestive behavior of grazing cattle. *Comput. Electron. Agric.* **2016**, *127*, 64-75. doi: <https://doi.org/10.1016/j.compag.2016.05.015>.
- (229) Wang, H.; Fapojuwo, A. O.; Davies, R. J. A Wireless Sensor Network for Feedlot Animal Health Monitoring. *IEEE Sensors J.* **2016**, *16*, 6433-6446. doi: 10.1109/jsen.2016.2582438.

- (230) Beng, L. T.; Kiat, P. B.; Meng, L. N.; Cheng, P. N., *Field testing of IoT devices for livestock monitoring using Wireless Sensor Network, near field communication and Wireless Power Transfer*. 2016 IEEE Conference on Technologies for Sustainability (SusTech), **2016**, pp. 169-173. doi: 10.1109/SusTech.2016.7897161.
- (231) Barriuso, L. A.; Villarrubia González, G.; De Paz, F. J.; Lozano, Á.; Bajo, J. Combination of Multi-Agent Systems and Wireless Sensor Networks for the Monitoring of Cattle. *Sensors (Basel)* **2018**, *18*. doi: 10.3390/s18010108.
- (232) Choi, S. G.; Chimeddorj, G.; Altankhuyag, B.; Dunkhorol, S., *Design and implementation of a GPS-enabled mobile wireless sensor network for livestock herd tracking in mongolian nomadic herding*. 2016 11th International Forum on Strategic Technology (IFOST), **2016**, pp. 423-427. doi: 10.1109/ifost.2016.7884144.
- (233) Le, G. T.; Tran, T. V.; Lee, H. S.; Chung, W. Y. Long-range batteryless RF sensor for monitoring the freshness of packaged vegetables. *Sensors and Actuators, A: Physical* **2016**, *237*, 20-28. doi: 10.1016/j.sna.2015.11.013.
- (234) Steiner, M.-S., Meier, R. J., Duerkop, A., Wolfbeis, O.S. Chromogenic Sensing of Biogenic Amines Using a Chameleon Probe and the Red Green Blue Readout of Digital Camera Images. *Anal. Chem.* **2010**, *82*, 8402-8405. doi: 10.1021/ac102029j.
- (235) Azab, H. a.; El-Korashy, S. a.; Anwar, Z. M.; Khairy, G. M.; Steiner, M.-S.; Duerkop, A. High-throughput sensing microtiter plate for determination of biogenic amines in seafood using fluorescence or eye-vision. *Analyst* **2011**, *136*, 4492. doi: 10.1039/c1an15049a.
- (236) Rukchon, C.; Nopwinyuwong, A.; Trevanich, S.; Jinkarn, T.; Suppakul, P. Development of a food spoilage indicator for monitoring freshness of skinless chicken breast. *Talanta* **2014**, *130*, 547-554. doi: <https://doi.org/10.1016/j.talanta.2014.07.048>.
- (237) Chen, Y.; Fu, G.; Zilberman, Y.; Ruan, W.; Ameri, S. K.; Miller, E.; Sonkusale, S., *Disposable colorimetric geometric barcode sensor for food quality monitoring*. 2017 19th International Conference on Solid-State Sensors, Actuators and Microsystems (TRANSDUCERS), **2017**, pp. 1422-1424. doi: 10.1109/transducers.2017.7994325.
- (238) Khatua, S.; Goswami, S.; Biswas, S.; Tomar, K.; Jena, H. S.; Konar, S. Stable Multiresponsive Luminescent MOF for Colorimetric Detection of Small Molecules in Selective and Reversible Manner. *Chem. Mater.* **2015**, *27*, 5349-5360. doi: 10.1021/acs.chemmater.5b01773.
- (239) Hoang, A. T.; Cho, Y. B.; Park, J. S.; Yang, Y.; Kim, Y. S. Sensitive naked-eye detection of gaseous ammonia based on dye-impregnated nanoporous polyacrylonitrile mats. *Sens. Actuators, B* **2016**, *230*, 250-259. doi: 10.1016/j.snb.2016.02.058.
- (240) Roales, J.; Pedrosa, J. M.; Guillén, M. G.; Lopes-Costa, T.; Pinto, S. M. A.; Calvete, M. J. F.; Pereira, M. M. Optical detection of amine vapors using ZnTriad porphyrin thin films. *Sens. Actuators, B* **2015**, *210*, 28-35. doi: 10.1016/j.snb.2014.12.080.
- (241) Yang, H.; Kim, D.; Kim, J.; Moon, D.; Song, H. S.; Lee, M.; Hong, S.; Park, T. H. Nanodisc-Based Bioelectronic Nose Using Olfactory Receptor Produced in

Escherichia coli for the Assessment of the Death-Associated Odor Cadaverine. *ACS nano* **2017**, *11*, 11847-11855. doi: 10.1021/acsnano.7b04992.

- (242) Liu, S. F.; Petty, A. R.; Sazama, G. T.; Swager, T. M. Single-Walled Carbon Nanotube/Metalloporphyrin Composites for the Chemiresistive Detection of Amines and Meat Spoilage. *Angew. Chem. Int. Ed.* **2015**, *54*, 6554-6557. doi: 10.1002/anie.201501434.
- (243) Azzarelli, J. M.; Mirica, K. A.; Ravnsbæk, J. B.; Swager, T. M. Wireless gas detection with a smartphone via rf communication. *Proc. Natl. Acad. Sci. U.S.A.* **2014**, *111*, 18162-18166. doi: 10.1073/pnas.1415403111.
- (244) Hezinger, A.; Mohr, G. J.; Schmidt, J.; Stich, M.; Trupp, S., *Packaging having an indicator area*. WO Application WO 2012/152531 A1, Nov. 15, 2012.
- (245) Abad, E.; Zampolli, S.; Marco, S.; Scorzoni, A.; Mazzolai, B.; Juarros, A.; Gómez, D.; Elmi, I.; Cardinali, G. C.; Gómez, J. M.; Palacio, F.; Cicioni, M.; Mondini, A.; Becker, T.; Sayhan, I. Flexible tag microlab development: Gas sensors integration in RFID flexible tags for food logistic. *Sens. Actuators, B* **2007**, *127*, 2-7. doi: 10.1016/j.snb.2007.07.007.
- (246) Sharma, N.; Zhong, Q.; Chen, Z.; Choi, W.; McMillan, J. P.; Neese, C. F.; Schueler, R.; Medvedev, I.; De Lucia, F.; K., O., *200-280GHz CMOS RF Front-End of Transmitter for Rotational Spectroscopy*. Paper presented at the IEEE Symposia on VLSI Technology and Circuits, Honolulu, Hawaii, **2016**.
- (247) Mouazen, A. M.; Kuang, B. On-line visible and near infrared spectroscopy for in-field phosphorous management. *Soil Tillage Res.* **2016**, *155*, 471-477. doi: 10.1016/j.still.2015.04.003.
- (248) Ahmad, F.; Weimin, D.; Qishuo, D.; Hussain, M.; Jabran, K. Forces and Straw Cutting Performance of Double Disc Furrow Opener in No-Till Paddy Soil. *PLoS One* **2015**, *10*, e0119648. doi: 10.1371/journal.pone.0119648.
- (249) Fried, M.; Broeshart, H., *The Soil-Plant System*. (Academic Press, New York, **1967**), pp. 368. doi: 10.1016/B978-0-12-395728-3.X5001-5.
- (250) O'Connor, T. F.; Zaretski, A. V.; Savagatrup, S.; Printz, A. D.; Wilkes, C. D.; Diaz, M. I.; Sawyer, E. J.; Lipomi, D. J. Wearable organic solar cells with high cyclic bending stability: Materials selection criteria. *Sol. Energy Mater. Sol. Cells* **2016**, *144*, 438-444. doi: <https://doi.org/10.1016/j.solmat.2015.09.049>.
- (251) Mathew, A. G.; Cissell, R.; Liamthong, S. Antibiotic resistance in bacteria associated with food animals: a United States perspective of livestock production. *Foodborne Pathog. Dis.* **2007**, *4*, 115-133. doi: 10.1089/fpd.2006.0066.
- (252) Holmberg, S. D.; Osterholm, M. T.; Senger, K. A.; Cohen, M. L. Drug-Resistant Salmonella from Animals Fed Antimicrobials. *N. Engl. J. Med.* **1984**, *311*, 617-622. doi: 10.1056/NEJM198409063111001.
- (253) Fey, P. D.; Safranek, T. J.; Rupp, M. E.; Dunne, E. F.; Ribot, E.; Iwen, P. C.; Bradford, P. A.; Angulo, F. J.; Hinrichs, S. H. Ceftriaxone-Resistant Salmonella Infection Acquired by a Child from Cattle. *N. Engl. J. Med.* **2000**, *342*, 1242-1249. doi: 10.1056/NEJM200004273421703.

- (254) Sergie, M., "Qatar Is Shipping In 3,000 Cows From California, Arizona and Wisconsin", can be found under <https://www.bloomberg.com/news/articles/2018-03-08/flying-cows-floating-cows-qatar-busts-a-boycott-to-get-milk>, **2018**.
- (255) www.c2sense.com - from farm to table. **2016**.
- (256) Emanuele II, V. A.; Panicker, G.; Gurbaxani, B. M.; Lin, J.-M. S.; Unger, E. R. Sensitive and Specific Peak Detection for SELDI-TOF Mass Spectrometry Using a Wavelet/Neural-Network Based Approach. *PLoS One* **2012**, *7*, e48103. doi: 10.1371/journal.pone.0048103.
- (257) Lin, W.; Wang, J.; Zhang, W.-J.; Wu, F.-X. An unsupervised machine learning method for assessing quality of tandem mass spectra. *Proteome Sci.* **2012**, *10*, S12. doi: 10.1186/1477-5956-10-S1-S12.
- (258) Kalegowda, Y.; Harmer, S. L. Classification of time-of-flight secondary ion mass spectrometry spectra from complex Cu-Fe sulphides by principal component analysis and artificial neural networks. *Anal. Chim. Acta* **2013**, *759*, 21-27. doi: 10.1016/j.aca.2012.11.001.
- (259) Bade, R.; Bijlsma, L.; Miller, T. H.; Barron, L. P.; Sancho, J. V.; Hernández, F. Suspect screening of large numbers of emerging contaminants in environmental waters using artificial neural networks for chromatographic retention time prediction and high resolution mass spectrometry data analysis. *Sci. Total Environ.* **2015**, *538*, 934-941. doi: 10.1016/j.scitotenv.2015.08.078.
- (260) Munro, K.; Miller, T. H.; Martins, C. P. B.; Edge, A. M.; Cowan, D. A.; Barron, L. P. Artificial neural network modelling of pharmaceutical residue retention times in wastewater extracts using gradient liquid chromatography-high resolution mass spectrometry data. *J. Chromatogr. A* **2015**, *1396*, 34-44. doi: 10.1016/j.chroma.2015.03.063.
- (261) Valletta, E.; Kučera, L.; Prokeš, L.; Amato, F.; Pivetta, T.; Hampl, A.; Havel, J.; Vaňhara, P. Multivariate Calibration Approach for Quantitative Determination of Cell-Line Cross Contamination by Intact Cell Mass Spectrometry and Artificial Neural Networks. *PLoS One* **2016**, *11*, e0147414. doi: 10.1371/journal.pone.0147414.
- (262) Miller, J. H.; Schrom, B. T.; Kangas, L. J., in *Artificial Neural Networks. Methods in Molecular Biology, Vol. 1260* (Ed.: Cartwright, H.), Springer, New York, NY, **2015**, pp. 89-100. doi: 10.1007/978-1-4939-2239-0_6.
- (263) Kumozaki, S.; Sato, K.; Sakakibara, Y. A Machine Learning Based Approach to de novo Sequencing of Glycans from Tandem Mass Spectrometry Spectrum. *IEEE/ACM Trans. Comput. Biol. Bioinform.* **2015**, *12*, 1267-1274. doi: 10.1109/TCBB.2015.2430317.
- (264) Golubović, J.; Birkemeyer, C.; Protić, A.; Otašević, B.; Zečević, M. Structure-response relationship in electrospray ionization-mass spectrometry of sartans by artificial neural networks. *J. Chromatogr. A* **2016**, *1438*, 123-132. doi: 10.1016/j.chroma.2016.02.021.
- (265) Frandsen, H.; Janfelt, C.; Lauritsen, F. R. Fast and direct screening of polyaromatic hydrocarbon (PAH)-contaminated sand using a miniaturized membrane inlet mass

- spectrometer (mini-MIMS). *Rapid Commun. Mass Spectrom.* **2007**, *21*, 1574-1578. doi: 10.1002/rcm.3000.
- (266) Wright, S.; Malcolm, A.; Wright, C.; O'Prey, S.; Crichton, E.; Dash, N.; Moseley, R. W.; Zaczek, W.; Edwards, P.; Fussell, R. J.; Syms, R. R. A. A Microelectromechanical Systems-Enabled, Miniature Triple Quadrupole Mass Spectrometer. *Anal. Chem.* **2015**, *87*, 3115-3122. doi: 10.1021/acs.analchem.5b00311.
 - (267) Cooks, R. G.; Ouyang, Z.; Takats, Z.; Wiseman, J. M. Ambient Mass Spectrometry. *Science* **2006**, *311*, 1566. doi: 10.1126/science.1119426.
 - (268) Blakeman, K. H.; Wolfe, D. W.; Cavanaugh, C. A.; Ramsey, J. M. High Pressure Mass Spectrometry: The Generation of Mass Spectra at Operating Pressures Exceeding 1 Torr in a Microscale Cylindrical Ion Trap. *Anal. Chem.* **2016**, *88*, 5378-5384. doi: 10.1021/acs.analchem.6b00706.
 - (269) Pulliam, C. J.; Bain, R. M.; Wiley, J. S.; Ouyang, Z.; Cooks, R. G. Mass spectrometry in the home and garden. *J. Am. Soc. Mass Spectrom.* **2015**, *26*, 224-230. doi: 10.1007/s13361-014-1056-z.
 - (270) Gilliland, W. M., Jr.; Mellors, J. S.; Ramsey, J. M. Coupling Microchip Electrospray Ionization Devices with High Pressure Mass Spectrometry. *Anal. Chem.* **2017**, *89*, 13320-13325. doi: 10.1021/acs.analchem.7b03484.
 - (271) Wu, Q. H.; Tian, Y.; Li, A. L.; Andrews, D.; Hawkins, A. R.; Austin, D. E. A Miniaturized Linear Wire Ion Trap with Electron Ionization and Single Photon Ionization Sources. *J. Am. Soc. Mass Spectrom.* **2017**, *28*, 859-865. doi: 10.1007/s13361-017-1607-1.
 - (272) Li, A.; Hansen, B. J.; Powell, A. T.; Hawkins, A. R.; Austin, D. E. Miniaturization of a planar-electrode linear ion trap mass spectrometer. *Rapid Commun. Mass Spectrom.* **2014**, *28*, 1338-1344. doi: 10.1002/rcm.6906.
 - (273) Hansen, B. J.; Niemi, R. J.; Hawkins, A. R.; Lammert, S. A.; Austin, D. E. A Lithographically Patterned Discrete Planar Electrode Linear Ion Trap Mass Spectrometer. *J. Microelectromech. Syst.* **2013**, *22*, 876-883. doi: 10.1109/jmems.2013.2248128.
 - (274) Lynch, K. B.; Chen, A. P.; Liu, S. R. Miniaturized high-performance liquid chromatography instrumentation. *Talanta* **2018**, *177*, 94-103. doi: 10.1016/j.talanta.2017.09.016.
 - (275) Barney, B. L.; Daly, R. T.; Austin, D. E. A multi-stage image charge detector made from printed circuit boards. *Rev. Sci. Instrum.* **2013**, *84*, 114101. doi: 10.1063/1.4828668.
 - (276) Gerbig, S.; Neese, S.; Penner, A.; Spengler, B.; Schulz, S. Real-Time Food Authentication Using a Miniature Mass Spectrometer. *Anal. Chem.* **2017**, *89*, 10717-10725. doi: 10.1021/acs.analchem.7b01689.
 - (277) Syms, R. R. A.; Wright, S. MEMS mass spectrometers: the next wave of miniaturization. *J. Micromech. Microeng.* **2016**, *26*, 023001. doi: 10.1088/0960-1317/26/2/023001.

- (278) Tian, Y.; Higgs, J.; Li, A.; Barney, B.; Austin, D. E. How far can ion trap miniaturization go? Parameter scaling and space-charge limits for very small cylindrical ion traps. *J. Mass Spectrom.* **2014**, *49*, 233-240. doi: 10.1002/jms.3343.
- (279) Almeida, A.; Kolarich, D. The promise of protein glycosylation for personalised medicine. *Biochim. Biophys. Acta* **2016**, *1860*, 1583-1595. doi: 10.1016/j.bbagen.2016.03.012.
- (280) Morelle, W.; Michalski, J. C. Analysis of protein glycosylation by mass spectrometry. *Nat. Protoc.* **2007**, *2*, 1585-1602. doi: 10.1038/nprot.2007.227.
- (281) Zhang, J.; Rector, J.; Lin, J. Q.; Young, J. H.; Sans, M.; Katta, N.; Giese, N.; Yu, W.; Nagi, C.; Suliburk, J.; Liu, J.; Bensussan, A.; DeHoog, R. J.; Garza, K. Y.; Ludolph, B.; Sorace, A. G.; Syed, A.; Zahedivash, A.; Milner, T. E.; Eberlin, L. S. Nondestructive tissue analysis for ex vivo and in vivo cancer diagnosis using a handheld mass spectrometry system. *Sci. Transl. Med.* **2017**, *9*, ean3968. doi: 10.1126/scitranslmed.aan3968.
- (282) Hamilton, S. E.; Mattrey, F.; Bu, X.; Murray, D.; McCullough, B.; Welch, C. J. Use of a miniature mass spectrometer to support pharmaceutical process chemistry. *Org. Process Res. Dev.* **2014**, *18*, 103-108. doi: 10.1021/op400253x.
- (283) Bristow, T. W. T.; Ray, A. D.; O'Kearney-Mcmullan, A.; Lim, L.; McCullough, B.; Zammataro, A. On-line monitoring of continuous flow chemical synthesis using a portable, small footprint mass spectrometer. *J. Am. Soc. Mass. Spectrom.* **2014**, *25*, 1794-1802. doi: 10.1007/s13361-014-0957-1.
- (284) Laksshman, S.; Bhat, R. R.; Viswanath, V.; Li, X. L. DeepBipolar: Identifying genomic mutations for bipolar disorder via deep learning. *Hum. Mutat.* **2017**, *38*, 1217-1224. doi: 10.1002/humu.23272.
- (285) Tapan, S.; Wang, D. H. A Further Study on Mining DNA Motifs Using Fuzzy Self-Organizing Maps. *IEEE Trans. Neural Netw. Learn. Syst.* **2016**, *27*, 113-124. doi: 10.1109/tnnls.2015.2435155.
- (286) Manning, T.; Sleator, R. D.; Walsh, P. Biologically inspired intelligent decision making: a commentary on the use of artificial neural networks in bioinformatics. *Bioengineered* **2014**, *5*, 80-95. doi: 10.4161/bioe.26997.
- (287) Lucassen, A.; Houlston, R. S. The challenges of genome analysis in the health care setting. *Genes* **2014**, *5*, 576-585. doi: 10.3390/genes5030576.
- (288) Lowe Jr., W. L.; Reddy, T. E. Genomic approaches for understanding the genetics of complex disease. *Genome Res* **2015**, *25*, 1432-1441. doi: 10.1101/gr.190603.115.
- (289) van der Lee, T. B. J.; Bonants, P. Next Generation Sequence Technology reveals bacteria and viruses. *Prophyta Annual* **2017**, 42-43.
- (290) Goodwin, S.; McPherson, J. D.; McCombie, W. R. Coming of age: ten years of next-generation sequencing technologies. *Nat. Rev. Genet.* **2016**, *17*, 333-351. doi: 10.1038/nrg.2016.49.

- (291) Wetterstrand, K. A., "DNA Sequencing Costs: Data from the NHGRI Genome Sequencing Program (GSP) Available at: www.genome.gov/sequencingcostsdata.", can be found under <https://www.genome.gov/sequencingcostsdata/>, **2017**.
- (292) Herper, M., "Illumina Promises To Sequence Human Genome For \$100 -- But Not Quite Yet", can be found under <https://www.forbes.com/sites/matthewherper/2017/01/09/illumina-promises-to-sequence-human-genome-for-100-but-not-quite-yet/#4228d073386d>, **2017**.
- (293) Rothberg, J. M.; Hinz, W.; Rearick, T. M.; Schultz, J.; Mileski, W.; Davey, M.; Leamon, J. H.; Johnson, K.; Milgrew, M. J.; Edwards, M.; Hoon, J.; Simons, J. F.; Marran, D.; Myers, J. W.; Davidson, J. F.; Branting, A.; Nobile, J. R.; Puc, B. P.; Light, D.; Clark, T. A., et al. An integrated semiconductor device enabling non-optical genome sequencing. *Nature* **2011**, 475, 348. doi: 10.1038/nature10242.
- (294) Sahm, F.; Schrimpf, D.; Jones, D. T. W.; Meyer, J.; Kratz, A.; Reuss, D.; Capper, D.; Koelsche, C.; Korshunov, A.; Wiestler, B.; Buchhalter, I.; Milde, T.; Selt, F.; Sturm, D.; Kool, M.; Hummel, M.; Bewerunge-Hudler, M.; Mawrin, C.; Schüller, U.; Jungk, C., et al. Next-generation sequencing in routine brain tumor diagnostics enables an integrated diagnosis and identifies actionable targets. *Acta Neuropathol.* **2015**, 131, 1-8. doi: 10.1007/s00401-015-1519-8.
- (295) Erlich, Y. A vision for ubiquitous sequencing. *Genome Res.* **2015**, 25, 1411-1416. doi: 10.1101/gr.191692.115.
- (296) Lan, F.; Demaree, B.; Ahmed, N.; Abate, A. R. Single-cell genome sequencing at ultra-high-throughput with microfluidic droplet barcoding. *Nat. Biotechnol.* **2017**, 35, 640-646. doi: 10.1038/nbt.3880.
- (297) DuVall, J. A.; Le Roux, D.; Thompson, B. L.; Birch, C.; Nelson, D. A.; Li, J.; Mills, D. L.; Tsuei, A.-c.; Ensenberger, M. G.; Sprecher, C.; Storts, D. R.; Root, B. E.; Landers, J. P. Rapid multiplex DNA amplification on an inexpensive microdevice for human identification via short tandem repeat analysis. *Anal. Chim. Acta* **2017**, 980, 41-49. doi: <https://doi.org/10.1016/j.aca.2017.04.051>.
- (298) Zhu, Z.; Jenkins, G.; Zhang, W.; Zhang, M.; Guan, Z.; Yang, C. J. Single-molecule emulsion PCR in microfluidic droplets. *Anal. Bioanal. Chem.* **2012**, 403, 2127-2143. doi: 10.1007/s00216-012-5914-x.
- (299) Guan, Y.; Mayba, O.; Sandmann, T.; Lu, S.; Choi, Y.; Darbonne, W. C.; Leveque, V.; Ryner, L.; Humke, E.; Tam, N. W. R.; Sujathasarma, S.; Cheung, A.; Bourgon, R.; Lackner, M. R.; Wang, Y. High-Throughput and Sensitive Quantification of Circulating Tumor DNA by Microfluidic-Based Multiplex PCR and Next-Generation Sequencing. *J. Mol. Diagn.* **2017**, 19, 921-932. doi: <https://doi.org/10.1016/j.jmoldx.2017.08.001>.
- (300) Fluidigm Inc., "Fluidigm, Access Array System, Specifications", can be found under <https://www.fluidigm.com/products/access-array#specifications>, **2017**.
- (301) Oxford Nanopore Technologies, "MinION, portable real-time sequencer product page", can be found under <https://nanoporetech.com/products/minion>, **2018**.

- (302) GenapSys Inc., "*GenapSys Gene Electronic Nano-Integrated Ultra-Sensitive (GENIUS) technology*", can be found under <http://www.genapsys.com/product2/productwithfeatures.html>, **2015**.
- (303) MC10 Inc., "*MC10 devices, Products*", can be found under <https://www.mc10inc.com/>, **2018**.
- (304) AgaMatrix, "*Connected Products for Diabetes Care.*", can be found under <http://agamatrix.com/>, **2018**.
- (305) Senseonics Inc., "*Eversense CGM System.*", can be found under <https://ous.eversenseddiabetes.com/products/>, **2016**.
- (306) Senseonics Inc., "*Senseonics Announces CE Mark Approval for Eversense® XL CGM System*", can be found under <http://www.senseonics.com/investor-relations/news-releases/2017/09-12-2017-213230489>, **2017**.
- (307) Senseonics Inc., "*Senseonics submits Eversense® Continuous Glucose Monitoring system PMA to FDA*", can be found under <http://www.senseonics.com/investor-relations/news-releases/2016/10-27-2016-214918103>, **2016**.
- (308) Basil Leaf Technologies, L., "*Basil Leaf Technologies - product page*", can be found under <http://www.basilleaftech.com/our-solutions/>, **2018**.
- (309) XPRIZE Foundation Inc., "*Qualcomm tricorder Xprize - Final Frontier Medical Devices.*", can be found under <https://tricorder.xprize.org/teams/final-frontier-medical-devices>, **2018**.
- (310) Two Pore Guys Inc., "*Molecular DX - A Universal Biomarker Development Platform*", can be found under http://twoporeguys.com/molecular_dx/, **2018**.
- (311) MyDx Inc., "*MyDx Product page*", can be found under <https://www.mydxlife.com/>, **2017**.
- (312) MyDx Inc., "*Detailed product information - CannaDx.*", can be found under <https://www.mydxlife.com/cannadx/>, **2017**.
- (313) Cropio, "*Farming management software*", can be found under <https://about.cropio.com/de/>, **2017**.
- (314) Bosch Japan, "*Plantect™ smart agriculture solutions - Bosch launches innovative disease prediction service using sensors and artificial intelligence*", can be found under <http://www.bosch.co.jp/press/rbjp-1706-05/?lang=en>,
- (315) Kruize, J. W.; Wolfert, J.; Scholten, H.; Verdouw, C. N.; Kassahun, A.; Beulens, A. J. M. A reference architecture for Farm Software Ecosystems. *Comput. Electron. Agric.* **2016**, 125, 12-28. doi: 10.1016/j.compag.2016.04.011.
- (316) Geipel, J.; Jackenkroll, M.; Weis, M.; Claupein, W. A Sensor Web-Enabled Infrastructure for Precision Farming. *ISPRS Int. J. Geo-Inf.* **2015**, 4, 385-399. doi: 10.3390/ijgi4010385.
- (317) Ünal, I.; Topakci, M. Design of a Remote-controlled and GPS-guided Autonomous Robot for Precision Farming. *Int. J. Adv. Robot. Syst.* **2015**, 1. doi: 10.5772/62059.

- (318) Eastwood, C. R.; Chapman, D. F.; Paine, M. S. Networks of practice for co-construction of agricultural decision support systems: Case studies of precision dairy farms in Australia. *Agric. Syst.* **2012**, *108*, 10-18. doi: <https://doi.org/10.1016/j.agsy.2011.12.005>.
- (319) Ripe Technology Inc., "*Ripe.io*", can be found under <http://www.ripe.io/>, **2018**
- (320) Bryzek, J.; Grace, R., "*The Trillion Sensors Initiative*", can be found under <http://www.cmmmagazine.com/cmm-articles/the-trillion-sensors-initiative/>, **2014**.
- (321) Bogue, R. Towards the trillion sensors market. *Sens. Rev.* **2014**, *34*, 137-142. doi: 10.1108/SR-12-2013-755.
- (322) Krishna, A., "*Changing the Way the World Works: IBM Research's '5 in 5' "*", can be found under <https://www.ibm.com/blogs/research/2018/03/ibm-research-5-in-5-2018/>, **2018**.
- (323) HP Development Company L.P., "*CeNSE*", can be found under <http://www8.hp.com/us/en/hp-information/environment/cense.html>, **2018**.
- (324) Intel Corporation, "*Context Awareness to Radically Change How We Interact with Technology*", can be found under <https://newsroom.intel.com/news-releases/context-awareness-to-radically-change-how-we-interact-with-technology/>, **2010**.
- (325) Shields, N., "*Qualcomm doubles down on the IoT with new Vision Intelligence platform*", can be found under <https://www.businessinsider.de/qualcomm-vision-intelligence-platform-iot-2018-4?r=US&IR=T>, **2018**.
- (326) Desai, N., "*IBM scientists team with The Weather Company to bring edge computing to life*", can be found under <https://www.ibm.com/blogs/research/2017/02/bringing-edge-computing-to-life/>, **2017**.
- (327) Yeow, K.; Gani, A.; Ahmad, R. W.; Rodrigues, J. J. P. C.; Ko, K. Decentralized Consensus for Edge-Centric Internet of Things: A Review, Taxonomy, and Research Issues. *IEEE Access* **2018**, *6*, 1513-1524. doi: 10.1109/access.2017.2779263.
- (328) Ren, J.; Guo, H.; Xu, C.; Zhang, Y. Serving at the Edge: A Scalable IoT Architecture Based on Transparent Computing. *IEEE Netw.* **2017**, *31*, 96-105. doi: 10.1109/mnet.2017.1700030.
- (329) Lopez, P. G.; Montresor, A.; Epema, D.; Datta, A.; Higashino, T.; Iamnitchi, A.; Barcellos, M.; Felber, P.; Riviere, E. Edge-centric Computing: Vision and Challenges. *Comput. Commun. Rev.* **2015**, *45*, 37-42. doi: 10.1145/2831347.2831354.
- (330) Esposito, C.; Castiglione, A.; Pop, F.; Choo, K. K. R. Challenges of Connecting Edge and Cloud Computing: A Security and Forensic Perspective. *IEEE Cloud Computing* **2017**, *4*, 13-17. doi: 10.1109/mcc.2017.30.
- (331) Intel News Byte, "*Intel Democratizes Deep Learning Application Development with Launch of Movidius Neural Compute Stick*", can be found under <https://newsroom.intel.com/news/intel-democratizes-deep-learning-application-development-launch-movidius-neural-compute-stick/>, **2017**.

- (332) Novak, J.; Melenhorst, M.; Micheel, I.; Pasini, C.; Fraternali, P.; Rizzoli, A. E. Integrating behavioural change and gamified incentive modelling for stimulating water saving. *Environ. Modell. Softw.* **2018**, *102*, 120-137. doi: 10.1016/j.envsoft.2017.11.038.
- (333) Chen, Y.; Elenee Argentinis, J. D.; Weber, G. IBM Watson: How Cognitive Computing Can Be Applied to Big Data Challenges in Life Sciences Research. *Clin. Ther.* **2016**, *38*, 688-701. doi: 10.1016/j.clinthera.2015.12.001.
- (334) George, S.; Karly, S.; Ala Eldin, O.; Shuo, L.; Clement, C.; Udeshaya, W.; Safieddin, S.-N.; Richard, H. Non-Invasive Monitoring of Glucose Level Changes Utilizing a mm-Wave Radar System. *International Journal of Mobile Human Computer Interaction (IJMHCI)* **2018**, *10*, 10-29. doi: 10.4018/ijmhci.2018070102.
- (335) Mar, V. J.; Soyer, H. P. Artificial intelligence for melanoma diagnosis: How can we deliver on the promise? *Ann. Oncol.* **2018**, mdy193-mdy193. doi: 10.1093/annonc/mdy193.
- (336) Luechtefeld, T.; Marsh, D.; Rowlands, C.; Hartung, T. Machine learning of toxicological big data enables read-across structure activity relationships (RASAR) outperforming animal test reproducibility. *Toxicol. Sci.* **2018**, kfy152-kfy152. doi: 10.1093/toxsci/kfy152.
- (337) Jo, Y.; Park, S.; Jung, J.; Yoon, J.; Joo, H.; Kim, M.-h.; Kang, S.-J.; Choi, M. C.; Lee, S. Y.; Park, Y. Holographic deep learning for rapid optical screening of anthrax spores. *Sci. Adv.* **2017**, *3*, e1700606. doi: 10.1126/sciadv.1700606.
- (338) Dehaene, S.; Lau, H.; Kouider, S. What is consciousness, and could machines have it? *Science* **2017**, *358*, 486-492. doi: 10.1126/science.aan8871.
- (339) George, D.; Lehrach, W.; Kansky, K.; Lázaro-Gredilla, M.; Laan, C.; Marthi, B.; Lou, X.; Meng, Z.; Liu, Y.; Wang, H.; Lavin, A.; Phoenix, D. S. A generative vision model that trains with high data efficiency and breaks text-based CAPTCHAs. *Science* **2017**, *358*. doi: 10.1126/science.aag2612.

Chapter 3: PAMAM dendrimers: A multifunctional nanomaterial for ECL biosensors

Abstract

Polyamido amine (PAMAM) dendrimers have been shown to function as electrochemiluminescence (ECL) co-reactant and have the inherent capability of improving immobilization of molecules on surfaces due to their dendritic structure. Here, we investigated the combination of both of these properties as the basis for biosensor development. Dendrimers with 5, 8, 10 and 16 terminal amine groups, respectively, were used. These were covalently coupled to biotin as model recognition site, and tagged with $\text{Ru}(\text{bpy})_3^{2+}$ via adsorption. Due to their hydrophilicity, Ru-dendrimers showed significantly improved electrochemical activity in comparison to the standard tripropylamine (TPA) assisted ECL and similar luminescence yields even though 10 fold less dendrimer concentration was required in comparison to TPA. Best signals were obtained for D8 and D10 dendrimers. These Ru-dendrimers were subsequently used for the quantification of streptavidin, as its binding to the biotin-tag caused a proportional decrease in ECL signal with a dynamic range of 5 nM to 1 μM . These preliminary studies demonstrate that PAMAM dendrimers can function as responsive signal generators in solution-based ECL-bioassays with an assumed even higher impact when being immobilized directly on the electrode-surface.

This chapter has been published.

Sudeshna Chandra, Michael Mayer, Antje J. Baeumner, *Talanta*, **2017**, 168, 126-129, DOI: 10.1016/j.talanta.2017.03.016

Author contributions:

SC, MM and AJB planned the experiments. SC did most of the experiments and wrote the initial draft of the manuscript. MM performed some experiments. MM and AJB revised the manuscript. AJB is corresponding author.

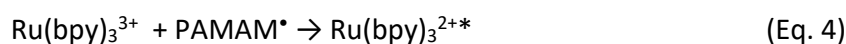
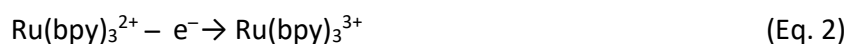
1. Introduction

Electrogenerated chemiluminescence (ECL) involves the generation of electroactive species which can undergo highly-energetic electron transfer (redox or enzymatic) reactions that emit light upon relaxation to the ground state. This technique has attracted attention due to its application in medical diagnostics, pharmacy, food and environmental analysis.¹ Commonly used ECL reagents (luminophores) are luminol, quantum dots and tris(2,2'-bipyridyl) ruthenium(II) ($\text{Ru}(\text{bpy})_3^{2+}$) and their analogues, among which $\text{Ru}(\text{bpy})_3^{2+}$ is most frequently used due to its available low oxidation potential, high emission yield, and low cost.² Commonly, a co-reactant (mostly tripropylamine, TPA) is used to enhance the sensitivity of the Ru-based ECL system.³ However, TPA is toxic, volatile, and is required in high concentrations (~ 100 mM), which leads to an increase in background noise. Further, TPA exhibits slow electrochemical oxidation that limits the ECL efficiency. Moreover, TPA is basic in nature and surfactants are needed to bring it close to the electrode surface to enable an efficient electron transfer. All these drawbacks prompted researchers to find alternative co-reactants. Here, tertiary amines are interesting as they show higher ECL efficiencies than primary and secondary amines.⁴ In fact, several parameters contribute to the overall performance of an ECL assay such as hydrophilicity, luminescence lifetime, wavelength of emission, the location of the excited state within the complex, and the redox potential of ground and excited states. The ability to control these parameters depends on the luminophore and the co-reactant, which ultimately enhances the sensitivity and specificity of the assay either by providing longer excited-state lifetime or by reducing the redox potential, respectively.^{5,6} Of late, nanoparticles are found to enhance the ECL signal because of their ability to diffuse into the solution layer near the electrode, thereby enhancing the ECL signals. As they possess a large surface area they also provide many binding sites for attaching biomolecules of interest.^{7,8} Among the studied nanomaterials, the hyper-branched, three-dimensional polyamidoamine (PAMAM) dendrimers received considerable interest as they bear a substantial number of primary, secondary and most importantly tertiary amine groups. Furthermore, it is anticipated that PAMAM dendrimers can not only serve as co-reactant to the ECL

luminophores,⁹ but can simultaneously serve as a multifunctional label loaded with luminophores and biomolecules.¹⁰ Kim et al.¹¹ reported an enhanced ECL of Ru(bpy)₃²⁺ with TPA co-reactant on ITO electrodes that were modified with dendrimers encapsulating nanoparticles. Using these modified electrodes, nicotine was detected with a ~210-fold increase of the ECL signals in comparison to signals obtained from bare ITO. Similarly, Lin et al.¹² constructed an ECL platform by functionalizing a PAMAM dendrimer with titanate nanotubes. In this work, we have explored the ECL co-reactant pathway of Ru(bpy)₃²⁺ using plain PAMAM dendrimers as postulated by Xiong et al.¹³ (Equations 1-5). It is proposed that PAMAM in solution is oxidized along with the luminophore (Ru(bpy)₃²⁺) at the same electrode potential to form Ru(bpy)₃³⁺ and excited PAMAM^{•+}. Then, Ru(bpy)₃³⁺ is reduced by PAMAM^{•+} to produce Ru(bpy)₃^{2+*}, ensuing emission of light. We studied this mechanism by varying the dendrimer core molecules (ethylenediamine and triethylenetriamine) and using different numbers of peripheral amine groups.

2. Assay Principles

Based on the terminal amine groups, the PAMAM dendrimers were classified as D5, D8, D10 and D16 having 5, 8, 10 and 16 -NH₂ groups, respectively (Figure S1). To trigger an ECL signal, the dendrimers were oxidized at the electrode surface generating a radical. At the same time, Ru(II) is oxidized to Ru(III) which in turn is reduced and excited by the deprotonated dendrimer radical. Luminescence occurs consequently by radiative relaxation of the excited Ru(II).



The ECL platform based on Ru-dendrimers (Ru-D5, Ru-D8, Ru-D10 and Ru-D16) was then used to study the binding of biotin to streptavidin as straightforward affinity binding model as depicted in Fig. 1.

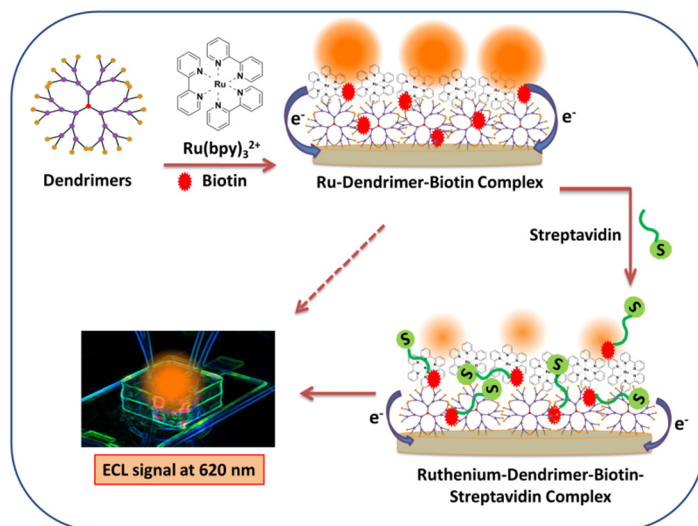


Fig. 1. Schematic representation of the dendrimer-ECL platform for the biotin-streptavidin assay

3. Materials and Methods

An indium tin oxide (ITO) electrode coated on PET (polyethylene terephthalate) foil, Ag wire and Pt wire were used as working, pseudo reference and counter electrodes, respectively. An Autolab potentiostat was used for the ECL measurements. The PMT voltage was set to 620 V and the set potential was maintained at +1.5V. Luminescence spectra were measured using a 620 nm emission wavelength. For CV measurements with $\text{Ru}(\text{bpy})_3^{2+}$ and its associated analysis, the potential was scanned from +0.5 to +1.7 V with a step potential of 0.01 V and scan rate of 50 mV/sec.

The dendrimers (D5 and D10) and (D8 and D16) were synthesized from initiator cores diethylenetriamine and ethylenediamine, respectively with branching monomers (methyl acrylate and ethylenediamine) by Michael addition-amidation reaction.^{14,15}

Typically, 10 mM dendrimers were incubated with $\text{Ru}(\text{bpy})_3^{2+}$ (0.1 mM) for 5 hours in a buffer solution of pH 9.0 with glycine-NaOH buffer. KCl (0.1 M) was used as supporting

electrolyte. No surfactant was used for the ECL measurements. For experiments employing streptavidin, the ITO cells were blocked with 0.1% BSA solution for 30 minutes and washed prior to use. For biofunctionalization of the dendrimers, they were tagged with biotin using NHS-biotin (0.1 mg in 30 μ L total volume of glycine buffer pH 9.0) by incubation under magnetic stirring for 3 hours. In the case of experiments with streptavidin, an additional incubation for 30 minutes was used. Here, varying concentrations of streptavidin (SA) were made from the stock solution (200 μ M) by serial dilution in the same glycine buffer.

4. Results and Discussion

Based on previous knowledge^{10,11} it can be predicted that dendrimers with their layered architecture and structural homogeneity have the potential to serve multiple purposes in an ECL reaction. They offer a large reactive surface area for both, the immobilization of proteins/nucleic acids and simultaneously function as co-reactant for the ECL luminophore. Furthermore, the residual terminal amines render stable aqueous dendrimer dispersions. The primary and tertiary amine groups of PAMAM dendrimers are mostly responsible for ECL reactions, whereas the latter are more efficient as co-reactants than the former since the electron-donating alkyl side chains have a tendency to enhance ECL.¹⁶ Further, it is known that the enhancement of ECL intensity is also correlated with the amine structure wherein the amines with an α -hydrogen atom are easily oxidized to form a cation radical that in turn can deprotonate easily to form strongly reducing free-radical species.¹⁶ Thus, the ability of all dendrimers studied here to act as co-reactant was expected.

Initial experiments in which dendrimers were adsorbed to the ITO surface demonstrated, that a layer of dendrimers does effectively inhibit the ruthenium-based ECL reaction. At the same time, it became clear that the dendrimers could function as co-reactants in solution. As the primary and tertiary amines of the G1.0-G3.0 PAMAM dendrimers are fully deprotonated at pH 10, we assume that both participate in the ECL mechanism. Based on these results the assay was changed. As the dendrimers are highly hydrophilic, they could also be used in solution. In addition, Yuan et al.² had

already shown that the ECL reaction time, the electron transfer efficiency and consequently the ECL signal were enhanced when adding luminophore and coreactant simultaneously to the electrode surface. Therefore, dendrimers and the luminophore were incubated for 30 min prior to the ECL measurements, also no immobilization such as simple absorption was performed. The preliminary studies showed best ECL performances of the D8 (ethylenediamine core) and D10 (triethylenetriamine core) dendrimers with respect to the reliability of the data obtained and signal height, so that these two systems were further characterized with respect to their electrochemical performances (Figure S2).

Figure 2 demonstrates the electroactivity of the PAMAM dendrimers at 10 mM (Ru-D8 and Ru-D10) in comparison to the conventional co-reactant TPA (100 mM). The cyclic voltammograms show that direct oxidation of the $\text{Ru}(\text{bpy})_3^{2+}$ started at the same electrode potential ($\sim +0.9$ V vs pseudo Ag/AgCl). Maximum ECL emission can be observed at +1.5V similar to TPA-assisted ECL. Further, an apparent increase in the oxidation current suggested that the dendrimers exhibited a very good electrocatalytic effect on the oxidation of $\text{Ru}(\text{bpy})_3^{2+}$ even though they are present at a 10-fold lower concentration than TPA. We assume that this enhancement is due to the hydrophilic nature of the dendrimers in contrast to the hydrophobicity of TPA. Ruthenium can more easily access the electrode surface under hydrophilic conditions which consequently leads to an enhanced electron transfer (Fig. 2) and also luminescence signal (data not shown). Further, the presence of multiple amine groups in the dendrimers unlike TPA, is directly correlated with the enhancement of the ECL intensity since the α -H atom of the amine is easily oxidized and the newly formed cation radical can deprotonate easily to form reducing free radical species.¹⁶

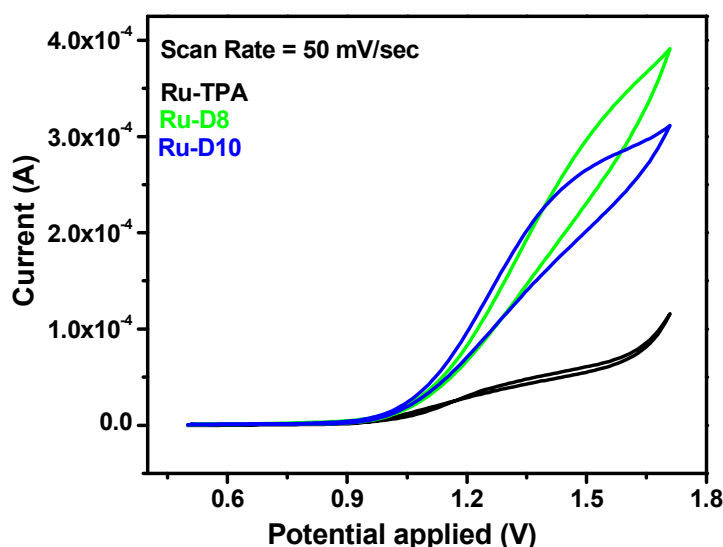


Fig. 2. Comparison of the electroactivity of Ru-D8 and Ru-D10 with Ru-TPA

Based on these findings, the dendrimer ruthenium concept was explored to simultaneously function as co-reactant and as biorecognition element in a bioassay, using biotin-streptavidin as affinity binding model. The dendrimers were chemically modified with an abundance of biotin, while keeping at least one free primary amine group per dendrimer statistically to serve as co-reactant. (This resulted in lower ECL activity as described further below.) In the assay, biotinylated dendrimers, tris(2,2'-bipyridine)ruthenium(II) and streptavidin were incubated for 30 minutes prior to addition to the ITO electrodes. The expected decrease in the luminescence intensity of Ru-D8 (Figure S3) and Ru-D10 (data not shown) upon specific streptavidin binding was clearly detectable.

To further investigate this finding, the influence of the binding interaction of biotin and streptavidin on the ECL reaction was also monitored by the change in the luminescence intensity with time. Figures 3 demonstrate the ECL decay of Ru-D10 in presence of biotin and streptavidin. While the biotinylation did not alter the ECL signal trace of the Ru-D10 significantly, the reaction with streptavidin causes a two-fold drop in signal. We assume that the streptavidin binding causes steric hindrance for the ECL mechanism or affects the diffusion process to the electrode surface. In the case of the Ru-D8 complexes also the biotinylation led to a decrease in signal. We assume this is due to fewer primary amine groups available after the biotinylation reaction and further optimization of the biotinylation reaction in the future is warranted.

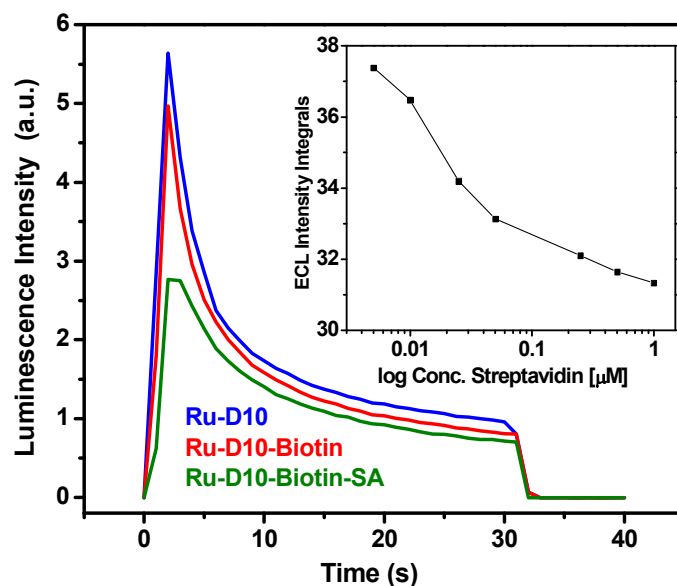


Fig. 3. Changes in the ECL intensity of Ru-D10 over time on immobilization with biotin and streptavidin. Inset: Dose-response ECL intensity curve showing decrease in luminescence with increase in the concentration of streptavidin.

Finally, the detection principle was assessed by subjecting the Ru-Dendrimer-Biotin solution to different concentrations of streptavidin (Figure S4). The ECL intensity decreased with an increase in the streptavidin concentration as depicted in the dose responsive curve which is due to specific binding between the analyte streptavidin to the dendrimer-coupled biotin. The calibration curve of ECL versus logarithm concentration of SA showed an exponential relationship in a dynamic range from 0.005 to 1 μM. The regression equation was found to be $I = 31.7 (\log C_{SA}) - 1.74$ with a correlation coefficient of $R = 0.97523$ where I is the ECL intensity and C is the concentration of streptavidin.

Table 1 Changes in Zeta potential values of Ru-D8 and Ru-D10 upon immobilization with biotin and streptavidin

Sl. No.	Samples	Zeta Potential (mV) \pm S.D
1	D8	-19.1 \pm 1.3
2	D8-Ru	-7.5 \pm 2.7
3	D8-Ru-Biotin	-12.8 \pm 4.0
4	D8-Ru-Biotin-Streptavidin	-3.99 \pm 0.3
5	D10	-34.9 \pm 2.4
6	D10-Ru	-26.2 \pm 4.4
7	D10-Ru-Biotin	-32.4 \pm 7.4
8	D10-Ru-Biotin-Streptavidin	-9.89 \pm 3.6

Finally, the potential stability of the dendrimer complex in buffer solution (0.1 M glycine-NaOH buffer, pH 9.0; 25°C) was assessed using zeta potential measurements. (Table 1). The refractive index of the dendrimers was experimentally found to be 1.334. Upon modification with Tris(2,2'-bipyridine)ruthenium(II) and biotin, the zeta potential changes as expected. Interestingly, the addition of streptavidin indicates that the complexes become less colloiddally stable due to the positive charge of the protein (+20 mV at pH \leq 8).¹⁷ A schematic representation of the above is shown in Figure S4. Further experiments need to be carried out to determine, how this contributes to the sensitive signal response upon streptavidin binding.

5. Conclusion

The dendrimer-Ru(bpy)₃²⁺ approach shows promise as analytical platform for the direct detection of bioaffinity events. The dendrimers function as efficient immobilization matrix due to their tethered structures and primary amine groups. Simultaneously they function as highly efficient coreactant due to their primary and tertiary amine groups. In fact, Newkome et al.¹⁸ postulated in a similar mechanism that Ru-species promote and stabilize the inter-dendrimer assembly on electrode surfaces by joining the individual dendrimers and interacting the (bipyridine) ligand with the exterior amine groups of the dendrimers. The presence of primary and tertiary amines in the PAMAM dendrimers therefore provides for specific coupling reactions and for ECL enhancement. The proposed assay here is based on a homogeneous format allowing full distribution of the biorecognition element (here biotin) within the sample. Preliminary studies with immobilized dendrimers indicate increased sensitivity, which will be studied in more detail in the future.

6. References

- (1) Richter, M. M. Electrochemiluminescence (ECL). *Chem. Rev.* 2004, *104*, 3003-3036. doi: 10.1021/cr020373d.
- (2) Yuan, Y.; Gan, X.; Chai, Y.; Yuan, R. A novel electrochemiluminescence aptasensor based on in situ generated proline and matrix polyamidoamine dendrimers as coreactants for signal amplification. *Biosens. Bioelectron.* 2014, *55*, 313-317. doi: <https://doi.org/10.1016/j.bios.2013.12.010>.
- (3) Wu, B.; Hu, C.; Hu, X.; Cao, H.; Huang, C.; Shen, H.; Jia, N. Sensitive ECL immunosensor for detection of retinol-binding protein based on double-assisted signal amplification strategy of multiwalled carbon nanotubes and Ru(bpy)₃²⁺ doped mesoporous silica nanospheres. *Biosens. Bioelectron.* 2013, *50*, 300-304. doi: <https://doi.org/10.1016/j.bios.2013.06.045>.
- (4) Liu, X.; Shi, L.; Niu, W.; Li, H.; Xu, G. Environmentally Friendly and Highly Sensitive Ruthenium(II) Tris(2,2' -bipyridyl) Electrochemiluminescent System Using 2-(Dibutylamino)ethanol as Co-Reactant. *Angew. Chem. Int. Ed.* 2006, *46*, 421-424. doi: 10.1002/anie.200603491.
- (5) Zhou, M.; Robertson, G. P.; Roovers, J. Comparative Study of Ruthenium(II) Tris(bipyridine) Derivatives for Electrochemiluminescence Application. *Inorg. Chem.* 2005, *44*, 8317-8325. doi: 10.1021/ic0510112.
- (6) Brooks, S. C.; Vinyard, D. J.; Richter, M. M. Electrogenated chemiluminescence of (bis-bipyridyl)ruthenium(II) acetylacetonate complexes. *Inorg. Chim. Acta* 2006, *359*, 4635-4638. doi: <https://doi.org/10.1016/j.ica.2006.05.031>.
- (7) Chang, Z.; Zhou, J.; Zhao, K.; Zhu, N.; He, P.; Fang, Y. Ru(bpy)₃²⁺-doped silica nanoparticle DNA probe for the electrogenerated chemiluminescence detection of DNA hybridization. *Electrochim. Acta* 2006, *52*, 575-580. doi: <https://doi.org/10.1016/j.electacta.2006.05.036>.
- (8) Spehar-Deleze, A.-M.; Schmidt, L.; Neier, R.; Kulmala, S.; de Rooij, N.; Koudelka-Hep, M. Electrochemiluminescent hybridization chip with electric field aided mismatch discrimination. *Biosens. Bioelectron.* 2006, *22*, 722-729. doi: <https://doi.org/10.1016/j.bios.2006.02.013>.
- (9) Perez-Tejeda, P.; Prado-Gotor, R.; Grueso, E. M. Electrochemiluminescence of the [Ru(bpy)₃]²⁺ Complex: The Coreactant Effect of PAMAM Dendrimers in an Aqueous Medium. *Inorg. Chem.* 2012, *51*, 10825-10831. doi: 10.1021/ic301239x.

- (10) Mankbadi, M. R.; Barakat, M. A.; Ramadan, M. H.; Woodcock, H. L.; Kuhn, J. N. Iron Chelation by Polyamidoamine Dendrimers: A Second-Order Kinetic Model for Metal–Amine Complexation. *The Journal of Physical Chemistry B* 2011, *115*, 13534-13540. doi: 10.1021/jp208546a.
- (11) Kim, Y.; Kim, J. Modification of Indium Tin Oxide with Dendrimer-Encapsulated Nanoparticles To Provide Enhanced Stable Electrochemiluminescence of Ru(bpy)₃²⁺/Tripropylamine While Preserving Optical Transparency of Indium Tin Oxide for Sensitive Electrochemiluminescence-Based Analyses. *Anal. Chem.* 2014, *86*, 1654-1660. doi: 10.1021/ac403415m.
- (12) Lin, Y.; Dai, H.; Xu, G.; Yang, T.; Yang, C.; Tong, Y.; Yang, Y.; Chen, G. Enhanced luminol electrochemiluminescence triggered by an electrode functionalized with dendrimers modified with titanate nanotubes. *Microchimica Acta* 2013, *180*, 563-572. doi: 10.1007/s00604-013-0963-1.
- (13) Xiong, C.; Wang, H.; Yuan, Y.; Chai, Y.; Yuan, R. A novel solid-state Ru(bpy)₃²⁺ electrochemiluminescence immunosensor based on poly(ethylenimine) and polyamidoamine dendrimers as co-reactants. *Talanta* 2015, *131*, 192-197. doi: <https://doi.org/10.1016/j.talanta.2014.07.072>.
- (14) Dietrich, S.; Chandra, S.; Georgi, C.; Thomas, S.; Makarov, D.; Schulze, S.; Hietschold, M.; Albrecht, M.; Bahadur, D.; Lang, H. Design, characterization and magnetic properties of Fe₃O₄-nanoparticle arrays coated with PEGylated-dendrimers. *Mater. Chem. Phys.* 2012, *132*, 292-299. doi: <https://doi.org/10.1016/j.matchemphys.2011.11.015>.
- (15) Chandra, S.; Patel, M. D.; Lang, H.; Bahadur, D. Dendrimer-functionalized magnetic nanoparticles: A new electrode material for electrochemical energy storage devices. *J. Power Sources* 2015, *280*, 217-226. doi: <https://doi.org/10.1016/j.jpowsour.2015.01.075>.
- (16) Parveen, S.; Aslam, M. S.; Hu, L.; Xu, G., *Electrogenerated Chemiluminescence-Protocols and Applications*. SpringerBriefs in Molecular Science (BRIEFSMOLECULAR)(Springer, Berlin, Heidelberg, 2013). doi: 10.1007/978-3-642-39555-0.
- (17) Green, N. M. AVIDIN. 4. STABILITY AT EXTREMES OF PH AND DISSOCIATION INTO SUB-UNITS BY GUANIDINE HYDROCHLORIDE. *Biochem. J* 1963, *89*, 609.
- (18) Newkome, G. R.; He, E.; Moorefield, C. N. Suprasupermolecules with Novel Properties: Metallodendrimers. *Chem. Rev.* 1999, *99*, 1689-1746. doi: 10.1021/cr9800659.

7. Supplementary Information

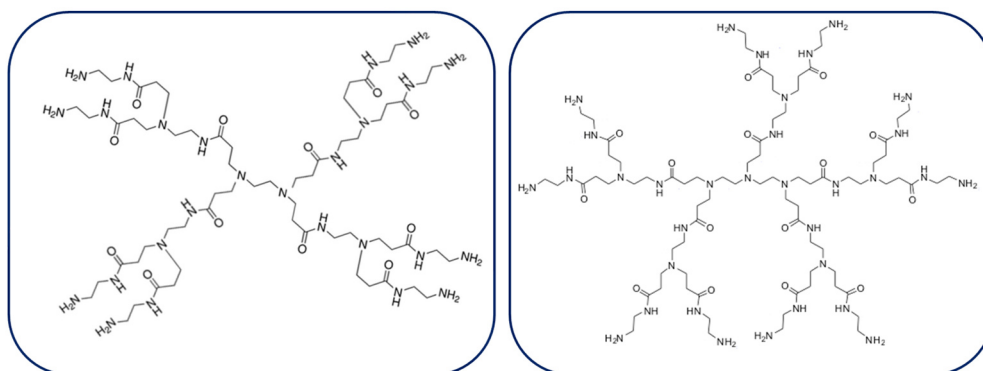


Figure S1. Structure of D8 and D10-PAMAM dendrimers.

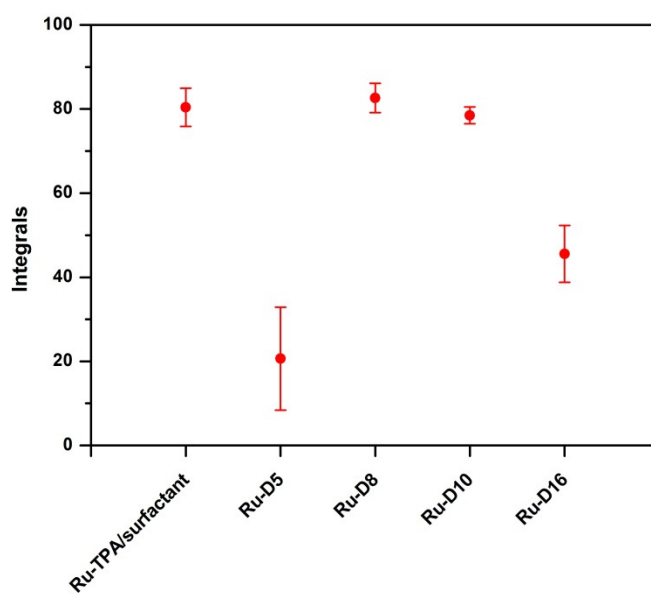


Figure S2. Comparison of signal intensities between different dendrimers and the standard Ru/TPA system.

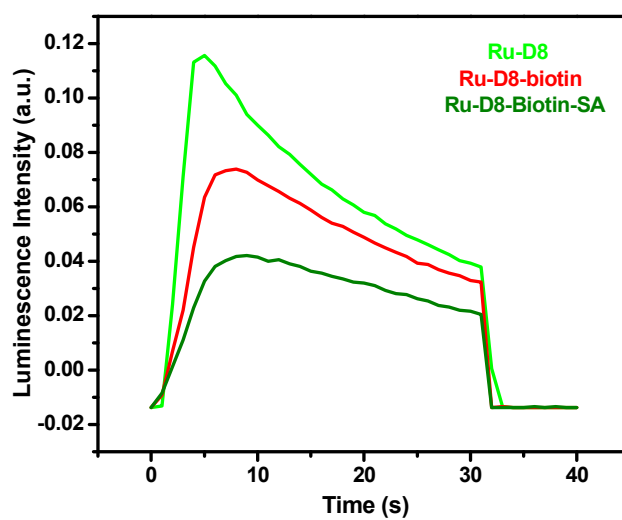


Figure S3. Changes in the ECL intensity of Ru-D8 over time on immobilization with biotin and streptavidin.

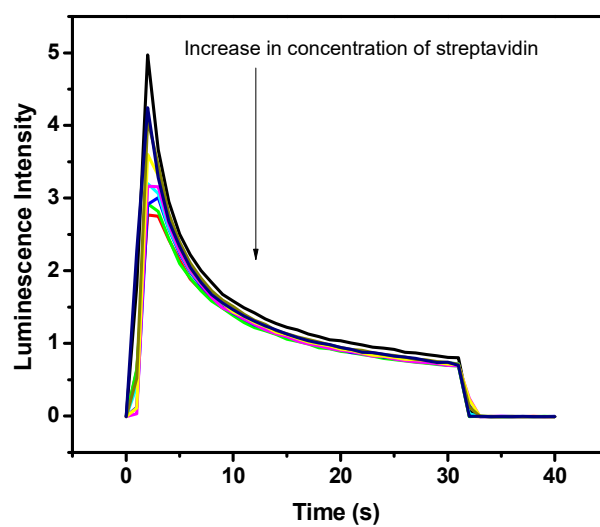


Figure S4. Dose-responsive ECL intensity curve showing decrease in luminescence with increase in the concentration of streptavidin.

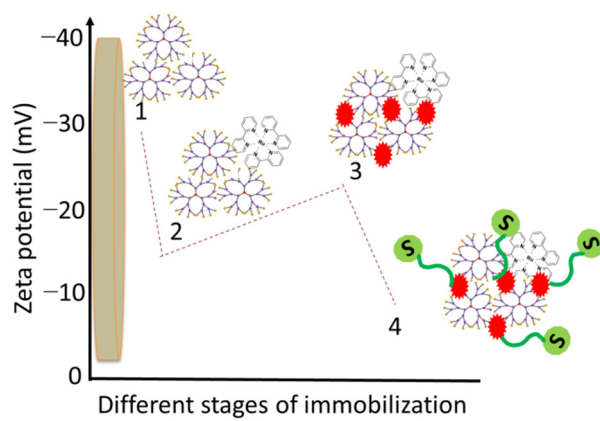


Figure S5. Change in zeta potential at different stages of immobilization.

Chapter 4: Electrochemiluminescence Bioassays with a Water-Soluble Luminol Derivative Can Outperform Fluorescence Assays

Abstract

The most efficient and commonly used electrochemiluminescence (ECL) emitters are luminol, $[\text{Ru}(\text{bpy})_3]^{2+}$, and derivatives thereof. Luminol stands out due to its low excitation potential, but applications are limited by its insolubility under physiological conditions. The water-soluble *m*-carboxy luminol was synthesized in 15 % yield and exhibited high solubility under physiological conditions and afforded a four-fold ECL signal increase (vs. luminol). Entrapment in DNA-tagged liposomes enabled a DNA assay with a detection limit of 3.2 pmol L^{-1} , which is 150 times lower than the corresponding fluorescence approach. This remarkable sensitivity gain and the low excitation potential establish *m*-carboxy luminol as a superior ECL probe with direct relevance to chemiluminescence and enzymatic bioanalytical approaches.

This chapter has been published.

Michael Mayer, Shigehiko Takegami, Michael Neumeier, Simone Rink, Axel Jacobi von Wangelin, Silja Schulte, Moritz Vollmer, Axel G. Griesbeck, Axel Duerkop, Antje J. Baeumner, *Angew. Chem. Int. Ed.* **2018**, 57, 408, DOI: 10.1002/anie.201708630

Author contributions:

MM carried out most of the experimental work (ECL, all assays, ECL characterization of *m*-carboxy luminol and characterization and synthesis of *m*-carboxy luminol liposomes, surfactant& matrix study, data evaluation and partly the luminol liposome syntheses), ST performed most of the luminol liposome syntheses and their full characterization. MN did the *m*-carboxy luminol synthesis and full characterization and respective data evaluation. SR supported bioassays and assay measurements, AJvW supported synthesis validation, SS did the first synthesis of *m*-carboxy luminol, MV optimized that synthesis, AGG supported synthesis design, project administrators were AD and AJB. MM wrote most of the manuscript, MN wrote the *m*-carboxy luminol synthesis and -characterization part of the manuscript. MM, MN, AJvW, AGG, AD and AJB revised the manuscript. AJB is corresponding author.

1. Introduction

Since its ascent with A.J. Bard's work on $[\text{Ru}(\text{bpy})_3]^{2+}$ based ECL in 1972¹ and the discovery of its great benefits towards other analytical techniques, ECL nowadays plays a major role in highest-sensitivity (bio)detection applications.^{2,3} Most analytical applications employ only few ECL luminophores, focusing on $[\text{Ru}(\text{bpy})_3]^{2+}$ and luminol. Yet new nanomaterials such as quantum dots and electrode coatings find recently considerable attention.⁴⁻⁶ Luminol-ECL was first described in 1928.⁷ Due to its very low excitation potential of +0.5 V (*vs. Ag/AgCl; on gold electrodes) it is compatible with a large variety of working electrode materials and offers benefits towards electrode fouling resistance and long-term stability in contrast to $[\text{Ru}(\text{bpy})_3]^{2+}$ - ECL (+1.2 V, *). Also, transparent electrode materials like indium tin oxide can be used allowing more flexibility in terms of detection and easy combination with microfluidic systems. In analytical chemistry, signal enhancement and improvement of assay sensitivity remain a vital area of research⁸⁻¹⁰ where the combination of the essentially background-free ECL with signal amplification via nanovesicles such as liposomes¹¹ provides untapped possibilities. A signal enhancement of up to three orders of magnitude¹² can be obtained by the incorporation of a multitude of reporters in the inner cavity and the introduction of surficial recognition moieties. We have recently reported the facile synthesis of a family of substituted luminol derivatives with high chemiluminescence (CL) quantum yields,^{13,14} however their poor solubility in aqueous buffer systems does not enable their use in bio/liposome assays. Alternative hydrophobic or hydrophilic luminol derivatives, modified either at the amino functionality or the benzene ring (see Table S2) do not exhibit any better performance in ECL (few were better in CL) than the parent luminol **1**.¹⁵ In this work, we present the synthesis of a new luminol derivative, with a carboxyl group modification in the benzene-ring, to significantly enhance solubility in aqueous buffers while additionally increasing ECL yields. The new molecule shows favorable ECL capabilities in comparison to the parent luminol. If encapsulated into liposomes, DNA could be detected in a very simple manner yet at excessively low concentrations (attomolar level) in a sandwich assay using ECL signal transduction (Figure 1).

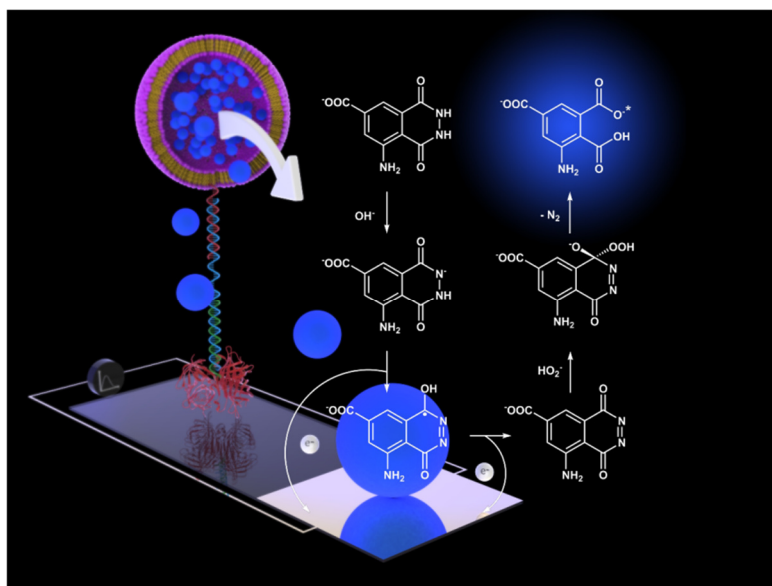
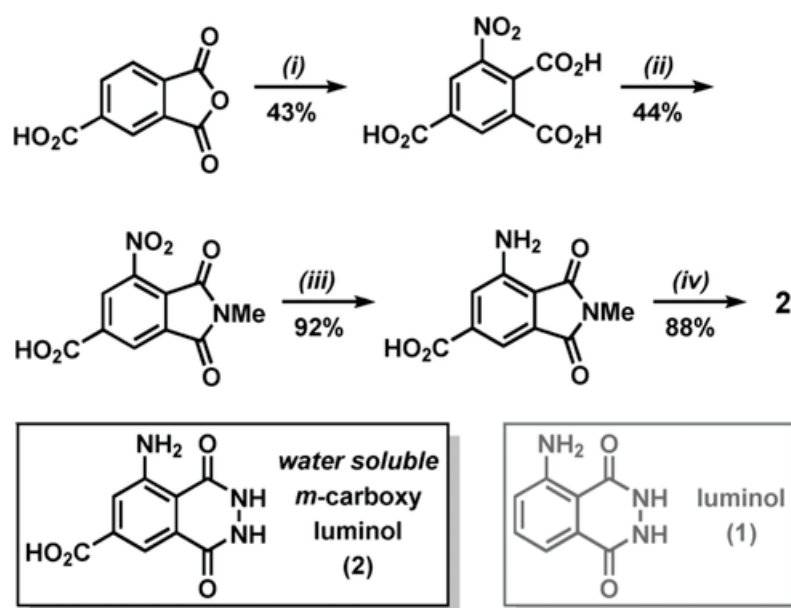


Figure 1. Assay with the proposed luminol ECL reaction and the nucleic acid sandwich structure on a streptavidin anchor with a top-bound liposome with encapsulated *m*-carboxyl luminol **2**. (CAD-liposome model provided by Andrei Georgescu)

2. Results and Discussion

We synthesized a hydrophilic luminol derivative by introduction of a carboxylate-substituent at the benzene ring. As there is no report of this strategy *via* late-stage aromatic derivatization, we decided to build up the luminol scaffold from the suitably decorated starting material trimellitic anhydride (Scheme 1). Following a literature report,¹⁶ a three-step sequence led to the corresponding phthalimide, which was then subjected to hydrazinolysis to give the desired *m*-carboxyl luminol **2** in 15% overall yield. This has the additional merit of providing an anchor for bioorthogonal conjugation.



Scheme 1. Synthesis of *m*-carboxy luminol **2**. i) KNO₃, H₂SO₄, 120 °C, 45 h; ii) 1,3-dimethylurea, 170 °C, 30 min; iii) H₂, Pd/C, r.t., 5 h; iv) hydrazine hydrate, 120 °C, 6 h.

Analytical characterization of the luminol derivative focused on its ability to function as ECL emitter. Using the parent luminol ECL conditions, a 4-fold higher signal intensity was obtained for the *m*-carboxy luminol vs. parent luminol in aqueous buffer (Figure S3). This is remarkable because quenching generally becomes more prevalent in more polar solvents and commonly decreases luminescence yields of probes by enhanced radiationless decay. At the same time, the favorably low excitation potential and the emission wavelength of 425 nm are retained (Figures S3 - S5) suggesting that **2** follows a similar ECL pathway as described for **1**.¹⁷

Subsequently, we utilized the *m*-carboxy luminol **2** in a bioassay. Here, we took further advantage of the signal enhancement strategy afforded by liposomes and developed a DNA hybridization assay. Liposomes were therefore synthesized using the standard protocol¹⁸ but with 22 mmol L⁻¹ of **2** in 0.2 mol L⁻¹ Hepes buffer (pH 8.6) as encapsulant solution. Characterization of the liposomes revealed successful and highly reproducible formation and typical data regarding size, stability and composition (Tables 1 and S4). For comparison, we aimed at the entrapment of **1** within liposomes by a literature procedure.^{19,20} However, the solubility of **1** under various conditions (Table S3) was lower than published²⁰ which prevented its encapsulation in liposomes. Even though a broad range of liposome syntheses was studied, none led to liposomes containing

sufficient amounts of parent luminol **1**. Furthermore, luminol leakage resulted in very limited stability and prohibited characterization or bioassay application (Table S3). In contrast, the *m*-carboxy luminol-liposomes were long-term stable upon storage at 10 °C²¹ which was in addition significantly increased with respect to earlier data.¹⁹

Table 1. Properties of the *m*-carboxy luminol liposomes.

Liposome data	Value
Hydrodynamic diameter	271 nm
Polydispersity index	0.22
Surface ζ potential	−24 mV
Phospholipid content	5.9 mmol L ^{−1}
Total lipid content	10.9 mmol L ^{−1}
Encapsulant concentration	22 mmol L ^{−1}
Liposome volume fraction	ca. 14 %
Calculated concentration of 2 in liposomes	ca. 16.8 mmol L ^{−1}
Encapsulation efficiency	77 %

The new *m*-carboxy luminol-liposomes were then investigated for the detection of DNA derived from pathogenic organisms in a microtiter plate assay format. The target sequence was a DNA derived from the *C. parvum* heat shock protein 70 (hsp70) mRNA which we had used previously in the development of microtiterplate, microfluidic and lateral-flow assays.²²⁻²⁴ We obtained a typical sigmoidal calibration curve (Figure 2) after minor assay optimization.²⁵ The latter included the choice of detergent used to release encapsulants from the liposomes which offers a further way to enhance the ECL signal.²⁶

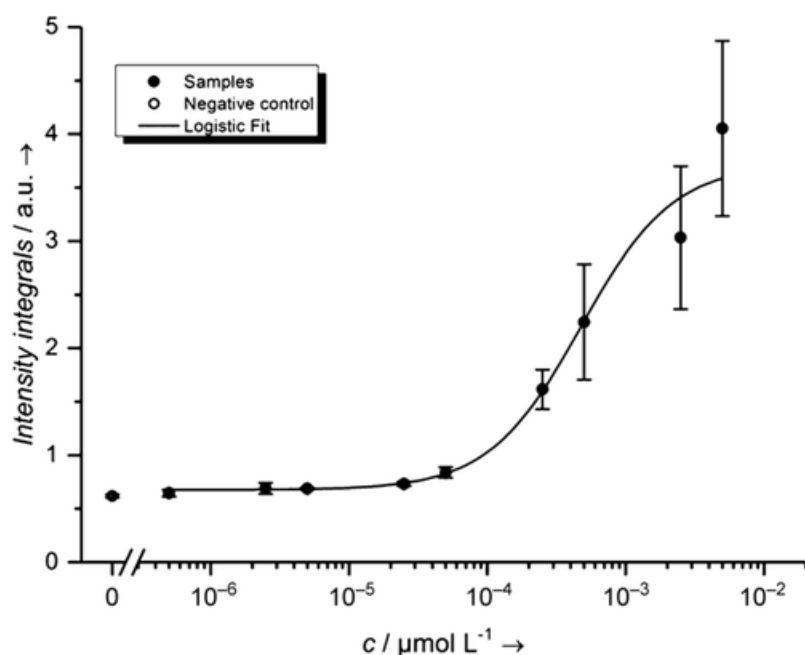


Figure 2. Calibration curve for target DNA sequence of *C. parvum* (hsp70).

The limit of detection (3σ) was 3.2 pmol L^{-1} , which corresponds to 400 amol of target DNA per test. This is about 150 times lower than previously demonstrated optimized limits of detection using a fluorescence-based liposome assay and the same type of liposome/lipid compositions.¹⁸ With only 17 mmol L^{-1} *m*-carboxy luminol entrapped in the liposomes vs. 150 mmol L^{-1} sulforhodamine B in the case of the fluorescent liposomes,¹⁸ the lower limit of detection afforded by the ECL liposomes is therefore more than significant with a total enhancement factor of almost 1500.

Table 2. Comparison of matrix effects through real samples on 100 pmol L⁻¹ DNA sequence. [18]

Sample	Signal recovery ^[a]	Intensity integrals ^[b]
Reference	100 ± 5	0.42 ± 0.02
River water	105 ± 23	0.44 ± 0.09
Soil extract	119 ± 13	0.50 ± 0.05
Bovine serum	95 ± 3	0.40 ± 0.01

[a] Given in % ± standard deviations in %. [b] Given in arbitrary units (a.u.) ± standard deviations.

Furthermore, the minimal matrix effects that were observed upon spiking 100 pmol L⁻¹ DNA sequences into various complex matrices demonstrate the strength of the background-free ECL assay principle (Table 2).

3. Conclusion

In summary, we synthesized and characterized the new *m*-carboxy luminol **2** and demonstrated its outstanding performance in bioassays.²⁸ Due to its high solubility under physiological conditions, its low oxidation potential, its high ECL yield, and the presence of a bioorthogonal functional group, **2** is highly attractive for a variety of analytical applications from which the parent luminol **1** is precluded. For example, ECL can be easily miniaturized into microfluidic systems.²⁹ Thus, one takes advantage of the absence of scattered excitation light, its low inherent background, the highly localized signal generation and minimized instrumental hardware. These are all advantages especially in comparison to miniaturized fluorescence detection. Therefore, the successful combination of *m*-carboxy luminol with liposomes reported here is a promising signal amplification tool for point-of-care and in-field detection for DNA or RNA sequences. Further approaches for bioassays can take advantage of the covalent coupling capabilities through the carboxylate group. *m*-Carboxy luminol enables studies under physiological conditions and provides efficient signal enhancement and thus bears the potential to replace luminol and [Ru(bpy)₃]²⁺ in most of their bioanalytical applications. This opens up new possibilities in chemiluminescence-based cellular imaging, *in vivo* detection of biomarkers such as ROS, highly sensitive point-of-care sensing and microarray technologies.

4. References

- (1) Tokel, N. E.; Bard, A. J. Electrogenated chemiluminescence. IX. Electrochemistry and emission from systems containing tris(2,2'-bipyridine)ruthenium(II) dichloride. *J. Am. Chem. Soc.* **1972**, *94*, 2862-2863. doi: 10.1021/ja00763a056.
- (2) Hu, L.; Xu, G. Applications and trends in electrochemiluminescence. *Chem. Soc. Rev.* **2010**, *39*, 3275-3304. doi: 10.1039/b923679c.
- (3) Lu, L.; Li, J.; Kang, T.; Cheng, S. Bi-functionalized aptasensor for ultrasensitive detection of thrombin. *Talanta* **2015**, *138*, 273-278. doi: 10.1016/j.talanta.2015.03.016.
- (4) Carrara, S.; Arcudi, F.; Prato, M.; De Cola, L. Amine-Rich Nitrogen-Doped Carbon Nanodots as a Platform for Self-Enhancing Electrochemiluminescence. *Angew. Chem. Int. Ed.* **2017**, *56*, 4757-4761. doi: 10.1002/anie.201611879.
- (5) Chen, Y.; Zhou, S.; Li, L.; Zhu, J.-j. Nanomaterials-based sensitive electrochemiluminescence biosensing. *Nano Today* **2017**, *12*, 98-115. doi: 10.1016/j.nantod.2016.12.013.
- (6) Tan, J.; Xu, L.; Li, T.; Su, B.; Wu, J. Image-Contrast Technology Based on the Electrochemiluminescence of Porous Silicon and Its Application in Fingerprint Visualization. *Angew. Chem. Int. Ed.* **2014**, *53*, 9822-9826. doi: 10.1002/anie.201404948.
- (7) Harvey, N. Luminescence during Electrolysis. *J. Phys. Chem.* **1928**, *33*, 1456-1459. doi: 10.1021/j150304a002.
- (8) Jin, Q.; Li, M.; Polat, B.; Paidi, S. K.; Dai, A.; Zhang, A.; Pagaduan, J. V.; Barman, I.; Gracias, D. H. Mechanical Trap Surface-Enhanced Raman Spectroscopy for Three-Dimensional Surface Molecular Imaging of Single Live Cells. *Angew. Chem. Int. Ed.* **2017**, *56*, 3822-3826. doi: 10.1002/anie.201700695.
- (9) Du, Y.; Pothukuchy, A.; Gollihar, J. D.; Nourani, A.; Li, B.; Ellington, A. D. Coupling Sensitive Nucleic Acid Amplification with Commercial Pregnancy Test Strips. *Angew. Chem. Int. Ed.* **2017**, *56*, 992-996. doi: 10.1002/anie.201609108.
- (10) Shintaku, H.; Palko, J. W.; Sanders, G. M.; Santiago, J. G. Increasing Hybridization Rate and Sensitivity of Bead-Based Assays Using Isotachophoresis. *Angew. Chem. Int. Ed.* **2014**, *53*, 13813-13816. doi: 10.1002/anie.201408403.

- (11) Pattni, B. S.; Chupin, V. V.; Torchilin, V. P. New Developments in Liposomal Drug Delivery. *Chem. Rev.* **2015**, *115*, 10938-10966. doi: 10.1021/acs.chemrev.5b00046.
- (12) Edwards, K. A.; Baeumner, A. J. Liposomes in analyses. *Talanta* **2006**, *68*, 1421-1431. doi: 10.1016/j.talanta.2005.08.044.
- (13) Griesbeck, A. G.; Díaz-Miara, Y.; Fichtler, R.; Jacobi von Wangelin, A.; Pérez-Ruiz, R.; Sampedro, D. Steric Enhancement of the Chemiluminescence of Luminols. *Chem. Eur. J.* **2015**, *21*, 9975-9979. doi: 10.1002/chem.201500798.
- (14) Pérez-Ruiz, R.; Fichtler, R.; Diaz Miara, Y.; Nicoul, M.; Schaniel, D.; Neumann, H.; Beller, M.; Blunk, D.; Griesbeck, A. G.; Jacobi von Wangelin, A. On the photophysical properties of new luminol derivatives and their synthetic phthalimide precursors. *J. Fluoresc.* **2010**, *20*, 657-664. doi: 10.1007/s10895-010-0598-0.
- (15) See supplementary information, chapter 5.3.1
- (16) Ribi, M. A.; Wei, C. C.; White, E. H. Energy transfer involving derivatives of luminol. *Tetrahedron* **1972**, *28*, 481-492. doi: 10.1016/0040-4020(72)84012-2.
- (17) Wilson, R.; Akhavan-Tafti, H.; DeSilva, R.; Schaap, A. P. Comparison between acridan ester, luminol, and ruthenium chelate electrochemiluminescence. *Electroanalysis* **2001**, *13*, 1083-1092. doi: 10.1002/1521-4109(200109)13:13<1083::AID-ELAN1083>3.0.CO;2-D.
- (18) Edwards, K. A.; Baeumner, A. J. Optimization of DNA-tagged liposomes for use in microtiter plate analyses. *Anal. Bioanal. Chem.* **2006**, *386*, 1613-1623. doi: 10.1007/s00216-006-0743-4.
- (19) Nakonechny, F.; Firer, M. A.; Nitzan, Y.; Nisnevitch, M. Intracellular antimicrobial photodynamic therapy: A novel technique for efficient eradication of pathogenic bacteria. *Photochem. Photobiol.* **2010**, *86*, 1350-1355. doi: 10.1111/j.1751-1097.2010.00804.x.
- (20) Rakthong, P.; Intaramat, A.; Ratanabanangkoon, K. Luminol encapsulated liposome as a signal generator for the detection of specific antigen-antibody reactions and nucleotide hybridization. *Anal. Sci.* **2010**, *26*, 767-772. doi: 10.2116/analsci.26.767.
- (21) See supplementary information, chapter 5.3.5
- (22) Edwards, K. A.; Curtis, K. L.; Sailor, J. L.; Baeumner, A. J. Universal liposomes: Preparation and usage for the detection of mRNA. *Anal. Bioanal. Chem.* **2008**, *391*, 1689-1702. doi: 10.1007/s00216-008-1992-1.
- (23) Connelly, J. T.; Nugen, S. R.; Borejsza-Wysocki, W.; Durst, R. A.; Montagna, R. A.; Baeumner, A. J. Human pathogenic *Cryptosporidium* species bioanalytical detection method with single oocyst detection capability. *Anal. Bioanal. Chem.* **2008**, *391*, 487-495. doi: 10.1007/s00216-008-1967-2.

- (24) Esch, M. B.; Locascio, L. E.; Tarlov, M. J.; Durst, R. A. Detection of Viable *Cryptosporidium parvum* Using DNA-Modified Liposomes in a Microfluidic Chip. *Anal. Chem.* **2001**, 73, 2952-2958. doi: 10.1021/ac001508n.
- (25) See supplementary information, chapter 5.3.7
- (26) See supplementary information, chapter 5.3.6
- (27) See supplementary information, chapter 5.2.8.
- (28) Detection of DNA spiked into various matrices was chosen as powerful example demonstrating assay stability and high sensitivity of the ECL liposome approach. Detection of nucleic acids after their extraction from a matrix or after their amplification through a molecular biological approach results in cleaner matrices and is therefore significantly simpler. The applicability to extracted and amplified RNA and DNA sequences was shown previously²³ through fluorescent liposomes.
- (29) Kadimisetty, K.; Malla, S.; Sardesai, N. P.; Joshi, A. A.; Faria, R. C.; Lee, N. H.; Rusling, J. F. Automated multiplexed ecl immunoarrays for cancer biomarker proteins. *Anal. Chem.* **2015**, 87, 4472-4478. doi: 10.1021/acs.analchem.5b00421.

5. Supplementary Information

5.1 Abbreviations

DLS	Dynamic light scattering
DPPC	1,2-dipalmitoyl-sn-glycero-3- phosphocholine
DPPG	1,2-dipalmitoyl-sn-glycero-3[phospho-rac-(1-glycerol)],sodium salt
DPPE-GA	1,2-dipalmitoyl-sn-glycero-3-phosphoethanolamine-N-(glutaryl), sodium salt
<i>ee</i>	Encapsulation efficiency
ITO	Indium tin oxide
<i>m</i> -carboxy luminol	8-Amino-1,4-dioxo-1,2,3,4-tetrahydrophthalazine-6-carboxylic acid
PdI	Polydispersity index
Ru(bpy) ₃ ²⁺	Tris(2,2'-bipyridyl)ruthenium(II)
λ_{Em}	Emission wavelength

5.2 Experimental Procedures

5.2.1 Materials

For the *m*-carboxy luminol synthesis, all reagents and solvents were purchased from commercial suppliers (Aldrich, Alfa, Fluka, Merck) and used as received. DPPC, DPPG, DPPE-GA, 1.0 μ m and 0.4 μ m filter membranes and filter supports were purchased from Avanti Polar Lipids (Alabaster, U.S.). Fetal bovine serum (FBS Superior) was obtained from Biochrom (Germany). Cholesterol, Ficoll 400, Sephadex G50 (medium), sodium citrate (dihydrate) and Zonyl-FSN-100 were obtained from SigmaAldrich (Taufkirchen,

Germany). BSA (albumin fraction V from bovine serum), di-potassium hydrogen phosphate, formamide, Glycine, potassium chloride, potassium dihydrogen phosphate, sodium azide, sodium hydroxide (1 mol L^{-1} in water) and sucrose were bought from Merck (Germany). Hydrogen peroxide (30% v/v in water), HEPES and sodium chloride were purchased from VWR (Germany), hydrochloric acid (1 mol L^{-1} solution in water) was bought from Fluka (Germany) and Tris was obtained from Affymetrix (Ohio, U.S.). Nucleic acid sequences were obtained from Life Technologies GmbH (Darmstadt, Germany). Rotilabo, sterile syringe filters ($0.45 \mu\text{m}$ pore size) were bought from Carl Roth (Germany).

5.2.2 Buffers and reaction mixes

0.1 mol L^{-1} glycine-NaOH buffer for ECL was prepared by dilution of an appropriate amount of glycine in millipore water and adjustment of the pH to 9.0 with 1 mol L^{-1} sodium hydroxide solution. Liposome outer buffer consisted of 10 mmol L^{-1} glycine-NaOH at a pH of 8.6, 200 mmol L^{-1} NaCl, 0.1% NaN_3 and 113 mmol L^{-1} sucrose with a solution osmolality of 524 mosm/kg. The *m*-carboxy luminol ECL mix consisted of $100 \mu\text{mol L}^{-1}$ *m*-carboxy luminol (**2**), 30 mmol L^{-1} H_2O_2 , 0.1 mol L^{-1} KCl, and varying surfactant amount or presence in glycine-NaOH buffer. Washing buffer, contained 0.01% BSA and 0.05% Tween 20 in 1xPBS buffer at pH 7.4. 1xPBS buffer, consisted of 137 mmol L^{-1} NaCl, 2.7 mmol L^{-1} KCl, 10 mmol L^{-1} Na_2HPO_4 and 1.8 mmol L^{-1} KH_2PO_4 at a pH of 7.4. Potassium phosphate buffer contained 50 mmol L^{-1} K_2HPO_4 , 50 mmol L^{-1} KH_2PO_4 and 1 mmol L^{-1} EDTA at pH 7.5. Hybridization buffer (9xSSC) was made from 1.35 mol L^{-1} NaCl, 0.135 mol L^{-1} sodium citrate, 0.01% (w/v) NaN_3 , 30% (v/v) formamide and 0.2% (w/v) Ficoll 400 at a pH of 7.0. Hepes-saline-sucrose (HSS) buffer was prepared from 10 mmol L^{-1} Hepes, 200 mmol L^{-1} NaCl, 0.01% (w/v) NaN_3 and a varying sucrose level, adjusted to the same osmolality as the liposome outer buffer. The pH was set to 7.0. The lysis mixture consisted of 30 mmol L^{-1} H_2O_2 , 0.5 wt. % Zonyl FSN 100 and 0.1 mol L^{-1} KCl in 0.1 mol L^{-1} glycine-NaOH buffer at pH 9.0.

5.2.3 *m*-Carboxy luminol synthesis

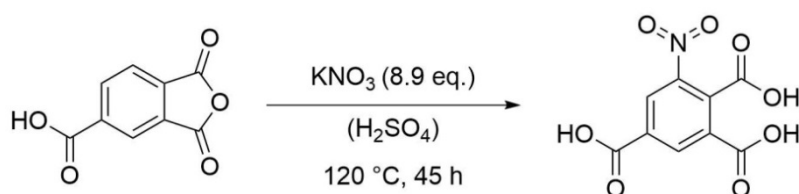
Hydrogenation reactions were performed in an autoclave with manometer stable until 10 bar of gas pressure. Purity and structure confirmation of isolated products was performed by ^1H NMR, ^{13}C NMR, high resolution mass spectrometry (HRMS) and infrared spectroscopy (IR). NMR spectral data were collected on a Bruker Avance 300 (300 MHz for ^1H ; 75 MHz for ^{13}C) spectrometer, a Bruker Avance 400 (400 MHz for ^1H ; 100 MHz for ^{13}C) spectrometer and a Bruker Avance 600 cryo (600 MHz for ^1H ; 150 MHz for ^{13}C) at 20 °C. Chemical shifts are reported in δ/ppm , coupling constants J are given in Hertz. Solvent residual peaks were used as internal standard for all NMR measurements. The quantification of ^1H cores was obtained from integrations of appropriate resonance signals. Abbreviations used in NMR spectra: s – singlet, d – doublet, bs – broad singlet. HRMS was carried out by the Central Analytics at the department of chemistry, University of Regensburg. Abbreviations used in HRMS: M – molar mass of target compound, ESI – electrospray ionization. IR spectra were recorded on an Agilent Cary 630 FTIR spectrometer using an ATR unit at ambient temperature. Abbreviations used in IR spectra: b – broad, s – strong, m – medium, w – weak. Melting points were measured on a SRS OptiMelt MPA 100 machine.

5.2.4 Detailed procedures for the synthesis of *m*-carboxy luminol

In our approach, the first step in the reaction sequence (see scheme **1**) was the nitration of trimellitic anhydride **1**, which resembles an electron-poor aromatic and hence harsh conditions had to be applied. As expected, these conditions led to the opening of the anhydride to the free acid moieties, which was clearly confirmed by NMR and IR data. In the second step the phthalimide moiety was introduced via condensation with 1,3-dimethylurea to yield compound **3**. Reduction of the nitro-group and subsequent hydrazinolysis afforded luminol **5** in 15% yield over four steps. As the first two steps give rather moderate yields, due to the harsh conditions applied and the modestly effective recrystallizations, we are currently investigating the optimization of these steps as well as further conjugation protocols to employ *m*-carboxy luminol as a covalent label in bioassays. Another possible synthesis route for an introduction of

COOH-groups into the benzene ring part of luminol would be a multicomponent reaction with introduction of two carboxy groups in 5- and 7- position of the final luminol as reported by *Neumann et al.*⁵¹ This approach was not favored as it could influence the ECL reaction to a greater extent, it would add unspecificity towards future use with bioconjugation reactions and furthermore did not seem very promising from a synthesis strategy point-of-view, due to the aldehyde that would have been necessary to be used.

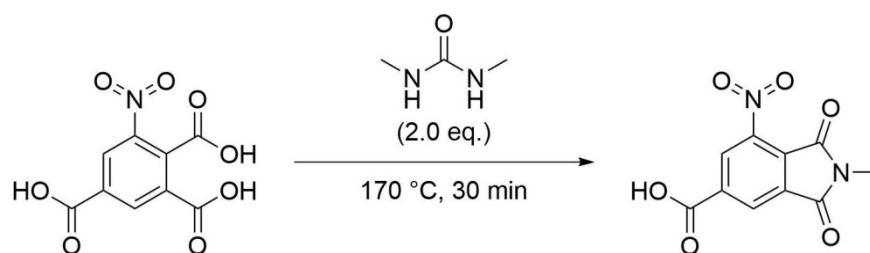
6-Nitrobenzene-1,2,4-tricarboxylic acid



The procedure was based on earlier prescriptions.⁵² Trimellitic anhydride (6.00 g, 31.2 mmol) was dissolved in concentrated sulfuric acid (97%, 50 mL) with stirring at 90°C. Potassium nitrite (16.0 g, 158 mmol) was added in portions over 30 minutes and the mixture was heated to 120°C for 22 hours. Another portion of potassium nitrite (6.00 g, 59.3 mmol) was added and heated to 120°C for six hours, before a final portion of potassium nitrite (6.00 g, 59.3 mmol) was added and heated to 120°C for 16 hours. Then, the mixture was poured on ice and extracted with diethyl ether (3 x 200 mL). The combined organic phases were dried over magnesium sulfate and filtered. After evaporation of the solvent, the crude residue was crystallized from benzene saturated with diethyl ether under slow evaporation of the volatile solvent. Contrary to the expectations, the anhydride was opened during the reaction and 6-nitrobenzene-1,2,4-tricarboxylic acid (3.40 g, 13.3 mmol, 43%) was obtained as a slightly off-white solid. Nitration in 5-position also occurred and the corresponding product could not be separated via crystallization (5% in first crystallization fraction).

¹H NMR (400 MHz, DMSO-*d*₆): δ = 14.07 (bs, 3H), 8.66 (d, *J* = 1.6 Hz, 1H), 8.64 (d, *J* = 1.6 Hz). **¹³C NMR** (100 MHz, DMSO-*d*₆): δ = 165.4, 165.0, 164.4, 146.6, 135.0, 133.9, 132.7, 131.7, 128.0. **HRMS** (ESI): *m/z* = calcd. for C₉H₅NO₈[−] (−H): 253.9942, found: 253.9955. **IR** (ATR, neat): $\tilde{\nu}$ [cm^{−1}] = 3350–2200 (bs, COOH), 1700 (s, COOH), 1548 (m, NO₂), 1349 (m, NO₂), 1260 (s, COOH). **M.p.**: decomposition at 265°C.

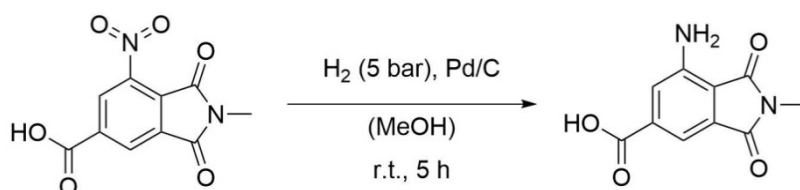
4-Carboxy-6-nitro-*N*-methylphthalimide



The procedure was based on earlier descriptions.⁵² 6-Nitrobenzene-1,2,4-tricarboxylic acid (2.00 g, 8.43 mmol) and 1,3-dimethylurea were melted and heated to 170 °C with stirring for 30 minutes. After cooling to room temperature the solid mixture was dissolved in water (20 mL) and ethyl acetate (20 mL). The organic phase was separated, washed with water (20 mL) again, and then extracted with saturated aqueous sodium bicarbonate solution (20 mL). The extract was acidified with concentrated HCl. The precipitate was filtered off and recrystallized from ethanol/water. 4-Carboxy-6-nitro-*N*-methylphthalimide (920 mg, 3.68 mmol, 44%) was obtained as pale yellow needles.

¹H NMR (400 MHz, DMSO-*d*₆): δ = 14.24 (bs, 1H), 8.65 (d, *J* = 1.2 Hz, 1H), 8.39 (d, *J* = 1.6 Hz), 3.07 (s, 3H). **¹³C NMR** (100 MHz, DMSO-*d*₆): δ = 165.4, 164.3, 162.9, 144.2, 137.8, 134.6, 128.6, 126.4, 125.8, 24.4. **HRMS** (ESI): *m/z* = calcd. for C₁₀H₆N₂O₆[−] (−H): 249.0153, found: 249.0167. **IR** (ATR, neat): $\tilde{\nu}$ [cm^{−1}] = 3350–2200 (bs, COOH), 1778 (m, imide), 1693 (s, COOH), 1543 (m, NO₂), 1356 (m, NO₂), 1260 (m, COOH). **M.p.**: 228°C.

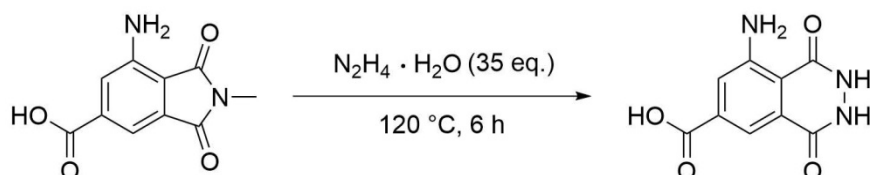
6-Amino-4-carboxy-*N*-methylphthalimide



The procedure was based on earlier descriptions.^{S2} 4-Carboxy-6-nitro-*N*-methylphthalimide (400 mg, 1.60 mmol) and palladium (10% on activated carbon, 50.0 mg) were suspended in methanol (14 mL). The atmosphere was changed from oxygen to hydrogen (5 bar) and the mixture was stirred at room temperature for five hours. The mixture was filtered and the residue repeatedly washed with boiling methanol (200 mL) until only catalyst was left insoluble. Evaporation of the solvent gave 6-amino-4-carboxy-*N*-methylphthalimide (324 mg, 1.47 mmol, 92%) as a yellow solid.

¹H NMR (300 MHz, DMSO-*d*₆): δ = 13.45 (bs, 1H), 7.61 (d, *J* = 1.1 Hz, 1H), 7.32 (d, *J* = 1.1 Hz), 6.64 (s, 2H), 2.97 (s, 3H). **¹³C NMR** (75 MHz, DMSO-*d*₆): δ = 169.0, 167.6, 166.3, 146.1, 136.8, 133.1, 122.7, 111.9, 110.0, 23.5. **HRMS** (ESI): *m/z* = calcd. for C₁₀H₈N₂O₄^{−•} (−H): 219.0411, found: 219.0422. **IR** (ATR, neat): $\tilde{\nu}$ [cm^{−1}] = 3500–2100 (bs, COOH), 3481 (m, NH₂), 3366 (m, NH₂), 1730 (m, imide), 1681 (s, COOH). **M.p.**: decomposition at 285°C.

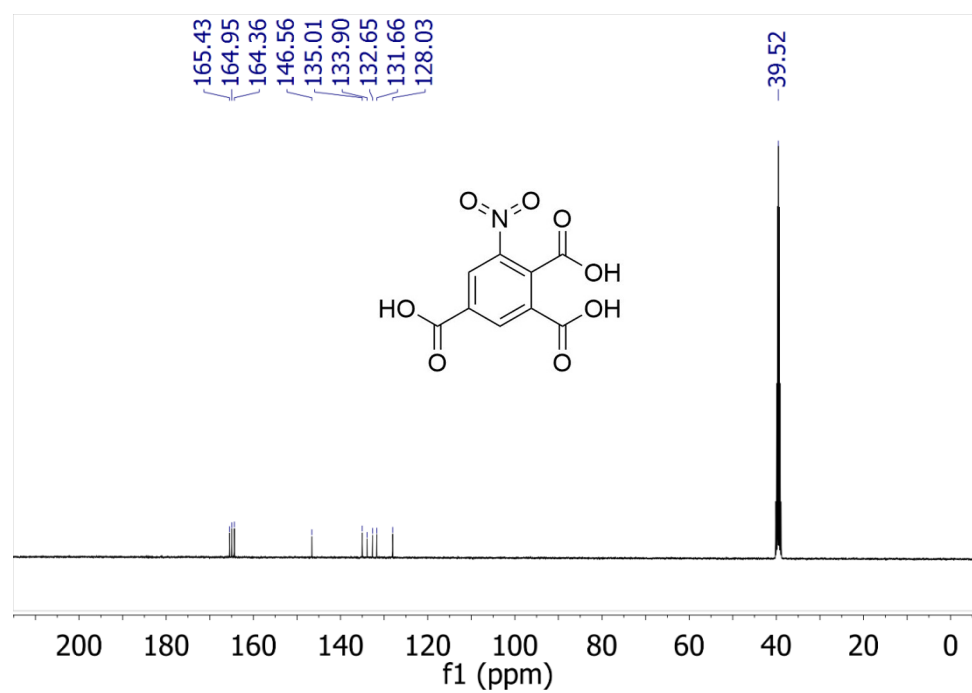
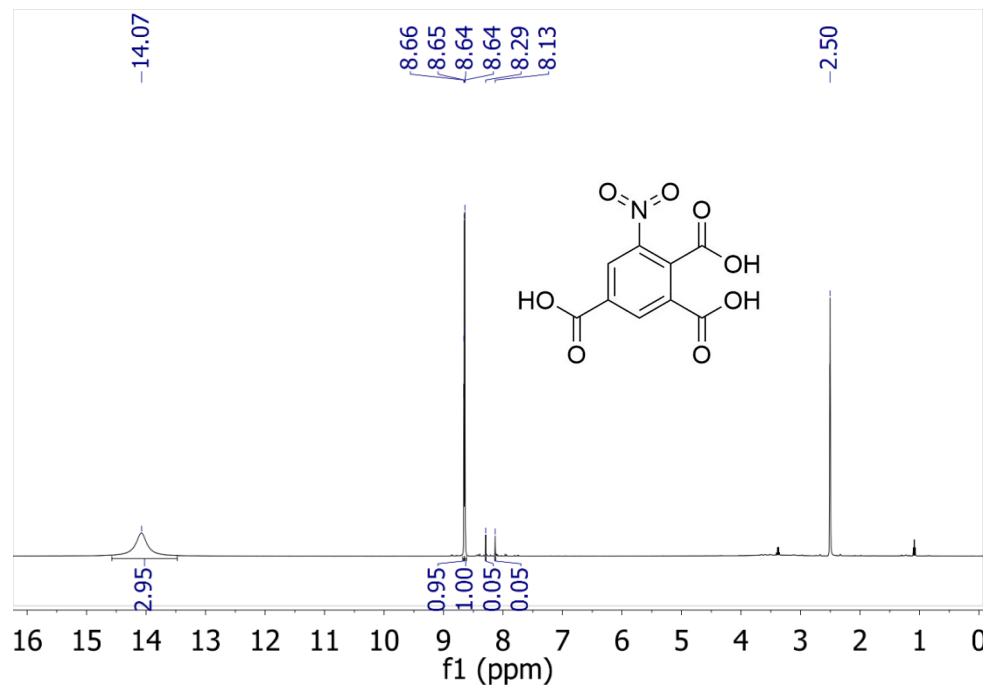
8-Amino-1,4-dioxo-1,2,3,4-tetrahydrophthalazine-6-carboxylic acid

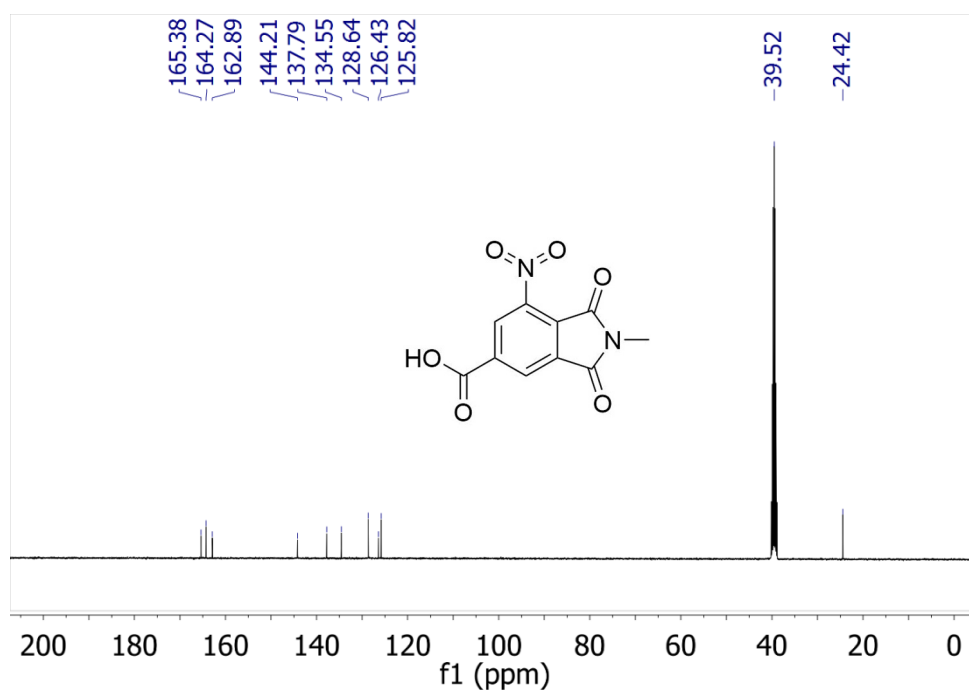
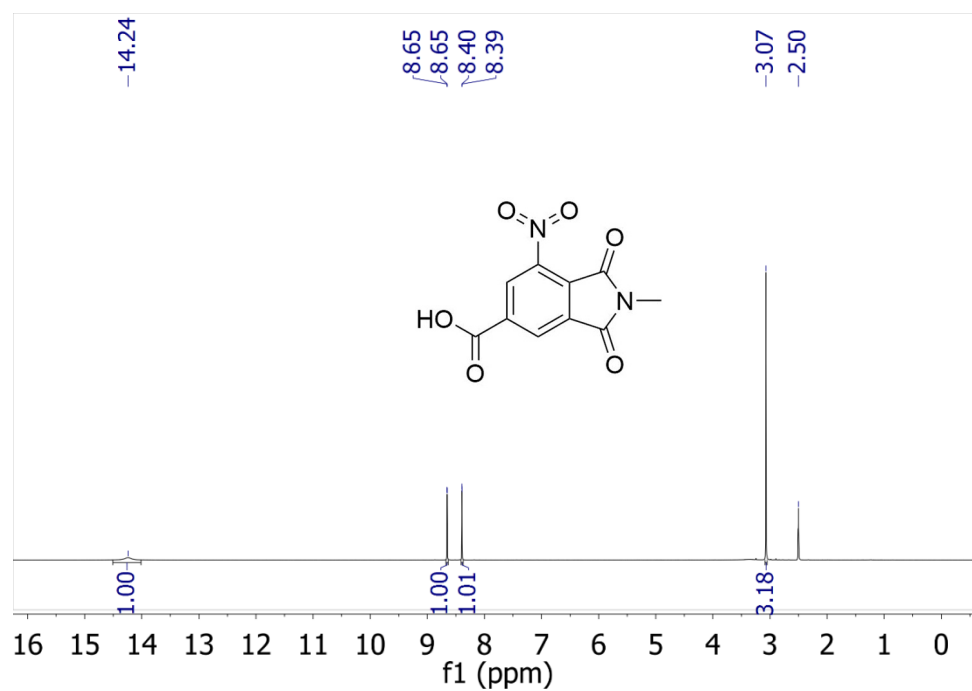


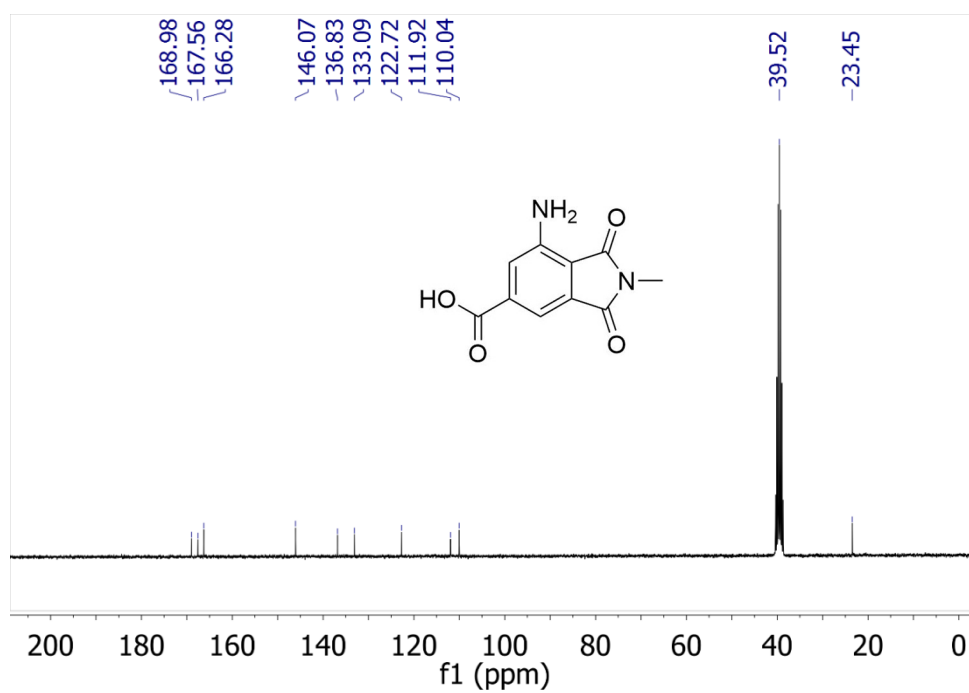
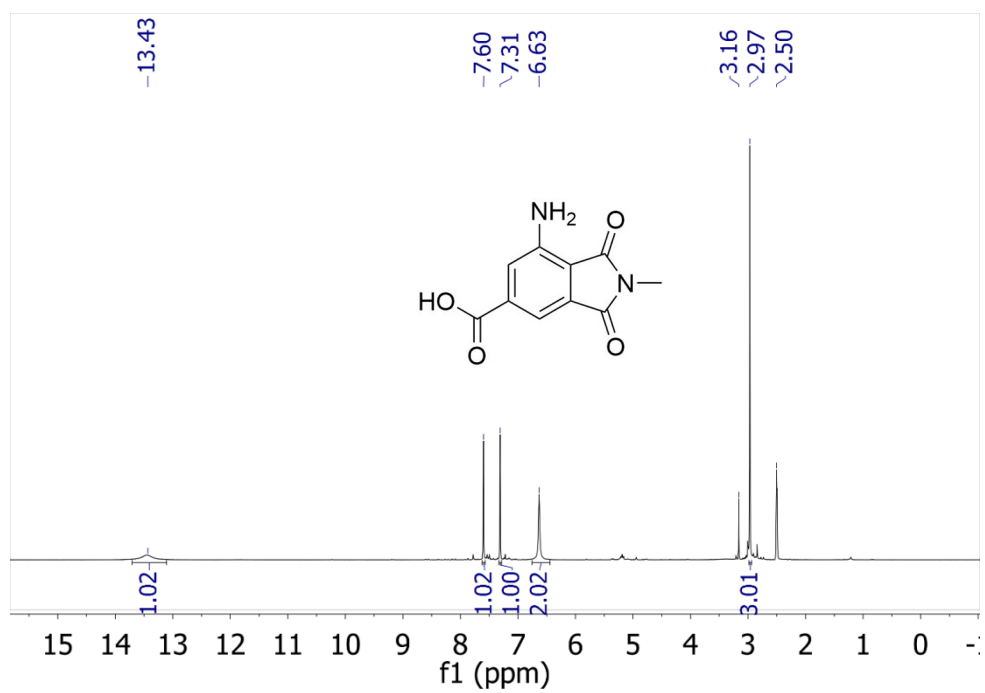
The procedure was based on earlier prescriptions.^{S1} 6-Amino-4-carboxy-*N*-methylphthalimide (250 mg, 1.14 mmol,) was suspended in hydrazine hydrate (2.00 mL, 39.7 mmol) and heated to 120 °C for six hours with stirring in a pressure tube under N₂ atmosphere. After cooling to room temperature the volatile compounds were removed in vacuum. The residue was suspended in hot methanol (2 x 20 mL) and filtered off. After drying in high vacuum 8-amino-1,4-dioxo-1,2,3,4-tetrahydrophthalazine-6-carboxylic acid (221 mg, 1.00 mmol, 88%) was obtained as a slight yellow solid.

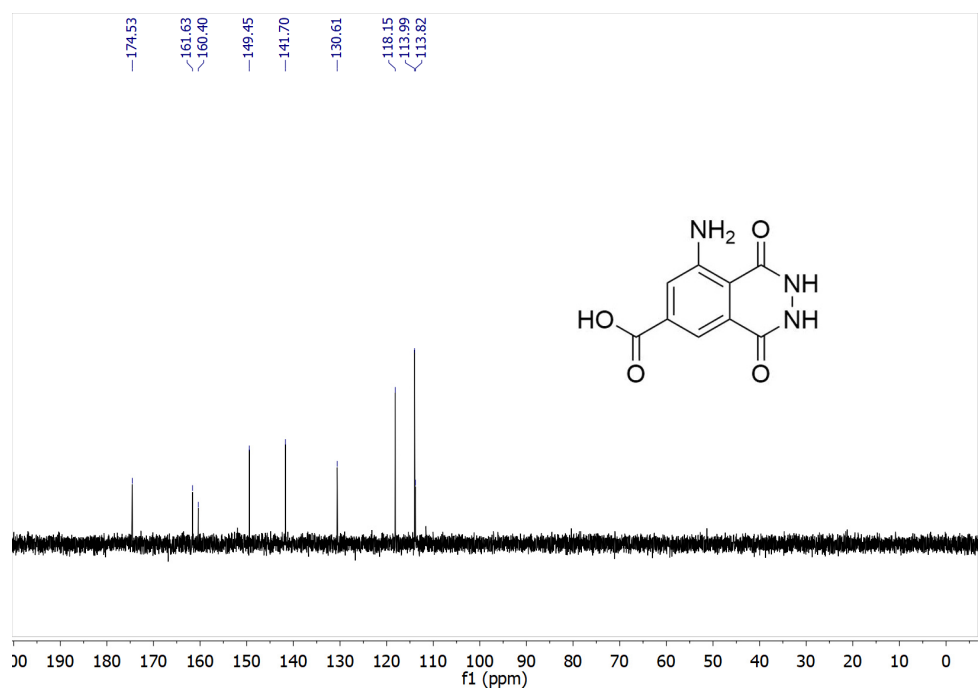
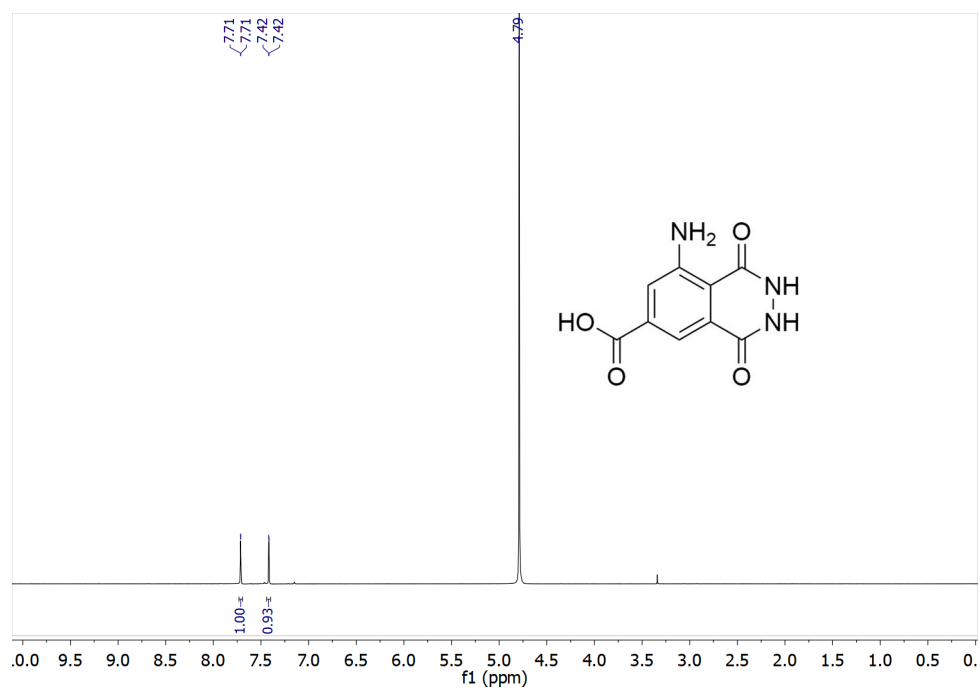
¹H NMR (400 MHz, D₂O): δ = 7.71 (d, J = 1.6 Hz, 1H), 7.42 (d, J = 1.6 Hz, 1H). **¹³C NMR** (100 MHz, D₂O): δ = 174.5, 161.6, 160.4, 149.5, 141.7, 130.6, 118.2, 114.0, 113.8. **HRMS** (ESI): m/z = calcd. for C₉H₇N₃O₄⁻ (–H): 220.0364, found: 220.0370. **IR** (ATR, neat): $\tilde{\nu}$ [cm⁻¹] = 3500–2100 (bs, COOH), 3444 (m, NH₂), 3295 (m, NH₂), 1625 (s, COOH). **M.p.**: > 300 °C.

5.2.5 Selected NMR spectra of isolated products









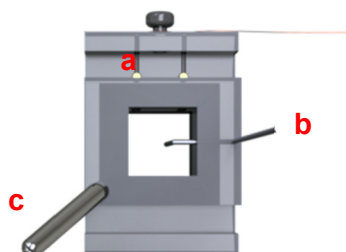
5.2.6 Liposome synthesis

Liposomes encapsulating carboxy-luminol were prepared according to an established protocol from Edwards et al.⁵³ with modifications in buffer composition. Briefly, DPPC, DPPG and cholesterol (40.9 μmol , 20.1 μmol and 51.7 μmol) were dissolved in a mixture of 3 mL CHCl_3 and 0.5 mL MeOH in a round bottom flask. Then, 50 μL of a 300 $\mu\text{mol L}^{-1}$ dilution of cholesteryl tagged reporter probe (diluted with a mixture of methanol/formamide of 1:4 (v/v); matching 0.013 mol% of total lipid content) were added and the mixture was intensely sonicated in a ultrasonication bath (VWR ultrasonic cleaner, model USC 300 THD) at 47 °C. After all solids had been solubilized, 2 mL of preheated (47°C) encapsulant solution (29 mmol L^{-1} *m*-carboxy luminol (**2**) in 0.2 mol L^{-1} Hepes buffer set to a final pH of 8.6 and a solution osmolality of 433 mosm/kg) were added to the mixture which was further sonicated at 47 °C for 5 minutes. Solvent was evaporated at 47 °C and further 2 mL of encapsulant solution was added during the evaporation procedure. Subsequently, liposomes were extruded through 1.0 μm and subsequently 0.4 μm filter membranes. Finally, the solution was purified using a size-exclusion column (2 cm x 8 cm) with Sephadex G 50 as stationary phase and eluted with liposome outer buffer with a speed of ~ 5 ml/min. It was dialyzed against outer liposome buffer overnight in a Spectrum Labs, Spectra/Por standard tubing dialysis membrane with a pore size of 12-14 kDa. The purified solutions were stored at 10 °C protected from light.

5.2.7 ECL measurements

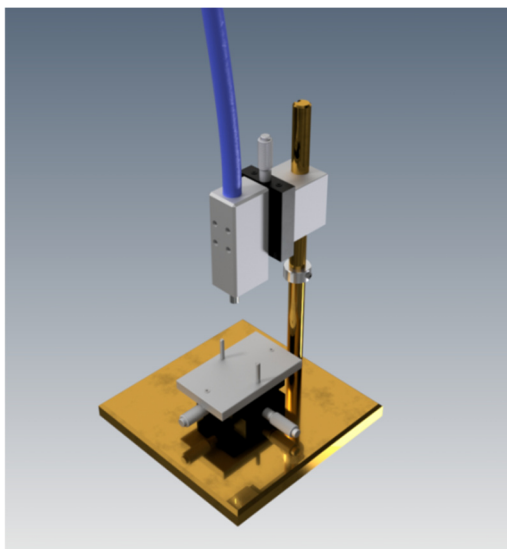
All ECL measurements were performed with a 3-electrode setup, consisting of a ITO – working electrode (WE, sheet electrode on PET foil), a Pt-counter electrode (CE, wire, 0.5 mm diameter) and an Ag-wire pseudo reference electrode (RE, 2.0 mm diameter) inside a self-designed, 3-D-printed minicell fabricated within collaboration with the Sensorik-Applikations Zentrum of the OTH Regensburg (figure S1).

Figure S1. Mini-cell for ECL measurements (top view) with integrated electrodes. (a: gold coated spring feather contact pins establishing contact to the WE connected with a copper wire; b: Pt-CE (d= 0.5 mm); c: Ag-*Pseudo*RE; at the bottom of the cell: sealing rubber bonded onto the cell bottom).



The active WE-area is $\sim 50 \text{ mm}^2$. The cell was fixed onto a self-designed, manually operated xyz-linear stage (figure S2), allowing for exact positioning of the optical fiber for emission readout above the cell opening.

Figure S2. linear xyz-stage for ECL-cell placement and optical fiber adjustment.



Electrical connection was established with an Autolab MAC 08121 potentiostat (Autolab BV, Netherlands) connected to a PC, operating the Autolab Nova software for operation. We used amperometric recording with a constant potential over 30 seconds. Optical readout was done with an Aminco Bowman, AB 2 spectrofluorimeter via a y-shaped bifurcated optical fiber (diameter = 10 mm). All ECL measurements were obtained, recording the luminescence signal for 40 seconds, while a constant excitation potential was applied for 30 seconds during that time. Different emission monochromator wavelengths were used, while the slit-width was always opened to 16 nm. PMT voltages were altered for different experiments. All measurements were done with a measuring volume of 120 μL . All signals are given as intensity integrals over the total acquisition time, integrated with the software of the luminescence spectrometer, if not otherwise stated. The composition of the ECL reaction mixture always contained 30 mmol L^{-1} H_2O_2 as coreactant, 0.1 mol L^{-1} KCl as electrolyte. Partially, surfactant was added and a 0.1 mol L^{-1} glycine-NaOH buffer at pH 9.0 was used throughout. Cyclic voltammetry (CV) measurements were done with a 3-electrode setup, using a gold disk electrode ($d = 1.6$ mm) as WE, a Pt-wire ($d = 0.5$ mm) as CE and an Ag/AgCl reference electrode with solutions of the ECL mix or buffer with the respective luminol species. CV conditions are given in the figure captions or footnotes.

5.2.8 Liposome characterization

The dialyzed liposomes were characterized by means of ECL signal, size distribution, surface ζ -potential and phospholipid content. For the ECL measurements, liposome solution was diluted 1:10 in the ECL reaction mixture. A solution with intact liposomes, one with lysed liposomes and a reference solution with 100 $\mu\text{mol L}^{-1}$ luminol were measured. Liposomes were lysed by addition of surfactant and vigorous mixing. With these values, the lysis ratio, the encapsulated *m*-carboxy luminol amount and long-time stability were determined. The size and size distribution of the liposomes was measured, using a Zetasizer Nano, model ZEN3600 device (Malvern Instruments, UK). The dynamic light scattering (DLS) measurements were done with a standard disposable polystyrene cuvette filled with 1 mL of sample solution. Liposome suspensions were diluted 1:100 with liposome outer buffer to reach a phospholipid

concentration of about 100 $\mu\text{mol L}^{-1}$. The device settings of the Zetasizer were set to backscattering mode with an angle of 173° and 120 s of equilibration time at 20 °C. 30 consecutive measurements were performed. From the autocorrelation data, the mean hydrodynamic diameter and the polydispersity index (Pdl) were extracted. The ζ -potential was determined from the mean electrophoretic mobility with the same device with a DTS-1070 folded capillary cell (Malvern Instruments). The phospholipid content of the liposomes was analyzed, using inductively coupled plasma atomic emission spectroscopy (ICP-AES). Here, dilutions were prepared, using a 1:150 dilution of liposome solution in 0.5 mol L^{-1} HNO_3 with a total sample volume of 3 mL. As reference solution, 100 $\mu\text{mol L}^{-1}$ Na_2HPO_4 in 0.5 mol L^{-1} HNO_3 was used, corresponding to an established measurement protocol.⁵⁴ The measurements were done on a Spectro Flame-EOP (Spectro Analytical Instruments GmbH, Kleve, Germany).

5.2.9 Surfactant study

Different surfactants were tested for their effect on the ECL signal of *m*-carboxy luminol. They were chosen according to a range of different HLB (hydrophilic-lipophilic balance) values ranging from 2 to 18: Zonyl® FSN-100 (HLB: 2.1⁵⁵), octylglucoside (HLB: 12.6⁵⁶), Triton-X-100 (HLB: 13.5⁵⁶), Tween 20 (HLB: 16.7⁵⁶), and Brij S 100 (HLB: 18⁵⁷). The surfactants were added to a standard luminol ECL mix in different concentrations.

5.2.10 Sandwich hybridization assay

The assay was performed with minor modifications according to an established and optimized protocol for DNA-tagged liposomes with similar size to the *m*-carboxy luminol (**2**) liposomes.⁵³ In this case, DNA sequences from *C. parvum* were chosen as model system. The chosen sequences are corresponding to heat shock protein 70 coding mRNA, as these have been proven as suitable analyte.^{53, 58} Three matching sequences were used, divided into capture probe (CP), target sequence (tDNA) and reporter probe (RP) [CP: 5'-biotinyl-AGATTCGAAGAACTCTGCGC-3'; tDNA: 5'-

AAGGACCAGCATCCTTGAGTACTTTCTCAACTGGAGCTAAAGTTGCACGGAAGTAATCAGCGC
 AGAGTTCTTCGAATCTAGCTCTACTGATGGCAACTGA-3'; RP: 5'- GTGCAACTTTAGCTCCAG
 TT-cholesteryl-3']. First, streptavidin-coated microtiterplates (KaiSA-96 Lockwell) from
 Kaivogen (Turku, Finland) with a reported binding capacity of >15 pmol biotin/well
 were washed 2x with 200 µL washing buffer, followed by a single washing step with 200
 µL PBS buffer. Then, 100 µL of the biotinylated capture probe, diluted to a
 concentration of 0.1 µmol L⁻¹ with 50 mmol L⁻¹ potassium phosphate buffer were
 pipetted to each well. Incubation for 30 minutes at room temperature was performed
 with slight agitation (60 rpm) of the plates. Afterwards, unbound capture probe was
 removed and the plate was allowed to dry for a minute. The plates were further
 washed with 2x200 µL washing buffer and then 2x200 µL hybridization buffer. Then,
 100 µL of target DNA diluted to appropriate concentrations was added to each well.
 The probes were incubated at RT for 30 minutes with shaking. Unbound target DNA
 was removed, washed with 2x200 µL HSS buffer. Finally, 100 µL of diluted liposome
 suspension was added to each well and incubated at RT for 30 minutes under agitation.
 Then the liposome supernatant was removed, washed with 3x200 µL HEPES-saline
 sucrose buffer. Bound liposomes were lysed using 125 µL of lysis mixture, incubated at
 RT for 5 minutes under shaking. ECL measurements of all samples were performed
 while covering the remaining wells with parafilm to avoid evaporation. Data evaluation
 was done with the Software Origin (Version 2017; OriginLab Corporation, MA, U.S.A).
 As curve fit equation, a four-parameter logistic model was chosen (equation S1) with A₁
 being the response at a concentration of zero, A₂ is the response at saturation, x is the
 analyte concentration, x₀ is the analyte concentration at half-maximum response and p
 is the slope factor.^{S9}

Equation S1. Formula of 4-point logistic fit model.^{S10-S11}

$$y = \frac{A_1 - A_2}{1 + \left(\frac{x}{x_0}\right)^p} + A_2$$

The limit of detection was determined from the relation “signal_{LOD} = mean value_{negative control} + 3*standard deviation_{negative control}”,^{S12-S13} with the corresponding C_{LOD} (concentration at the limit of detection) value being derived from the 4-point logistic

fit.” The herein used 4-point-logistic non-linear fit model was chosen based on statistical quality considerations, revealing a R^2 value of 0.97 and an adjusted R^2 of 0.96 for our model. These were the best obtained values when comparing to a 5-point logistic model and others (all contained in the Origin software). This and the lowest obtained weighted sum of squares error, the lowest value for χ^2 (reduced) for our fit model and a comparison of the 4-point and the 5-point logistic fit model via an AIC and F-test, strengthened our choice.

5.2.11 Optimization of sandwich assay protocol steps

A simple optimization study for a maximum enhancement of the assay performance without changing major protocol parameters was done. All tested conditions are described in table **S1**. The variation No. 1 was tested for influence on the hybridization performance with a pH differing by >1.5 units. Variant No. 3 has been shown to be more effective previously in an LFA format.^{S3} Variant No. 4 was investigated to account for the new detection format. Agitation effects (No. 6), and longer incubation times (No. 5) have not been described previously.

Table S1. List of assay protocol variations with applied changes. All tests were done with a tDNA concentration of 5 nmol L⁻¹.

No.	Assay protocol step	Variation factor	Difference
1	Liposome/target strand hybridization	Buffer composition (Outer buffer from liposomes instead of HSS buffer)	Equals to pH change from 7.0 to 8.6, otherwise no difference
2	Blocking of the MTP	Washing buffer composition	Only PBS instead of washing buffer
3	Liposome/target strand hybridization	Preincubation of tDNA and liposome solution (10min.), then addition to capture strand on MTP (30 min.)	Dilution of tDNA in liposome solution, then addition to MTP
4	Liposome dilution	Dilution of liposomes	Phospholipid conc. of 0.026 mmol L ⁻¹ (1:5)
5	Liposome/target strand hybridization	Incubation time	30, 45 and 60 minutes
6	All incubation steps	Agitation during incubation	As described: no agitation

5.2.12 Effect of matrices

Various matrices were chosen. One was river water from the river Danube in Regensburg, the second species was a soil sample extract from a normal soil covered with lawn. The third matrix was fetal bovine serum (FBS). The soil sample was diluted 1:1 (v/v) with millipore water to deliver an aqueous extract. Further sample preparation of the river water sample and the soil sample included filtering through a 0.45 µm syringe filter. The FBS sample was added without further treatment. These different sample matrices were spiked with the target DNA, keeping the sample at 33% of the final volume. Distilled water was used as reference. For all samples a target DNA concentration of 125 pmol L⁻¹ was chosen. This spiking procedure was chosen to demonstrate that luminol-liposomes can be used for direct detection in these various matrices, without or with only minimal sample clean-up. In bioassays, in which DNA (or RNA) sequences are first isolated and amplified prior to detection, sensing via luminol-liposomes will be even less affected by the clean sample components.

5.3 Results and Discussion

5.3.1 Luminol derivatives comparison

Table S2. Literature comparison of different luminol derivatives and their ECL/CL enhancement properties.

Derivative	Description	Conditions	ECL/CL enhancement factor ^[a]	References
Luminol	Standard luminol (commercially available)	pH 9.0, EC: static potential +0.8V	1 (ECL/CL)	-
<i>m</i> -Carboxy luminol	<i>Our new luminol derivative</i>	pH 9.0, EC: static potential +0.8V	3.8 (ECL)	<i>This work</i>
ABEI	N-(4-aminobutyl)-N-ethylisoluminol (commercially available)	pH 10.0 , EC: static potential +1.0V	No comparison available, ≈1 (CL) ^{S14}	S15
LC11/TF46	Amphiphilic derivatives, functionalized via amino group (synthesis report in literature ^{S16})	pH 9.0	<0.1 (ECL)	S16
Luminol imide derivatives	Hydrophobic luminol derivatives, all functionalized via amino group, luminol “dimers”, “trimers”, cholesterol coupled derivative (synthesis report in literature ^{S17})	pH 8.0, EC: linear sweep +0.45-+0.85V	<0.1-0.6 (ECL)	S17
N-(β-carboxyl- propionyl)luminol	Hydrophilic functionalization of luminol via amino group (synthesis report in literature ^{S18})	pH 9.5, EC: pulse up to ~+1.8V	Not sufficient data for comparison available	S18
Various others	Different luminol derivatives with different substituents, no ECL (synthesis reports in literature ^{S14, S19-S26})	CL, pH 12.0 ^{S23}	All CL, <1-20 (Φ ^[b] compared)	S14, S19-S26

[a] Enhancement factor is obtained by published limits of detection, or by comparisons to luminol ECL or CL in the respective articles. In all instances, authors compared luminol and new derivatives under equal measurement conditions. Here, standard luminol is arbitrarily set to 1 (for better comparison purposes) and enhancement factors are given as ratio to 1 as a formal mathematical normalization which enables a comparison between the different literature values irrespective of individual PMT voltages used. (It may be noted though that it cannot be deduced from literature data, if the ratio of one derivative to the parent molecule always remains constant for different PMT voltages, but it is the case for the *m*-COOH-luminol/luminol ratio). [b] Φ is the absolute chemiluminescence quantum yield, here compared to Φ_{Luminol} = 0.012.^{S27}

5.3.2 Luminol liposomes

Here, preparation iterations included different synthesis protocols, different lipid compositions and lipid charges, varying membrane fluidity, varying pH values, pH gradients, altering dialysis conditions, varying luminol concentrations, summarized in table **S3**. In the end, we concluded that luminol was not sufficiently hydrophilic in order to remain inside the liposomes. Instead, upon encapsulation it would diffuse through the bilayer resulting in “empty” liposomes.

Table S3. Preparation procedures employed for obtaining standard-luminol based liposomes.

Synthesis variations	Lipid composition	Phospholipid content	Luminol content	Remarks
Reverse phase evaporation	(DPPC/DPPG/cholesterol) 10:5:6.6	N.D. ^[a]	N.D.	Standard protocol
Reverse phase evaporation	(DPPC/DPPG) 10:5	13.6 mmol L ⁻¹	1.77 mmol L ⁻¹	-
Reverse phase evaporation	(DPPC/DPPG) 7.5:7.5	11.4 mmol L ⁻¹	1.95 mmol L ⁻¹	-
Reverse phase evaporation	(DPPC/DPPG/DPPE-GA) 10:5:1	13.1 mmol L ⁻¹	3.1 mmol L ⁻¹	-
Reverse phase evaporation	(DPPC/DPPG/DPPE-GA) 7.5:7.5:1	11.9 mmol L ⁻¹	4.1 mmol L ⁻¹	-
Reverse phase evaporation –pH gradient	(DPPC/DPPG/DPPE-GA) 7.5:7.5:1	N.D.	7.7 mmol L ⁻¹	Outer buffer: 10 mM MES buffer (pH 5.5), No dialysis
Reverse phase evaporation	(DPPC/DPPG/DPPE-GA) 7.5:7.5:1	N.D.	N.D.	Luminol sodium salt instead of free acid
Reverse phase evaporation-luminol saturated outer phase	(DPPC/DPPG/DPPE-GA) 7.5:7.5:1	2.5 mmol L ⁻¹	N.D.	Outer buffer: HSS, pH 7.5, 8 mM luminol
Reverse phase evaporation-luminol saturated outer phase	(DPPC/DPPG/DPPE-GA/DPPE-biotin) 7.5:7.5:1:0.2	3.9 mmol L ⁻¹	N.D.	Outer buffer: HSS, pH 7.5, 10 mM luminol sodium salt

[a] N.D.: concentration too low to be determined; for all cases.

5.3.3 *m*-Carboxy luminol ECL

Figure S3. Maximum ECL emission intensities and emission maxima.

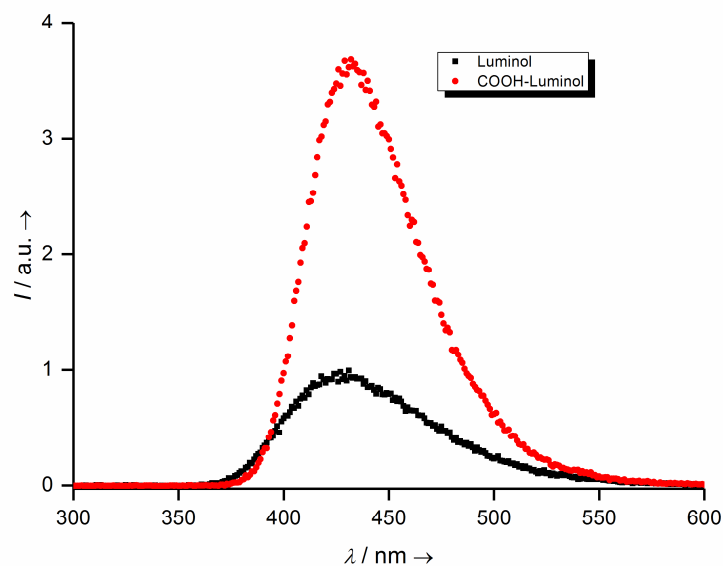
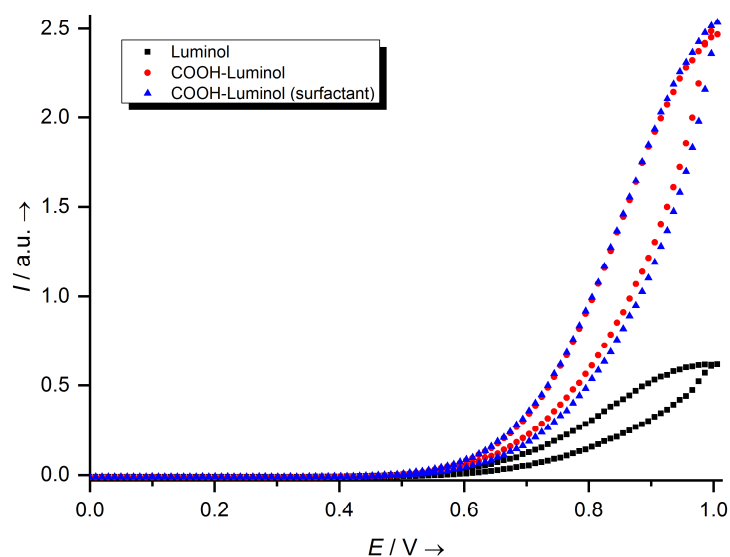


Figure S4. Excitation potential dependent luminescence intensity^[a].

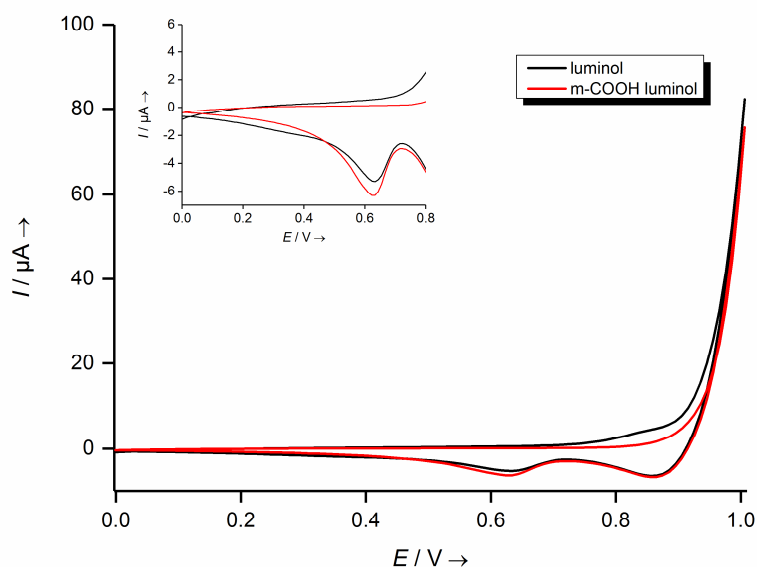


[a] “ I ” is the abbreviation for the luminescence intensity, in this case. The optimum excitation potential, giving the highest signal intensity was about equal between both species with a slight shift for the luminol derivative. Earlier saturation (i.e. no further signal

rise with rising potential) was observed for luminol ECL compared to *m*-carboxy luminol ECL.

Successive CV analysis of both, normal luminol and *m*-carboxy luminol indicate an equal signal decay progress of both species as shown in the subsequent figure.

Figure S5. CV cycles for luminol and *m*-carboxy luminol solutions to compare electroactivity [b].



[b] “*I*” is the abbreviation for the current in this figure. Conditions: 10 $\mu\text{mol L}^{-1}$ luminol or *m*-carboxy luminol solution in millipore H_2O with 0.1 mol L^{-1} KCl as electrolyte. Working electrode: gold disc electrode with a diameter of 1.6 mm, counter electrode: Pt-wire with a diameter of 0.5 mm and reference electrode: Ag/AgCl-reference electrode. Scan rate of 50 mV/sec. with a step potential of 0.01 V. Luminol solution diluted from a 1 mmol L^{-1} stock solution of luminol in 0.1 mol L^{-1} Tris-HCl buffer @ pH 8.5; *m*-carboxy luminol from a stock solution in H_2O . The slightly different peak form between +0.7 and +0.8 V results from the included Tris-HCl buffer (not shown for better overview).

5.3.4 *m*-Carboxy luminol liposomes

Reproducibility of liposome formation was tested between several different prepared batches and is shown in table **S4**.

Table S4. Reproducibility of liposome formation.

Batch No.	DLS (size) / nm	ζ -potential / mV	PdI	Phospholipid content / mmol L ⁻¹	Total lipid content / mmol L ⁻¹
1	270	-21	0.19	5.5	10.2
2	271	-24	0.22	5.9	10.9
3	279	-24	0.18	8.8	16.3
4	274	-28	0.19	7.2	13.3

The long-term stability of the *m*-carboxy luminol liposomes (storage at 10 °C) was determined by comparing intact liposomes vs. those lysed using a detergent. Colloidal stability, no lysis and no drop in ECL signal was observed for at least 5 weeks of storage (table **S5**).

Table S5. Liposome stability data from one batch^[a].

Liposome stability data	Intact liposomes / ECL signal	Lysed liposomes / ECL signal	Lysis ratio / %	<i>m</i> -carboxy luminol / ECL signal	DLS (size) / nm	ζ-potential / mV	Luminol reference / ECL signal	Temperature / °C
Day 0	3.14±0.27	102±1	3	70.5±1.6	322±9	-	52.9±1.9	19.5
1 week	4.89±0.22	103±0	5	82.6±2.4	309±1	-22±3	59.4±1.6	19.5
2 weeks	6.72±0.37	132±5	5	107±2	306±4	-22±3	74.6±1.9	25
3 weeks	5.41±0.92	133±2	4	110±1	291±13	-22±2	74.0±2.5	25
4 weeks	4.34±0.52	114±3	4	93.6±1.3	300±7	-24±1	66.6±2.1	22
5 weeks	5.81±0.22	122±2	5	101±3	274±5	-28±2	69.2±2.1	24

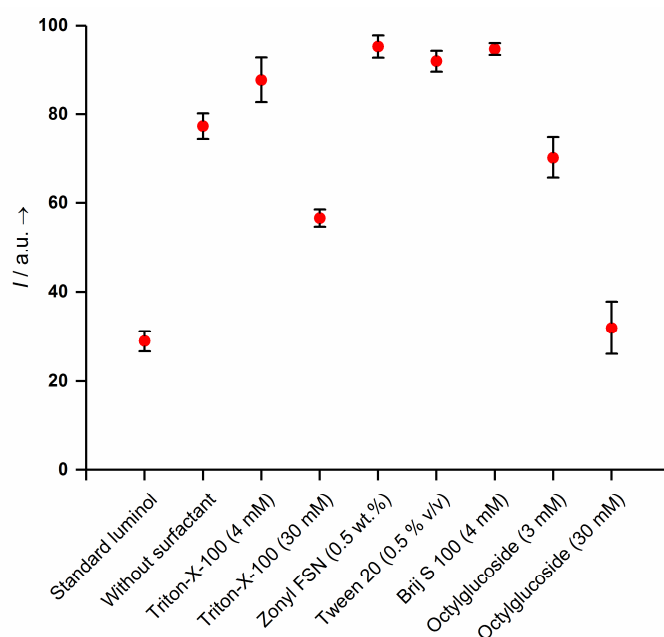
[a] *Luminol reference* is a 100 μmol L⁻¹ standard luminol ECL solution measured as reference signal to account for signal changes with varying conditions at different measurement days. *m*-Carboxy luminol is a 100 μmol L⁻¹ *m*-carboxy luminol (**2**) solution measured as second reference signal to indicate stability or instability of *m*-carboxy luminol in solution. *Lysis ratio* is given as the percentage value of the intact liposomes ECL signal divided by the lysed liposomes ECL signal. It indicates progressive stability or instability of liposomes with time (i.e. encapsulant leakage). *Intact and lysed liposomes* were measured with liposome solution diluted 1:20. As lysis detergent, 4 mmol L⁻¹ of Triton-X-100 were used. All ECL signals are given as intensity integrals (*n*=4) in arbitrary units. Generally, stability is estimated from ECL data with lysis ratio, DLS data indicating major changes in size and ζ-potential values indicating altered colloidal stability. *Temperature* is the ambient temperature during measurements, logged. Stability data in Table retrieved from one single liposome batch.

It is known that those liposomes are stable for over 1 year when encapsulating fluorophores or redox couples.^{S4} In contrast, Nakonechny et al.^{S28} showed 50% degradation in ECL signal upon storage for 3 weeks at 8°C and Rakhtong et al.^{S29} don't show any stability data.

5.3.5 Surfactants as lysis and ECL enhancing agents

In order to release luminol from the liposomes for ECL detection in the assay, detergents are commonly used. As they are also known to either quench or enhance ECL signals^{S30-S33} a range of surfactants at different concentrations was investigated according to different HLB values in order to create different hydrophobic/hydrophilic conditions on the electrode surface. It was found, that the HLB values were not the dominating factor influencing the ECL reactions (figure **S6**). For example Zonyl FSN (low HLB value) and Brij S 100 in low concentrations (high HLB value) both enhanced the ECL signal, whereas octylglucoside (OG) (medium HLB value) quenched the signal already at low concentrations. The HLB values therefore have no primary effect on luminol ECL. Here, it is important to note that OG, which is the predominantly used detergent for liposome lysis in bioassays^{S34} significantly quenched the ECL signal. Ultimately, Zonyl FSN 100 in medium concentration was chosen as lysis reagent as it enhances the ECL signal and has good water solubility.

Figure S6. Surfactant study – missing HLB correlation^[a].



[a] 100 $\mu\text{mol L}^{-1}$ *m*-carboxy luminol was used for comparison with added surfactant in given concentrations. 0.5 wt.% Zonyl FSN \approx 4.8 mmol L^{-1} and 0.5 wt.% Tween 20 \approx 4.5 mmol L^{-1}

5.3.6 Optimization of sandwich assay protocol steps

Here, we used detection probes and DNA target sequences for the detection of *Cryptosporidium parvum*^{S35} and further optimized assay conditions to adjust to the ECL detection format (table S6). As expected, no conditions pertaining to the new detection format itself (also not the altered buffer conditions or detergent use) but rather to DNA hybridization conditions affected signals obtained. For example, an elevated incubation temperature during the DNA hybridization lead to an increase of 20% as did lengthening the incubation time from 30 to 60 minutes. Interestingly, higher liposome concentrations provided higher signals without increasing the background signals.

Table S6. Hybridization assay protocol variations – comparison for maximum efficiency All tests were done with a target DNA concentration of 5 nmol L⁻¹. Signals are given as ECL intensity integrals [a.u.].

Condition	Signal
<i>Negative control</i>	0.04 ± 0.01
Reference conditions	1.6 ± 0.1
Assay buffer variation	1.7 ± 0.1
No blocking	1.5 ± 0.1
Preincubation of tDNA and liposomes	1.1 ± 0.2
37°C incubation	1.9 ± 0.1
1:5 liposome dilution	1.9 ± 0.0
30 min. incubation	1.9 ± 0.1
45 min. incubation	2.4 ± 0.1
60 min. incubation	2.4 ± 0.0

5.3.7 Effect of matrices

Matrix effects have the potential to prevent successful transfer of bioassays to real sample environments (clinical diagnostics, molecular biology, biodefense).^{S36} Therefore, the assay format was tested for matrix effects from potentially real samples. A river water sample, a soil extract and fetal bovine serum were chosen as representative bioassay matrices causing typically high background signals in fluorescence assays.^{S37-S38} The samples were mixed with target DNA and directly applied to our assay (figure 2). None of the samples showed significant influence on the assay compared to the negative controls, i.e. buffer or water used as spiking solutions, respectively. This indicates that our assay is well suited as a robust method for pathogen detection in different environmental samples.

5.4 References

- (1) Neumann, H.; Klaus, S.; Klawonn, M.; Strübing, D.; Hübner, S.; Gördes, D.; Wangelin, A. J. v.; Lalk, M.; Beller, M. A New Efficient Synthesis of Substituted Luminols Using Multicomponent Reactions. *Zeitschrift für Naturforschung B* **2004**, *59*, 431-438. doi: 10.1515/ZNB-2004-0411.
- (2) Ribi, M. A.; Wei, C. C.; White, E. H. Energy transfer involving derivatives of luminol. *Tetrahedron* **1972**, *28*, 481-492. doi: 10.1016/0040-4020(72)84012-2.
- (3) Edwards, K. A.; Baeumner, A. J. Optimization of DNA-tagged liposomes for use in microtiter plate analyses. *Anal. Bioanal. Chem.* **2006**, *386*, 1613-1623. doi: 10.1007/s00216-006-0743-4.
- (4) Fenzl, C.; Hirsch, T.; Baeumner, A. J. Liposomes with High Refractive Index Encapsulants as Tunable Signal Amplification Tools in Surface Plasmon Resonance Spectroscopy. *Anal. Chem.* **2015**, *87*, 11157-11163. doi: 10.1021/acs.analchem.5b03405.
- (5) Jureller, S., Hariott; Kerschner, J. L.; Murphy, D. S., *Dry cleaning system with low HLB surfactant*. U.S. Patent US 6,461,387 B1, Feb. 4, 2000.
- (6) Kastner, M., *Protein liquid chromatography*. (Elsevier, New York, **1999**), pp. 941.
- (7) SigmaAldrich, "Brij® S 100 product information", can be found under <http://www.sigmaaldrich.com/catalog/product/aldrich/466387?lang=de®ion=D E>, **2017**.
- (8) Stinear, T.; Matusan, A.; Hines, K.; Sandery, M. Detection of a single viable *Cryptosporidium parvum* oocyst in environmental water concentrates by reverse transcription-PCR [published erratum appears in *Appl Environ Microbiol* 1997 Feb;63(2):815]. *Appl. Environ. Microbiol.* **1996**, *62*, 3385-3390.
- (9) Gottschalk, P. G.; Dunn, J. R., "Bio-Plex suspension array system: Fitting Brendan's five-parameter logistic curve", can be found under <http://www.brendan.com/PDF%20files/Bio-Rad%20Bulletin%203022%20-%20StatLIA5PL.pdf>, **2006**.
- (10) Dunn, J., in *The Immunoassay Handbook*, 4 ed. (Ed.: Wild, D.), Elsevier, **2013**, chap. 3.6, pp. 323-336. doi: 10.1016/B978-0-08-097037-0.00022-1.
- (11) Origin 2017G (OriginLab, Northampton, MA, USA).
- (12) Geiß, S.; Einax, J. W. Comparison of detection limits in environmental analysis –is it possible? An approach on quality assurance in the lower working range by verification. *Fresenius J. Anal. Chem.* **2001**, 673-678. doi: 10.1007/s002160100710.

- (13) Harris, D. C., 9 ed., W.H. Freeman & Company New York, NY **2016**, chap. 5, pp. 103.
- (14) Gundermann, K.-D.; Drawert, M. Konstitution und Chemilumineszenz, I. Sterische Resonanzhinderung bei alkylierten Amino-phthalhydraziden. *Chem. Ber.* **1962**, *95*, 2018-2026. doi: 10.1002/cber.19620950825.
- (15) Yang, M.; Liu, C.; Qian, K.; He, P.; Fang, Y. Study on the electrochemiluminescence behavior of ABEI and its application in DNA hybridization analysis. *Analyst* **2002**, *127*, 1267-1271. doi: 10.1039/b205783b.
- (16) Jiao, T.; Leca-Bouvier, B. D.; Boullanger, P.; Blum, L. J.; Girard-Egrot, A. P. Electrochemiluminescent detection of hydrogen peroxide using amphiphilic luminol derivatives in solution. *Colloids Surf. A* **2008**, *321*, 143-146. doi: 10.1016/j.colsurfa.2008.02.021.
- (17) Jiao, T.; Huang, Q.; Xiao, Y.; Shen, X.; Zhou, J.; Gao, F. Electrochemiluminescent Detection of Hydrogen Peroxide via Some Luminol Imide Derivatives with Different Substituent Groups. *J. Chem.* **2013**, *2013*, 1-6. doi: 10.1155/2013/375372.
- (18) Chen, G. N.; Lin, R. E.; Zhuang, H. S.; Zhao, Z. F.; Xu, X. Q.; Zhang, F. Study of electrogenerated chemiluminescence of N-(β -carboxyl-propionyl)luminol. *Anal. Chim. Acta* **1998**, *375*, 269-275. doi: 10.1016/S0003-2670(98)00459-0.
- (19) Drew, H. D. K.; Pearman, F. H. 5. Chemiluminescent organic compounds. Part II. The effect of substituents on the closure of phthalhydrazides to 5- and 6-membered rings. *J. Chem. Soc.* **1937**, 26. doi: 10.1039/jr9370000026.
- (20) White, E. H.; Bursey, M. M. Analogs of Luminol. Synthesis and Chemiluminescence of Two Methoxy-Substituted Aminophthalic Hydrazides. *J. Org. Chem.* **1966**, *31*, 1912-1917. doi: 10.1021/jo01344a055.
- (21) Brundrett, R. B.; Roswell, D. F.; White, E. H. Yields of chemically produced excited states. *J. Am. Chem. Soc.* **1972**, *94*, 7536-7541. doi: 10.1021/ja00776a042.
- (22) Brundrett, R. B.; White, E. H. Synthesis and chemiluminescence of derivatives of luminol and isoluminol. *J. Am. Chem. Soc.* **1974**, *96*, 7497-7502. doi: 10.1021/ja00831a018.
- (23) Griesbeck, A. G.; Díaz-Miara, Y.; Fichtler, R.; Jacobi von Wangelin, A.; Pérez-Ruiz, R.; Sampedro, D. Steric Enhancement of the Chemiluminescence of Luminols. *Chem. Eur. J.* **2015**, *21*, 9975-9979. doi: 10.1002/chem.201500798.
- (24) Omote, Y.; Miyake, T.; Ohmori, S.; Sugiyama, N. The Chemiluminescence of Acyl Luminols. *Bull. Chem. Soc. Jpn.* **1966**, *39*, 932-935. doi: 10.1246/bcsj.39.932.
- (25) Dodeigne, C.; Thunus, L.; Lejeune, R. Chemiluminescence as a diagnostic tool. A review. *Talanta* **2000**, *51*, 415-439. doi: 10.1016/S0039-9140(99)00294-5.

- (26) White, E. H.; Roswell, D. F. Chemiluminescence of organic hydrazides. *Acc. Chem. Res.* **1970**, *3*, 54-62. doi: 10.1021/ar50026a003.
- (27) Ando, Y.; Niwa, K.; Yamada, N.; Irie, T.; Enomoto, T.; Kubota, H.; Ohmiya, Y.; Akiyama, H. Development of a quantitative bio/chemiluminescence spectrometer determining quantum yields: Re-examination of the aqueous luminol chemiluminescence standard. *Photochem. Photobiol.* **2007**, *83*, 1205-1210. doi: 10.1111/j.1751-1097.2007.00140.x.
- (28) Nakonechny, F.; Firer, M. A.; Nitzan, Y.; Nisnevitch, M. Intracellular antimicrobial photodynamic therapy: A novel technique for efficient eradication of pathogenic bacteria. *Photochem. Photobiol.* **2010**, *86*, 1350-1355. doi: 10.1111/j.1751-1097.2010.00804.x.
- (29) Rakthong, P.; Intaramat, A.; Ratanabanangkoon, K. Luminol encapsulated liposome as a signal generator for the detection of specific antigen-antibody reactions and nucleotide hybridization. *Anal. Sci.* **2010**, *26*, 767-772. doi: 10.2116/analsci.26.767.
- (30) Zu, Y.; Bard, A. J. Dependence of Light Emission of the Tris (2,2') bipyridylruthenium (II)/ Tripropylamine System on Electrode Surface Hydrophobicity. *Anal. Chem.* **2001**, *73*, 3960-3964. doi: 10.1021/ac010230b.
- (31) Workman, S.; Richter, M. M. The Effects of Nonionic Surfactants on the Tris (2,2' - bipyridyl)ruthenium(II)-Tripropylamine Electrochemiluminescence System. *Anal. Chem.* **2000**, *72*, 5556-5561. doi: 10.1021/ac000800s.
- (32) Rypka, M.; Lasovský, J. Micellar halide and energy transfer effects in electrochemiluminescence. *J. Electroanal. Chem.* **1996**, *416*, 41-45. doi: 10.1016/S0022-0728(96)04698-0.
- (33) Marquette, C. a.; Ravaud, S.; Blum, L. J. Luminol Electrochemiluminescence-Based Biosensor for Total Cholesterol Determination in Natural Samples. *Anal. Lett.* **2000**, *33*, 1779-1796. doi: 10.1080/00032710008543158.
- (34) Ullman, E. F.; Tarnowski, T.; Felgner, P.; Gibbons, I. Use of liposome encapsulation in a combined single-liquid reagent for homogeneous enzyme immunoassay. *Clin. Chem.* **1987**, *33*, 1579-1584.
- (35) Edwards, K. A.; Curtis, K. L.; Sailor, J. L.; Baeumner, A. J. Universal liposomes: Preparation and usage for the detection of mRNA. *Anal. Bioanal. Chem.* **2008**, *391*, 1689-1702. doi: 10.1007/s00216-008-1992-1.
- (36) Gaster, R. S.; Hall, D. A.; Nielsen, C. H.; Osterfeld, S. J.; Yu, H.; Mach, K. E.; Wilson, R. J.; Murmann, B.; Liao, J. C.; Gambhir, S. S.; Wang, S. X. Matrix-insensitive protein assays push the limits of biosensors in medicine. *Nature Medicine* **2009**, *15*, 1327-1332. doi: 10.1038/nm.2032.

- (37) Zipper, H.; Buta, C.; Lämmle, K.; Brunner, H.; Bernhagen, J.; Vitzthum, F. Mechanisms underlying the impact of humic acids on DNA quantification by SYBR Green I and consequences for the analysis of soils and aquatic sediments. *Nucleic Acids Res.* **2003**, *31*, e39. doi: 10.1093/nar/gng039.
- (38) Chiu, M. L.; Lawi, W.; Snyder, S. T.; Wong, P. K.; Liao, J. C.; Gau, V. Matrix Effects-A Challenge Toward Automation of Molecular Analysis. *J Lab Autom* **2010**, *15*, 233-242. doi: 10.1016/j.jala.2010.02.001.

Chapter 5: Surfactant Interactions with Luminol and *m*-Carboxy Luminol Electrochemiluminescence

Abstract

Luminol is a major probe in (bio)analysis for chemiluminescence (CL) and electrochemiluminescence (ECL) detection technologies. Surfactants are added to ECL assay cocktails to enhance signals, yet not much is known regarding their effects on luminol ECL. In-depth understanding was gained here through a broad study with various bioanalytically relevant surfactants (cationic, anionic and non-ionic), four common electrode materials and two luminol derivatives. We found that in contrast to CL, the effect surfactants have on luminol ECL is complex. Also, it cannot be predicted based on general surfactant characteristics such as ionic nature, HLB value and CMC. Neither surface nor bulk solution effects are predominant. For example, the postulated hydrophobic surface effects surfactants have in ruthenium-based ECL are only partially mirrored here and in fact are not throughout beneficial. We found that surfactants act in an all-encompassing mechanism, including surface electrochemistry, their solution and interfacial phases and finally also the chemical luminescence pathway. This can lead to dramatic differences in signals obtained, ranging from 2 – 5 fold increases to total quenching. We conclude that careful surfactant selection is crucial for any (bio)analytical luminol ECL reaction to obtain synergistic effects between the nature of the surfactant, electrode material and the bioanalytical demands.

This chapter is intended for publication.

Michael Mayer, Maximilian Hahn, Florian Gerstl, Thomas Köwer, Simone Rink, Axel Duerkop, Antje J. Baeumner

Author contributions:

MM, AJB and AD planned most of the experiments. MM did most of the experimental work and wrote the manuscript. FG, TK and SR helped with the ECL measurements. MH provided expertise, discussed and revised the surfactant adsorption models on electrodes, and this part of the manuscript. MM, AD and AJB revised the manuscript. AJB is corresponding author.

1. Introduction

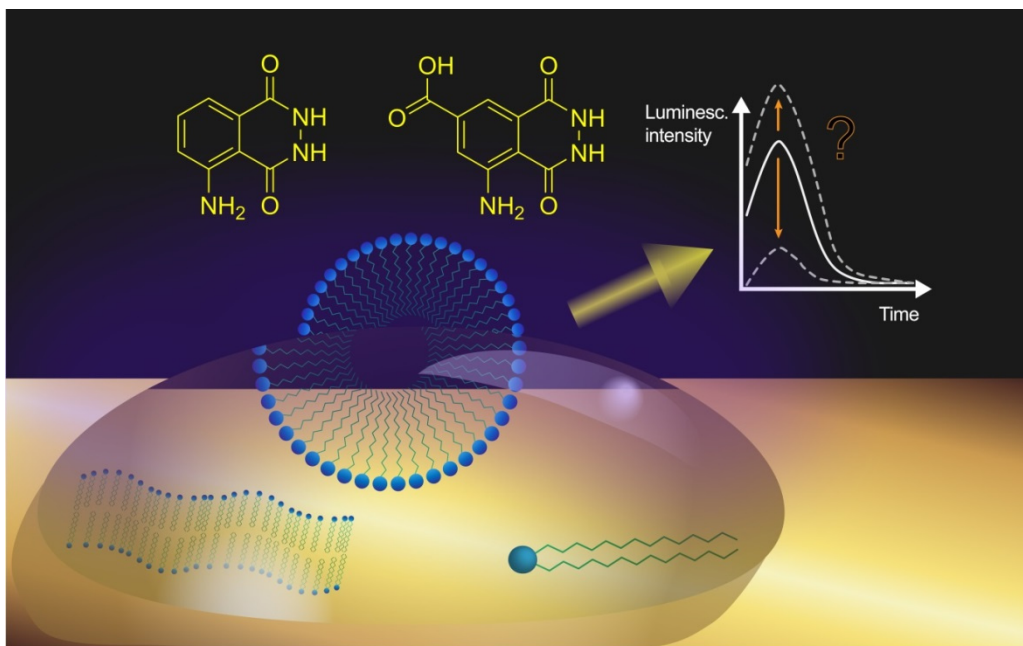


Figure 1: Surfactant effects on luminol/*m*-COOH luminol ECL chemistry.

Surfactants served as soap since ancient Egyptian times and became global commodities since the mid-20th century with a large global market share today in an overwhelming number of applications from household and daily life use to industry and research.¹ Their application in ECL goes back to early results on their effects on osmium- and ruthenium-based ECL systems.^{2,3} Later they have been found to be crucial in Ru(bpy)₃²⁺ based coreactant ECL to enhance the signal yield.⁴ However, surfactants have also been shown to quench ECL processes^{5,6} and the underlying mechanisms are not straightforward.⁷ Luminol has ever been one of the most used and common ECL compounds.⁸ However, there are only few reports about luminol ECL associated with surfactants and the synergistic or counteracting effects, and almost all are solely focusing on microemulsion effects or don't use the luminol-H₂O₂ system.^{5,9-12} We have recently discovered that *m*-carboxyluminol ECL on ITO electrodes is influenced by surfactants which were essential in the associated liposome-based bioassay.¹³ In fact, surfactants are essential tools in bioanalysis, including cell lysis,¹⁴ electrophoresis,¹⁵ protein methods¹⁶ and DNA extraction¹⁷ or also as practical additives, e.g. preventing reactant adsorption on microfluidic system sidewalls.¹⁸ Removing the detergents prior

to detection is typically cumbersome or not always possible. Frequently used surfactants include Cetyltrimethylammonium bromide (CTAB), Octyl glucoside (OG), N-Lauroylsarcosinate, Brij[®] representatives, Triton-X-100, Tween 20, and Sodium dodecyl sulfate (SDS).^{15,16,19-21} Understanding their effect on luminol ECL is hence essential.

The hydrophilic-lipophilic-balance (HLB) value of a surfactant is an empirical measure of its intrinsic hydrophobic/hydrophilic attributes. The system is only strongly valid for nonionic surfactants but was extended by Davies *et al.*²² to ionic surfactants so that it may serve as a rough classification with respect to their dispersibility in water and oil systems. In general, a small number indicates an oil dispersible surfactant and a large number indicates water dispersibility ($HLB > 7$).²² The critical micellar concentration (cmc) is the concentration of a surfactant above which the concentration of surfactants adsorbed to the water-air or water-solid interfaces reaches a critical level where no further surfactant molecules can be incorporated and micelles are formed in the bulk aqueous phase.²³ These micelles can e.g. act as microreactors establishing an altered microenvironment inside and take up and stabilize luminophores in CL or ECL.^{9,24} Thus, investigating the relation of the surfactants' parameters i.e. HLB or cmc values and possible signal enhancement or quenching can provide important insights into the nature of these effects.

In this work, we show for the first time, the concentration dependent influence of 13 different surfactants on the ECL process of luminol and its hydrophilic derivative *m*-carboxy luminol (Figure S1) on up to four different working electrode materials, i.e. gold, ITO, hydrophilized ITO (H-ITO) and laser scribed graphene (LSG) electrodes generating specific answers to the general question posed in Figure 2.

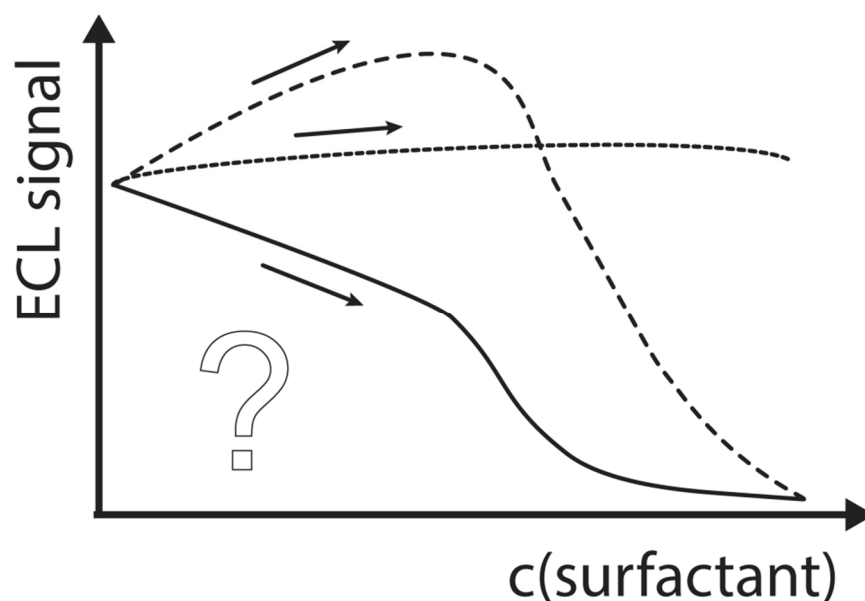


Figure 2: Signal progression of luminol ECL emissions upon addition of surfactants.

The employed surfactants were chosen according to their general nature, i.e. being anionic, cationic, zwitterionic or nonionic, their HLB values indicating their amphiphilic behavior, their structural classification and their highlighted usage in biochemical assays and techniques (Table 1). We correlated the ECL emission intensities to different concentrations of all surfactants and evaluated possible critical micellar concentration (CMC) effects. Furthermore, we investigated the resulting emission properties in the ECL process upon surfactant addition and also the electrochemical behavior, characterized via cyclic voltammetry measurements to also evaluate transferred charge amounts during ECL. Finally, we highlight mechanistical contributions towards the signal influencing effects of the various surfactants to aid in an intelligent assay design and choice of surfactant/electrode systems.

Surfactant	Type	HLB ^[a]	cmc ^[b]
N-Lauroylsarcosinate	Anionic	30 ²⁵	14.6 ²⁶
Sodium dodecyl sulfate (SDS)	Anionic	40 ²³	8.2 ²⁷
Sodium benzene sulfonate (SBS)	Hydrotrope		n.a.
Cetyltrimethylammonium bromide (CTAB)	Cationic	10 ^{28,29}	1.0 ³⁰
Dimethyl dioctadecyl ammonium chloride (distearyldimonium chloride)	Cationic	n.a. calcd.)	(-1 n.a.
Cocoamidopropyl betaine (DEHYTON PK 45)	Zwitterionic	n.a.	1.7-2.9 ³¹
Brij® 93	Nonionic	4 ³²	n.a.
Brij® S-100	Nonionic	18 ³³	0.02 ³⁴
Merpol® A	Nonionic	6.7 ³⁵	0.005% ³⁵
<i>n</i> -Octyl-β-D-glucoside (OG)	Nonionic	12.6 ³⁰	20-25 ³⁰
Triton-X-100	Nonionic	13.5 ³⁰	0.24 ³⁰
Tween® 20	Nonionic	16.7 ³⁰	0.059 ³⁰
Zonyl FSN 100	Nonionic	2.1 ³⁶	0.05-0.1 ³⁷

[a] *Caution: only strongly valid for nonionic surfactants!* [b] given in mmol/L if not otherwise stated. Caution: given for pure solutions, influence of supporting electrolyte (KCl) not included.

Table 1. List of screened surfactants and their typical data.

2. Experimental part

2.1 Materials

Brij® S-100, Dimethyl dioctadecyl ammonium chloride, Brij® 93, Indium tin oxide coated PET foil (surface resistivity: 60 Ω/cm^2), Luminol, Merpol® A, Triton-X-100, Tween® 20 and Zonyl-FSN-100 were obtained from SigmaAldrich (Taufkirchen, Germany). SDS was obtained from AppliChem (Darmstadt, Germany). Glycine, potassium chloride and sodium hydroxide (1 mol L⁻¹ in water) were bought from Merck (Germany). CTAB, CTAC, Hydrogen peroxide (30% v/v in water), potassium ferrocyanide and potassium ferricyanide were purchased from VWR (Germany). DEHYTON PK 45 was obtained at 30% from BASF, Germany. N-Lauroylsarcosine sodium salt was bought from Fluka (Germany). Octylglucoside was obtained from Carl Roth (Germany). *m*-Carboxy luminol was synthesized as described previously.¹³

2.2 Buffers and reaction mixtures

0.1 mol L⁻¹ glycine-NaOH buffer for ECL was prepared by dilution of an appropriate amount of glycine in millipore water and adjustment of the pH to 9.0 with 1 mol L⁻¹ sodium hydroxide solution. The luminol or *m*-carboxy luminol ECL reaction mix consisted of 100 $\mu\text{mol L}^{-1}$ luminol or *m*-carboxy luminol, 30 mmol L⁻¹ H₂O₂, 0.1 mol L⁻¹ KCl, and varying surfactant amount or presence in glycine-NaOH buffer. Surfactant dilutions were obtained in the described concentrations upon dilution with millipore water.

2.3 ECL measurements

All ECL measurements were performed with a 3-electrode setup, consisting of an ITO – working electrode (WE, sheet electrode on PET foil, 5 mil ITO layer, surface resistivity: 60 $\Omega/\text{sq.}$) or gold working electrode, a Pt-counter electrode (CE, wire, 0.5 mm diameter) and an Ag-wire pseudo reference electrode (RE, 2.0 mm diameter) inside a self-designed, 3-D-printed minicell positioned on a xyz-linear stage which were both described earlier.¹³ Electrical connection was established with an Autolab MAC 08121 potentiostat (Autolab BV, Netherlands) connected to a PC, operating the Autolab Nova software for operation. We used amperometric recording with a constant potential

over 30 seconds. Optical readout was done with an Aminco Bowman, AB 2 spectrofluorimeter via a y-shaped bifurcated optical fiber (diameter = 10 mm) with the excitation source switched off. All ECL measurements were obtained, recording the luminescence signal for 40 seconds, while a constant excitation potential was applied for 30 seconds during that time. For gold-WEs, a potential of +0.5V vs. Ag-wire and for ITO-WEs, a potential of +0.8V vs. Ag-wire was set. Different emission monochromator wavelengths were used, while the slit-width was always opened to 16 nm. PMT voltages were altered for different experiments. All measurements were done with a solution volume of 120 μ L. All signals are given as intensity integrals over the total acquisition time, integrated with the software of the luminescence spectrometer, if not otherwise stated.

2.4 ITO electrode hydrophilisation

The as obtained ITO electrodes (described above), were treated with oxygen plasma on a PlasmaFlecto 10 plasma cleaner (PlasmaTechnology GmbH, Germany) with following protocol similar to a published procedure:³⁸ for 4 minutes and 20 seconds (equals to 5 min. @ 50 W) with 60 W power, 100% oxygen at a total amount of 15 sccm, and a set vacuum of 0.2 mbar (equal to 150 mTorr) at room temperature. After treatment, the ITO electrodes were stored under Millipore water prior to usage to avoid carbonaceous contamination as good as possible. The protective coating foil on the ITO surface was only removed immediately prior to plasma treatment and all electrodes were treated right before the measurement and directly used after.

2.5 LSG electrodes

LSG electrodes were prepared, following a reported procedure³⁹ employing a Kapton® HN foil (125 μ m thickness) from CMC (CMC Klebetechnik GmbH, Germany) on a ULS (Universal Laser Systems GmbH, Austria), VLS 2.30 system (30W CO₂-laser @ 10.6 μ m) with a 2 inch lens. Settings were: in-focus (-0.7 mm above focus), 1% power, 10% speed (13 cm/s), image density 7 (1000 pulses per inch (x-direction), 2000 lines per inch (y-direction)), without borders.

2.6 Resistivity measurements

The measurements were done on a KEITHLEY, 175 autoranging multimeter (Tektronix, OR, U.S.A.). The ITO sheets were contacted directly via clamps with a lateral distance of 0.5 cm for all measurements. Triple measurements were performed.

2.7 CL measurements

Chemiluminescence measurements were performed according to a beforehand optimized protocol with 100 $\mu\text{mol L}^{-1}$ of each luminol species, 5 mmol L^{-1} H_2O_2 , with 100 nmol L^{-1} hemin as catalyst in 0.1 mol L^{-1} carbonate buffer at a pH of 10.5 and varying surfactant concentrations. Stock solutions of the surfactants were diluted in the same carbonate buffer at pH 10.5. Readings were taken in a white, polystyrene flat bottom microtiter plate (Porvair Science Ltd., Wrexham, UK) with 200 μL measurement volume per well. The reaction was started for each well prior to the reading upon addition of H_2O_2 in buffer. Readings were done on a BioTek SYNERGY neo2 (BioTek Instruments, Inc., VT, USA) reader in luminescence mode, with the respective luminescence filter, 1s of integration time, optics on top position, read height of 4 mm and a gain of 55. Blanks were recorded for each well prior to the respective CL measurement.

2.8 Contact angle measurements

Contact angles were measured, using the sessile drop method on a DataPhysics OCA 15EC (DataPhysics Instruments GmbH, Germany) device and data analysis was done with the corresponding SCA 20 software (DataPhysics Instruments GmbH). A droplet volume of 5 μL was used per measurement with Millipore water as contacting liquid. Repetitive measurements were done on fresh surface spots.

2.9 CV measurements

Cyclic voltammetry (CV) measurements were done either in the described ECL cell or with a 3-electrode setup, using a gold disk electrode ($d = 1.6 \text{ mm}$) as WE, a Pt-wire ($d = 0.5 \text{ mm}$) as CE and an Ag/AgCl reference electrode, all obtained from Bioanalytical Systems, Inc. (West Lafayette, IN, U.S.A.) with solutions of the ECL mix or buffer with the respective luminol species. CV conditions are given in the figure captions or footnotes.

2.10 Emission Scans

Emission scans were done under ECL conditions, at the described spectrofluorimeter with an emission wavelength scan between 300 and 600 nm and a scan rate of 10 nm per second.

2.11 Liposome lysis study

The liposome lysis study was done with 150 mmol L⁻¹ Sulforhodamine B encapsulating liposomes with a standard composition.⁴⁰ The liposomes were diluted 1:1000 prior to use. Surfactants were used in following concentrations: Zonyl FSN-100, 0.5 % (v/v); OG, 30 mmol L⁻¹ or 30 μmol L⁻¹; CTAB, 250 μmol L⁻¹; Tween® 20, 4.5 mmol L⁻¹; N-Lauroylsarcosinate, 250 μmol L⁻¹. Measurements were done in a black, Greiner Bio-One, MICROLON® microtiter plate with 100 μL total volume per well. Fluorescence signals were read at a BMG, FLUOstar® OPTIMA microtiter plate reader (λ_{Exc} = 545 nm, λ_{Em} = 590 nm, detector gain 1400).

3. Results and Discussion

Surfactant effects on luminol CL have been described numerous times in literature, yet our results demonstrate that those findings cannot be directly translated to an ECL detection system. For example, while Liu *et al.* have reported⁴¹ a strong enhancement effect of Triton-X-100 (up to a concentration of 60 mM⁴¹) on the luminol/H₂O₂ CL system, we have observed both, enhancement and quenching effects on the luminol ECL systems (depending on the electrodes used), and an overall signal decrease with higher surfactant concentrations (Figure S9). Liu *et al.* deduced the enhancement effect to an enrichment of luminol or excited luminol species inside Triton-X-100 micelles, but it is clear that the situation is more complex in ECL, when electrode surfaces are needed for the overall reaction. Thus, surfactants can influence the solubility of the luminophore and coreactants, the electrochemical reaction kinetics and the luminescence kinetics. Hence, we thoroughly investigated different classes of surfactants with respect to the **surfactant nature** (anionic, cationic or nonionic), **CMC** or **HLB values**, and different, typical electrode materials used in (bio)analysis. We investigated the effect on electrochemical and luminescence contributions by assessment of anodic **EC currents**, and the **ECL** emission and trace, respectively.

3.1 Correlation with basic surfactant parameters.

No correlation between the inherent surfactant nature (cationic, anionic or nonionic) and either enhancement or quenching effects on luminol ECL was found (Figures S2-S14) and exemplary shown in table 2.

Detergent classification	Specific detergent	Electrode	Luminol species	Effect + = enhancing - = quenching
Anionic	SDS	H-ITO	COOH luminol	+
Anionic	SDS	ITO	COOH luminol	-
Cationic	CTAB	H-ITO	COOH luminol	++
Cationic	CTAB	Gold	COOH luminol	+/-
Nonionic	Brij S-100	H-ITO	COOH luminol	-
Nonionic	Brij 93	LSG	COOH luminol	+

Table 2. Relation between surfactant classification and their effect on the ECL signal: No correlation of enhancement/quenching and surfactant type is found.

Similarly, ECL enhancement or quenching for the systems studied are not generally dependent on micelle formation or presence while it might be supported or initiated by these effects in some cases (Tables S1 and S2). This is in contrast to findings by Liu et al. and others who found that surfactants when employed above the CMC significantly enhance the CL signal whereas they did not study effects below the CMC.^{41,42} For ECL, it was assumed that the micelles incorporate luminol species and thus promote the ECL process.⁹ However, as can be seen in Figure 3, this is not a general correlation. Most dramatic signal changes are observed with Tween20 in combination with gold electrodes, as it enhances luminol ECL below the stated CMC and quenches above, while quenching throughout is observed with *m*-carboxy luminol (Table S1), while on ITO, directly at the CMC, a raise in signal is observed. In other scenarios, the CMC has not such a distinct effect on the signals. It should be noted that surfactants are affected by electrolytes, which is indicated by the grey zone as an uncertainty range of the CMC based on literature data.

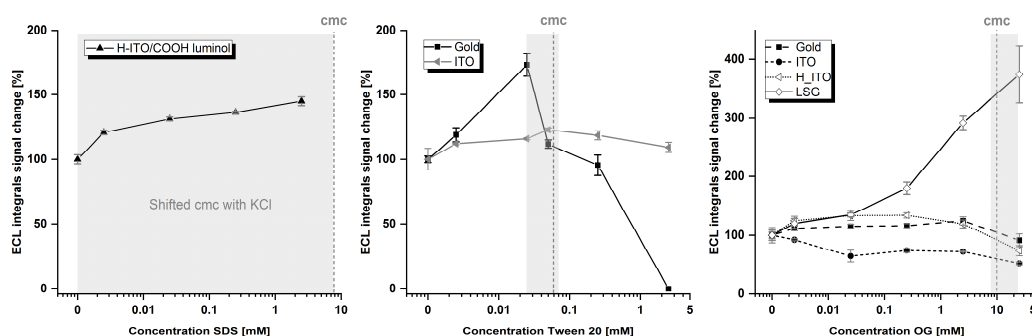


Figure 3. ECL/surfactant concentration curves for different surfactants with indicated CMC lines at the stated CMC values in water. **As a note:** CMC values at these lines do not consider the high electrolyte content in our systems. Grey-shaded areas specify approximation of CMC shifts correlating to our electrolyte contents, according to literature.⁴³⁻⁴⁶

Based on these findings, it is no surprise that also HLB values do not correlate to observed ECL signals. As depicted in Figure S16 (exemplary represented for ITO electrodes) no correlation for either luminol or *m*-carboxy luminol ECL could be found for all surfactants. The same was true for H-ITOs and gold electrodes. This implicates that the observed enhancing or quenching effects are unique to the surfactants, and cannot be solely related to polarity effects.

3.2 Electrochemiluminescence effects.

Surfactant effects on the ECL signal were more thoroughly studied using four common electrode materials. These were chosen to provide different surface properties and hence provoke different interfacial behavior of the surfactants, and because they are predominantly used in aqueous (bio)analytical applications. Gold⁴⁷ and ITO are defined as hydrophobic (carbonaceous contaminations, see chapter S), H-ITO as hydrophilic and the porous LSG as hydrophilic and highly reactive surface (see also contact angle data in chapter 6.15). As the luminol ECL reactions, i.e. their determinant oxidation steps occur directly at the electrode surface, aggregation and mesoscale structuring of surfactant molecules at, or in the vicinity of the electrode, has a major influence on the observed luminol ECL reaction. As such, we have briefly summarized simplified adsorption models of the respective surfactants on different electrodes in Figure 4 and further discussed in chapter 6.3.3.

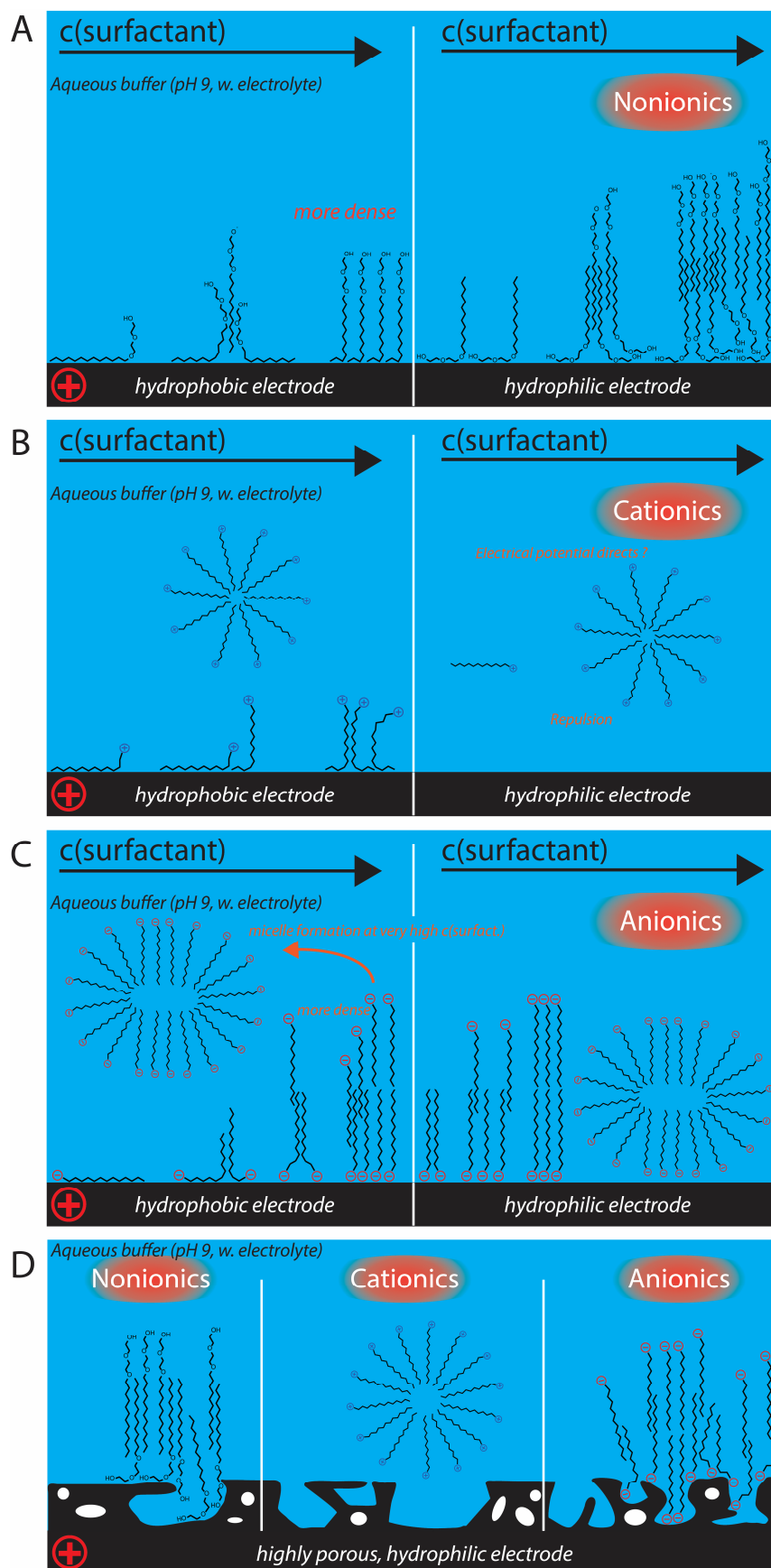


Figure 4 (A-D). Idealized, schematic surfactant adsorption models for different surfactants on varying electrode surfaces. Note: illustrated surfactant sizes not scaled to real dimensions. “+” indicates the positive electrode potential, present on all electrode variants.

Other boundary layer constituents or ECL reagents not shown for simplicity. **A** depicts exemplary a hydrophobic, nonionic surfactant, adsorbing in rising concentration, **B** shows cationic surfactants adsorption, **C** illustrates anionic surfactant adsorption – each on a hydrophilic and hydrophobic, positively charged surface. **D** outlines the situations with porous, hydrophilic electrodes like LSGs.

However, these general predictions cannot be corroborated, as these are very complicated in our systems including several unknown factors and the results demonstrate that our outlined models are insufficient to depict an overall trend in all surfactant/electrode combinations (in detail, chapter 6.3.3). The complexity of surfactant-electrode-luminol species interchange and the resulting ECL influence is outlined on the distinct ECL effects in chapter 6.3.2 (Fig. S2-S14). The cationic surfactant CTAB is a good example. On ITO electrodes it enhanced both ECL signals of luminol and *m*-carboxy luminol at an optimum concentration of 25 μ M CTAB. In both cases, the signal vs. CTAB concentration followed the same trend: gradual increase up to the optimum enhancement and a fast signal decrease with higher concentrations. On gold electrodes, only for *m*-carboxy luminol, an enhancement up to \sim 140% was observed (at 2.5 and 25 μ M) and then a decline to a final value around 50% for concentrations of 2.5 mM. Instead, for luminol, quenching was observed at all CTAB concentrations (Figure S4). In the case of H-ITOs, no quenching occurred at all, and the largest signal enhancement was found for both luminols for intermediate CTAB concentrations of 100 μ M (\sim 270% and 170% for *m*-carboxy luminol and luminol, respectively) (Figure S4). Finally, on LSGs, signal enhancement was less than observed on gold for the hydrophilic *m*-carboxy luminol. At the same time, the largest enhancement with CTAB for any electrode type was obtained at highest CTAB concentrations for luminol on LSG (\sim 200%) (Figure S4). In contrast to these findings, another cationic surfactant, dimethyl dioctadecyl ammonium chloride, quenched ECL signals in all studies, Fig. S5 (its low solubility limited the breadth of the studies) making it clearly of limited use for (bio)analytical assays. This is just an excerpt to illustrate the complexity and independence of any rules, the ECL influence of any surfactant follows.

Overall, the following trends can be concluded considering all studied aspects: **(1)** For all ionic and non-ionic surfactants it is found that the head group plays an important role given by their interface reactions with the electrode surface but a charge is not automatically needed to dramatically influence the ECL signal. **(2)** As to be expected,

the hydrophobicity of the surfactants is less important or unfavorable in stabilizing the charged *m*-carboxy luminol vs. luminol as seen for example with Zonyl FSN, yet **(3)** hydrophobicity itself is not an indicator for strong enhancement or quenching as outlined before and seen when directly comparing Brij S-100 and Brij 93 (Figures S12 and S13). **(4)** Quenching of the ECL signals is never following a Stern-Volmer relationship and **(5)** does not simply relate to turbidity resulting from cloud point concentrations; e.g. strong two-phase former Brij 93 does not cause quenching whereas the hydrotrope SBS causes quenching (Fig. S12 and S6). **(6)** Hydrophilic surfaces and highly active surfaces such as the H-ITO and LSGs, respectively, benefit most from the use of surfactants. Here a clear enhancing trend is seen for almost all surfactants throughout the whole concentration range. This suggests a cumulative impact towards enhanced residence probabilities of luminol ECL reactants directly at the electrode surface, compared to naturally hydrophobic electrodes. Beyond these trends, gives chapter 6.3.2 a thorough explanation of all distinct ECL effects for each surfactant.

In Table 3 the best performing surfactants for each of the two luminol molecules and for each of the four electrode types are identified as a guide for bioanalytical assay development. Signal enhancements up to almost 5-fold could be achieved in the case of the highly porous LSG electrodes, which is likely due to an increase in available surface area.

Electrode-luminol combinations	Surfactant	Maximum signal enhancement [%]	c(surfactant)@ maximum enhancement [mM]
Gold /Luminol	Tween 20	175	0.025
Gold /COOH luminol	OG	145	0.25
ITO /Luminol	CTAB	150	0.025
ITO /COOH luminol	CTAB	165	0.025
H-ITO /Luminol	Brij 93	300	25
H-ITO / COOH luminol	CTAB	275	0.1
LSG /Luminol	N-Lauroylsarcosinate	475	25
LSG /COOH luminol	N-Lauroylsarcosinate	215	25

Table 3. Best performing surfactants on the different electrode types

3.3 Surfactant effects on the underlying electrochemical reactions of ECL.

The influence of surfactants on the electrochemical reaction kinetics was further investigated using cyclic voltammetry. Various surfactants in buffer and in ECL reaction mixtures were compared on a gold electrode to identify general trends. It was found that (1) the CVs shifted to a more anodic current with the complete ECL mix compared to the surfactants in buffer alone. (2) The peak shape differed most in the region between +0.5 and +0.9 V during the forward cycle for the different surfactant/ECL solutions while the overall shape was relatively similar for all tested examples. (3) N-Lauroylsarcosinate differed from all other surfactants as no difference was observed between buffer and ECL mix responses. (4) There is no overall trend observable between the total charge transferred and ECL quenching or enhancement observed (Figure 4).

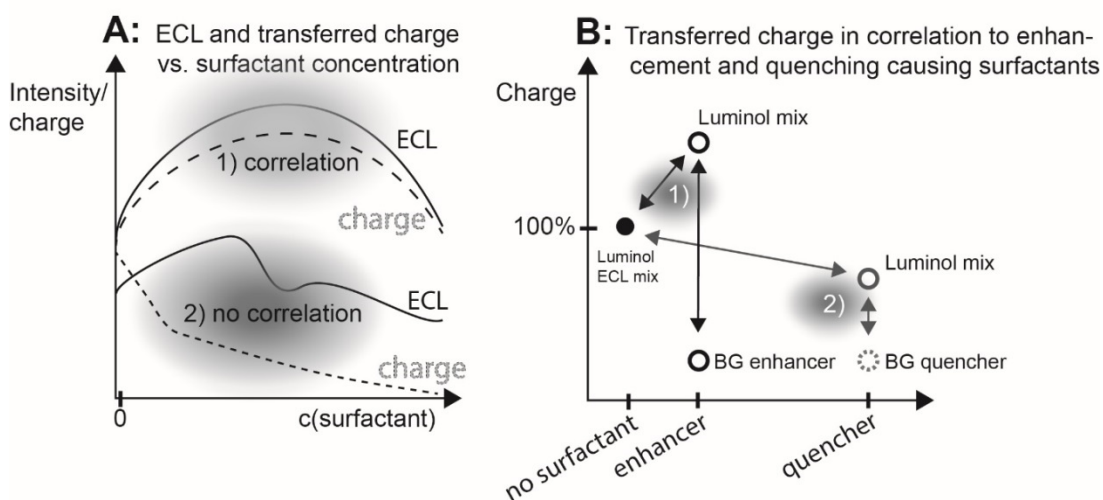


Figure 5. Schematic representation of relevant parameters in luminol ECL that are influenced by surfactants. **(A)** correlation between the ECL signal and electrochemical charge transferred vs. the surfactant concentration. **(B)** correlation between electrochemical charge transferred with respect to enhancing or quenching nature of the surfactant.

Specifically, for some surfactants the total transferred charge is increased if these are enhancing the ECL reactions and lowered if quenching is present (case 1, Fig. 5A) (figure 6 and chapter 6.3.2 and 6.10). However, these changes are not proportional to the extent of ECL enhancement or quenching. Furthermore, for other surfactants no

correlation exists at all (case 2, *Fig. 5A*), (*Figure 6 A-D* and *Table 4*). Here, surfactants that quench the ECL signal have either no, an increasing or a decreasing effect on the transferred charge.

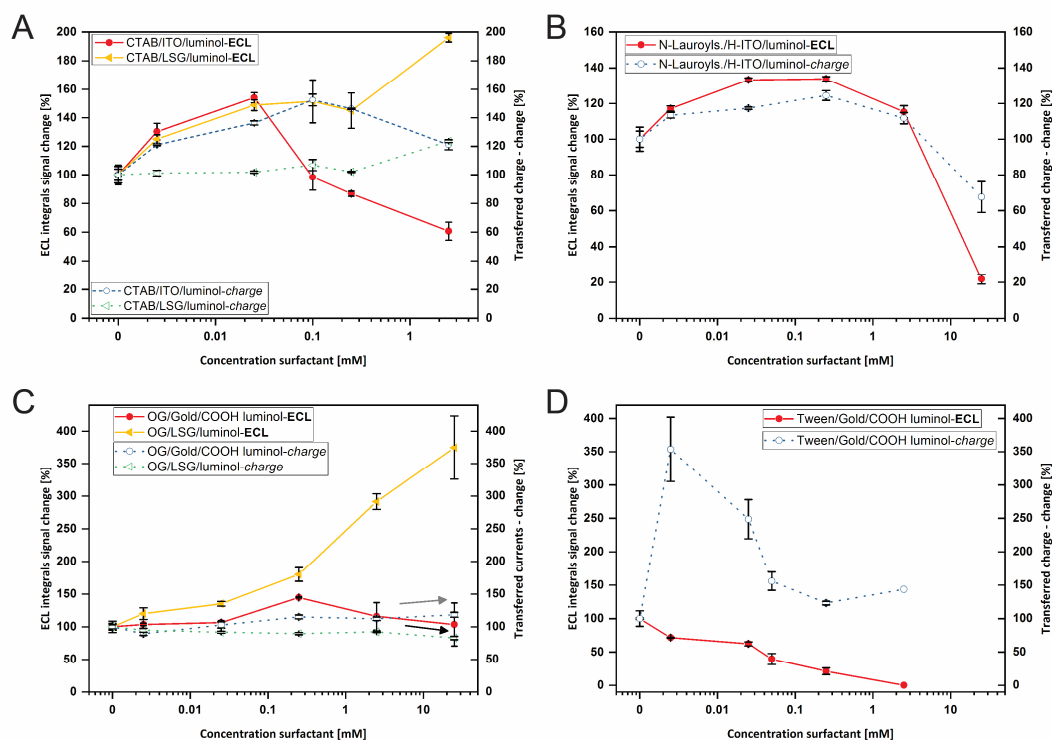


Figure 6. (A-D) Overlay of ECL response (“ECL”, left) and EC charges (“EC”, right) for several surfactants. **A** depicts a trend of the response progressions for ECL and transferred charge for CTAB, N-Lauroylsarcosinate in **B** does the same, even more overlapping, while OG and Tween 20 in **C** and **D** show disproportional behavior between both responses.

Example	Currents for ECL+surfactants vs. surfactant BG (*)	ECL/EC response for ECL solutions with surfactants (**)	Trend	Sources
N-Lauroylsarc. /ITO/L (Quencher)	Enhanced	Quenched/Quenched	Yes	Fig. S2 (ECL), S25(EC), S35 (BGcurrentQ)
Tween/Gold/L (Enhancer)	Enhanced	Enhanced/Enhanced	Yes	Fig. S9. (ECL), S31(EC), S36 (BGCurrent E)
Tween/Gold/COL	-	Enhanced/Quenched	No	Fig 4, Fig S36 (BGcurrentE)
CTAB/Gold/COL	-	Quenched/Enhanced	No	Fig. S3 (ECL), Fig. S26/EC)

Table 4. Different possibilities in current response (transferred charges) and luminescence behavior that depict the unique situation for each surfactant (L represents luminol and COL, *m*-carboxy luminol).

3.4 Investigation toward a correlation between surfactant effects on EC, CL and ECL.

During the EC studies, it was found that in the case of ECL-signal quenching, the surfactant's effect is not solely based on hindering charge transfer but also negatively affecting the luminescence generation (e.g. Figs. S36C, S4). We then performed a detailed CL study using a luminol/H₂O₂ CL system by testing both luminol species and several of the surfactants as employed before in the ECL systems. As expected, in many cases surfactant effects seen in CL reactions did not correlate to the corresponding ECL reaction. In general, CL signals are enhanced at lower surfactant concentrations and quenched at high surfactant concentrations, while the picture is very diverse, as discussed above, for ECL reactions. An extreme example is CTAB. It mildly quenched the signals on gold and ITO electrodes in ECL (max. quenching of 50%, Fig. S4), but completely eliminated signals in CL (>4% remaining signal, Fig. S39A). In the case of H-ITOs, CTAB even enhanced the ECL signal significantly.

In the scientific literature only anecdotal data exist to-date, identifying surfactant conditions that enhance luminol ECL. For example, Chu *et al.* used a CTAB microemulsion system,¹¹ Xiuhua *et al.*¹⁰ added further hydrophobic components (heptane, n-butanol). Chen *et al.* employed 2,2-Dichlorovinyl-dimethyl-phosphat (DDVP), a pesticide as coreactant for luminol ECL with a very high pH around 13.5 while they tested some more surfactants e.g. CTA(X), Tween-100 and SDS and found solely cationics to improve ECL.⁹ Also Rypka *et al.* investigated CTAX effects on a luminol/air ECL system with bipolar pulsed excitation.⁵ The good enhancing performance of CTAB was thought to be supported by bromide being the counterion of CTA⁺, and thus electrogenerated bromine or hypobromite can help with coreactant oxidation as previously reported for Ru(bpy)₃²⁺ ECL or as a halide effect on luminol ECL.^{5,48} However, we could not see this effect as a pronounced factor upon a test with CTAB vs. CTAC, (Figure S15), where CTAB and CTAC had practically the same effect on both luminol species ECL processes.

4. Conclusion

In conclusion, the effect surfactants have on luminol ECL is complex and cannot be predicted based on general surfactant characteristics such as ionic nature, HLB index and CMC. This means that extrapolation based on existing data or general predictions for not-yet studied surfactant/electrode pairs is currently not possible. However, some general trends can be concluded that are caused when chemiluminescence, solution-based or electrochemical effects dominate, respectively. Thus, at very low surfactant concentrations a small increase in ECL was often observed which can be attributed to an enhanced wetting of the electrode surfaces and no disturbance of diffusion processes to the electrode. At higher surfactant concentrations, the electrode adsorption behavior and also bulk solution-based processes like micellization or surfactant phase transitions and as such stabilization or destabilization of luminol species govern the ultimate ECL efficiency. Finally, at very high surfactant concentrations, either electrode blocking, surfactant induced electron transfer suppression or chemical quenching contribute to the overall effect on ECL signals. With respect to the electrode surfaces a general electrode hydrophilization prior to usage – especially for intrinsically hydrophobic electrode materials – is most beneficial in symbiosis with surfactants towards an enhancement effect. In the case of bioanalytical luminol-ECL assays, careful selection of a surfactant is mandatory considering the varying effect surfactants have on the detection system. Ultimately, when assay design allows a smart selection of a symbiotic surfactant/electrode pair, up to 5-fold signal enhancement effects are available for maximum assay sensitivity.

5. References

- (1) Karsa, D. R.; Joel, H., *Chemistry and Technology of Surfactants*. Farn, R. J., Ed., (Blackwell Publishing Ltd., **2007**). doi: 10.1002/9780470988596
- (2) Mc Cord, P.; Bard, A. J. Electrogenerated chemiluminescence Part 54. Electrogenerated chemiluminescence of ruthenium(II) 4,4'-diphenyl-2,2'-bipyridine and ruthenium(II) 4,7-diphenyl-1,10-phenanthroline systems in aqueous and acetonitrile solutions. *J. Electroanal. Chem. Interfacial Electrochem.* **1991**, *318*, 91-99. doi: 10.1016/0022-0728(91)85296-2
- (3) Ouyang, J.; Bard, A. J. Electrogenerated Chemiluminescence. 50. Electrochemistry and Electrogenerated Chemiluminescence of Micelle Solubilized Os(bpy)₃²⁺. *Bull. Chem. Soc. Jpn.* **1988**, *61*, 17-24. doi: 10.1246/bcsj.61.17
- (4) Li, F.; Zu, Y. Effect of Nonionic Fluorosurfactant on the Electrogenerated Chemiluminescence of the Tris(2,2'-bipyridine)ruthenium(II)/Tri-n-propylamine System: Lower Oxidation Potential and Higher Emission Intensity. *Anal. Chem.* **2004**, *76*, 1768-1772. doi: 10.1021/ac035181c
- (5) Rypka, M.; Lasovský, J. Micellar halide and energy transfer effects in electrochemiluminescence. *J. Electroanal. Chem.* **1996**, *416*, 41-45. doi: 10.1016/S0022-0728(96)04698-0
- (6) Marquette, C. a.; Ravaud, S.; Blum, L. J. Luminol Electrochemiluminescence-Based Biosensor for Total Cholesterol Determination in Natural Samples. *Anal. Lett.* **2000**, *33*, 1779-1796. doi: 10.1080/00032710008543158
- (7) Kirschbaum-Harriman, S.; Duerkop, A.; Baeumner, A. J. Improving ruthenium-based ECL through nonionic surfactants and tertiary amines *Analyst* **2017**, *142*, 2648-2653. doi: 10.1039/C7AN00197E
- (8) Miao, W. Electrogenerated chemiluminescence and its biorelated applications. *Chem. Rev.* **2008**, *108*, 2506-2553. doi: 10.1021/cr068083a
- (9) Chen, X. M.; Lin, Z. J.; Cai, Z. M.; Chen, X.; Wang, X. R. Electrochemiluminescence detection of dichlorvos pesticide in luminol-CTAB medium. *Talanta* **2008**, *76*, 1083-1087. doi: 10.1016/j.talanta.2008.05.007
- (10) Xiuhua, W.; Chao, L.; Yifeng, T. Microemulsion-enhanced electrochemiluminescence of luminol-H₂O₂ for sensitive flow injection analysis of antioxidant compounds. *Talanta* **2012**, *94*, 289-294. doi: 10.1016/j.talanta.2012.03.042
- (11) Chu, H.-H.; Wu, Y.; Di, J.-W.; Tu, Y.-F. Study on sensitization of ECL of luminol with microemulsion in neutral medium *Chin. J. Anal. Lab.* **2006**, 6-9.
- (12) Lasovský, J.; Grambal, F. 815-MICELLAR COMPLEXES OF ENERGY TRANSFER *. *Bioelectrochem. Bioenerg.* **1986**, *15*, 95-102. doi: 10.1016/0302-4598(86)80008-3
- (13) Mayer, M.; Takegami, S.; Neumeier, M.; Rink, S.; Jacobi von Wangelin, A.; Schulte, S.; Vollmer, M.; Griesbeck, A. G.; Duerkop, A.; Baeumner, A. J.

- Electrochemiluminescence Bioassays with a Water-Soluble Luminol Derivative Can Outperform Fluorescence Assays. *Angew. Chem. Int. Ed.* **2018**, 57, 408-411. doi: 10.1002/anie.201708630
- (14) Krady, M. M.; Zeng, J.; Yu, J.; MacLauchlan, S.; Skokos, E. A.; Tian, W.; Bornstein, P.; Sessa, W. C.; Kyriakides, T. R. Thrombospondin-2 Modulates Extracellular Matrix Remodeling during Physiological Angiogenesis. *Am. J. Pathol.* **2008**, 173, 879-891. doi: 10.2353/ajpath.2008.080128
 - (15) Liu, J.; Zhao, J.; Li, S.; Zhang, L.; Huang, Y.; Zhao, S. A novel microchip electrophoresis-based chemiluminescence immunoassay for the detection of alpha-fetoprotein in human serum. *Talanta* **2017**, 165, 107-111. doi: 10.1016/j.talanta.2016.12.038
 - (16) Feroz, H.; Kwon, H.; Peng, J.; Oh, H.; Ferlez, B.; Baker, C. S.; Golbeck, J. H.; Bazan, G. C.; Zydney, A. L.; Kumar, M. Improving extraction and post-purification concentration of membrane proteins. *Analyst* **2018**, 143, 1378-1386. doi: 10.1039/c7an01470h
 - (17) Sekikawa, T.; Kawasaki, Y.; Katayama, Y.; Iwahori, K. A simple method for extracting DNA from *Cryptosporidium* oocysts using the anionic surfactant LSS. *New Biotechnol.* **2011**, 29, 139-143. doi: 10.1016/j.nbt.2011.08.007
 - (18) Han, B.; Xu, Y.; Zhang, L.; Yang, X.; Wang, E. Surface modification of poly(dimethylsiloxane) microchips using a double-chained cationic surfactant for efficiently resolving fluorescent dye adsorption. *Talanta* **2009**, 79, 959-962. doi: 10.1016/j.talanta.2009.04.030
 - (19) Johnson, M. Detergents: Triton X-100, Tween-20, and More. *Mater. Methods.* **2013**, 3, 163. doi: 10.13070/mm.en.3.163.
 - (20) Jung, S. T.; Kim, M. S.; Seo, J. Y.; Kim, H. C.; Kim, Y. Purification of enzymatically active human lysyl oxidase and lysyl oxidase-like protein from *Escherichia coli* inclusion bodies. *Protein Expression Purif.* **2003**, 31, 240-246. doi: 10.1016/S1046-5928(03)00217-1
 - (21) Serna-Domínguez, M. G.; Andrade-Michel, G. Y.; Arredondo-Bernal, H. C.; Gallou, A. Two efficient methods for isolation of high-quality genomic DNA from entomopathogenic fungi. *J. Microbiol. Methods* **2018**, 148, 55-63. doi: 10.1016/j.mimet.2018.03.012
 - (22) Davies, J. T., A QUANTITATIVE KINETIC THEORY OF EMULSION TYPE. I. PHYSICAL CHEMISTRY OF THE EMULSIFYING AGENT. Gas/Liquid and Liquid/Liquid Interfaces. Proceedings of 2nd International Congress Surface Activity, **1957**, pp. 426-438.
 - (23) Chern, C.-S., in *Principles and Applications of Emulsion Polymerization*, John Wiley & Sons, Inc., Hoboken, New Jersey, **2008**, chap. 2.2, pp. 28. doi: 10.1002/9780470377949
 - (24) Hadjianestis, J.; Nikokavouras, J. Luminol chemiluminescence in micellar media. *J. Photochem. Photobiol., A* **1992**, 67, 237-243. doi: 10.1016/1010-6030(92)85232-J
 - (25) Ash, M., *Handbook of Preservatives*. Ash, M. a. I., Ed., (Synapse Information Resources, Inc., New York, **2004**), pp. 873.

- (26) SigmaAldrich, "*N-Lauroylsarcosinate sodium salt product information*", can be found under <https://www.sigmaaldrich.com/catalog/product/sial/y0001772?lang=de®ion=DE>, **2017**.
- (27) Mukerjee, P.; Mysels, K. J. Critical micelle concentrations of aqueous surfactant systems. Prepared under contract for the Office of Standard Reference Data, National Bureau of Standards of NSRDS-NBS 36, Washington, DC 20234, 1971 v + 227 pp. 20.5 × 27 cm. Price \$3.75. *J. Pharm. Sci.* **1972**, 61, 319. doi: 10.1002/jps.2600610254
- (28) Sherman, P., in *Emulsion Science* (Ed.: Sherman, P.), Academic Press, London, **1968**, pp. 131-212.
- (29) Barut, K. D.; Coskun Ari, F. F.; Öner, F. Development and Characterization of a Cationic Emulsion Formulation as a Potential pDNA Carrier System. *Turk. J. Chem.* **2005**, 29, 27-40.
- (30) Kastner, M., *Protein liquid chromatography*. (Elsevier, New York, **1999**), pp. 941. doi:
- (31) Dai, C.; Zhao, J.; Yan, L.; Zhao, M. Adsorption behavior of cocamidopropyl betaine under conditions of high temperature and high salinity. *J. Appl. Polym. Sci.* **2014**, 131. doi: 10.1002/app.40424
- (32) SigmaAldrich, "*Brij® 93 product information*", can be found under <https://www.sigmaaldrich.com/catalog/product/aldrich/388866?lang=de®ion=DE>, **2017**.
- (33) SigmaAldrich, "*Brij® S 100 product information*", can be found under <http://www.sigmaaldrich.com/catalog/product/aldrich/466387?lang=de®ion=DE>, **2017**.
- (34) Hait, S. K.; Moulik, S. P. Determination of Critical Micelle Concentration (CMC) of Nonionic Surfactants by Donor–Acceptor Interaction with Iodine and Correlation of CMC with Hydrophile–Lipophile Balance and Other Parameters of the Surfactants. *J. Surfact. Deterg.* **2001**, 4, 303-309. doi: 10.1007/s11743-001-0184-2
- (35) Stepan Company, "*Merpel A Product Bulletin*.", can be found under <https://www.stepan.com/products/Surfactants/MERPOL%C2%AE/MERPOL%C2%AE-A.aspx>, **2006**.
- (36) Jureller, S., Hariott; Kerschner, J. L.; Murphy, D. S., *Dry cleaning system with low HLB surfactant*. U.S. Patent US 6,461,387 B1, Feb. 4, 2000.
- (37) Škvarla, J.; Uchman, M.; Procházka, K.; Tošner, Z.; Garamus, V. M.; Pispas, S.; Štěpánek, M. Micellization of Zonyl FSN-100 fluorosurfactant in aqueous solutions. *Colloids Surf. A* **2014**, 443, 209-215. doi: 10.1016/j.colsurfa.2013.11.021
- (38) Zhong, Z.; Zhong, Y.; Liu, C.; Yin, S.; Zhang, W.; Shi, D. Study on the surface wetting properties of treated indium-tin-oxide anodes for polymer electroluminescent devices. *Phys. Status Solidi A* **2003**, 198, 197-203. doi: 10.1002/pssa.200306583

- (39) Fenzl, C.; Nayak, P.; Hirsch, T.; Wolfbeis, O. S.; Alshareef, H. N.; Baeumner, A. J. Laser-Scribed Graphene Electrodes for Aptamer-Based Biosensing. *ACS Sens.* **2017**, *2*, 616-620. doi: 10.1021/acssensors.7b00066
- (40) Edwards, K. A.; Baeumner, A. J. Optimization of DNA-tagged liposomes for use in microtiter plate analyses. *Anal. Bioanal. Chem.* **2006**, *386*, 1613-1623. doi: 10.1007/s00216-006-0743-4
- (41) Liu, X.; Li, A.; Zhou, B.; Qiu, C.; Ren, H. Chemiluminescence determination of surfactant Triton X-100 in environmental water with luminol-hydrogen peroxide system. *Chem. Cent. J.* **2009**, *3*, 7. doi: 10.1186/1752-153X-3-7
- (42) Hasebe, T.; Nagao, J.; Kawashima, T. Simultaneous Flow Injection Determination of Acetylcholine and Choline Based on Luminol Chemiluminescence in a Micellar System with On-Line Dialysis. *Anal. Sci.* **1997**, *13*, 93-98. doi: 10.2116/analsci.13.93
- (43) Niño, M. R. R.; Patino, J. M. R. Surface tension of bovine serum albumin and tween 20 at the air-aqueous interface. *J. Am. Oil Chem. Soc.* **1998**, *75*, 1241. doi: 10.1007/s11746-998-0169-6
- (44) Ortiz-Tafoya, M. C.; Tecante, A. Physicochemical characterization of sodium stearyl lactylate (SSL), polyoxyethylene sorbitan monolaurate (Tween 20) and κ-carrageenan. *Data in Brief* **2018**, *19*, 642-650. doi: 10.1016/j.dib.2018.05.064
- (45) Mukerjee, P.; Chan, C. C. Effects of High Salt Concentrations on the Micellization of Octyl Glucoside: Salting-Out of Monomers and Electrolyte Effects on the Micelle–Water Interfacial Tension1. *Langmuir* **2002**, *18*, 5375-5381. doi: 10.1021/la020059e
- (46) Dutkiewicz, E.; Jakubowska, A. Effect of electrolytes on the physicochemical behaviour of sodium dodecyl sulphate micelles. *Colloid. Polym. Sci.* **2002**, *280*, 1009-1014. doi: 10.1007/s00396-002-0723-y
- (47) Smith, T. The Hydrophilic Nature of a Clean Gold Surface. *J. Colloid Interface Sci.* **1980**, *75*, 51-55. doi: 10.1016/0021-9797(80)90348-3
- (48) Xu, G.; Pang, H. L.; Xu, B.; Dong, S.; Wong, K. Y. Enhancing the electrochemiluminescence of tris(2,2'-bipyridyl)ruthenium(II) by ionic surfactants. *Analyst* **2005**, *130*, 541-544. doi: 10.1039/b419269a

6. Supporting Information

6.1 Luminol and surfactant molecules

The in this study characterized luminol molecules were standard luminol and a luminol derivative, we recently reported.¹

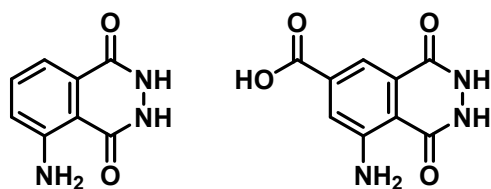
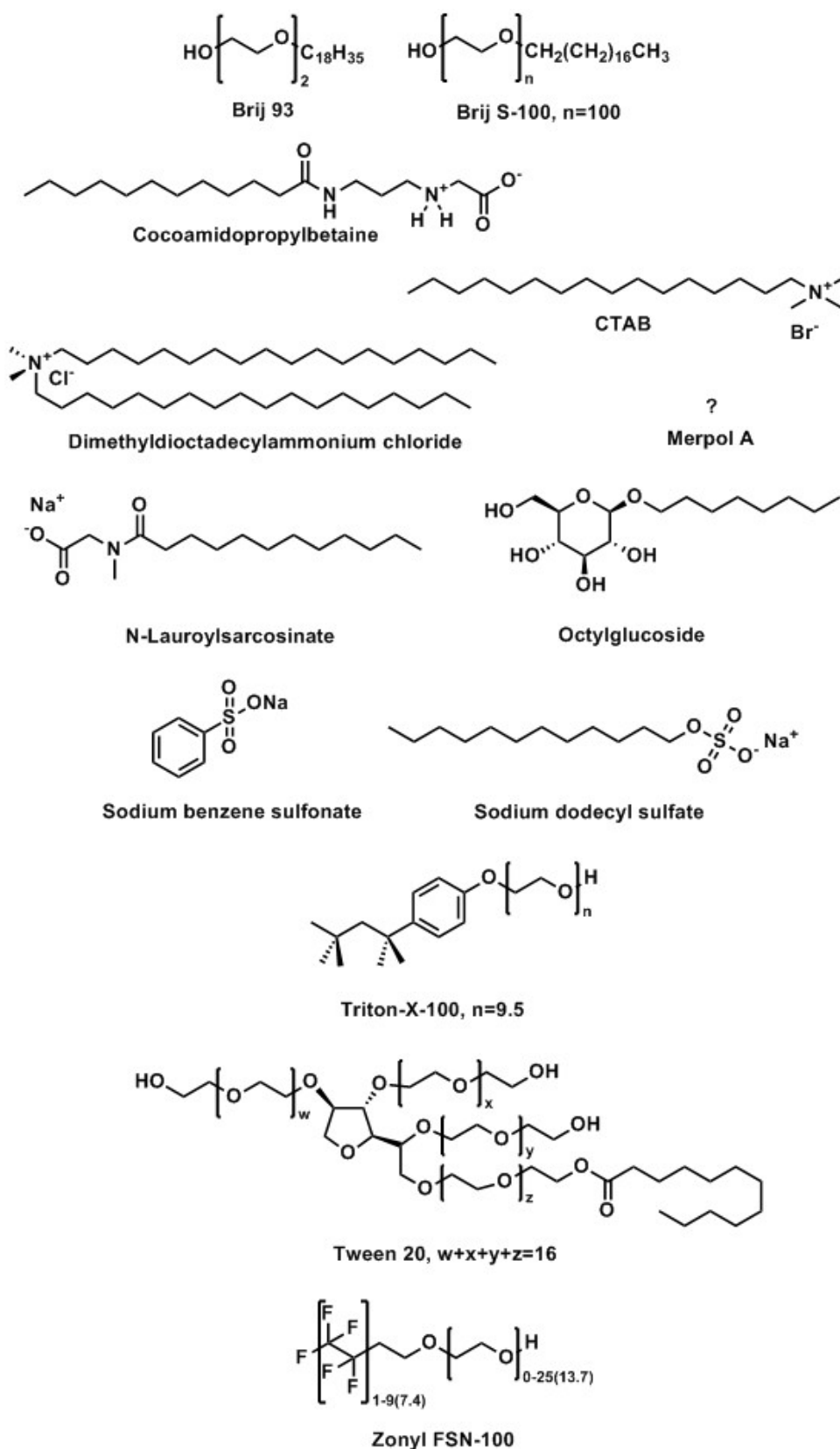


Figure S1. Structure of luminol and *m*-carboxyluminol.¹



Scheme S1. Structures of the employed surfactants in this study. Note: for Merpol A no exact chemical structure is known due to non-disclosure of the manufacturer and it is solely classified as alcohol phosphate.

6.2 Electrode area determination

For a comparison between the used working electrode materials ITO, hydrophilised ITO and gold, the active surface area of the electrodes was determined. Measurements were done on a PalmSens 4 portable potentiostat (Palm Sens BV, Netherlands) and data evaluation was done manually with the PStace 5 software package. Areas were calculated via the Randles-Sevcik equation upon data from CV measurements of ferri-/ferrocyanide solution on these electrodes. The used value for the diffusion coefficient for ferri-/ferrocyanide was $7.6 \times 10^{-6} \text{ cm}^2/\text{s}$ and the temperature value was 298 K and the number of transferred electrons was 1. For the measurements, the described ECL cell was used with either of the working electrodes and each time Pt as CE and the Ag-wire as *pseudo*RE. Each measurement was repeated 3 times on a fresh working electrode area of each material and triple rounds were measured during the CVs. CV conditions were as following: potential range between -0.6 V and +1.0 V (at the upper end relatively low to avoid the described electrode fouling reactions with ITO electrodes at potentials > +1.0 V). The scan rate was set to 50 mV/sec., the step potential was 0.01 V and the used reaction mixture was a 10 mM mixture of ferri-/ferrocyanide and 0.1 M KCl as supporting electrolyte in 10 mM phosphate buffer with a pH of 7.4.

6.3 ECL with chosen surfactants for luminol and *m*-carboxy luminol ECL on different electrodes

6.3.1 Remarks and settings

For these measurements, the PMT voltage was set to 800 V (ITO, hydrophilised ITO (H-ITO) and laser scribed graphene (LSG)) or 700 V/ 750 V (gold). The signals (i.e. intensity integral mean values) were normalized to the negative control (i.e. the data point without added surfactant) for each measurement series and the negative control being set to 100% (see figure S39 for absolute comparison between different electrodes). Thus, to highlight, the ECL signal response curves are with respect to highest overall intensity not fully equal and the signal on gold is approximately 5-10 times larger than on the other electrodes. All different surfactants were measured on an unused working electrode, the cell was cleaned and the reference electrode was polished and a new

AgCl layer deposited by immersion in 3 M KCl to avoid adsorption of surfactant remainders in the surface layer. For the measurements of dioctadecyldimethylammonium chloride and Merpol A on ITO, all signals were recorded at an emission wavelength of 430 nm and a PMT voltage of 850 V. Low solubility, poor performance and missing information about these surfactants prevented a full characterization for being rather less important.

6.3.2 Discussion.

In the case of anionic surfactants, two monianionic molecules were studied, N-Lauroylsarcosinate, a linear C₁₂-carboxylate species, with additional amide functionality and SDS, a linear C₁₂ sulfate. Here, SDS was slightly quenching both ECL processes with both luminols on ITO. Essentially the same was observed on gold, besides *m*-carboxy luminol being slightly enhancing and largely enhancing with both luminols on H-ITOs (~150-175%). Very high concentrations of SDS couldn't be measured as partly precipitating SDS was an issue, despite sufficient solubility was stated in literature, probably caused by the ECL reaction composition. On LSGs, the behavior was comparable to gold for *m*-carboxy luminol with slightly higher signals in the upper concentrations. For luminol however, the signal was steadily increasing with a steeper slope, until 200% enhancement at 2.5 mM.

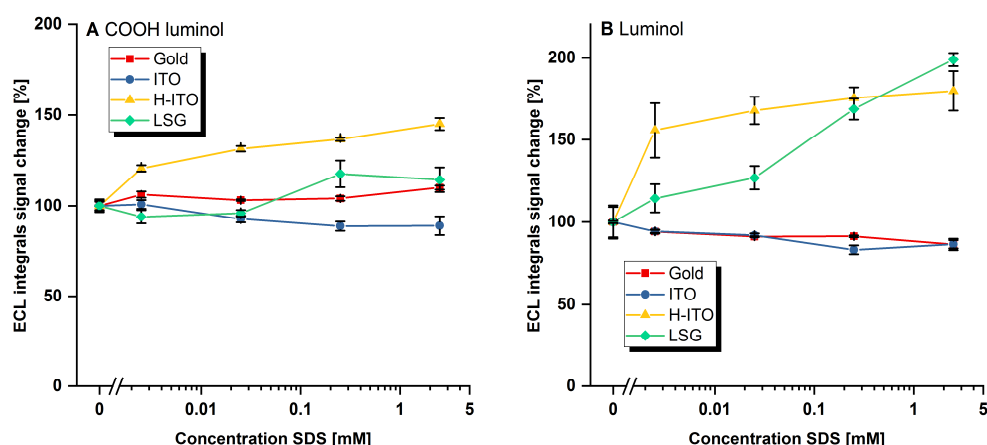


Figure S2. ECL signal dependence on SDS concentration.

N-Lauroylsarcosinate, had similar behavior for both luminols, being overall quenching on ITO electrodes. For gold and H-ITO for intermediate concentrations of surfactant (~0.1 mM) enhancing and then again quenching at high (≥ 1 mM) surfactant amounts was present. A special case was seen with luminol and gold, i.e. first enhancement, then a

signal drop to 75% (@1 mM) and then rise again to ~110%. The latter effect may be caused by N-Lauroylsarcosinate's CMC being around 15 mM. Finally, on LSGs, N-Lauroylsarcosinate, behaved differently as the ECL signal was enhanced very strongly for both luminols, reaching 220% for *m*-carboxy luminol at 25 mM. With luminol the strong enhancement started later from 25 μ M up and reached with almost 500% the largest overall enhancement of all surfactant with luminol, also at 25 mM.

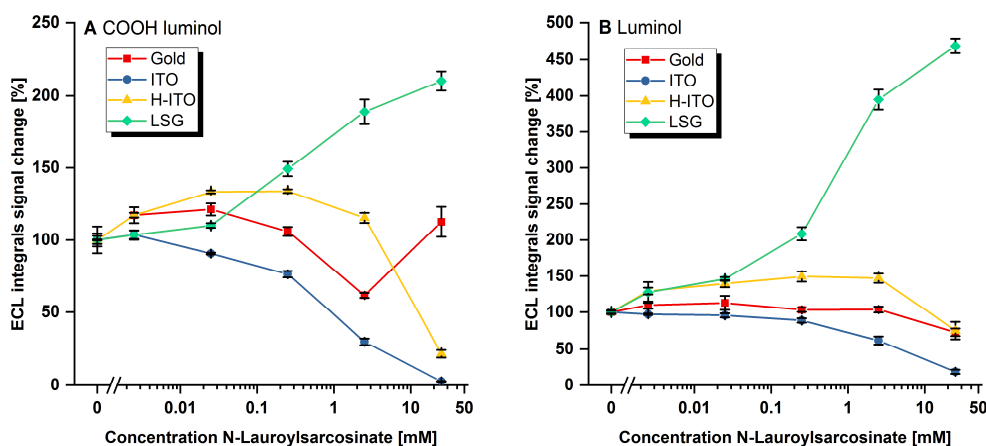


Figure S3. ECL signal dependence on N-Lauroylsarcosinate concentration.

The much steadier enhancement and lower pronounced quenching for SDS compared with N-Lauroylsarcosinate, suggests a better compatibility of the sulfate headgroup compared to the carboxyl group and the missing amide functionality with the electrode surface and the luminol ECL process on less surface active electrodes. In contrast, the behavior on LSG with N-Lauroylsarcosinate may be caused by its better compatibility, where the additional amide functionality and the carboxylate might aid. In fact, this suggests a major role of the head group nature irrespective of its charge as both are monoanionic.

The cationic surfactants response has been described exemplary in the main manuscript, thus being omitted here and their response is shown in figs. S4-S5.

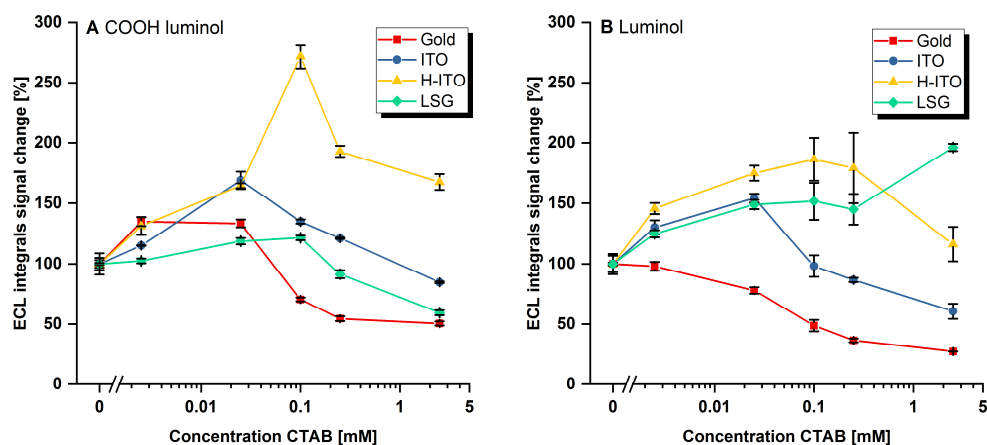


Figure S4. ECL signal dependence on CTAB concentration.

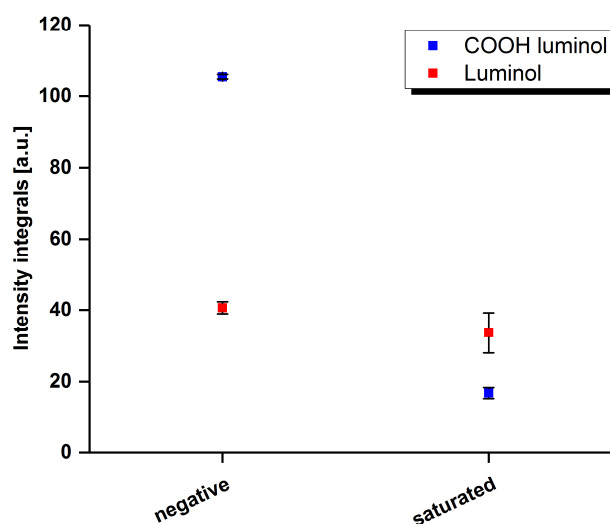


Figure S5. ECL signal dependence on Distearyltrimonium chloride concentration on ITO.

A special candidate is SBS, depicting a special surfactant class, a hydrotrope. As these do not form classical micelles, its behavior was interesting towards ECL influence. Despite its changes on the ECL on different electrodes were not large, some distinct effects could be observed. They varied between slight enhancement for H-ITOs, almost no influence on gold (despite a initial drop for *m*-carboxy luminol and then slow recovery of the signal to 100%) and a slight quenching effect for ITO, The present quenching effect without micelle formation or presence of large phase structures (in our concentration range²) suggests a nonexistent influence of turbidity effects causing the quenching behavior in our cases.

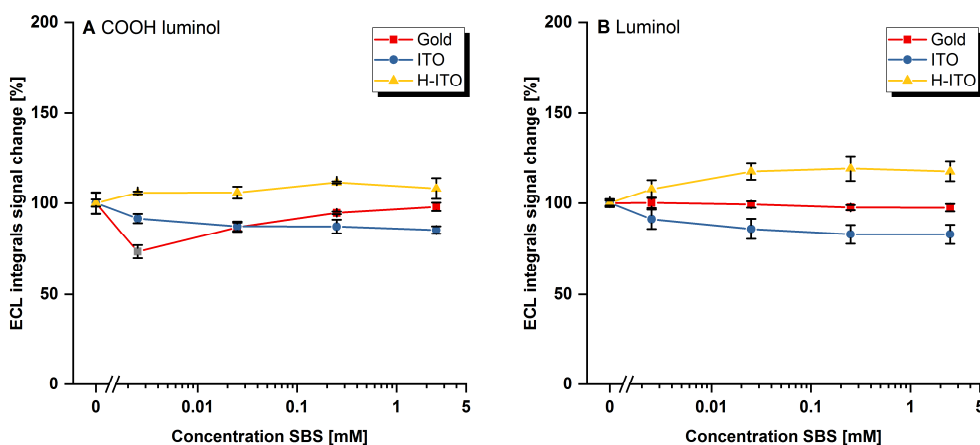


Figure S6. ECL signal dependence on SBS concentration.

Further, a second special surfactant is present with cocoamidopropyl betaine (DEHYTON PK 45), which is an amphoteric surfactant exhibiting neutral charge while having one cationic and one anionic functional group. Thus its response was rather interesting in comparison to nonionic or also ionic surfactants. Its behavior was rather in accordance with other surfactants, as the most beneficial enhancement effect for both luminols was observed with H-ITOs. Here, maximum enhancement was seen with medium surfactant concentrations and signal reduction with high concentrations occurred. On ITO, almost steady behavior was seen, while very slight quenching was present with higher concentrations. Finally on gold, both luminols differed as *m*-carboxy luminol exhibited a dip with 0.25 mM surfactant where the signal was quenched to $\sim 30\%$ and rised again slightly with higher concentrations. For pristine luminol, the signal was steady up to a concentration of 2.5 mM above which a signal rise to approximately 150% with 25 mM was observed. This behavior suggests an influence of possible surfactant solution phase behavior on gold electrodes while the other electrodes seem unaffected. Thus, there is possibly an additional effect, located in compliance of surface functionalities besides general hydrophobic- or hydrophilic electrode behavior.

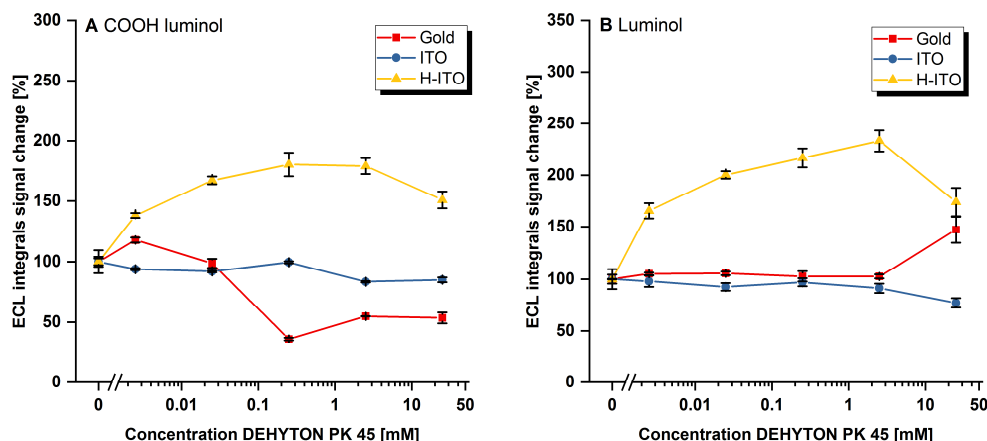


Figure S7. ECL signal dependence on Cocoamidopropyl betaine concentration.

In the case of nonionic surfactants, Octylglucoside was investigated that is a sugar derivative with a short to medium monoalkyl chain (C_8) readily used in biochemical methods. Steady quenching was here only observed for pristine ITOs, with both luminols down to $\sim 25\%$ signal. On gold electrodes, however, an enhancement is observed for both luminols, while that for *m*-carboxy luminol peaks at $250\ \mu\text{M}$ with 145% and then drops back to approximately 100% . Luminol only reaches a maximum of 125% signal yield for a higher concentration. With H-ITO, *m*-carboxy luminol only reaches 120% maximum enhancement while luminol approaches 140% and both are suspended to quenching at $25\ \text{mM}$ OG down to 50% and 75% signal for *m*-carboxy luminol and luminol, respectively. With LSGs, *m*-carboxy luminol reaches an enhancement up to 150% and then declines ($25\ \text{mM}$). With luminol, the overall largest enhancement can be observed with OG, reaching a value of almost 400% of the original signal, while the deviation also rises largely. This behavior with OG on LSG also imposes doubts on the role of the charge of the respective headgroup. Possibly, the cyclic hydrophilic headgroup is here also beneficial in the interaction with the electrode surface.

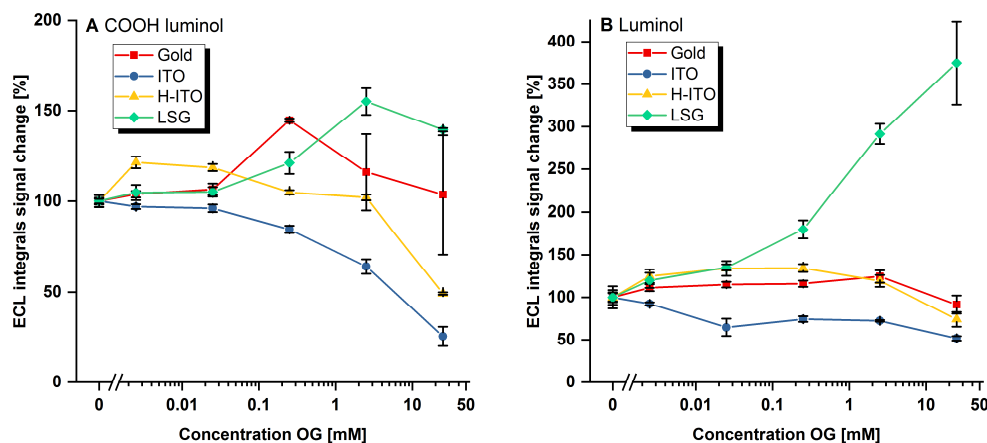


Figure S8. ECL signal dependence on Octyl glucoside concentration.

Triton-X-100, a short polyethyleneoxide (PEO) ether with a benzene ring and additional short C₄ chain exhibits enhancement with ITO and H-ITO with *m*-carboxy luminol and only with H-ITO for luminol. In both cases, with H-ITO, the signal rises steadily with rising surfactant concentration to peak in a signal of 160% and even 190% for *m*-carboxy luminol and luminol. With gold, luminol ECL is almost unchanged over the whole concentration range, but with *m*-carboxy luminol it is steadily quenched to 25% at 25 mM. With ITO, and *m*-carboxy luminol, the signal first increases and is reduced again at high concentrations, while for luminol, the signal is steadily quenched (65% at 25 mM). For LSGs, the signal with *m*-carboxy luminol is first slightly reduced, then starts slightly enhancing to peak off at high concentrations. For luminol, the signal reaches almost the enhancement as with H-ITOs but then peaks off in the higher mM range of surfactant.

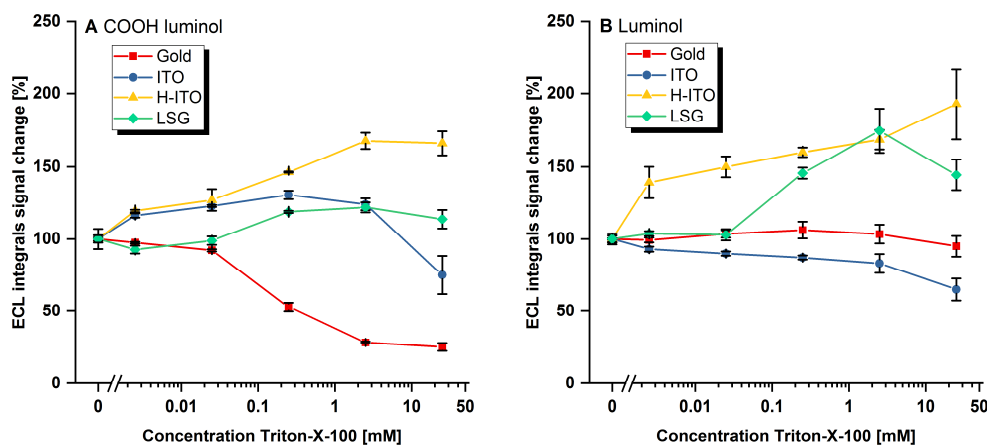


Figure S9. ECL signal dependence on Triton-X-100 concentration.

The ECL response with added Tween 20, a comparably bulky, hydrophilic PEO-fatty acid derivative manifested in enhancement with H-ITO and again large quenching at the maximum concentration with both luminols. It is assumed that phase transitions of the surfactant occurs at those concentrations above the CMC. Further, with *m*-carboxy luminol, a steady response was seen with ITO, a comparable behavior with LSGs and quenching from the beginning with gold. For luminol, enhancement on gold (175%), ITO and H-ITO was present while quenching occurred for all three to zero signal at 2.5 mM. On LSGs, however, quenching only occurred with 25 mM surfactant and steady enhancement up to 220% can be observed beforehand.

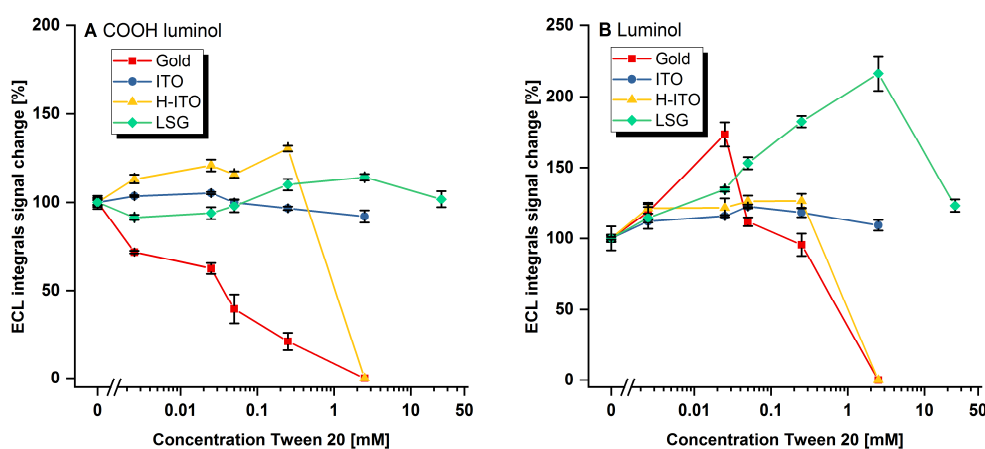


Figure S10. ECL signal dependence on Tween-20 concentration.

The third non-ionic surfactant, Zonyl FSN, is perfluorinated. It performs best on H-ITOs and LSG. On the H-ITO's, it steadily enhances the signal for both luminols over the whole concentration range, albeit stronger for *m*-carboxy luminol, while for *m*-carboxy luminol and ITO the signal stays constant and on gold, large quenching is observed. With luminol, on both, ITO and gold, the signal is quenched but in both cases only mildly. Finally on LSGs, the signal is enhanced first more slightly and then stronger (above 0.25 mM) to peak off at 2.5 mM and then decline again for *m*-carboxy luminol. For luminol, similarly, the signal first climbs slower to 175% at 0.25 mM above which the maximum of 400% is reached. It is assumed that the strongly hydrophobic perfluorinated tails interact preferably with itself instead of the solution and they can similarly to a SAM structure, accumulate on gold,³ and that the permanently charged *m*-carboxy luminol cannot be well stabilized. The polydispersity of Zonyl-FSN 100 composition can also yield quite varying microenvironments.⁴

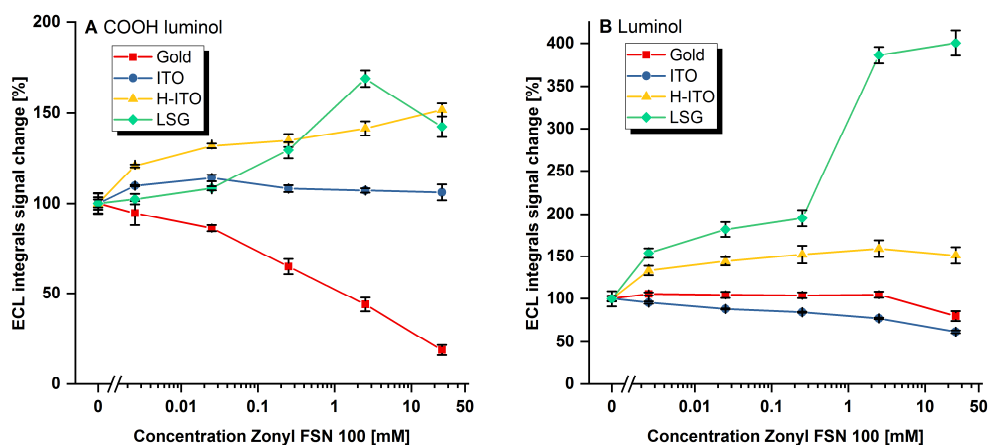


Figure S11. ECL signal dependence on Zonyl FSN 100 concentration.

The single alkyl-chain PEO surfactants, Brij® S-100 and Brij® 93 display interesting response behaviors. Brij® S-100 stands for a more hydrophilic candidate as it incorporates 100 ethylene oxide (EO) units with a C₁₈-chain, thus being well water dispersible. Here, ITO, H-ITO and gold cause quite similar behavior for both luminols, being very steady besides very little enhancement or signal reduction. Just luminol and H-ITOs are an exception, as the enhancement is stronger (135%) but also is very constant over the whole concentration range to only drop off slightly with 1 mM surfactant. LSGs, however, again are an exception for both luminols, being strong enhancers. For m-carboxy luminol up to 150%, peaking at 0.25 mM and then declining slowly. For luminol, the signal rises constantly and steeply up to 320% at 2.5 mM without peak off. Brij® 93 on the other hand is a very hydrophobic surfactant, with its 2 EO units and an equal C₁₈ chain length, also manifesting in being turbid (above cloud point) and thus being presumably present in a coacervate phase and a surfactant poor aqueous phase. This makes it interesting as this forms hydrophobic islands of fluid dispersed inside the solution phase and being able to influence the ECL process. Brij® 93 has almost no influence on ITO and gold electrodes for both luminol species, where the signal is basically unchanged over the whole concentration range. However, for LSG and H-ITOs the situation is different. Here, both electrodes have similar behavior, both are steadily enhancing the ECL signal with rising concentration over the whole range for both luminols. In this case, however, H-ITOs are the more efficient enhancers while LSGs are less steeply enhancing.

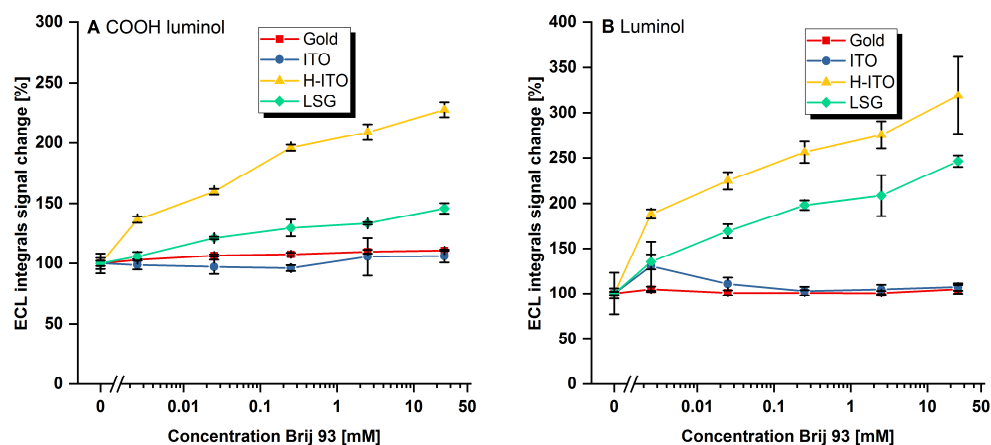


Figure S12. ECL signal dependence on Brij 93 concentration.

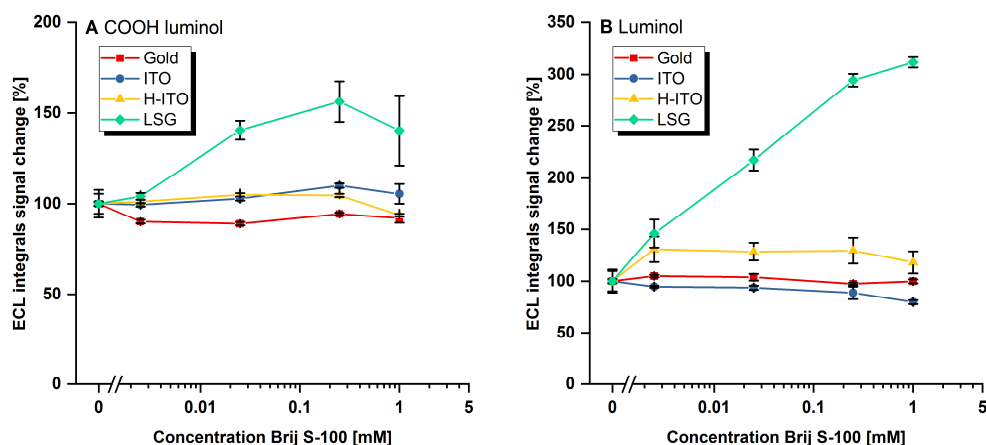


Figure S13. ECL signal dependence on Brij S-100 concentration.

Finally, for Merpel A only the behavior on ITO was characterized where with *m*-carboxy luminol the signal decreased slowly until 0.005% and above a sharp drop to zero was obtained. For luminol the signal was constant and dropped slightly above 0.01%.

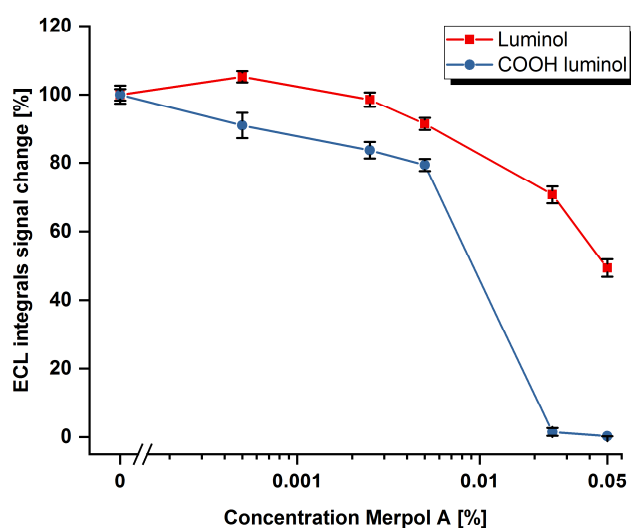


Figure S14. ECL signal dependence on Merpol A concentration on ITO.

6.3.3 Surfactant adsorption behavior on the employed electrode surfaces

This section gives a simplified discussion of general surface adsorption behavior, stating proposed contributions on the ECL enhancement or quenching characteristic, exemplary for the nonionic surfactant Brij 93, the cationic surfactant CTAB and the anionic surfactant SDS on different electrodes. As the luminol ECL reactions, i.e. their determinant oxidation steps occur directly at the electrode surface, aggregation and mesoscale structuring of surfactant molecules at, or in the vicinity of the electrode, has a major influence on the observed luminol ECL reaction. As such, we briefly discuss this important area in the following. The macroscopic electrode surface properties are here considered as well, with Gold and ITO being classified as hydrophobic electrodes (carbonaceous contamination!),⁵ H-ITO classified as hydrophilic⁶ and LSG as porous, hydrophilic electrode, respectively (as shown with contact angles in chapter 6.15). The discussion is limited to these three exemplary cases, as there are many factors, having critical influence on the actual surface situation. These are: the ionic strength and pH, the actual surfactant structures and how these - and their aggregation tendencies are influenced (e.g. CMC shifts) by entropic and enthalpic contributions to the free energy of the liquid system.⁷ Furthermore, specific effects arising from the potential at and the actual surface chemistry on the electrode, and especially for LSGs, their pore size distribution must be considered as well.

Nonionic surfactants

Surfactants are likely to adsorb onto hydrophobic electrodes in a way that as much of their nonpolar molecular surface is in close contact with the hydrophobic surface of the electrode. With increasing surfactant content in the aqueous solution, they aggregate presumably in a monolayer type of adsorbate layer with denser and more and more vertical structures with rising concentrations.⁸ Here, the molecular packing parameter, gives a measure to estimate the favored aggregates (e.g. spherical, rod-like or disc-like micelles or lamellar structures.⁹ In the case of a hydrophilic electrode, a surfactant like Brij 93, with a small hydrophilic part and a large hydrophobic area is likely to orient itself in a double layer structure at the surface with rising concentrations with their nonpolar surface in the middle and the headgroups oriented towards the electrode surface and the solution.¹⁰ while also structures like spherical bilayered vesicles or adsorbed, disc-like micelles can be expected. A surfactant with a large portion of a hydrophilic EO-headgroup compared to its nonpolar surface (e.g. Brij S-100) will rather form small aggregates or micelles, according to literature.¹¹ Exemplary, in the case of Brij 93, for gold and ITO electrodes, the surfactant addition has little overall influence besides a possibly slight improvement of the electrode environment for an increased presence probability for the luminols. On H-ITO, the not-so-dense packing of surfactants on the electrode surface can provide better accessibility for luminol molecules while still improving the milieu compared to no surfactant being present.

Cationic surfactants

The headgroup's contribution to the adsorption process of ionic surfactants is, in the case of cationic surfactants largely influenced by repulsive Coulomb interactions because of the positive electrode potential. In addition to that, the surface character of the electrode plays an important role. In this regard, it is to distinguish between electrodes with hydrophobic and hydrophilic surface environment, respectively (see also chapter 6.15). In the case of an electrode with an overall hydrophobic surface (due to carbonaceous contamination), for cationic surfactants we expect at low concentrations that they rather orient in a way that their tails maximize the contact area to the hydrophobic electrode and the headgroups sticking out into the solution.¹² At higher surfactant concentration, the surfactants are expected to aggregate in a monolayer on the electrode surface¹³ - with the headgroups oriented towards the

aqueous solution and also micelles can be formed. On hydrophilic electrodes, the adsorption of surfactant molecules onto the hydrophilic electrode surfaces is relatively unlikely for cationic surfactants (e.g. CTAB). This is mainly because of the balance between strong Coulomb repulsion among the positively charged headgroup and the positive electrode potential or possible attractive forces to the hydrophilic surface groups on the electrode. Influenced by entropy, the cationic surfactants thus rather arrange in micelles and might even undergo a potential-directed electrophoretic mobilization along the potential gradient away from the working electrode.

However, with a high ionic strength, electrolyte anions can also act in a shielding manner to weaken the long-range interactions and even enhance the attraction.¹⁴ Furthermore, it is known from literature that even adsorption of charged surfactants on equally charged surfaces is possible.¹⁵

In the exemplary case of CTAB, the observed ECL enhancement or quenching behavior on different electrodes, can be attributed to two effects: a different probability of presence for luminols, influenced by the surfactants at the electrode surface and also in possible stabilizing or destabilizing effects for the transition states in the ECL reaction and thus higher or lower reaction rates.

Anionic surfactants

For anionic surfactants on hydrophobic electrodes, the headgroups experience strong coulomb attraction, and through the tail hydrophobicity, it is likely for them to orient themselves in a way to maximize the contact area with both, their headgroups and tails to the surface. With rising concentration they are likely to align in a more vertical orientation, and also form micelles. For hydrophilic electrodes, a more vertical orientation is already given at low concentrations, as the hydrophilic surface and the surfactant tails do not match each other very well. Here, rather double layer structures can be formed¹⁶ and with increasing concentrations, micelles. To note here is that micellar structures, because of their mutual repulsion following their charge, can aid to expose free electrode space to a greater extent compared to double layers and thus allow more space for ECL reactants to approach the electrode. Exemplary in the case of SDS, the ECL quenching behavior on hydrophobic electrodes, would match an assumption of surfactants blocking the electrode towards accessibility for the hydrophobic luminol.

Porous, hydrophilic electrodes

Finally, on porous, hydrophilic electrodes, the surfactant orientations are expected to be similar to the hydrophilic electrodes. However, the much larger overall surface area and the pores can strongly influence the surfactant behavior on these electrodes and through the 3D-environment inside the pore structure, an orientation in micelle-like structures compared to double layers can be expected. Overall, surfactants are expected to enter the pores and gradually cover the surface. More polar surfactants cover more surface area as the hydrophilic surface groups improve adsorption. Additionally, the environment of the porous structure is likely to become more hydrophobic in general, which is also reflected in the larger enhancement of the more hydrophobic luminol compared to *m*-carboxy luminol.¹⁷

6.4 Surfactant's ECL signal effects with respect to their cmc

Table S1. Surfactants and ECL signal change plus correlation with cmc.- *m*-carboxy luminol given for selection of surfactants.

Surfactant	Maximum signal enhancement [%] *	c(surfactant)@ max. enhancement [mM]	cmc [mM]	Signal difference factor **	Electrode
N-Lauroylsarcosinate	215	25	14.6	~ 1	LSG
Sodium dodecyl sulfate (SDS)	140	2.5	8.2	?	H-ITO
Cetyltrimethylammonium bromide (CTAB)	272	0.1	1.0	~ 1.5	H-ITO
Octylglucoside (OG)	155	2.5	20-25	~ 1.1	LSG
Triton-X-100	168	2.5	0.24	0.9	H-ITO
Tween® 20	130	0.25	0.06	0.9	H-ITO
Zonyl FSN 100	170	2.5	0.05-0.1	~1.4	LSG

Table S2. Surfactants and ECL signal change plus correlation with cmc.- **luminol**, given for selection of surfactants.

Surfactant	Maximum signal enhancement [%] *	c(surfactant)@ max. enhancement [mM]	cmc [mM]	Signal change vs. signal @ cmc [%] **
N-Lauroylsarcosinate	475	25	14.6	~ 1.1
Sodium dodecyl sulfate (SDS)	195	2.5	8.2	?
Cetyltrimethylammonium bromide (CTAB)	195	2.5	1.0	1.1
Octylglucoside (OG)	370	25	20-25	1
Triton-X-100	190	25	0.24	1.3
Tween® 20	215	2.5	0.06	1.4
Zonyl FSN 100	400	25	0.05-0.1	2.2

*Signal enhancement or decrease in % relative to signal without surfactant added. “~” sign indicates approximation as employed surfactant concentrations and cmc concentrations are partly differing and thus an exact number cannot be stated.

$$Factor^{**} = \frac{\% \text{ maximum ECL signal enhancement}}{\% \text{ ECL Signal @cmc concentration}}$$

6.5 Luminol and *m*-carboxy luminol ECL with CTAB and CTAC

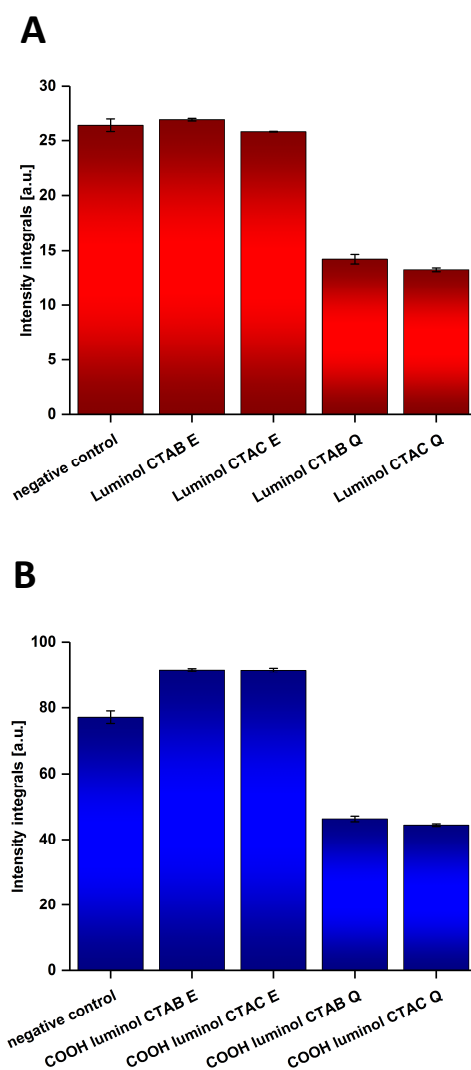


Figure S15. Direct comparison of ECL signals between CTAC and CTAB in enhancing and quenching concentrations for both luminol species. Concentrations of CTAB (E: 25 μ M; Q: 1 mM) and CTAC (E: 25 μ M; Q: 1 mM) and PMT voltage: 800 V.

6.6 HLB correlation to quenching/ enhancement with ECL signal or EC current

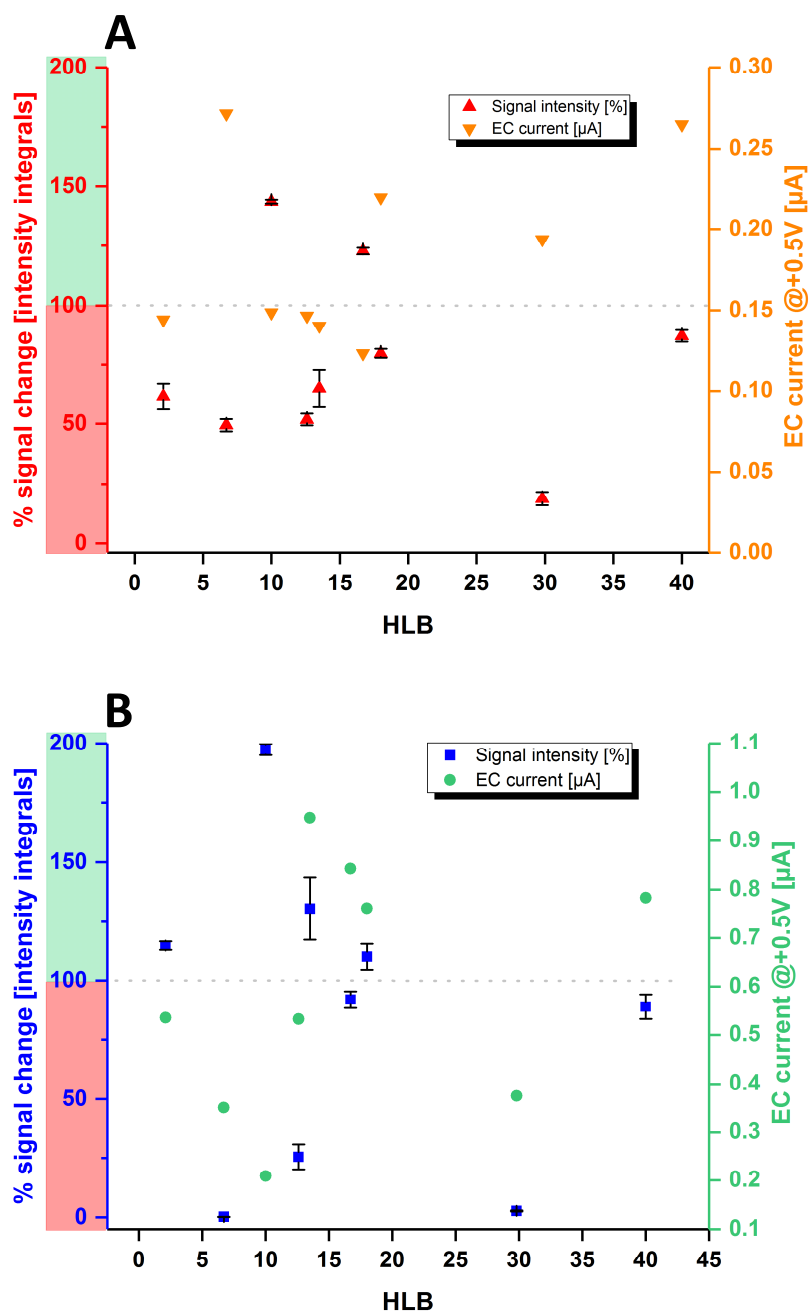


Figure S16. HLB correlation of ECL signal enhancement or quenching^[a] and anodic currents^[b] for luminol(A) and *m*-carboxy luminol (B) – analysis for pristine ITO electrodes.

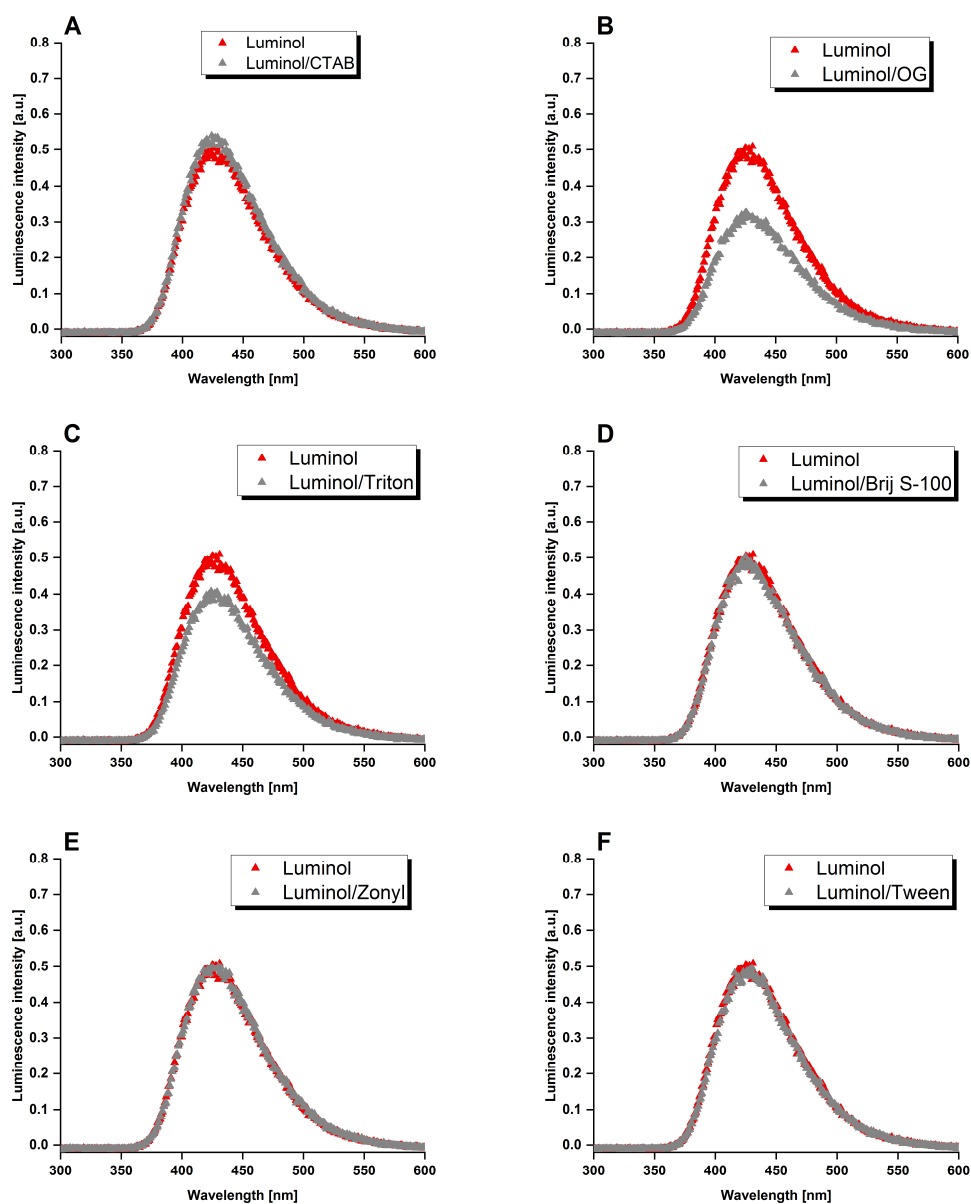
[a] %-Value for the optimum enhancement concentration or a large quenching concentration normalized to the negative control signal without added surfactant for

each data point (calculated from the intensity integral values and the negative control set to 100% signal). [b] taken from the cyclic voltamograms, each 2nd run assuming stabilized conditions at a potential of +0.5 V vs. Ag/AgCl (forward scan).

6.7 Luminescence emission scans

For these measurements, all signals were recorded with a PMT voltage of 750 V.

6.7.1 Luminol ECL



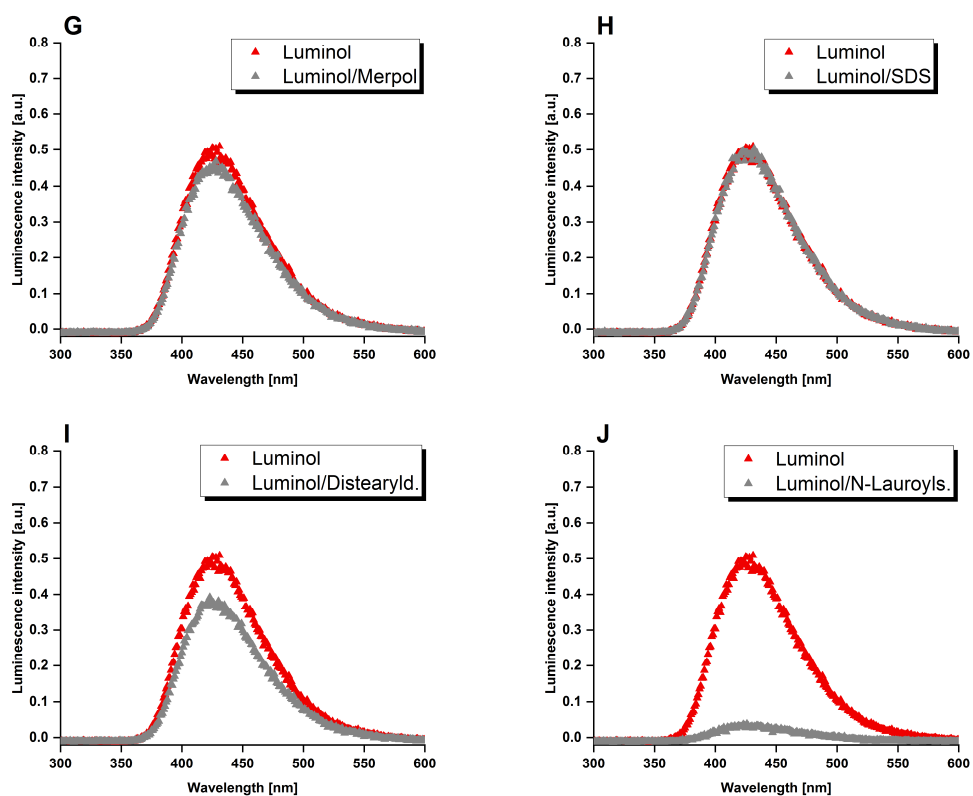
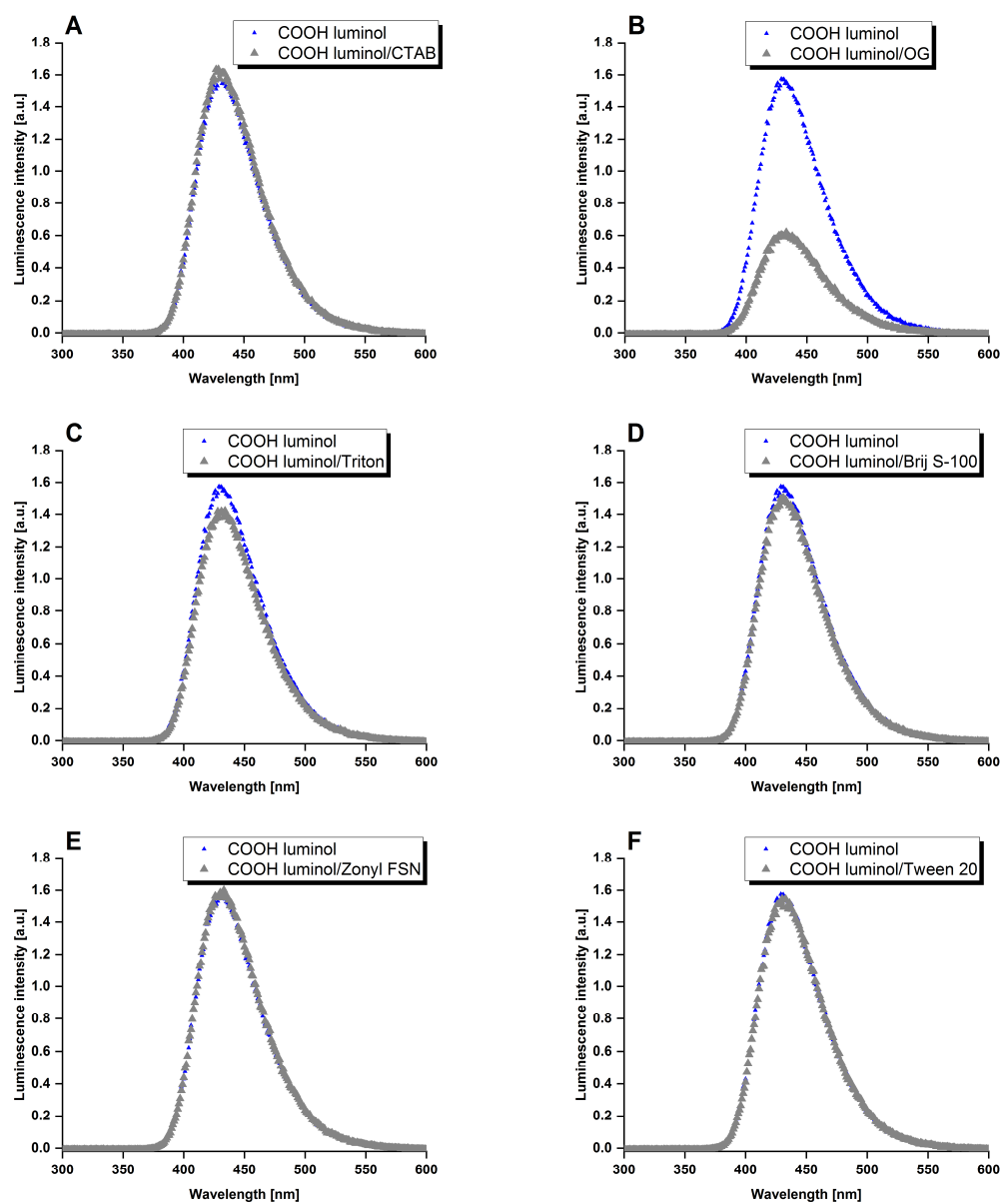


Figure S17 (a-j). Emission Scans of Luminol ECL with different added surfactants and w/o surfactant as reference.

6.7.2 *m*-Carboxy luminol ECL



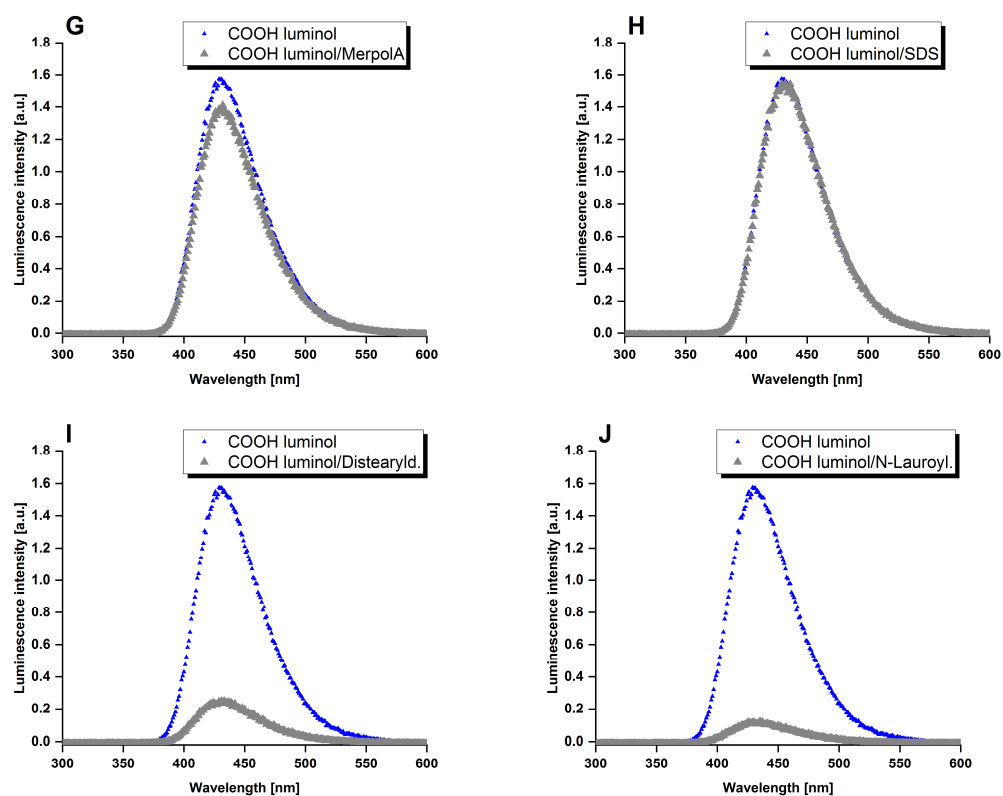


Figure S18 (a-j). Emission Scans of *m*-carboxy luminol ECL with different added surfactants and w/o surfactant as reference.

6.8 Cyclic voltammetry measurements

6.8.1 CV on Gold WEs

Selection of cyclic voltammograms which were recorded with a gold macro electrode ($d = 1.6$ mm), Pt CE and Ag/AgCl-RE from 0 V to +1.0 V at 50 mV/s scan rate and 0.001 V step potential. Gold WE's were cleaned via 1.0 μ m diamond polish, alumina polish and rinsing with millipore water and isopropanol prior to each new surfactant to remove contaminants. The concentration of the glycine-NaOH buffer at pH 9, employed here was 1 mM.

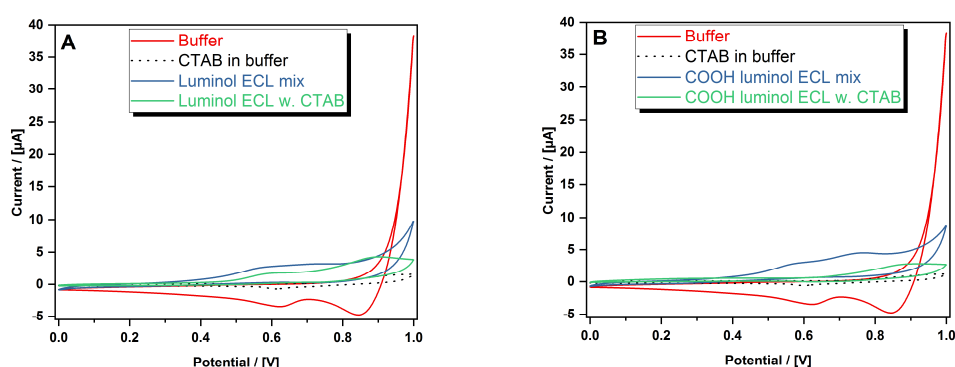


Figure S19. CV for a cationic representative, CTAB and both luminol species (**A** and **B**) where **A** is enhancing ECL emission and **B** is quenching ECL emission. Both at a surfactant concentration of 25 μ M.

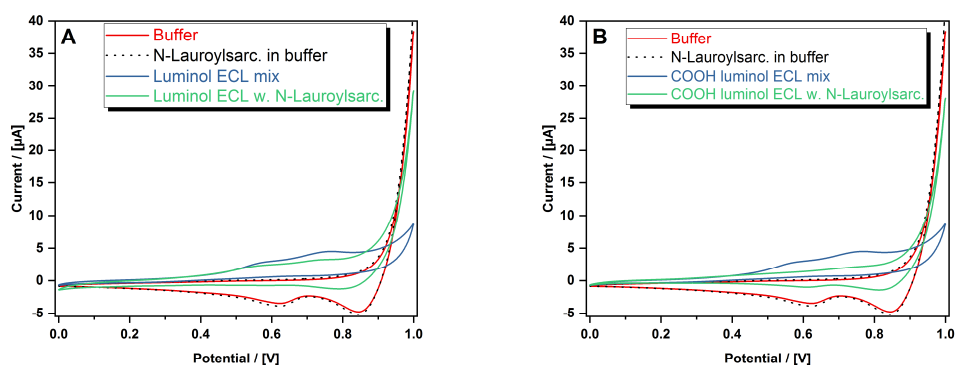


Figure S20. CV for an anionic representative, N-Lauroylsarcosinate and both luminol species (**A** and **B**) where **A** is neutral in ECL emission and **B** is enhancing ECL emission. Both at a surfactant concentration of 25 μ M.

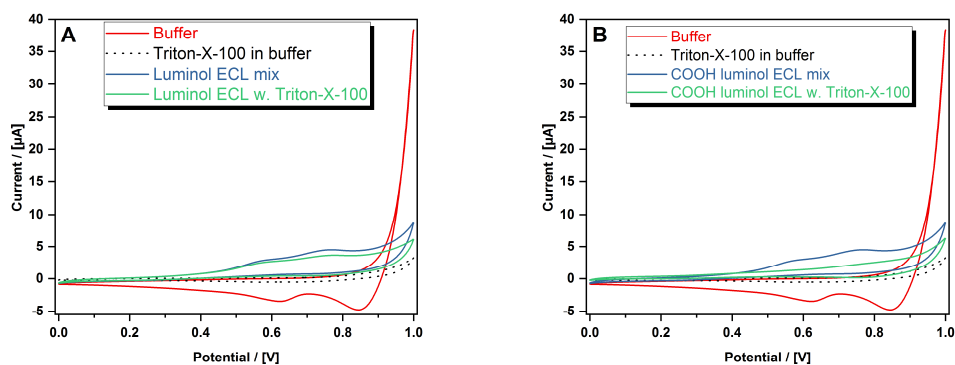


Figure S21. CV for a nonionic representative, Triton-X-100 and both luminol species (**A** and **B**) where **A** is neutral in ECL emission and **B** is quenching ECL emission. Both at a surfactant concentration of 1 mM.

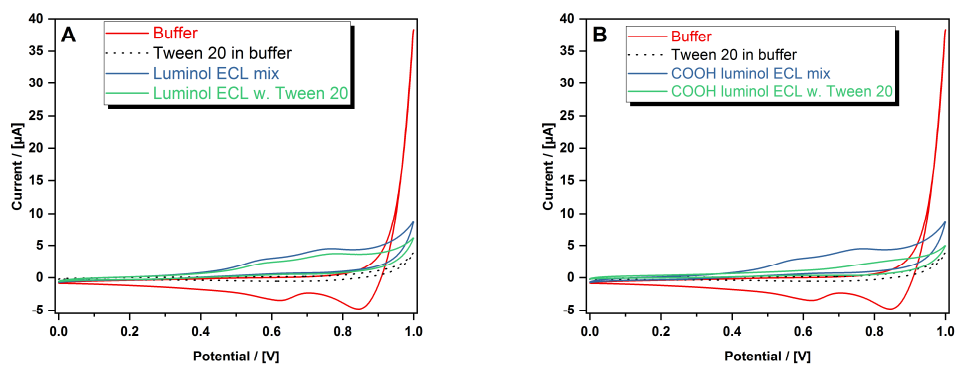


Figure S22. CV for a further nonionic representative, Tween-20 and both luminol species (**A** and **B**) where **A** is enhancing ECL emission and **B** is quenching ECL emission. **A** at a surfactant concentration of 25 μM and **B** at a surfactant concentration of 1 mM.

6.9 CV on ITO WEs

Settings were in the ECL cell with ITO-WE, Pt-wire-CE and Ag-wire-*pseudo* RE. Scans were done at 100 mV/s scan rate, 0.01 V step potential from 0 V to +1.0 V.

6.9.1 Luminol

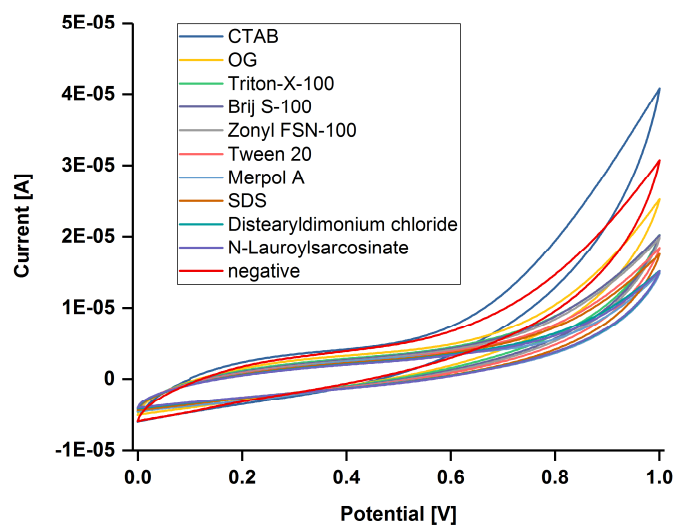


Figure S23. CV of luminol ECL with different surfactants on an ITO-WE in ECL cell.

6.9.2 *m*-Carboxy luminol

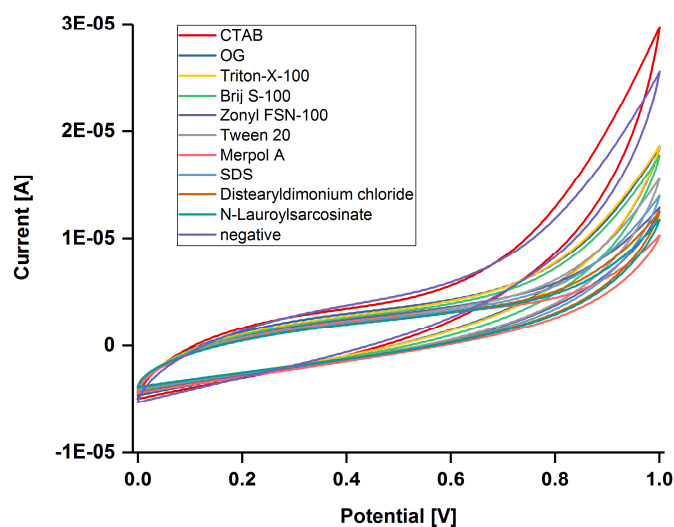


Figure S24. CV of *m*-carboxy luminol ECL with different surfactants on an ITO-WE in ECL cell.

6.10 Total charge transfer for different surfactants on various electrodes for both luminol species and background currents

The total charge amount was calculated via integration over the current vs. time curves from amperometric data of each ECL reaction. The values are given in %, normalized to transferred charge @ zero surfactant concentration (100%) for each surfactant. All values are mean values ($n=4$), \pm S.D. (in %).

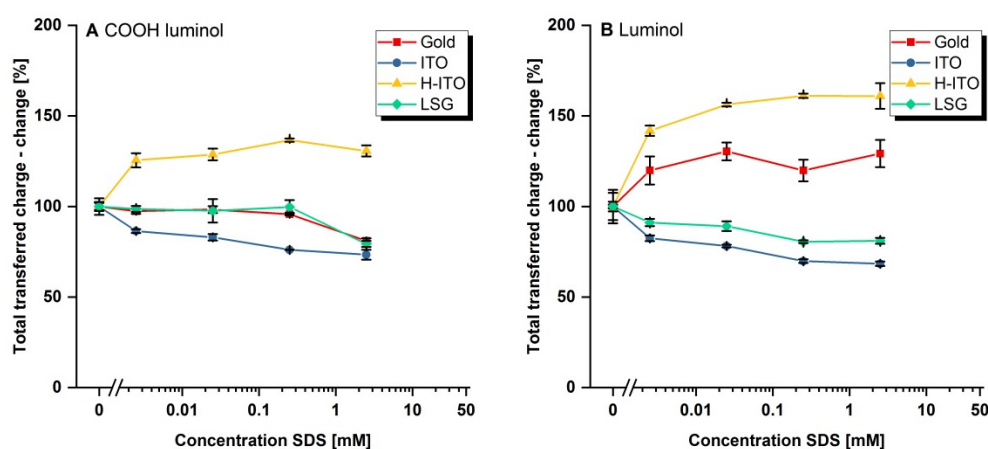


Figure S25. Overall charge transfer for SDS in response to surfactant concentration.

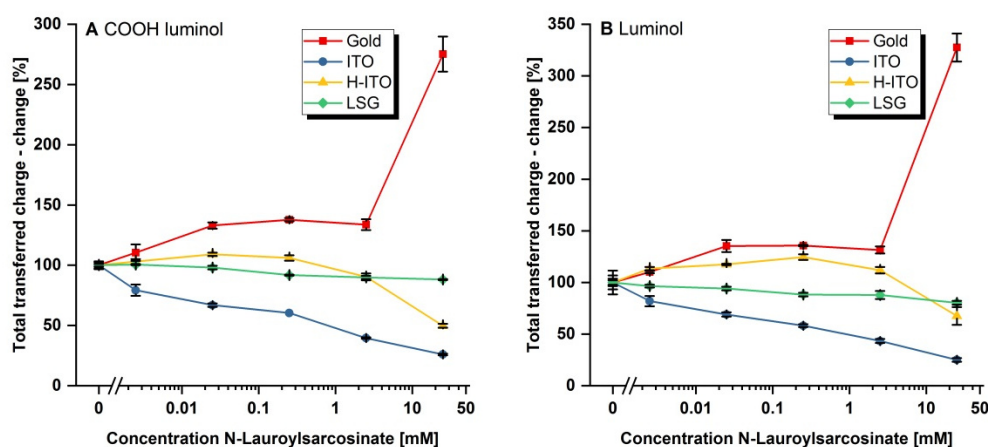


Figure S26. Overall charge transfer for N-Lauroylsarcosinate in response to surfactant concentration.

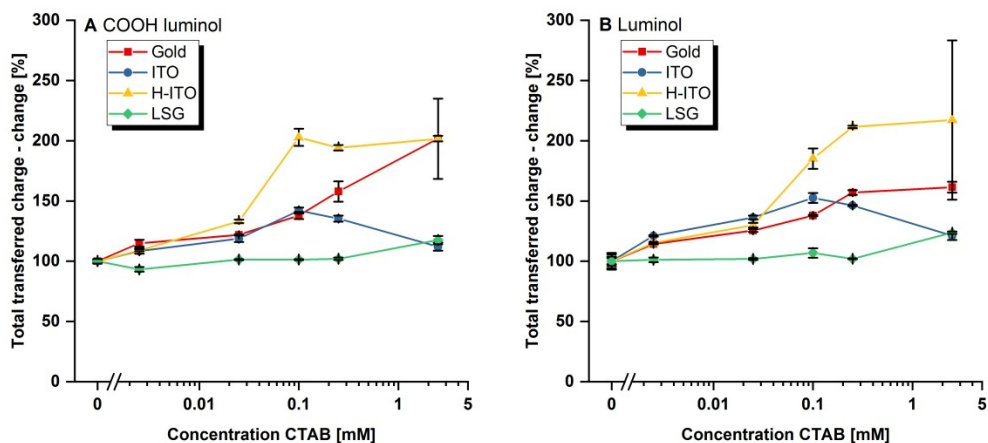


Figure S27. Overall charge transfer for CTAB in response to surfactant concentration.

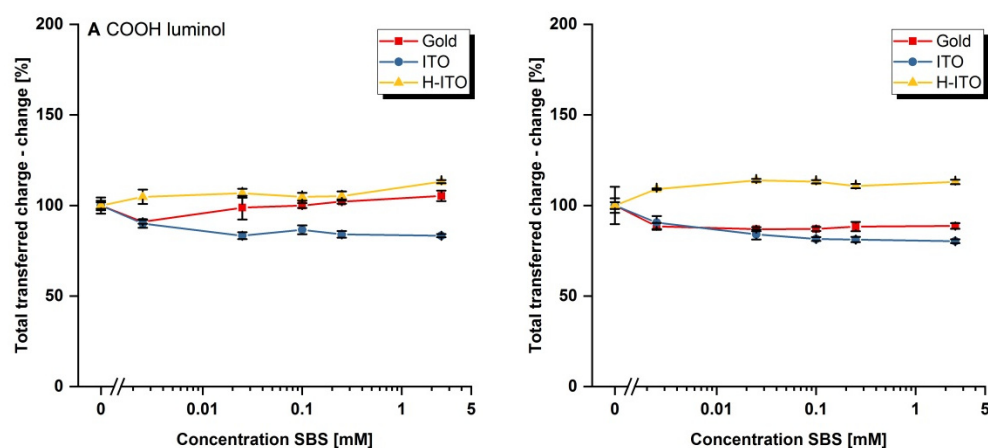


Figure S28. Overall charge transfer for SBS in response to surfactant concentration.

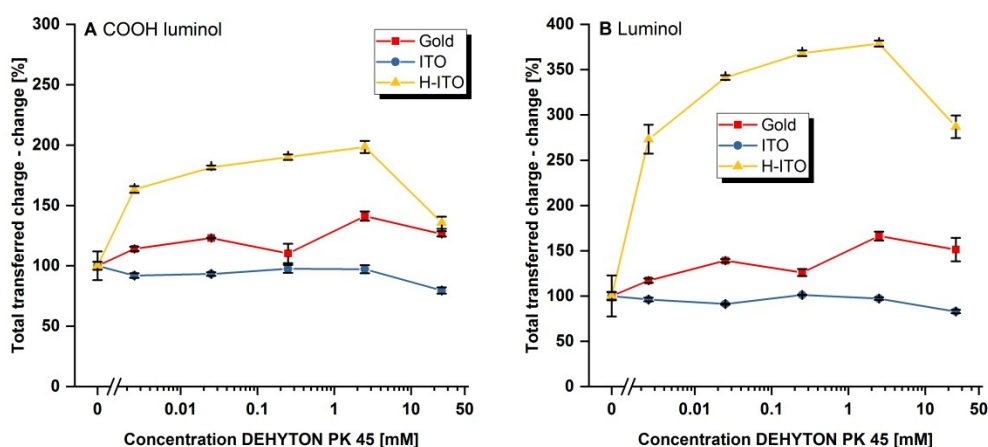


Figure S29. Overall charge transfer for Cocoamidopropyl betaine in response to surfactant concentration.

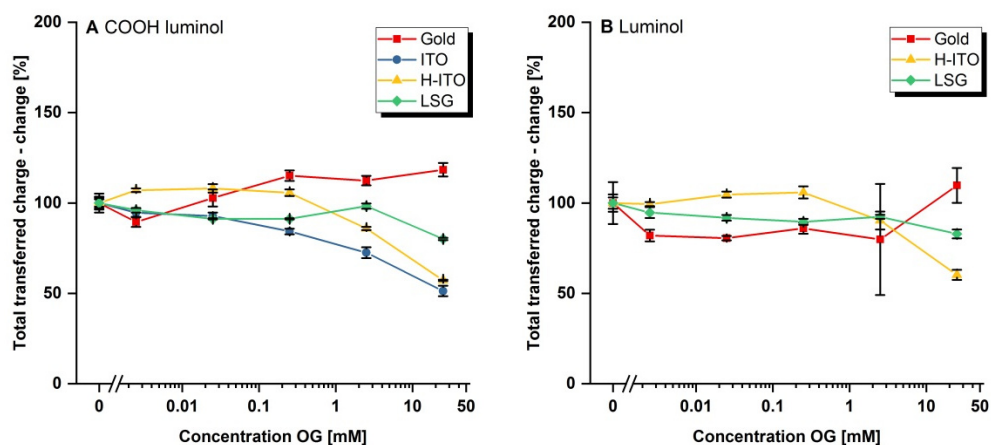


Figure S30. Overall charge transfer for Octyl glucoside in response to surfactant concentration.

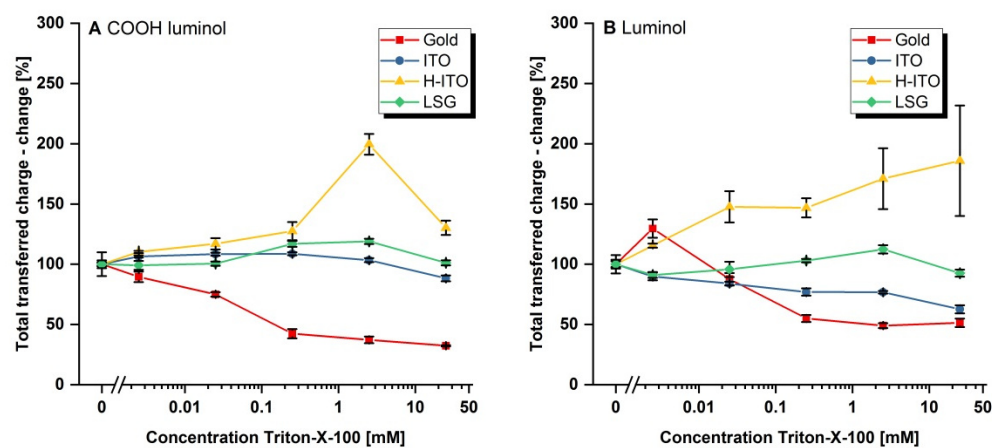


Figure S31. Overall charge transfer for Triton-X-100 in response to surfactant concentration.

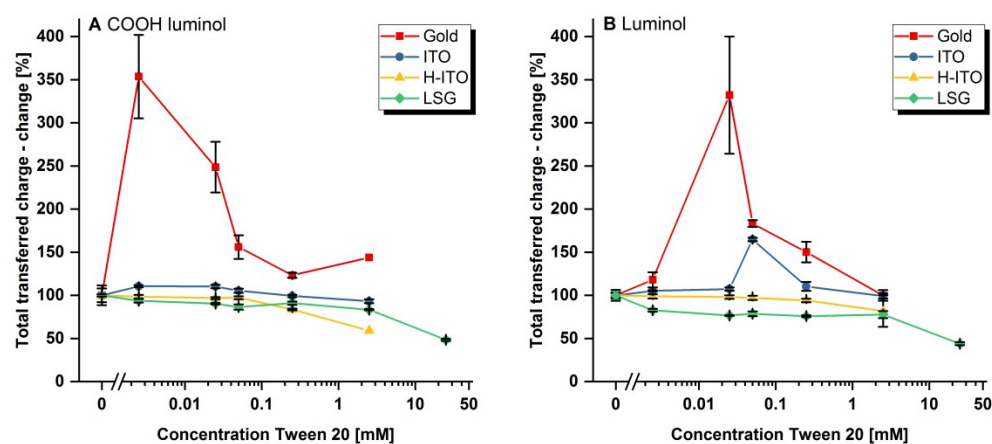


Figure S32. Overall charge transfer for Tween 20 in response to surfactant concentration.

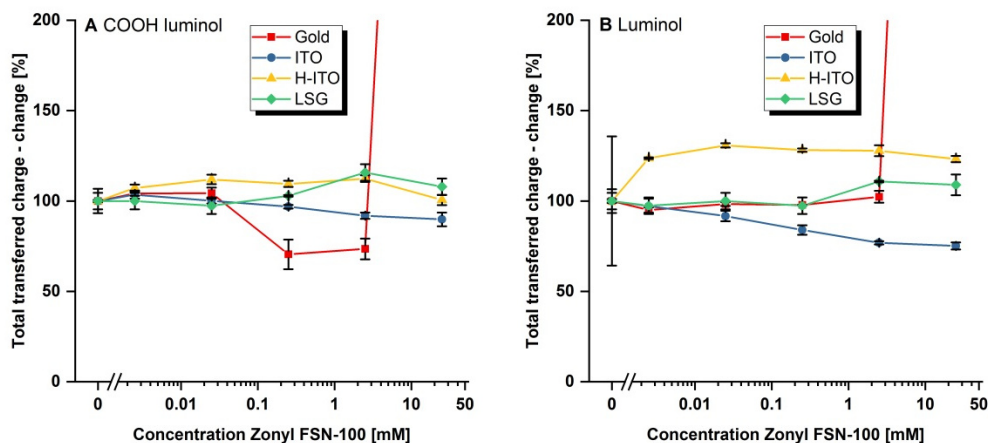


Figure S33. Overall charge transfer for Zonyl FSN 100 in response to surfactant concentration. Final values @ 2.5 mM surfactant on gold for both luminols approximately at 900% thus not shown.

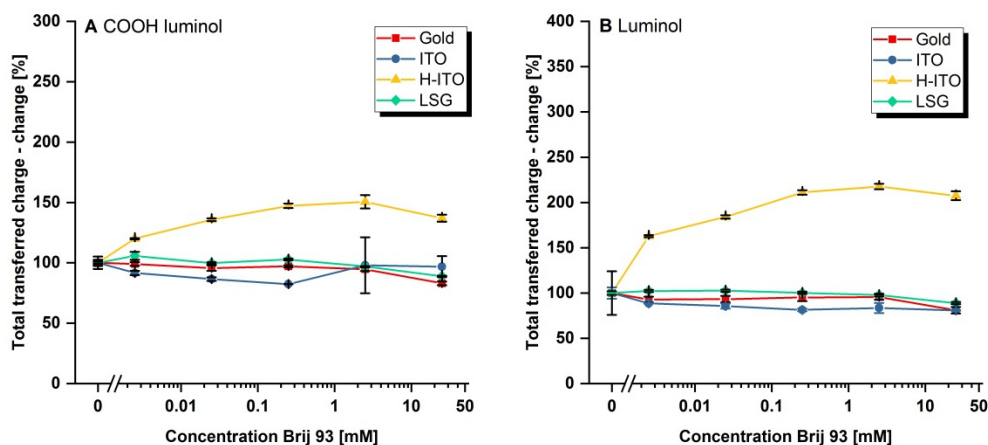


Figure S34. Overall charge transfer for Brij 93 in response to surfactant concentration.

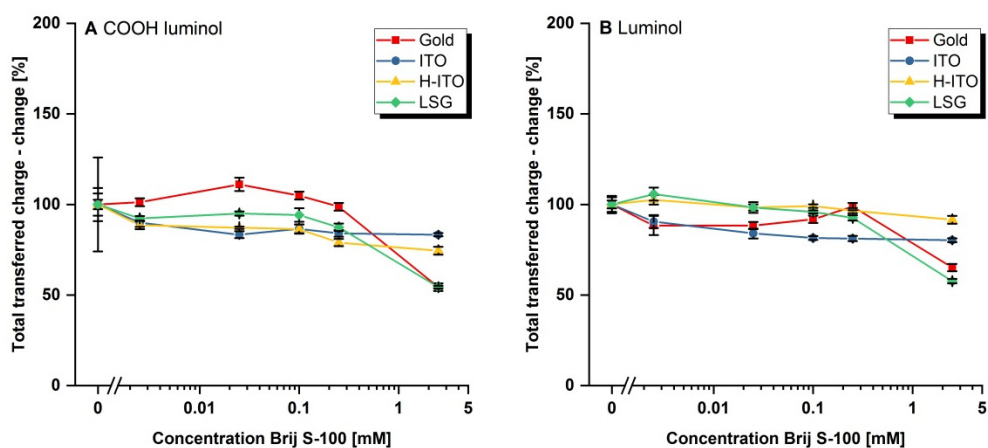
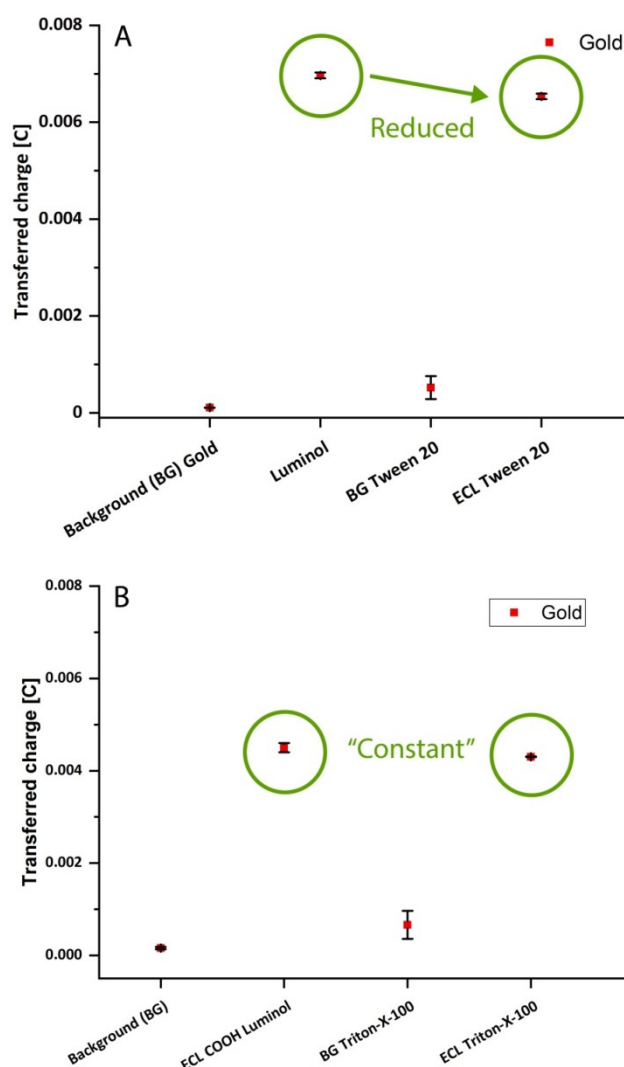


Figure S35. Overall charge transfer for Brij S 100 in response to surfactant concentration.

For background current measurements, we analyzed the overall transferred charges for a buffer solution, a buffer solution with surfactant in the highest quenching (2.5 mM or 25 mM) or optimal enhancement concentration, the luminol ECL mix (for both luminol species) and the luminol ECL mix with the same surfactant (in equal concentrations), respectively. We investigated exemplarily some quenching surfactants, i.e. Triton-X-100 on gold, N-Lauroylsarcosinate, OG and CTAB on ITO and some enhancing surfactants, i.e. Tween 20 on gold, CTAB on H-ITO and Triton-X-100 on ITO. For each case, we chose the respective luminol species which was quenching or enhancing respectively. Thus, we could cover all variants, to prove a persistent trend between all electrodes.



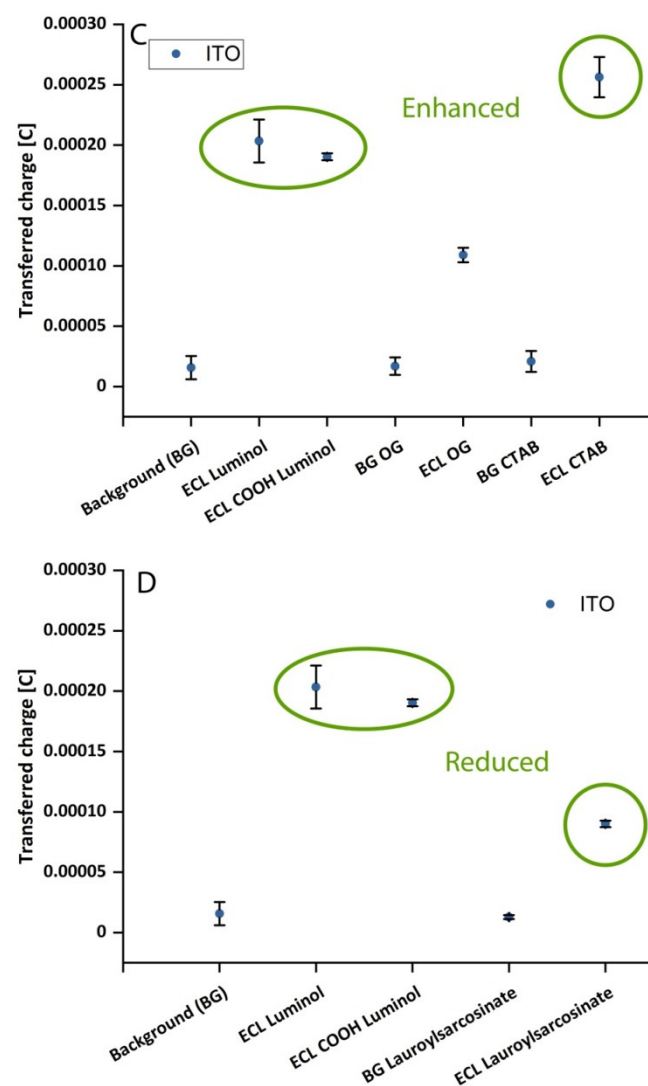
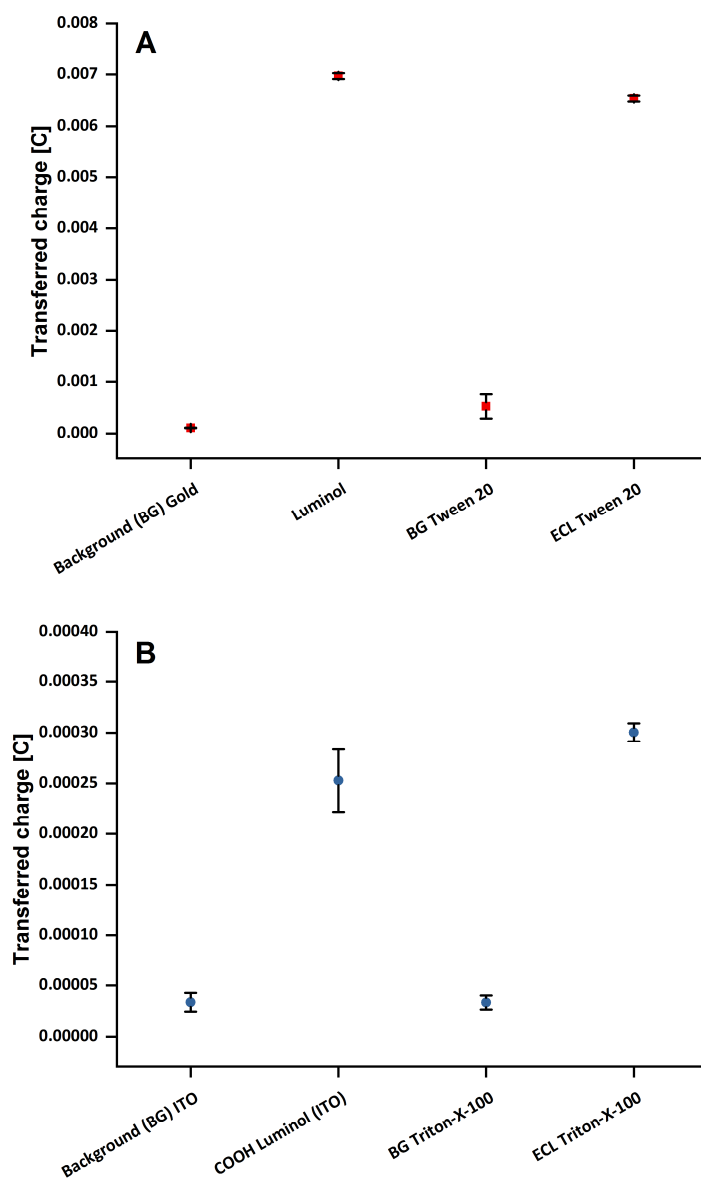


Figure S36 (A-D). Background current comparisons for ECL luminescence quenching surfactants on different electrodes. **A** depicts an ECL quencher with reduced charge transferred, **B** is an ECL quencher with almost no change in the total charge, **C** is an ECL quencher with an enhanced charge amount, transferred and **D** is an ECL quencher with less transferred charge.



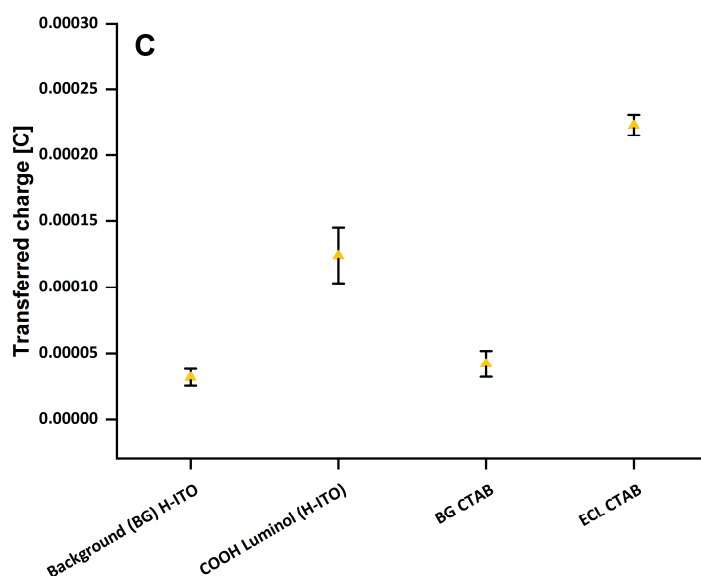


Figure S37 (A-C). Background current comparisons for ECL luminescence enhancing surfactants on three different electrodes. **A** depicts an ECL enhancer with slightly reduced charge transferred on gold, **B** is an ECL enhancer with a raised amount of the charge on pristine ITO and **C** is an ECL enhancer with enhanced charge amount transferred, on H-ITO.

6.11 Effect of buffer presence

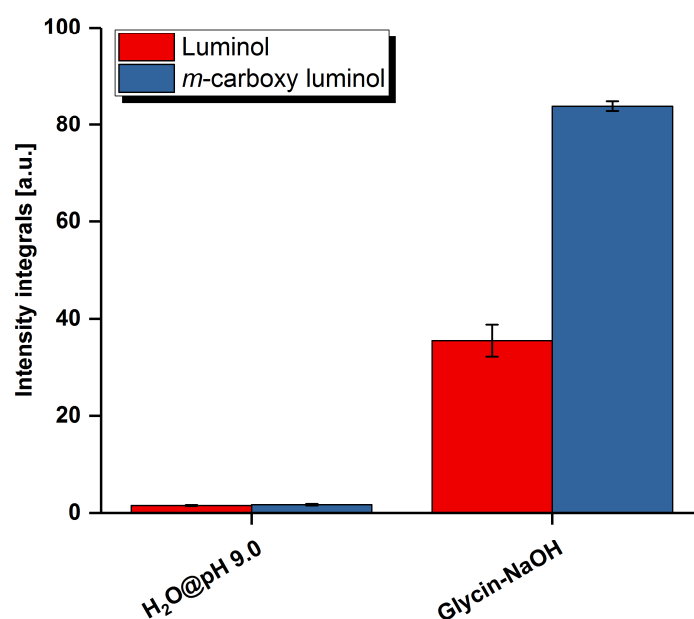


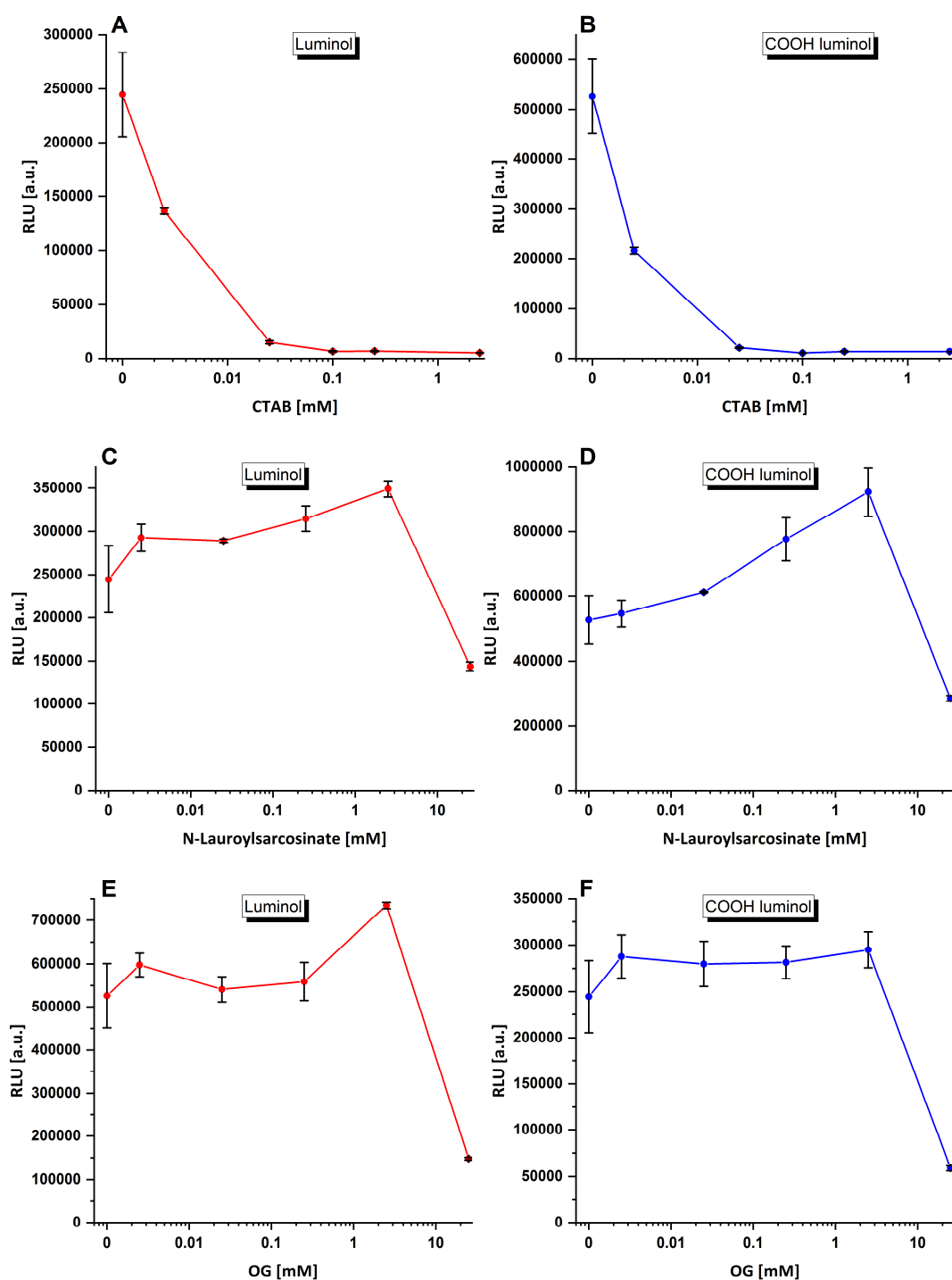
Figure S38. Effect of Glycine-NaOH buffer presence (0.1 M concentrated vs. Millipore water with equal pH value) on general ECL performance of luminol species.

Figure S38 illustrates the important effect that even the presence of the respective buffer has on ECL efficiency, versus a solution set to the same pH but without buffer capacities.

6.12 Electrode surface area calculation

The actual surface area of each working electrode was 0.49 cm^2 set by the ECL cell dimensions. The calculated surface areas via Randles-Sevcik were as following: $0.64 \pm 0.07 \text{ cm}^2$ for gold electrodes, $0.26 \pm 0.01 \text{ cm}^2$ for pristine ITO electrodes, $0.87 \pm 0.02 \text{ cm}^2$ for the LSG electrodes and $0.23 \pm 0.02 \text{ cm}^2$ for the hydrophilised ITOs whereas the last value has to be taken with care as the peak separation was $> 550 \text{ mV}$ and no dedicated oxidation peak was present for these curves and therefore the calculation is not truly reliable and just serves as rough approximation. This also suggests a change in electrode functionality through the hydrophilization process on the H-ITO electrodes. LSG electrodes display the overall largest surface area, being above the actual electrode area, also suggesting that the large enhancement effects with LSG are linked to the large surface and porosity of the electrode structures. However, the results show a small active electrode area for the ITO species compared to gold which is lower than the actual surface area. This counteracts the ECL results of the ITO species being more of enhancing nature, especially for the hydrophilised ones but also highlights the fact that gold is not generally in favor of pristine ITOs for each surfactant despite its intrinsic better performance. Again, this supports the assumption of a large contribution of the surface hydrophobicity or wetting properties and not only electron transfer rates or active surface area.

6.13 Chemiluminescence comparative measurements



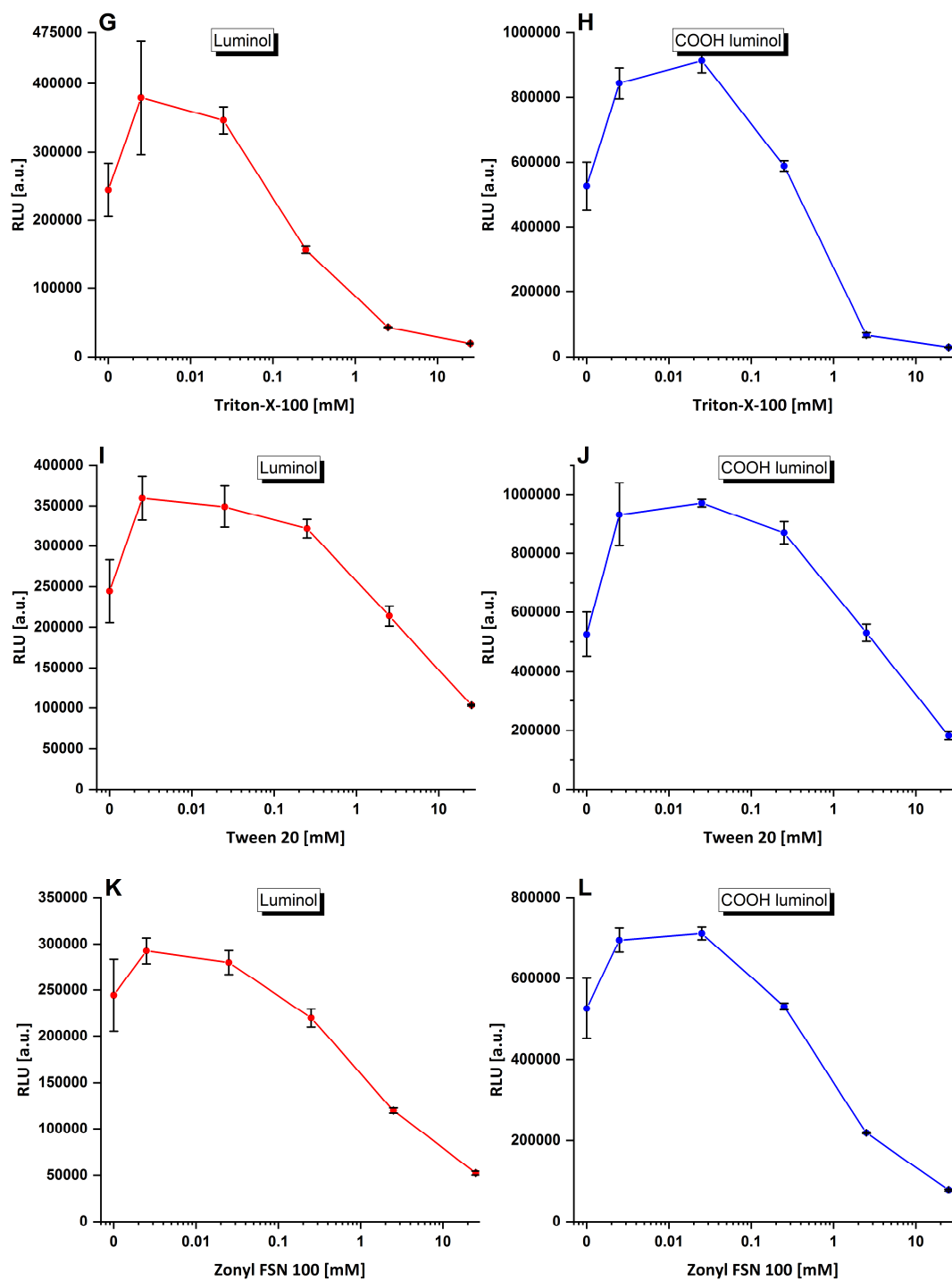


Figure S39 (A-L). Chemiluminescence response curves dependent on surfactant concentration.

6.14 Comparison of maximum absolute ECL signals on different electrodes

For direct comparison of the ECL signals on different electrodes used, their absolute signal intensities in ECL are compared in Figure S39. Here, the signals for both luminols without added surfactant were measured (800 V PMT) under equal conditions and all values referenced to the signal on gold electrodes set to 100%. As a note, for H-ITOs, the quality sometimes differed largely and while we could achieve a maximum signal of ~30-35% of that of gold, the low efficiency of ~4% for the worst ones, supports the idea of a partial electrode impairment through the hydrophilization procedure. Nevertheless, hydrophilized electrodes proved to be beneficial for enhancement with surfactants, thus the reported plasma procedure could be amended for a milder effect or a different hydrophilization method could be chosen. The absolute enhancement factor was approximately 3:1 for *m*-carboxy luminol : luminol on gold, ITO and H-ITO electrodes but a large factor of 11:1 (*m*-carboxy luminol : luminol) was found on LSG electrodes.

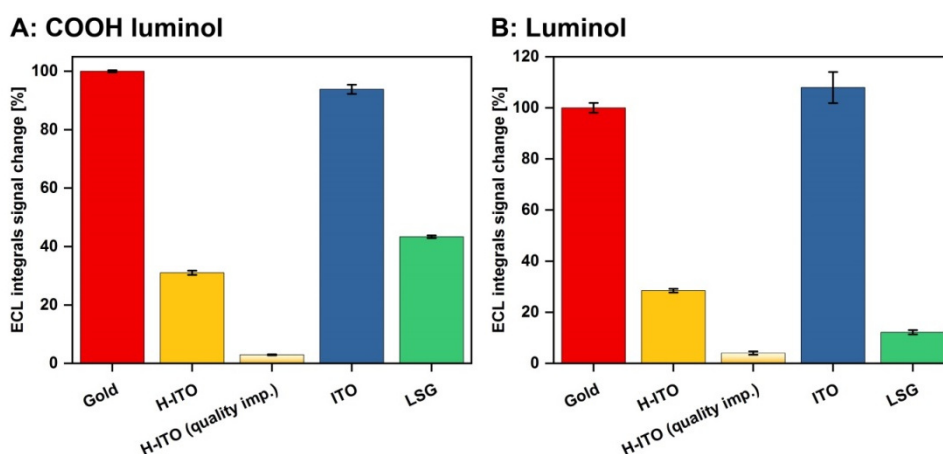
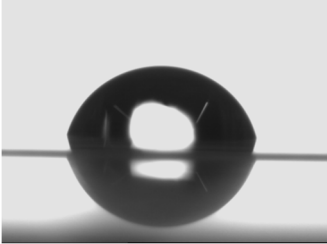
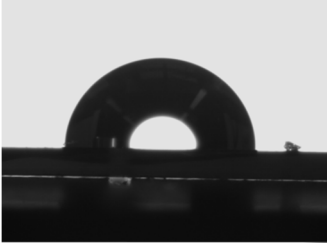



Figure S40 (A-B). Maximum absolute signals of luminol species ECL, given in %, without surfactant and normalized to gold (100%).

6.15 Contact angle measurements

For all 4 electrode materials, contact angles were determined and are shown in Table S3.

Table S3. Contact angle data on different electrodes.

Electrode	Contact angle / [°] ± SD [°]	Droplet image	Classification
ITO	77 ± 4		<i>hydrophobic</i>
Gold	91 ± 1		<i>hydrophobic</i>
H-ITO	39 ± 6		<i>hydrophilic</i>
LSG	“0”	Complete spreading	<i>porous, hydrophilic</i>

The contact angle of zero for LSG electrodes denotes the complete spreading on this electrode material, indicating its hydrophilicity. No possible image capturing of a contact angle was possible. For H-ITO, the contact angle measurement still involved a several minute long drying and thus exposure to ambient air, which presumably lead to an increased contact angle again. However, this was necessary to assure to keep the surface clean between plasma-treatment and the contact angle measurement and does more accurately reflect the real situation for ECL measurements.

In this case, some minutes of exposure to air, prior to the measurements are unavoidable due to the instrumentation setup routine. However, the contact angle is considerably lower compared to the pristine ITO, with much better wetting and can thus be defined as “hydrophilic”.

6.16 Surfactant effect on liposome lysis

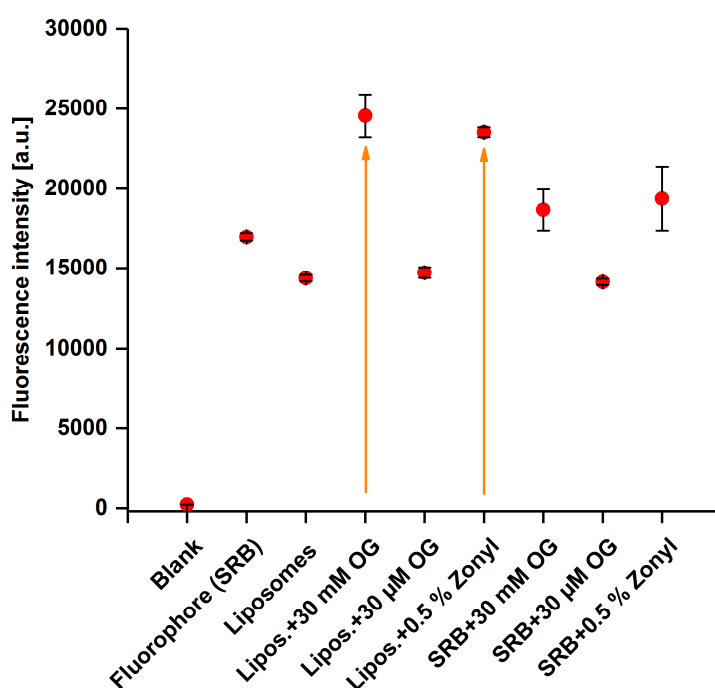


Figure S41. Fluorescence intensity of SRB and SRB encapsulated liposomes with the standard lysis surfactant vs. the optimum alternative

In Figure S41, the highest fluorescence signal for OG and Zonyl FSN-100 shows that these are the two most efficient lysis surfactants and non-quenchers. A small concentration of 30 μ M OG as comparison shows the need for a high surfactant concentration for efficient liposome lysis.

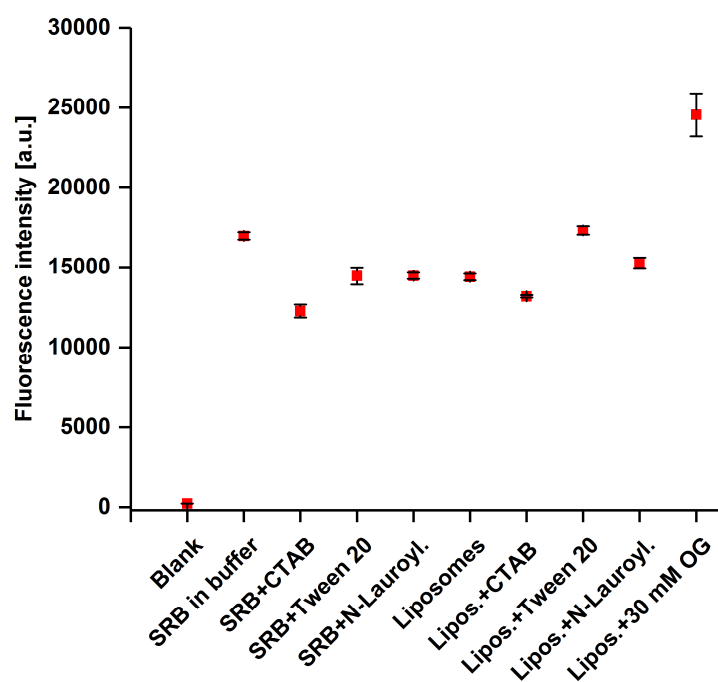


Figure S42. Fluorescence intensity of SRB and SRB encapsulated liposomes with quenching and non-lysis efficient surfactants

In Figure S42, other fluorescence signals are given for the remaining surfactants that have been screened. Here, as reference, the OG data point is given again.

6.17 References

- (S1) Mayer, M.; Takegami, S.; Neumeier, M.; Rink, S.; Jacobi von Wangelin, A.; Schulte, S.; Vollmer, M.; Griesbeck, A. G.; Duerkop, A.; Baeumner, A. J. Electrochemiluminescence Bioassays with a Water-Soluble Luminol Derivative Can Outperform Fluorescence Assays. *Angew. Chem. Int. Ed.* **2018**, *57*, 408-411. doi: 10.1002/anie.201708630
- (S2) Subramanian, D.; Anisimov, M. A. Phase behavior and mesoscale solubilization in aqueous solutions of hydrotropes. *Fluid Phase Equilib.* **2014**, *362*, 170-176. doi: 10.1016/j.fluid.2013.09.064
- (S3) Tang, Y.; Yan, J.; Zhu, F.; Sun, C.; Mao, B. Comparative Electrochemical Scanning Tunneling Microscopy Study of Nonionic Fluorosurfactant Zonyl FSN Self-Assembled Monolayers on Au(111) and Au(100): A Potential-Induced Structural Transition. *Langmuir* **2011**, *27*, 943-947. doi: 10.1021/la103812v
- (S4) Škvarla, J.; Uchman, M.; Procházka, K.; Tošner, Z.; Garamus, V. M.; Pispas, S.; Štěpánek, M. Micellization of Zonyl FSN-100 fluorosurfactant in aqueous solutions. *Colloids Surf. A* **2014**, *443*, 209-215. doi: 10.1016/j.colsurfa.2013.11.021
- (S5) Landoulsi, J.; Genet, M. J.; Fleith, S.; Touré, Y.; Liascukienė, I.; Méthivier, C.; Rouxhet, P. G. Organic adlayer on inorganic materials: XPS analysis selectivity to cope with adventitious contamination. *Appl. Surf. Sci.* **2016**, *383*, 71-83. doi: 10.1016/j.apsusc.2016.04.147
- (S6) Brumbach, M.; Veneman, P. A.; Marrikar, F. S.; Schulmeyer, T.; Simmonds, A.; Xia, W.; Lee, P.; Armstrong, N. R. Surface Composition and Electrical and Electrochemical Properties of Freshly Deposited and Acid-Etched Indium Tin Oxide Electrodes. *Langmuir* **2007**, *23*, 11089-11099. doi: 10.1021/la701754u
- (S7) Bauduin, P.; Zemb, T. Perpendicular and lateral equations of state in layered systems of amphiphiles. *Curr. Opin. Colloid Interface Sci.* **2014**, *19*, 9-16. doi: https://doi.org/10.1016/j.cocis.2014.02.002
- (S8) Grant, L. M.; Ederth, T.; Tiberg, F. Influence of Surface Hydrophobicity on the Layer Properties of Adsorbed Nonionic Surfactants. *Langmuir* **2000**, *16*, 2285-2291. doi: 10.1021/la990700l
- (S9) Nagarajan, R. Molecular Packing Parameter and Surfactant Self-Assembly: The Neglected Role of the Surfactant Tail. *Langmuir* **2002**, *18*, 31-38. doi: 10.1021/la010831y
- (S10) Bohmer, M. R.; Koopal, L. K.; Janssen, R.; Lee, E. M.; Thomas, R. K.; Rennie, A. R. Adsorption of nonionic surfactants on hydrophilic surfaces. An experimental and theoretical study on association in the adsorbed layer. *Langmuir* **1992**, *8*, 2228-2239. doi: 10.1021/la00045a027
- (S11) Levitz, P.; Van Damme, H. Fluorescence decay study of the adsorption of nonionic surfactants at the solid-liquid interface. 2. Influence of polar chain length. *J. Phys. Chem.* **1986**, *90*, 1302-1310. doi: 10.1021/j100398a020

- (S12) Xu, G.; Pang, H. L.; Xu, B.; Dong, S.; Wong, K. Y. Enhancing the electrochemiluminescence of tris(2,2'-bipyridyl)ruthenium(II) by ionic surfactants. *Analyst* **2005**, *130*, 541-544. doi: 10.1039/b419269a
- (S13) Ward, R. N.; Duffy, D. C.; Davies, P. B.; Bain, C. D. Sum-Frequency Spectroscopy of Surfactants Adsorbed at a Flat Hydrophobic Surface. *J. Phys. Chem.* **1994**, *98*, 8536-8542. doi: 10.1021/j100085a037
- (S14) Rosen, M. J.; Kunjappu, J. T., *Surfactants and Interfacial Phenomena*. (John Wiley & Sons, Inc., Hoboken, New Jersey, ed. 4th, 2012). doi: 10.1002/9781118228920
- (S15) Li, P.; Ishiguro, M. Adsorption of anionic surfactant (sodium dodecyl sulfate) on silica. *Soil Sci. Plant Nutr. (Abingdon, U. K.)* **2016**, *62*, 223-229. doi: 10.1080/00380768.2016.1191969
- (S16) Jiménez-Ángeles, F.; Khoshnood, A.; Firoozabadi, A. Molecular Dynamics Simulation of the Adsorption and Aggregation of Ionic Surfactants at Liquid–Solid Interfaces. *J. Phys. Chem. C* **2017**, *121*, 25908-25920. doi: 10.1021/acs.jpcc.7b09466
- (S17) Soria-Sánchez, M.; Maroto-Valiente, A.; Guerrero-Ruiz, A.; Nevskaya, D. M. Adsorption of non-ionic surfactants on hydrophobic and hydrophilic carbon surfaces. *J. Colloid Interface Sci.* **2010**, *343*, 194-199. doi: 10.1016/j.jcis.2009.10.082

Chapter 6: Microfabrication strategies for ECL detection

Abstract

Electrochemiluminescence is an intrinsically powerful detection technique, including features like versatility for all different assay formats and being able to be easily miniaturized. Microfabrication on the other hand, offers the advantages of automated, reproducible fluidics handling together with reduced detection volumes. This makes a fusion of both, ECL as detection technique and microfluidics for fluidics handling and as assay platform an attractive joint-venture for biosensing. Achieving that, not only enables a further means of signal amplification but also makes ECL ready for integration into all different systems for bioassays, i.e. for point-of-care (POC) diagnostics, small and automated benchtop- or portable, field application environments. Thus, a method for miniaturization that ideally adheres to principles of simple, cost effective fabrication with amenability for a scale-up is desirable to serve all application fields. In this chapter, design strategies and methods for a microfabricated system capable for multiple ECL detection are discussed and suggested. This includes considerations for the special requirements of both, the luminol-H₂O₂- and [Ru(bpy)₃]²⁺-tertiary amine-coreactant ECL systems and limitations of a dual use. These are demonstrated, using macro-electrode ECL characterizations on different electrode materials. Finally, laser scribed graphene (LSG) electrodes are suggested as interesting alternative for a miniaturized multi-ECL detection.

This chapter is not published.

Author contributions:

Michael Mayer did most of the experimental work and wrote this chapter. Christine Unger, Marion Vogl and Florian Gerstl contributed with ECL measurements on ITO and LSG electrodes. Andrei Georgescu contributed to this study initially with methodic and theoretical expertise and designed the layouts and CAD models for the PMMA-microfluidic structures. Jiří Houšť helped with bonding tests of PMMA with PET. Christian Griesche contributed with discussions to microfluidic design strategic ideas. The mechanical workshop of the faculty of chemistry at the University of Regensburg fabricated the metal templates for hot embossing and the bubble trap. Antje J. Baeumner was project administrator. Michael Mayer, Andrei Georgescu (initially), Antje J. Baeumner, Axel Duerkop and Thomas Hirsch discussed strategic decisions.

1. Introduction

Microfluidic approaches have experienced a long history of development¹ and exist today at a very sophisticated stage of development.²⁻⁵ The advantages⁶ of microfluidics are apparent and lie in reduced sample volumina, higher reproducibility, possible parallelization, reduced assay times, possible preconcentration or less dilution, easy automation, enhanced mobility, slow possible movements via flowrate control, shorter diffusion lengths and signal enhancement. The signal enhancement property is also given through the other named characteristics, microfluidics possesses. Exactly these features, a possible signal enhancement together with the qualification for portable and integrated solutions make microfluidics a further attractive tool that can be exploited for ECL detection. As in this case the material choice has to be matched with optical readout and further, the electrochemical side has to be miniaturized and interfaced, some challenges have to be overcome. Small-format image capturing and small-sized potentiostats are commercially available as also highlighted in the general introduction of this work. Thus, the critical points are the materials choice of electrodes, of substrates and their partly required transparency features for the ECL readout. Besides that, interfacing of electrodes at the contacting side and also with the rest of the microfluidic system can be challenging especially in the fabrication step of bonding. Exemplary, thinner electrodes like the ITO@ PET material used here, can be thermally bonded to another soft or hard polymer while thicker layers of electrodes like screen-printed carbon electrodes or laser scribed graphene (LSG) electrodes can cause problems with seamless integration.^{3,7} In this chapter, design considerations, transitioning from macroscopic ECL measurements on gold electrodes over ITO electrodes on PET interfaced to fluidic channels in PMMA and finally a possible solution employing printed LSG electrodes on polyimide are discussed. The incorporated capabilities and challenges with $[\text{Ru}(\text{bpy})_3]^{2+}$ -ECL requirements are outlined and depicted with the help of macroscopic ECL measurements. In this process flow, a new direct thermal bonding method for PET with PMMA is introduced. The inside that system contained ITO electrodes, are electrochemically tested (on-chip). Finally, LSG electrodes are suggested as an alternative electrode material, which is better suited for

a versatile ECL detection capability. $[\text{Ru}(\text{bpy})_3]^{2+}$ -ECL is finally tested for its characteristics and symbiosis with LSG electrodes.

1.1 Strategic route for ECL miniaturization in this project

The strategic workflow which directed microfabrication strategies in this study is outlined in Scheme 1. It depicts the route, outgoing from deposited gold-on-glass-electrodes for macroscopic ECL measurements without microfluidics towards LSG electrodes on polyimide as new basis for an electrochemical platform towards miniaturization of ECL detection. The design considerations here are depicted in advance of the results for a better illustration of the experimental strategies and decisions.



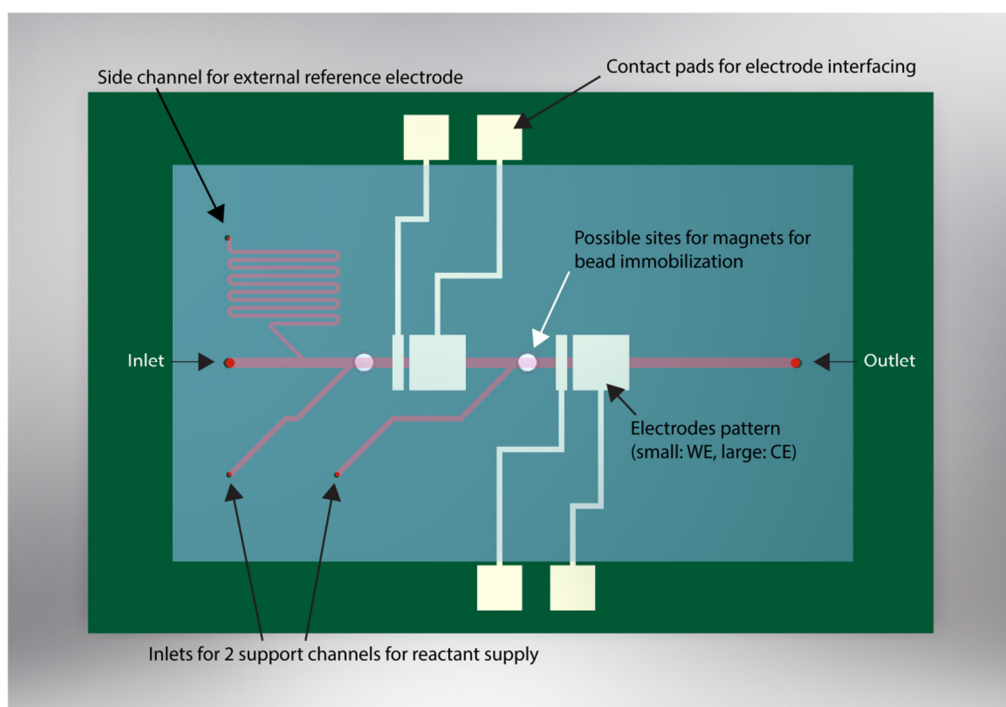
Scheme 1. Design considerations and materials choices balanced with qualification for ECL application and fabrication implications.

The colored circles illustrate the counterbalance between ECL performance, ECL usability and production complexity/cost balance as outlined in the following. The “gold standard” indicates a superior performance of gold electrodes for ECL signal efficiency with $[\text{Ru}(\text{bpy})_3]^{2+}$ -ECL. For luminol ECL this is no limiting factor as highlighted in **chapter 5** shown in the absolute electrode performance comparison where ITO and gold are in a same range. The usability for ECL denotes a decreasing and again increasing qualification of electrode and microfluidic design choices for multiple ECL detection

(outlined in the results in section 3). This is directed by the discovered limitation in the practical use of ITO electrodes with $[\text{Ru}(\text{bpy})_3]^{2+}$ -ECL, originating in a reduced stability for the required potential range. This includes modification of ITO electrodes. Finally with LSGs, the usability for multiple ECL application is rising again. The last field of fabrication complexity indicates a balance of cost and efforts of the chosen microfabrication method. Here, gold represents the poorest choice as deposition efforts (time and conditions!) and cost is very high, and a scale-up is limited. The photolithographic patterning of ITO electrodes represents already a better alternative, in terms of cost and complication while it additionally can be done with standard benchtop chemistry. However, that fabrication method still requires unique, personal preparation which cannot be automated very easily. The final route via LSG electrodes, which can be fabricated in a “printing”-like process, and thus be easily patterned in all desired layouts is the fastest and most cost-effective strategy. However, this approach has not been investigated in a microfluidic environment in this project, regarding bonding and interfacing and ECL. Thus, final conclusions towards its performance with multiple ECL systems are yet restricted.

1.2 Fluidic design strategies

Initially, a microfluidic chip layout was designed, with the constraint of a fluidic chip capable for electrochemical detection with two working- and counter electrode pairs integrated on the chip. The electrochemical part consisted of patterned ITO electrodes on polyethylene terephthalate (PET) foil and the fluidics part of channels in polymethyl methacrylate (PMMA) material. The layout (depicted in Scheme 2) contained following features: a total length from in- to outlet of 5 cm, a channel width of 500 μm , a channel depth of 75 μm , and a working electrode (WE) width of 1 mm and a counter electrode (CE) width of 2 mm. This includes a total volume of 6.5 μL in the whole chip and a volume at the working electrode area of 38 nL.



Scheme 2. Initial design of microfluidic system capable for multiple ECL detection. General layout and initial CAD design, created by Andrei Georgescu. Image reproduced on these data by the author. Further development of channel designs by the author.

The meandering side channel for the connection of a reference electrode (RE) was initially designated to keep the reagent solution inside the microfluidic system and avoid mixing at the solutions interface to the liquid junction to the outer reference electrode. Ultimately, this design was dismissed as introduction and removal of air bubbles into- and from the system caused problems with the meandering structure. For this reason, a self-built bubble trap was investigated. The design concept was based on a commercially available bubble trap from DARWIN microfluidics (Paris, France).⁸ However, the large inner volume of 44 μL contained in this model, was expected to be too large if sample injection was desired via the bubble trap. A similar type with a low inner volume of approximately 2 μL was designed with standard HPLC connector ports for 1/16th-outer diameter sized tubing. The bubble trap was fabricated in-house. As filter membranes, a 0.2 μm pore size and 1.5 mm thick PTFE membrane (DARWIN microfluidics) and a 0.05 μm pore size and 0.2 mm thick PTFE membrane from BOLA (Bohlender GmbH, Germany) were used.

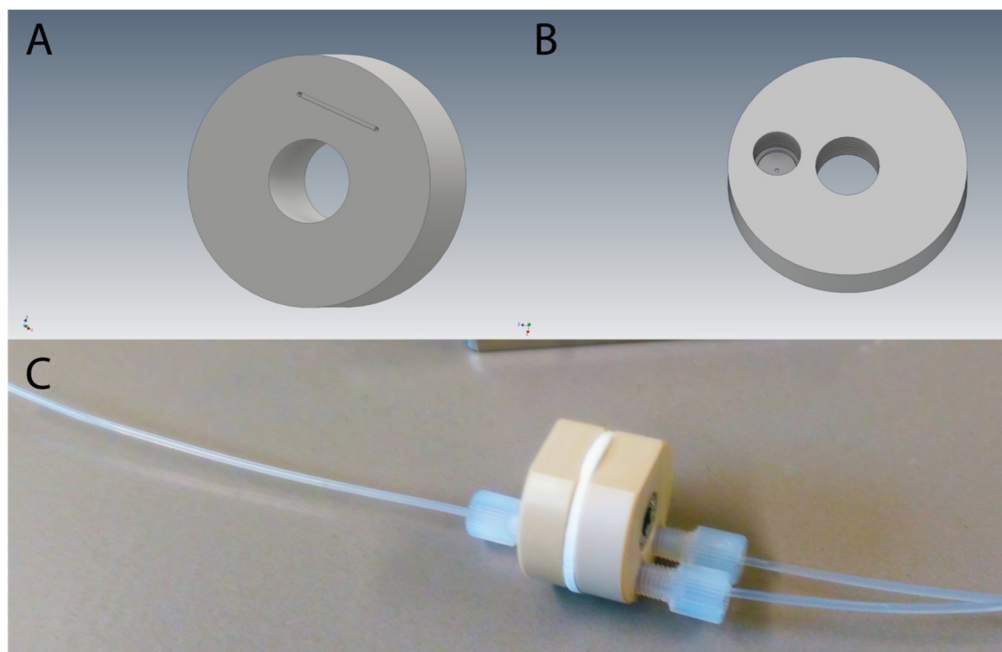


Figure 1 (A-C). Design of bubble trap, made from polyether ether ketone. **A** shows the microchannel in contact to the PTFE membrane with through holes to attachment ports on the other side. **B** shows the vacuum suction opening with the port connection and **C** the assembled trap.

Ultimately, a too high pressure in the system was necessary to move the fluid through the trap, presumably caused by the fluid interfacial tension and the small channel features. The required force was too large to be interfaced with the other parts of the microfluidic system while sustaining the pressures. Thus, a changed microfluidic channel layout was suggested. A mixing of the fluids was likely to be avoided via an adapted protocol for operating the fluidic system while a reference electrode port is moved closer to the outlet. This is shown in Figure 2.

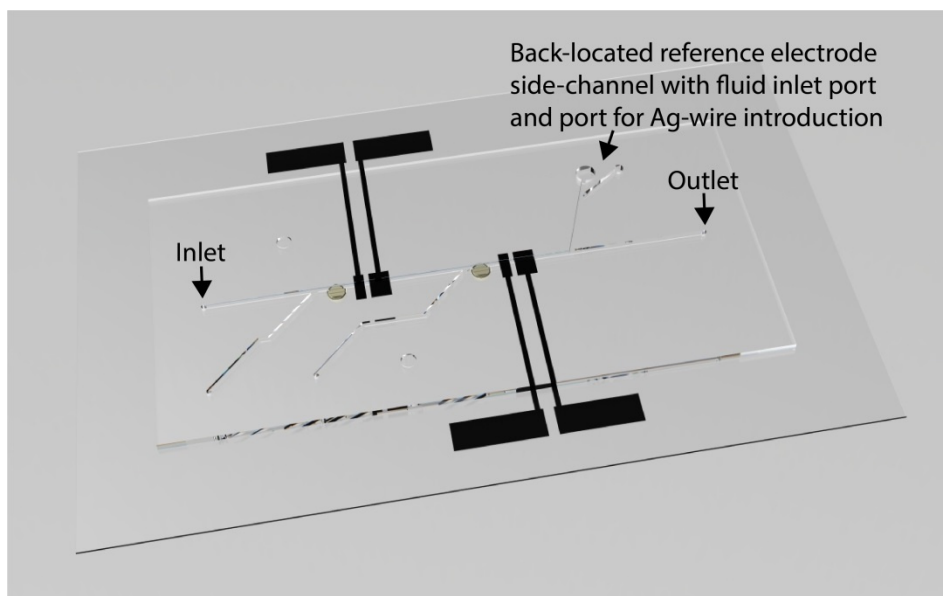


Figure 2. Possible microfluidic layout illustrating a reference electrode side channel shifted to the outlet side. Illustration is exemplary with a random electrode/material combination.

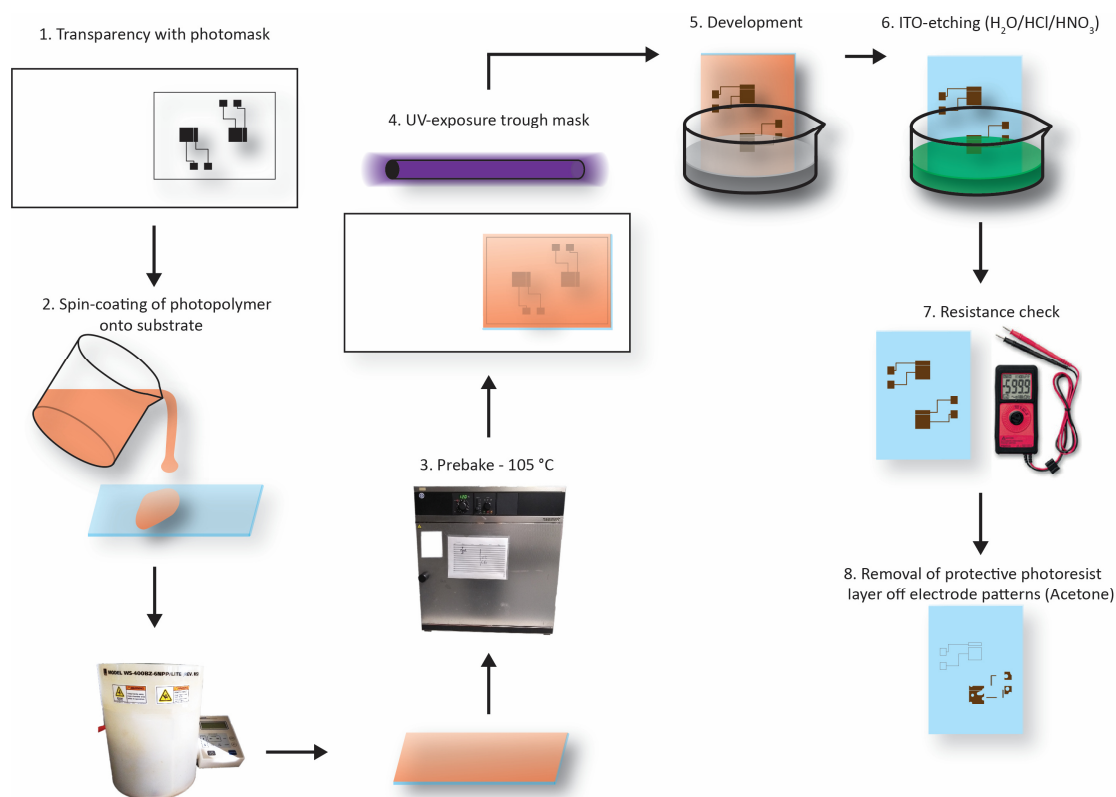
The further back-located side channel compared to the initial layout is designed for a possible introduction of an Ag-wire as reference electrode directly into the system. As such a long liquid junction between on chip WE/CE pairs and an external RE can be avoided. Alternatively a RE-port for a wire-RE introduction can be positioned in-line with the main channel downstream to the two WE/CE-electrode pairs. These design ideas however only depict further concepts which have to be tested towards practicability. Ultimately the introduction of a Ag-wire or Ag-layer reference electrode inside the chip is likely to improve the electrochemical performance compared to an outside-located reference electrode.

2. Materials & Methods

2.1 Materials

N-Butyldiethanolamine (NBEA), Ethanol (99%; v/v), Potassium hexacyanoferrate(II) trihydrate, Potassium hexacyanoferrate(III), Tetraethyl orthosilicate, Tris(2,2'-bipyridyl)ruthenium(II) chloride, Tripropylamine (TPA) and Zonyl FSN-100 fluorosurfactant solution were obtained from Sigma Aldrich. Ammonia (concentrated solution), Cetyltrimethylammonium bromide, Hydrochloric acid (37%), nitric acid (68%) and Potassium chloride were purchased from VWR. DuPont® D520 liquid nafion membrane solution was obtained from DuPont. S1813 photoresist and MF 321 developer were obtained from microresist technology GmbH (Berlin, Germany). LSG electrodes were prepared with the same parameters as described in chapter 5 of this work.

2.2 Photolithography of ITO foils.



Scheme 2. Benchtop photolithography and wet-etch procedure for the patterning of microfluidic structures into ITO-film.

As depicted in figure Scheme 2, a photolithography procedure was used to pattern microfluidic structures into the ITO film. As substrate, a ITO coated PET foil (thickness: 5 mil, resistivity $<60 \, \Omega/\text{sq}$, Sigma Aldrich, Germany) was used and coated with pre warmed S1813 positive photoresist (Dow Chemicals) on a WS-400BZ-6NPP/LITE (REV. MS) spin coater (Laurell Technologies Corporation, U.S.A.) with following parameters: 500 rpm for 5 seconds and following, 2000 rpm for 1 minute. Afterwards, a soft-baking step was performed in an oven at 105°C for 30 minutes. Subsequently, UV-exposure was done for 2 minutes on an Isel (isel Germany AG) model 2 UV illuminator after manual alignment with the photomask. The photomask was previously printed with an EPSON Stylus Photo 1500W using the AccuRIP droplet size control software (droplet size 5, fast mode) with the stock black ink on a standard inkjet transparency foil (folex, BG-32.5 RS plus from Folex Coating GmbH, Germany). The photomask was prepared a day prior to photolithography to allow for sufficient drying of the ink. Afterwards, the

development step was done via immersion in NaOH solution (7g/L) under mild agitation. After a rinsing step with Millipore water, the etching of the ITO film which was not protected by the photoresist was done. This included an etching step for 3 minutes in an acid mixture of H₂O : HCl : HNO₃ of 55 : 55 : 7 under mild agitation. Subsequently, immediate washing with Millipore water and drying under an N₂ stream followed. Afterwards, the remaining photoresist was removed via rinsing with Acetone for few seconds and a final washing step with Millipore water and drying followed. Finally, a careful inspection of the residual resistance on the remaining ITO features and surrounding PET foil was performed to assure successful etching. The prepared electrode substrates were stored protected from dust.

2.3 Silica-mesochannels (SMC) modification of ITO electrodes

Silica mesochannel modification of ITO electrodes has been done using a published procedure.^{9,10} As a difference to the reference, here ITO on PET foil was used instead of ITO on glass. Apparently, the fabrication method did macroscopically not seem to cause issues with the supporting polymer. To cope with the changed situation, the reported cleaning step in 1 M NaOH in Ethanol overnight was omitted here, to protect the PET substrate. However, as obtained ITO films on PET were used with the protective foil being removed prior to immersion in the growth solution, thus a contamination was avoided as good as possible. In detail, The amount of solvent mixture (Millipore water : Ethanol in a ratio of 70 : 30) was doubled to 100 mL. The other constituents were added in the given amounts, incorporating the larger volume. The growth step was done for 24h and the aging step over night. All other steps were done according to the protocol. A faint bluish-color indicated changes on the surface upon visual inspection. ECL characterization was done on the final, modified electrodes.

2.4 ECL and electrochemical measurements.

ECL measurements were performed as reported in **chapter 3** and **chapter 5** with the same Autolab potentiostat (Autolab BV; Netherlands) and AB2 spectrofluorimeter (Aminco Bowman) setup. The used ECL cell was described in **chapter 4**. The used volume of the ECL mixture was 120 µL in the ECL cell. All settings on the devices were as described while the distinct settings for [Ru(bpy)₃]²⁺-ECL were as following: a PMT voltage of 620V for ITO electrodes (if not otherwise stated) with the emission wavelength set to 620 nm and the applied electrical potential held at +1.5 V (vs. Ag-

wire). For measurements on LSG electrodes, the applied electrical potential was set to +1.1 V (vs. Ag-wire) and the emission wavelength was set to 595 nm after characterization, shown in the results section in this chapter. The $[\text{Ru}(\text{bpy})_3]^{2+}$ -ECL mix consisted of 100 μM $[\text{Ru}(\text{bpy})_3]^{2+}$, 10 or 50 mM N-Butyldiethanolamine, 2 % (v/v) HCl to compensate a buffer pH shift of the amine (10 mM), 0.1 M KCl and 0.05 wt. % Zonyl FSN. Cyclic voltammetry measurements were performed with the same Autolab potentiostat which was used for ECL. Luminol ECL capturing was performed at a wavelength of 430 nm with a slit width of 16 nm.

2.5 Hot embossing of PMMA

Hot embossing was done on a Specac Atlas 15T manual hydraulic press (Specac Limited, U.K.) hot press. In the process, a template (brass) with the positive structure of the microfluidic layout, which was fabricated on a Kern Evo micromill (Kern Mikrotechnik GmbH, Germany) from a CAD design made in Solidworks or Autodesk Inventor 2016 was placed on a stainless steel support plate. A 6 cm x 3 cm PMMA template with a thickness of 1.5 mm (Plexiglas® XT, clear from Kunststoff Acryl Design GmbH, Germany) was placed centered on top of the metal template. Following, a stainless steel cover plate was carefully centered on top and the assembly was placed centered on the bottom plate of the hot press. After lowering the upper plate and fixing the assembly against rotation with an initial low force of the upper plate, the temperature-time profile depicted in Figure 3 was applied.

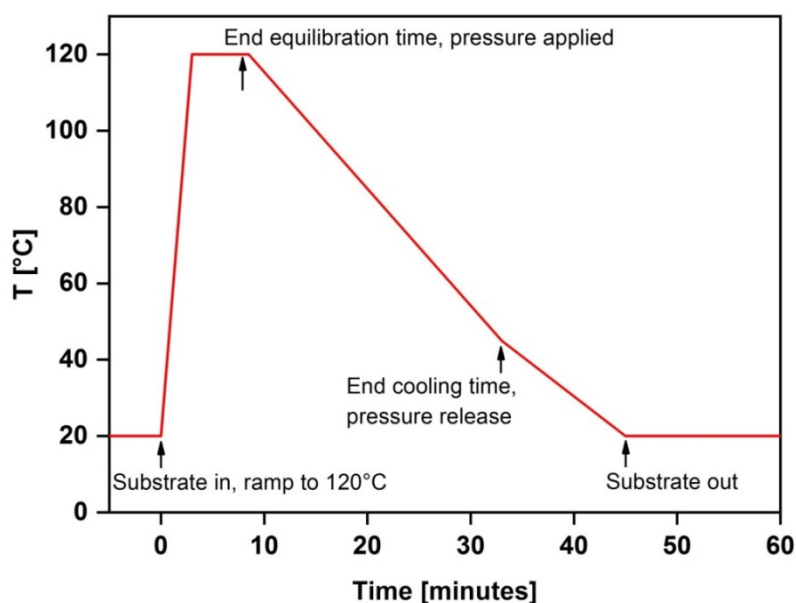


Figure 3. Hot embossing profile for PMMA microfluidic channels. Force applied: 500 N ($\sim 3.5 \text{ kg/cm}^2$ for used substrates).

After the cooling phase, the substrates were removed, PMMA templates that were sticking to the metal templates were carefully separated with a wafer tweezer and through-holes for fluidic connections were drilled at the inlet- and outlet ends of the fluidic structures through the PMMA with a Bosch PBD 40 table drill with a 1.25 mm diameter drill. Finally, contaminations from drilling were removed via quick rinsing with isopropanol and thorough drying under a N_2 -stream. The prepared substrates were stored protected from dust.

2.6 Thermal bonding of ITO@PET on PMMA (optimized procedure)

The bonding procedure of ITO @ PET with PMMA was performed as following. Prior to bonding a combined cleaning/activation step of both, the ITO@ PET electrode substrate as well as the PMMA fluidics part of the microfluidic chip was done. Therefore, both parts were first undertaken an Ar-plasma treatment. This was done on a HarrickPlasma PDC-002 on intensity level 2 with a constant, small Ar-gas flow. Subsequently, an UV-ozone treatment was performed. Both parts were placed in a UV-ozone-cleaner (Model 42, Jelight Company Inc., Irvine, U.S.A.) and an automated cleaning process was done for 5 minutes at a power rate of 30 mW/cm^2 with a constant O_2 -flow of 0.5 L/min.

The bonding step was done on the same Specac press model as the embossing step. Here, the substrates were oriented with activated surfaces to each other and aligned

with the electrode and fluidic features oriented properly, on top of a stainless steel support. This part was then centered on the lower plate of the hot press, which was maintained at 85 °C. Then, the upper plate was lowered to touch contact, fixing the assembly and the bonding profile shown in Figure 4 was run.

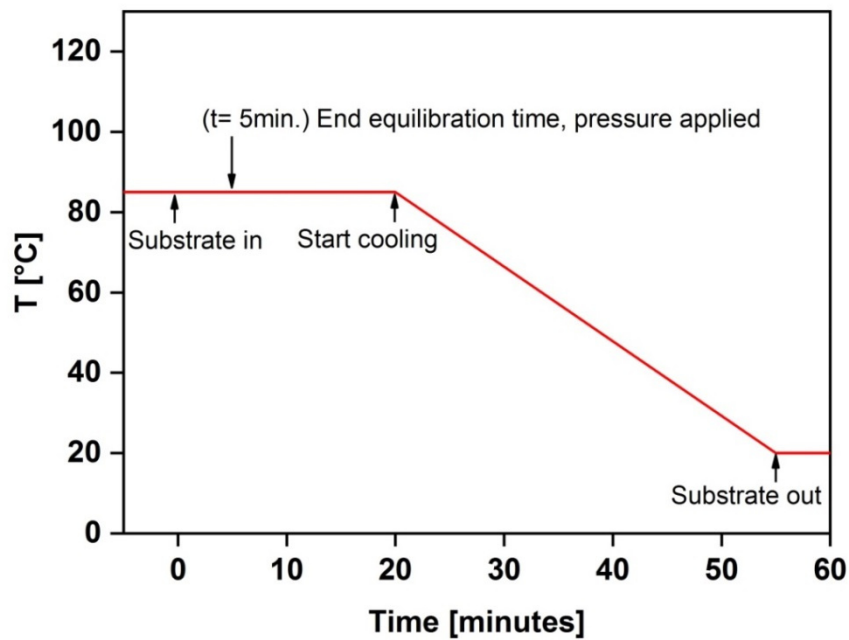


Figure 4. Temperature-time profile of ITO@PET on PMMA bonding (after optimization). Applied force was between 10-20 kN ($\sim 50 \text{ kg/cm}^2$). The force was maintained unchanged during the cooling phase and relieved, directed by the material's cooling-shrinkage effect. Remaining pressure was released at the time, the substrate was removed. Finally, the parts were set to rest for several hours to improve the bonding quality.

3. Results

3.1 Electrochemical implications towards materials choice and fabrication strategies

In this section, macroscopic ECL investigations are discussed. Initially, the usability of ITO electrodes for ECL was investigated with $[\text{Ru}(\text{bpy})_3]^{2+}$ -ECL. While the required potential of +1.5 V (vs. Ag-wire *pseudo*RE) indicated possible issues which have been reported at potentials above +1.0 V (vs. Ag-wire *pseudo*RE),¹¹ a confirmative longtime-ECL stability measurement with $[\text{Ru}(\text{bpy})_3]^{2+}$ -ECL suggested no problems (see Figure 5, ITO 1st test).

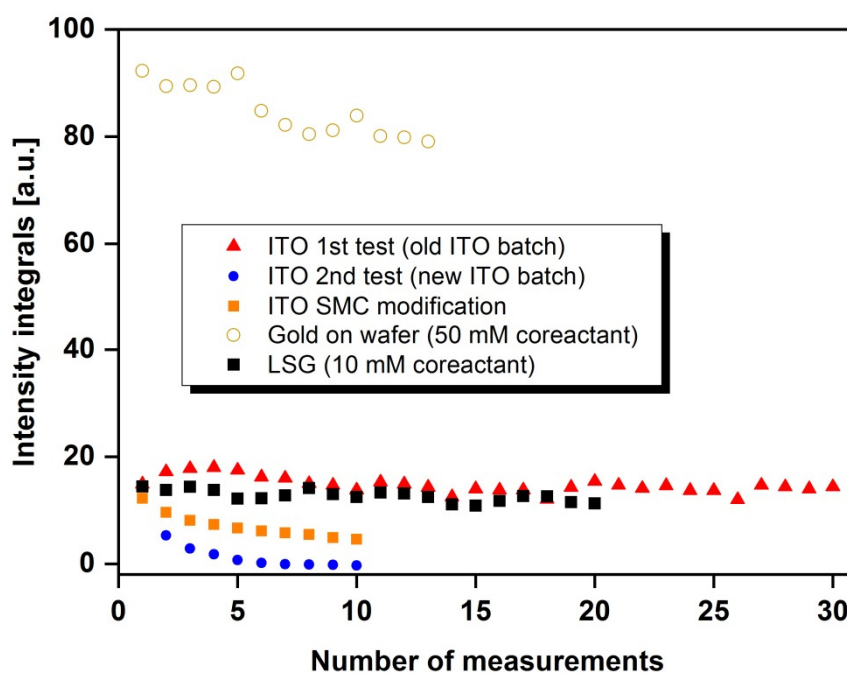


Figure 5. Electrode performance comparison and long-time stability with $[\text{Ru}(\text{bpy})_3]^{2+}$ -ECL. All measurements with comparable PMT voltages (600V and LSG 620V).

While the absolute ECL performance seems lower than on gold, the gold electrode ECL efficiency here has been determined with 50 mM NBEA as coreactant (Figure 5). However, in this case the performance rapidly declines as electrode fouling impedes the electrode functionality. This was the case even with a gold layer on a commercial wafer substrate which offers better stability than gold deposited on glass (e.g. tested

via a scratching test with a tweezer edge and confirming stronger gold layer bonding strength to the wafer). This has been investigated in an earlier master project and led to the limitation of $[\text{Ru}(\text{bpy})_3]^{2+}$ /NBEA-ECL to be used only with 10 mM NBEA to reduce fouling and enhance long-time stability.¹² Additionally, in further experiments, ITO caused stability issues which can be seen in Figure 5, depicted as second ITO test. The ultimate cause of this decline in performance has not been discovered however the most logical reason seems a behavior according to the reported ITO stability issues. Also, modification of ITO with SMCs, which is discussed below (chapter 3.3.1.) led to only marginal improvements (Figure 5). Ultimately, gold and ITO were dismissed for a multiple ECL miniaturization strategy. This was done for the complications with fabrication efforts and long-time stability issues for both electrode materials. Finally, LSG electrodes were investigated as an alternative material, maintaining an easy fabrication process but also sustaining the beneficial electrochemical conditions of carbon electrode materials against surface oxidation or high electrochemical background.¹³ Despite that this is a rather expectable behavior for a carbon electrode material,¹³ it was confirmed again via several long-time ECL stability tests (Figure 11).

3.2 Development of thermal bonding of PET with PMMA

Initially, the good performance of ITO for ECL resulted in using a process of photolithographic patterning of the ITO electrodes on PET as substrate and its fusion with PMMA containing the microfluidic structures after hot embossing. Thus a thermal bonding procedure between the two polymers was established. This approach of thermal bonding between PET and PMMA is not readily reported in literature. Other methods like solvent assisted bonding (of PMMA and PET) do however exist.¹⁴ This ethanol and UV-ozone-assisted bonding procedure was initially tested towards reproduction but could ultimately not be established successfully. Thus, direct thermal bonding between PET and PMMA was investigated. Initially, a sole UV-ozone treatment step was performed prior to the thermal bonding step. This however was not sufficient to assure a reliable bonding under any condition and led to separating parts in all cases. Subsequently, an Ar-plasma cleaning step was performed prior to the UV-ozone activation. This additional treatment which rather cleaned the surface than activate it

further improved the bonding quality. Finally, several bonding tests to find an optimum procedure were tested with an excerpt illustrated in Table 1.

Temperature [°C]	Force [kg/cm ²]	Duration [min]	Result
65	20	15	No bonding
75	40	5	Bonding not sufficient
85	10	15	Bonding not sufficient
85	25	15	Successful bonding
85	45	15	Successful bonding
85	-	30	*
95	10	15	No bonding
95	45	15	Bonding not sufficient
95	125	15	Successful bonding but channel narrowing
105	5	15	Melting
115	10	15	Melting

Table 1. Thermal bonding optimizations for PET/PMMA bonding. *Times longer than 15 minutes led to ultimately reduced bonding strengths.

Here, a temperature of at least 85°C was necessary, otherwise no sufficient bonding was achieved. Higher temperatures led to strong melting and channel feature shrinking with PMMA. The used temperature of 85°C is still below the glass transition temperature (T_g) of PMMA at approximately 105°C¹⁵ but slightly above the T_g of PET at approximately 75°C.¹⁶ This means, the here described thermal bonding is rather similar to a solvent-alike bonding process partially melting the polymers in contrast to a classical thermal bonding process which is often below the T_g of the involved polymers. However, for all successfully bonded chips, no disadvantage was found. The fluidic structures are contained in the PMMA polymer and were apparently not clogged by melted PET polymer. Macroscopically no visual defects or irregularities could be seen thus suggesting only a minor impact of a possible melting of the PET polymer. The lack of reports in literature on direct thermal bonding between both polymers lies presumably in PET having a low surface energy¹⁷ and thus causing problems towards a successful bonding behavior. Recently, Endo et al. have investigated a beneficial effect

of oxygen plasma treatment for direct bonding of PET with itself.¹⁸ This supports the here discovered route to directly thermally bond PET with PMMA with preceding Ar-Plasma and UV-Ozone treatment. However, the surface chemistries must be apparently different with the two distinct polymers applied here. The bonding duration was set to 15 minutes as longer times (30 minutes tested) led to reduced bonding strength and delamination of the parts after one day. This suggests an overexposure to heat - and presumably surface chemistry reactions during that phase. The final bonding protocol which was used after optimization is described in the materials part (chapter 2.6.) Finally, the produced chips were tested towards fluidics handling properties. Here, no leakage was observed for the optimized bonding procedure and overall, the chips could sustain total flow rates (aqueous solution) of approximately 300-400 μL per minute corresponding to a linear velocity of 0.13-0.18 m/sec. Higher flow rates were ultimately not tested and are in an irrelevant range for the here designated application of the microfluidic systems.

3.3 Electrochemical tests with $[\text{Ru}(\text{bpy})_3]^{2+}$ -ECL solutions on microfluidic ITO electrodes

Subsequently to the optimization of the microfluidic chips, on-chip ITO electrodes were characterized electrochemically. Here, Figure 6 **A** shows an exemplary cyclic voltammogram (CV) with $[\text{Ru}(\text{bpy})_3]^{2+}$ -ECL employing TPA as coreactant.

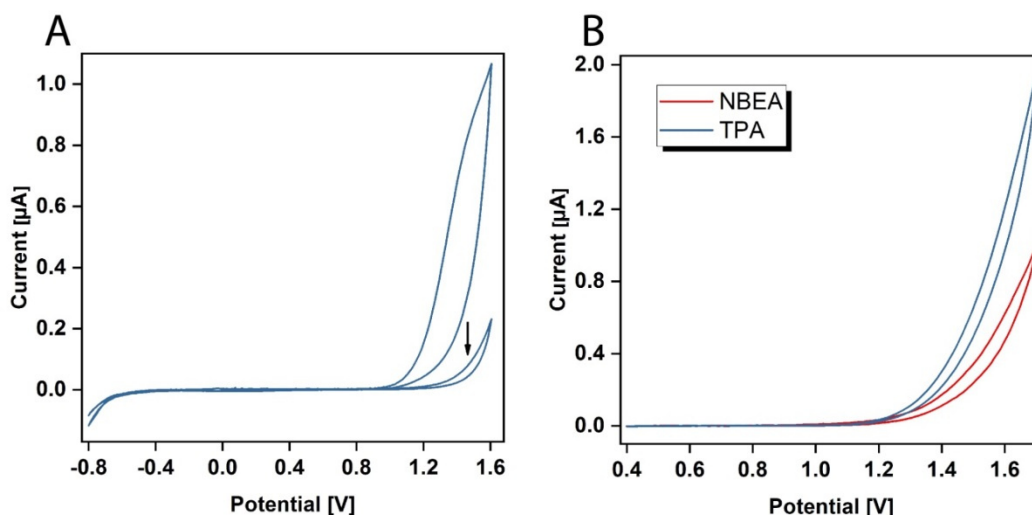


Figure 6 (A-B). **A** Cyclic voltammogram of ECL mix with tripropylamine as coreactant inside a microfluidic channel at a scan rate of 100 mV/sec., a step potential of 10 mV and 100 μM

[Ru(bpy)₃]²⁺ and 100 mM TPA without surfactant. **B** Comparison of the systems with coreactants TPA and NBEA on-chip.

This reflects a typical CV of [Ru(bpy)₃]²⁺-ECL with TPA on ITO electrodes¹⁹ with a large oxidation wave starting around +1.0 V (vs. Ag/AgCl-RE). The large drop in current response at the subsequent cycle depicts sacrificial ECL reagent consumption. This suggests a functional microfluidic chip for general ECL. In Figure 6 **B**, the comparison of the two coreactant systems with TPA and NBEA of [Ru(bpy)₃]²⁺-ECL are shown. However, this only represents a minimal characterization of the microfluidic system. Application of ferri-/ferrocyanide as reversible redox marker indicated a very poor electrochemical performance in the chip as exemplary depicted in Figure 7.

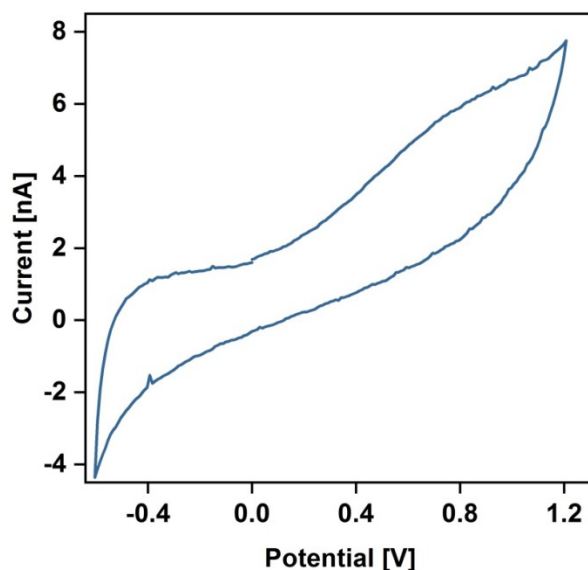


Figure 7. Cyclic voltammogram of 10 μ M ferri-/ferrocyanide on-chip at a scan rate of 100 mV/sec. with a step potential of 0.01 V, showing the fourth cycle.

Due to interfacing issues, at the connection site between ITO electrodes and the exterior and inconsistent stability, further studies are not shown here. This became also less important with the unfolding inexpedience of ITO for [Ru(bpy)₃]²⁺-ECL. Thus, modifications of ITO electrodes to protect the outer layer at the solution interface against surface oxidation were investigated.

3.4 ITO modifications

Several ITO treatment, coating and modification methods were tested for an improvement of ITO surface properties with $[\text{Ru}(\text{bpy})_3]^{2+}$ -ECL, as depicted in Table 2.

Surface modification	Effect
Electrochemical cleaning*	No improvement, electrode fouling.
Coating with Nafion membrane ⁺	No improvement, poor conductivity and noise level ECL.
Coating with Si-mesochannels	Slight improvement, stability not satisfying.

*indicates cleaning with voltammetric cycling in 1 M HCl or NaOH after initial measurements to remove increased oxide layers¹¹ on the surface. ⁺indicates drop coating of a Nafion® liquid membrane onto the ITO surface to protect the electrode while retaining diffusion permeability.

Table 2. Surface treatments of ITO@ PET electrodes.

Initially, an electrochemical cleaning process to reduce possibly increasing surface oxide layers in the ITO material was tested. Here, different solutions, i.e. potential sweep methods (scan rate: 100 mV/sec.) with p-toluenesulfonic acid in Isopropanol, KOH in Isopropanol, aqueous NaOH (1M) or HCl (1M) were applied after initial $[\text{Ru}(\text{bpy})_3]^{2+}$ -ECL reactions performed on these electrodes, to reduce forming oxide amounts again. None of these methods did improve the situation. It was concluded that the ITO was presumably irreversibly impaired and the supposedly increased amount of SnO_2 in the material¹¹ could not be reversely reduced and removed. Alternatively, a protective coating, employing a liquid Nafion membrane was tested. Therefore, a drop (25 μL) of the Nafion liquid membrane was drop-coated onto a fresh ITO electrode and the electrode was used for an ECL test after drying of the membrane. In this case, no improvement could be observed as visible in Figure 8.

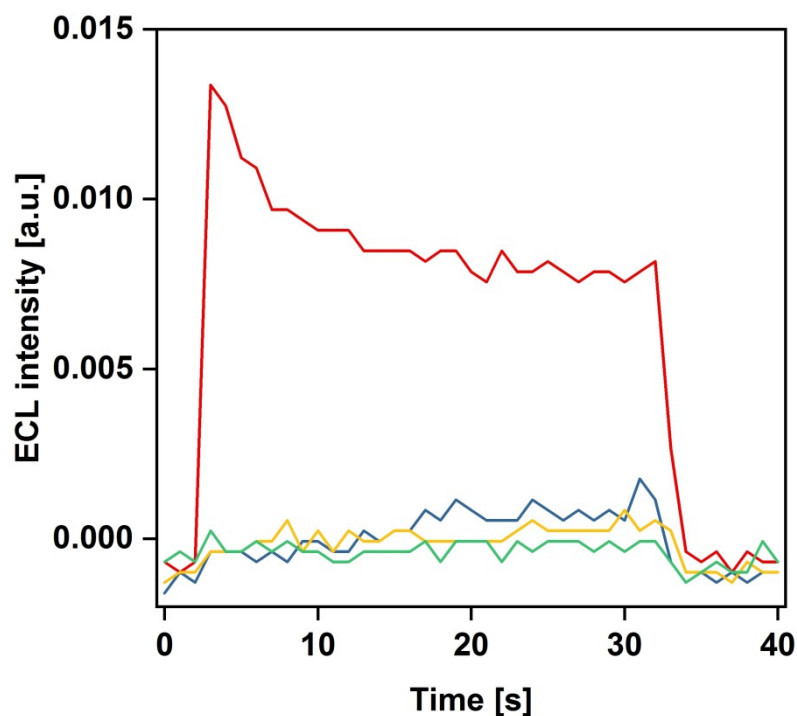


Figure 8. $[\text{Ru}(\text{bpy})_3]^{2+}$ -ECL with TPA (no surfactant) on Nafion coated ITO electrode. Different colors depict subsequent reactions with the red curve displaying the first ECL reaction.

The poor overall conductivity and low ECL response (Figure 8) led to the assumption that the electron transfer, diffusion- and redox processes across the membrane were too far hindered to allow a reasonable amperometric ECL excitation. Furthermore, the noise level of the emission after the first cycle also indicated degraded ITO functionality despite the Nafion coating. Finally, a reported method¹⁰ for modification of ITO electrodes with Silica mesochannels was investigated which is explained in detail in the following chapter 3.3.1.

3.4.1 SMC modified ITO electrodes.

As already depicted in Figure 5 (orange data points), the results of SMC modified ITO electrodes when tested with $[\text{Ru}(\text{bpy})_3]^{2+}$ did not show a noteworthy improvement towards the unmodified ITO electrodes. While the signal decline was minimally slower than with pristine ITO, the signal decayed to approximately 33% of the starting value within less than 10 repetitive ECL reactions on the same electrode. This does not reflect

a sufficient improvement for reasonable application of these electrodes. That dataset represents a typical example of several test sets which included variation of silane amounts and times and none was improving the situation. Though, some remarks to this method have to be added. The here applied method was amended from a reported procedure which used ITO layers on glass¹⁰ versus the here employed ITO on PET foil. However, this does not definitely explain the poor electrochemical performance as the ITO layer must not necessarily be affected by the substrate. Ultimately it cannot be excluded that a difference in the performance of ITO stability between the here performed measurements and the literature method lies in the different ECL conditions used. The literature procedure included a pH of 6.6 in PBS buffer with a potential sweep method between +0.6 V and +1.3 V for ECL excitation¹⁰ while the here employed method needs a pH of 9.0 in Glycine-NaOH buffer and a constant potential of +1.5V to get a meaningful ECL response. Thus, the less-basic pH value and overall lower potential can be imagined to reduce or decelerate ITO surface oxide formation which is thought to impede ITO performance.¹¹ Compared to previous findings,²⁰ however a low pH of 6.6 does not produce a desirable ECL response for powerful detection applications. Finally the unknown electrode area utilized in the reference method (for calculations of the exact silane ratio) can be imagined to impede an exact reproduction of the SMC composition. Additionally, the unknown absolute ECL value (e.g. versus the standard $[\text{Ru}(\text{bpy})_3]^{2+}/\text{TPA}$ system on gold) casts doubts on a definite improvement of ECL signals versus the here employed system with NBEA. Methods employing silica mesochannels and nafion membrane modifications of electrodes do seem to also work with intrinsically more stable carbon electrode materials.²¹ This raises the question if these layers rather work in a protective way against electrode surface fouling or function in a signal enhancing manner. Ultimately, the unknown factors and restricted success of a SMC modification of ITO in this study, led to the decision to dismiss ITO as electrode material for miniaturized ECL detection. Also in-general, such modification methods like SMC's include a relatively high fabrication effort and thus limit the practicability towards miniaturization-designated application.

3.5 [Ru(bpy)₃]²⁺-ECL characterization and luminol on LSG electrodes.

Carbon electrodes represent an interesting alternative for a multiple ECL detection capability as outlined in chapter 3.1. Here, the variant of LSG electrodes is a superior type of carbon material with respect to electrode patterning for microfabrication. However, its capability in ECL has only been tested with luminol ECL yet as shown in **chapter 5** of this thesis. Here, macroscopic ECL characterization of [Ru(bpy)₃]²⁺-ECL was done in order to investigate the general capability of LSG for this type of ECL, conditions and especially the electrode long-time stability.

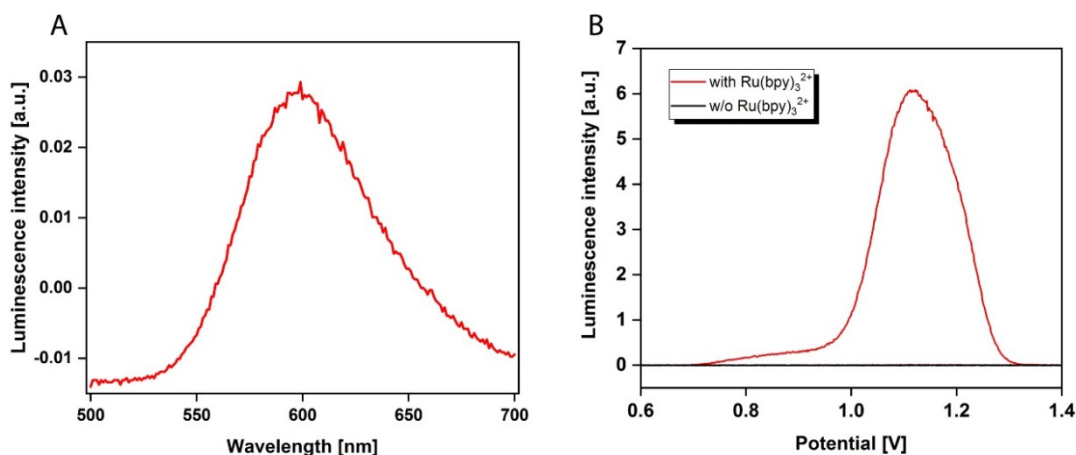


Figure 9 (A-B). A Emission scan of [Ru(bpy)₃]²⁺-ECL with NBEA and Zonyl FSN-100 at a speed of 5 nm/sec. a a potential of +1.2V. B Luminescence intensity versus potential scan without and with [Ru(bpy)₃]²⁺. Luminescence intensity units not corrected for absolute zero value.

First, an emission scan was performed to find the exact emission wavelength of the [Ru(bpy)₃]²⁺-ECL process. The resulting maximum of λ_{Em} at approximately 596 nm (Figure 9, A) depicts a shift of the typical emission wavelength of 620 nm for the tertiary amine oxidative-reductive coreactant ECL pathway of [Ru(bpy)₃]²⁺.¹¹ This suggests a possible influence of the porous LSG structure on the [Ru(bpy)₃]²⁺-ECL reaction mechanism, i.e. a possible interaction of the excited [Ru(bpy)₃]^{2+*} species with the graphene-alike electrode material. Also, with respect to a possible simultaneous ECL approach with [Ru(bpy)₃]²⁺- and luminol ECL this is just a minor shift of the emission wavelength which is still far enough separated from the 425 nm of the luminol emission. Subsequently, a luminescence intensity scan versus a potential sweep was

performed to find the exact $[\text{Ru}(\text{bpy})_3]^{2+}$ -ECL excitation potential. As visible in Figure 9B, for LSG electrodes the maximum emission can be observed at a working electrode potential of +1.1 V (vs. Ag-wire *pseudo*RE). The broad shoulder towards lower potentials, starting at approximately +0.7 V (vs. Ag-wire *pseudo*RE) indicates a low oxidation potential emission. This indicates similarity to the ECL reaction on other electrodes like gold.²⁰ Additionally, a reference scan was performed without added $[\text{Ru}(\text{bpy})_3]^{2+}$ -ECL to confirm the absence of any background luminescence, generated by the other solution constituents which was positive as visible in Figure 9B. Additionally, the optimum buffer system and pH value for the LSG electrodes was investigated. Here, Tris-HCl buffer at a pH of 8.5 proved to be the most efficient system for ECL signal generation as visible in Figure 10.

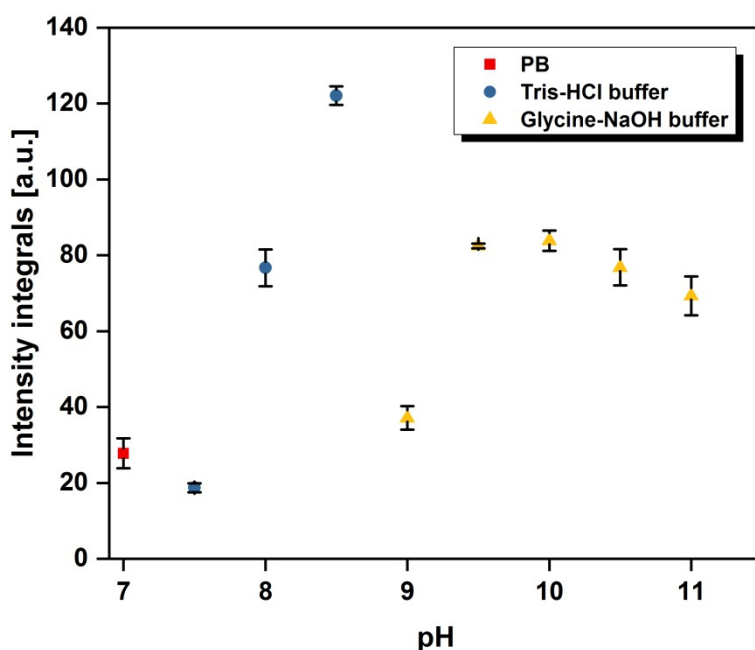


Figure 10. Buffer system and pH influence on the $[\text{Ru}(\text{bpy})_3]^{2+}$ -ECL efficiency on LSG electrodes. PMT voltage: 800V.

Larger pH values than 8.5 for a changed buffer system substantially reduced the ECL efficiency again. This is in agreement with previous findings²⁰ and again confirms that the Tris-system plays a special role in supporting the ECL efficiency of the $[\text{Ru}(\text{bpy})_3]^{2+}$ -ECL. Besides the suggested effect of the amino group being beneficial in the ECL process, a complex formation of Ruthenium(III) with Tris-(hydroxymethyl)-aminomethane has been reported.²² The revelation of the precise role of Tris in this ECL

process depicts an interesting topic for a future mechanistic study. With respect to assay efficiency, the approximately three times enhanced signal intensity with the Tris buffer system compared with Glycine–NaOH at a pH of 9.0 can be readily used as further source of enhancement. The optimum coreactant (e.g. NBEA vs. TPA) has not been experimentally confirmed for LSG electrodes. Though, it can be readily presumed that NBEA is in a similar way more efficient than the classical TPA on LSGs as on gold.²⁰ This is based on the effect that the enhanced efficiency of NBEA vs. TPA lies in the electron withdrawing effect of the hydroxyl groups inside the molecule. This intrinsic effect is likely not largely affected by the electrode material. Also, the hydrophilicity of the LSG electrodes (shown in chapter 5 of this work) is likely to aid in a preferred interaction with the more hydrophilic NBEA versus TPA bearing solely hydrophobic alkyl- sidechains. Finally, the most important study for the validation of LSG electrodes for multiple ECL application and miniaturization was a long-term stability test. This was repeated for three times on distinct LSG electrodes to assure a reliable outcome. Figure 11 depicts the results of independent experiments.

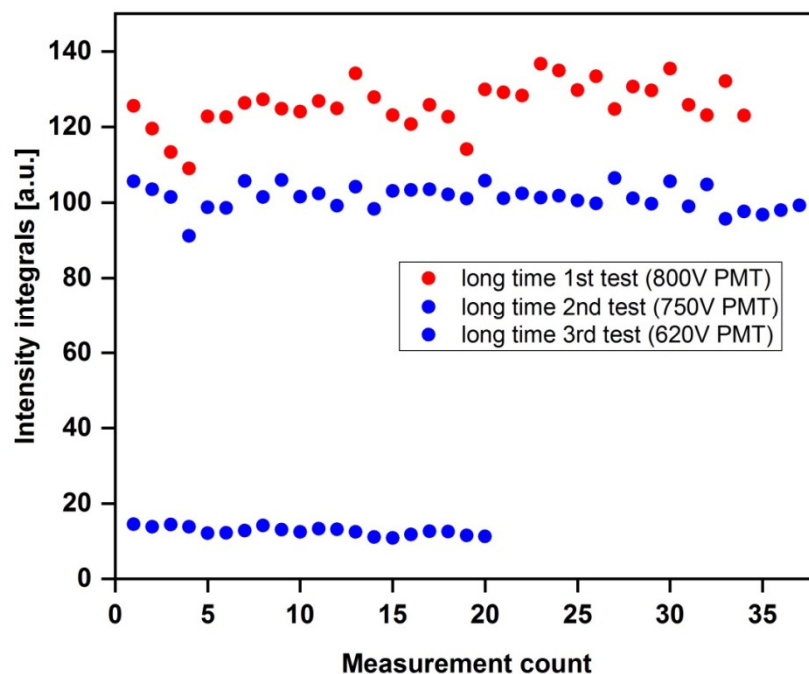


Figure 11. Long-term ECL stability tests with consecutive $[\text{Ru}(\text{bpy})_3]^{2+}$ -ECL measurements on LSG electrodes for 100 μM $[\text{Ru}(\text{bpy})_3]^{2+}$.

For a larger PMT value, the ECL signals are fluctuating more (in a range of approximately 10%), which is a rather typical effect for larger $[\text{Ru}(\text{bpy})_3]^{2+}$ -concentrations as employed here. Ultimately, the experimental results indicate a good long-term stability for $[\text{Ru}(\text{bpy})_3]^{2+}$ -ECL at +1.1 V (vs. Ag-wire *pseudo*RE) on LSG electrodes for almost 40 successive ECL reactions on one electrode without a visible loss in efficiency. This also suggests that the electrodes are not undergoing any major fouling reaction. Additionally, here a longtime test for luminol ECL on LSG electrodes was added. Assuming electrode affection with higher electrode potentials, this seems not an issue with luminol ECL being usually performed at +0.5 V (vs. Ag-wire *pseudo*RE) but contained species like the coreactant hydrogen peroxide as oxidizing species can supposedly also effect electrode materials. As shown in Figure 12, this was not the case and the electrodes performance remained unchanged over 35 consecutive luminol ECL reactions on the same electrode.

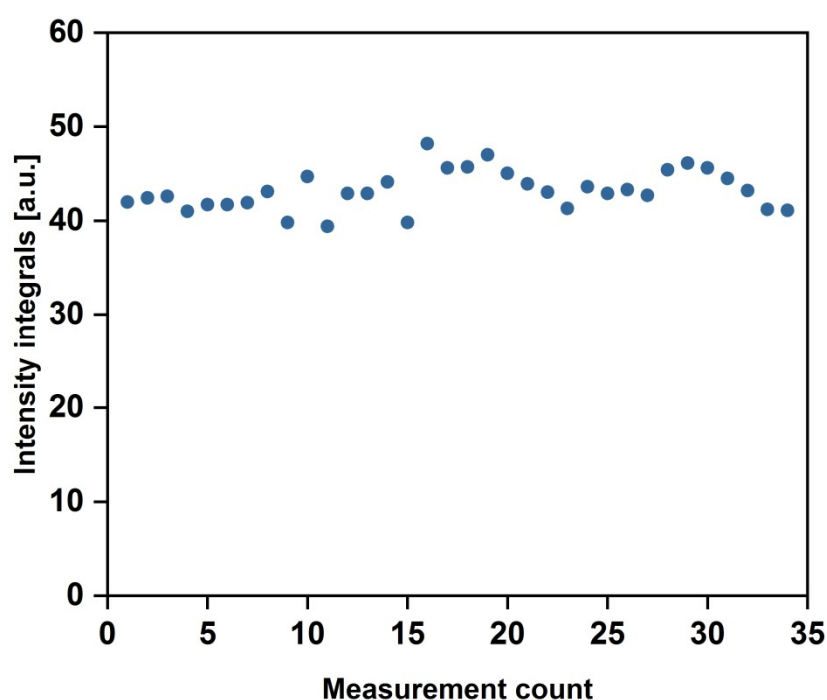


Figure 12. *m*-COOH luminol ECL on LSG electrodes. 100 μM *m*-COOH luminol, 50 μM Cetyltrimethylammonium bromide and 30 mM H_2O_2 . In 0.1 M Glycine NaOH buffer (0.1 M KCl) at pH 9.0 with a WE potential of +0.4 V, $\lambda_{\text{Em}} = 430 \text{ nm}$ and a PMT value of 850V.

Ultimately, these results indicate a good qualification for LSG electrodes as elements in miniaturization of versatile ECL detection devices that are capable of multiple detection.

4. Conclusions

The here presented strategies for miniaturization for ECL detection outline that this topic still represents a challenge when being restricted to simple fabrication and at the same time multiple ECL detection capabilities employing $[\text{Ru}(\text{bpy})_3]^{2+}$ -ECL and luminol ECL simultaneously are required. While gold electrodes work well for ECL in macroscopic conditions, the efforts and cost for miniaturization does not fit a simple fabrication concept. Additionally, the ultimately limited stability of gold films for $[\text{Ru}(\text{bpy})_3]^{2+}$ -ECL when used in its maximum efficiency is another disadvantage of gold. Here, a new direct, thermal bonding procedure for the interfacing of PMMA with PET for an electrochemical microfluidic chip has been developed. However this approach represents not an optimal solution for versatility and multiple ECL requirements. When using the combination of photolithographically patterned ITO electrodes on a PET substrate, the ability for ECL detection is electrochemically restricted to ECL reagents which are excited below +1.0 V (e.g. luminol). This is also valid for surface modified ITO electrodes. Electrochemically, the ITO electrodes inside the chip do show a response - and while macroscopically luminol ECL does work well on ITO, the true functionality inside the microfluidic systems must be further validated. Nevertheless, the usability for a luminol-only multiple detection system on one chip seems limited. Alternatively, a single-use, disposable application can be imagined. Here, the issue of electrode impairment does not seem as pronounced as with long-term stability also for $[\text{Ru}(\text{bpy})_3]^{2+}$ -ECL but inter-electrode signal repeatability must be a mandatory prerequisite. However, as ITO stability for a multiple ECL detection concept is not sufficient, a different microfabrication approach with respect to material choice and fabrication strategy is required. Exemplary, LSG electrodes represent here an interesting alternative. They sustain relatively large electrochemical potentials also covering $[\text{Ru}(\text{bpy})_3]^{2+}$ -ECL and are long-time stable under these conditions. Additionally, the ability to pattern these electrodes simply and freely creates a new route towards a simple microfabrication strategy. Nevertheless, the structural properties of LSG

electrodes of being relatively thick and comparable to screen printed electrodes in contrast to deposited layers of gold or semiconductor electrode materials can have influences on the fabrication and performance of microfluidics which has to be investigated further. The electrochemical performance of LSG electrodes for ECL has not been showing any issues, with respect to their porosity, stability and electron transfer^{23,24} properties in a macroscopic environment. This suggests good compliance with ECL signal generation, however, in a miniaturized environment this needs to be further validated. Thus, LSG electrodes can be proposed as electrochemical element for a multiple-ECL capable microfluidic system where the other part consists of a transparent polymer (for ECL signal transmission through the material). Here, bonding strategies that include interfacing via adhesive films can be suggested as these comply better with height irregularities.³ Addressing the challenges of interfacing, bonding and optimization of the on-chip ECL processes is an interesting task for future research projects.

5. References

- (1) Whitesides, G. M. The origins and the future of microfluidics. *Nature* **2006**, *442*, 368. doi: 10.1038/nature05058
- (2) Moutaux, E.; Charlot, B.; Genoux, A.; Saudou, F.; Cazorla, M. An integrated microfluidic/microelectrode array for the study of activity-dependent intracellular dynamics in neuronal networks. *Lab Chip* **2018**. doi: 10.1039/c8lc00694f
- (3) Temiz, Y.; Lovchik, R. D.; Kaigala, G. V.; Delamarche, E. Lab-on-a-chip devices: How to close and plug the lab? *Microelectron. Eng.* **2015**, *132*, 156-175. doi: 10.1016/j.mee.2014.10.013
- (4) Sackmann, E. K.; Fulton, A. L.; Beebe, D. J. The present and future role of microfluidics in biomedical research. *Nature* **2014**, *507*, 181. doi: 10.1038/nature13118
- (5) Kadimisetty, K.; Malla, S.; Bhalerao, K. S.; Mosa, I. M.; Bhakta, S.; Lee, N. H.; Rusling, J. F. Automated 3D-Printed Microfluidic Array for Rapid Nanomaterial-Enhanced Detection of Multiple Proteins. *Anal. Chem.* **2018**, *90*, 7569-7577. doi: 10.1021/acs.analchem.8b01198
- (6) Nge, P. N.; Rogers, C. I.; Woolley, A. T. Advances in Microfluidic Materials, Functions, Integration, and Applications. *Chem. Rev.* **2013**, *113*, 2550-2583. doi: 10.1021/cr300337x
- (7) Schrott, W.; Svoboda, M.; Slouka, Z.; Šnita, D. Metal electrodes in plastic microfluidic systems. *Microelectron. Eng.* **2009**, *86*, 1340-1342. doi: 10.1016/j.mee.2009.01.001
- (8) DARWIN microfluidics, *Bubble Trap for Microfluidics Kit*. <https://darwin-microfluidics.com/collections/microfluidic-accessories/products/microfluidic-bubble-trap> (accessed: 18th October 2018).
- (9) Teng, Z.; Zheng, G.; Dou, Y.; Li, W.; Mou, C.-Y.; Zhang, X.; Asiri, A. M.; Zhao, D. Highly Ordered Mesoporous Silica Films with Perpendicular Mesochannels by a Simple Stöber-Solution Growth Approach. *Angew. Chem. Int. Ed.* **2012**, *51*, 2173-2177. doi: 10.1002/anie.201108748
- (10) Zhou, Z.; Guo, W.; Xu, L.; Yang, Q.; Su, B. Two orders-of-magnitude enhancement in the electrochemiluminescence of Ru(bpy)₃²⁺ by vertically ordered silica mesochannels. *Anal. Chim. Acta* **2015**, *886*, 48-55. doi: 10.1016/j.aca.2015.06.005
- (11) Wilson, R.; Akhavan-Tafti, H.; DeSilva, R.; Schaap, A. P. Comparison between acridan ester, luminol, and ruthenium chelate electrochemiluminescence. *Electroanalysis* **2001**, *13*, 1083-1092. doi: 10.1002/1521-4109(200109)13:13<1083::AID-ELAN1083>3.0.CO;2-D
- (12) Mayer, M. *Luminol and ruthenium electrochemiluminescence for a dual ECL detection approach*. Master thesis, Regensburg, 2015.
- (13) McCreery, R. L. Advanced Carbon Electrode Materials for Molecular Electrochemistry. *Chem. Rev.* **2008**, *108*, 2646-2687. doi: 10.1021/cr068076m
- (14) Tran, H. H.; Wu, W.; Lee, N. Y. Ethanol and UV-assisted instantaneous bonding of PMMA assemblies and tuning in bonding reversibility. *Sens. Actuators, B* **2013**, *181*, 955-962. doi: 10.1016/j.snb.2012.11.060
- (15) Lin, C.-T.; Kuo, S.-W.; Huang, C.-F.; Chang, F.-C. Glass transition temperature enhancement of PMMA through copolymerization with PMAAM and PTCM

- mediated by hydrogen bonding. *Polymer* **2010**, *51*, 883-889. doi: 10.1016/j.polymer.2009.12.039
- (16) Zhang, Y.; Zhang, J.; Lu, Y.; Duan, Y.; Yan, S.; Shen, D. Glass Transition Temperature Determination of Poly(ethylene terephthalate) Thin Films Using Reflection–Absorption FTIR. *Macromolecules* **2004**, *37*, 2532-2537. doi: 10.1021/ma035709f
 - (17) Cioffi, M. O. H.; Voorwald, H. J. C.; Hein, L. R. O.; Ambrosio, L. Effect of cold plasma treatment on mechanical properties of PET/PMMA composites. *Composites Part A: Applied Science and Manufacturing* **2005**, *36*, 615-623. doi: 10.1016/j.compositesa.2004.08.006
 - (18) Endo, T.; Reddy, L.; Nishikawa, H.; Kaneko, S.; Nakamura, Y.; Endo, K. Composite Engineering – Direct Bonding of plastic PET Films by Plasma Irradiation. *Procedia Engineering* **2017**, *171*, 88-103. doi: 10.1016/j.proeng.2017.01.315
 - (19) Kim, Y.; Kim, J. Modification of Indium Tin Oxide with Dendrimer-Encapsulated Nanoparticles To Provide Enhanced Stable Electrochemiluminescence of Ru(bpy)₃²⁺/Tripropylamine While Preserving Optical Transparency of Indium Tin Oxide for Sensitive Electrochemiluminescence-Based Analyses. *Anal. Chem.* **2014**, *86*, 1654-1660. doi: 10.1021/ac403415m
 - (20) Kirschbaum-Harriman, S.; Duerkop, A.; Baeumner, A. J. Improving ruthenium-based ECL through nonionic surfactants and tertiary amines *Analyst* **2017**, *142*, 2648-2653. doi: 10.1039/C7AN00197E
 - (21) Cao, H.; Hu, X.; Hu, C.; Zhang, Y.; Jia, N. A novel solid-state electrochemiluminescence sensor for melamine with Ru(bpy)₃²⁺/mesoporous silica nanospheres/Nafion composite modified electrode. *Biosens. Bioelectron.* **2013**, *41*, 911-915. doi: 10.1016/j.bios.2012.10.004
 - (22) Dotson, R. L. Characterization of a diamagnetic Bi-nuclear ruthenium (III) complex of tris-(hydroxymethyl)-aminomethane. *Inorganic and Nuclear Chemistry Letters* **1972**, *8*, 353-355. doi: 10.1016/0020-1650(72)80011-4
 - (23) Nayak, P.; Kurra, N.; Xia, C.; Alshareef, H. N. Highly Efficient Laser Scribed Graphene Electrodes for On-Chip Electrochemical Sensing Applications. *Adv. Electron. Mater.* **2016**, *2*, 1600185. doi: 10.1002/aelm.201600185
 - (24) Fenzl, C.; Nayak, P.; Hirsch, T.; Wolfbeis, O. S.; Alshareef, H. N.; Baeumner, A. J. Laser-Scribed Graphene Electrodes for Aptamer-Based Biosensing. *ACS Sens.* **2017**, *2*, 616-620. doi: 10.1021/acssensors.7b00066

Chapter 7: Conclusions and perspectives

The findings obtained during this project underline the outstanding performance of luminol and $[\text{Ru}(\text{bpy})_3]^{2+}$ ECL together with various signal enhancement means as powerful detection systems for almost any bioanalytical problem. Biosensors will and must be an integral part of a future Internet of Things (IoT) e.g. in clinical diagnosis settings and *in-vivo* sensors. Though, this future vision is still far away, with respect to the many problems and challenges that have to be overcome until a functioning network is established. This includes topics like e.g. true long-term stability for *in-vivo* sensors or the need for more sophisticated and integrated solutions. Here, also barriers like the long route of FDA approval of new devices and the lack of matching categorizations for this device class in these agencies are apparent (Senseonics implantable glucose monitor is to date still the only approved *in-vivo* biosensor). Further obstacles are agreements on communication protocols and unique data formats that allow a seamless integration of any new device or lacking cooperation between research, industry and IT. This however does not mean that new developments should be stopped. In contrast, new ideas and progress are heavily needed and researchers can shape this evolution.

In view of that uprising Internet-of-Things dominated future of sensing and new trends towards patient-centralized diagnostics, versatile and sensitive detection techniques are important. The adaptability to all different dimensions from miniaturized and integrated to benchtop, standard laboratory devices depicts a flexibility which ECL displays. For all these different applications, ECL can play out its maximum efficiency when smartly coupled with different signal enhancement tools. Several options exist here which all exhibit their own advantages, depending on the respective application and chosen sensing route.

For a signal enhancement strategy employing $[\text{Ru}(\text{bpy})_3]^{2+}$ ECL together with PAMAM dendrimers, an application restricted to homogeneous assay formats represents the best option. Here, a combination of the sensing element together with the reporter moiety in one entity can be realized. This can also be extended that additionally to the biorecognition element and the coreactant functionality also the ECL reagent ($[\text{Ru}(\text{bpy})_3]^{2+}$) can be connected.¹ This allows up to a triple functionality. However, this

joint-venture also leads to some tradeoffs. In this regard it is important to mention that also the primary amino-groups can serve here in a coreactant-functionality.² The resulting blockade of outer amino functionalities through coupling to $[\text{Ru}(\text{bpy})_3]^{2+}$ or by the urgency to keep them free, in their original functionality for a role as ECL coreactant limits the ability to use these groups for attachment of biorecognition elements. This disadvantage also accounts for a dual coreactant/capturing element use or for other variations of such two or three-in-one functional variations. This limits the breadth of applications as possible reachable sensitivities are reduced either by limited capturing functions or by limited signal generation moieties. This more or less restricts the possible applications to assays requiring rather qualitative answers or these with a large abundance of analyte in the desired environment. A possibility to avoid this is, if the desired analyte takes the role of the coreactant³ and the dendrimers would serve as anchoring units to the electrode and for $[\text{Ru}(\text{bpy})_3]^{2+}$ immobilization with an enhanced ECL signal. It is imaginable that this enhances sensitivities via larger signals if both, the dendrimers and as well the analyte partly act in a coreactant role, thus comparable to the method of standard addition if linearity in the signal response persists. Besides that, an advantage for the detection of hydrophobic compounds like lipids in an aqueous environment can be envisioned. Here, the relative hydrophobicity of the dendrimers⁴ in their dendritic structure can be beneficial for a preferred interaction with hydrophobic compounds in biological buffer systems. Possible interactions with serum proteins – via their outer charge but also hydrophobic interactions⁵ and finally association with small aromatic hydrocarbons⁶ have been shown. Thus association of molecules can sterically limit either the electrode approximation of the resulting adducts or directly influence intra-dendrimer ECL reactivity and thus enable a quenching modulated dose-response ECL sensing of these interacting molecules.

In general, however, the application of dendrimer-enhanced ECL is limited by reduced aqueous dispersibility, especially when conjugated to $[\text{Ru}(\text{bpy})_3]^{2+}$ as shown earlier¹ and relatively high cost for commercially available PAMAM dendrimers. Finally, also in the case of a desired dual-detection approach, employing luminol and $[\text{Ru}(\text{bpy})_3]^{2+}$ -ECL in one solution, dendrimers have a disadvantage. Then they are not able to fully protect the ECL molecules from the environment (as e.g. liposomes do) as these are likely bound on their outer side. Thus, in this situation, the susceptibility of these two ECL reagents to mutual quenching which has been found⁷ cannot be eradicated, if both

dendrimer-sandwich constructs with luminol and $[\text{Ru}(\text{bpy})_3]^{2+}$ are within the diffusion range of a shared signal generating location.

In all these cases, a liposome-based enhancement approach represents a very different, but interesting alternative. Dispersibility of the here employed phospholipid/cholesterol – liposomes in aqueous buffer systems is a nonissue while the liposomes are at the same time more cost effective. More importantly, the possible signal enhancement capabilities as shown in the combination with *m*-carboxy luminol as ECL probe make them an outstanding reporter functionality. The general flexibility towards surface functionalization with different biorecognition elements like e.g. nucleic acids (or aptamers⁸), antibodies or binding proteins⁹ depicts their versatile role for different applications in all different bioassays. It has to be noted, that the here presented liposome application as signal enhancement means, is mostly limited to heterogeneous assay formats. That is, because a washing step prior to liposome lysis is necessary to remove unbound excess liposomes. Two rare cases make an exception, i.e. the direct sensing of liposome lysing compounds – if they do act in a proportional relation or an analyte-induced liposome aggregation and thus sedimentation which removes an analyte-concentration dependent amount of precipitate from the solution phase. The application range however, is in this regard not limited in an appreciable amount. The second part of this symbiosis shown here, *m*-carboxy luminol as new luminol derivative, represents a major improvement in all areas of luminol applications. This also accounts beyond ECL, which has been shown for CL applications.¹⁰ In that case, one issue became apparent, which is the limited solution-stability of *m*-carboxy luminol if exceeding a stand time beyond 5 weeks (10 °C, dark conditions; see chapter 4).

Though the comparative experiments in this work have suggested a similar ECL reaction mechanism for *m*-carboxy luminol as for standard luminol, it remains to identify that both species indeed follow the same mechanisms. However, some possible influencing factors on the reaction mechanism are suggested in the following paragraph. With its location at the 6-position of the aromatic ring, the carboxyl group is over two positions away from the amino-functionality - and also the next carbonyl group in the heterocyclic ring. Thus, it is unlikely to seminally change the reaction mechanism but it is likely to be able to influence e.g. sterically the position of that carbonyl group during the pathway. Thus it can change the probability for a transition in the excited state as it

has been suggested for other substituents in this position in CL.¹¹ Also, the amino functionality in the aromatic ring can presumably stabilize the reaction (without or after additional protonation at the amino or carbonyl group) via hydrogen bonding to the neighboring carbonyl group.¹¹ This is a step where the additional carboxyl group in *m*-carboxy luminol can presumably also influence the protonation and promote stronger hydrogen bonding via its electron withdrawing effect in the conjugated aromatic system to impact the reaction mechanism. Finally, the carboxyl group also leads to an enlargement of the conjugated system in the luminol molecule. While the results indicated that this apparently didn't change the emission wavelength it is likely to also be able to influence the reaction. These considerations were referred to literature covering the CL process of luminol. However, due to the similarity of both processes, ECL and CL, where the ECL process presumably always includes CL mechanistic reactions¹² at different possible steps all these considerations are likely for ECL as well. Thus, confirmation of the exact intermediate steps and molecular rearrangements during the reaction pathways and elucidation of the exact influence the carboxyl substituent has on them is a desirable future task.

The additive functionality that *m*-carboxy luminol incorporates versus pristine luminol and which directs its superior luminescence and solubility properties can also serve for a different purpose. The -COOH group enables coupling of the molecule e.g. via bioconjugation methods¹³ to other compounds or entities to create a new, immobilized luminol probe. The position of the coupling site is advantageous with respect to less influence (but not none) on the (E)CL reaction mechanism compared to e.g. functionalization at the amino group. However, such an additional use has to be reviewed critically. The gained water solubility via the additional ionic charge of a deprotonated carboxyl group and the beneficial luminescence effects are likely to be eradicated again. This is likely to happen when the carboxylic group is linked to another functional unit and loses its charge and properties as a single entity while a PEGylated spacer can probably avoid that to some extent. On the other hand, the directed introduction of a further functional group adjunct to the amino and carboxyl functionalities in the aromatic ring is presumably a complex synthesis task that also would increase the cost and efforts of synthesis. Besides questionable realization this last argument makes such a luminol probe rather unattractive for extensive use in many applications. As such, it remains to investigate how a functionalization of the *m*-

carboxy luminol towards a conjugation probe will affect its luminescence efficiencies and properties and how this application can be beneficially exploited in bioassays. Conceivable applications span a broad range from generation of heterogeneous, luminescent surfaces comparable to a luminous LED film (wound monitoring¹⁴, imaging¹⁵) to single probe labeling. This outlines several interesting applications that might benefit by a performance boost which an immobilized chemiluminescent probe can accomplish e.g. in comparison to classical fluorophores.

The important role of surfactants, being readily present in bioassays has been investigated in this work with respect to their influence on luminol ECL. The obtained results unearthed a complex symbiotic mechanism. To further dismantle this symbiosis and allocate certain contribution ratios of the surfactant effects on ECL efficiency is an interesting task for further studies. While this gives promise to interesting mechanistic findings, it is questionable if the possibility to fully resolve all certain mechanisms even exists with respect to the multitude of influences. A reduction of influencing factors on the other hand would most likely not reflect the real situation good enough for certain predictions. Experimental tools that can further help in this case are likely represented by Langmuir–Blodgett trough studies. Those can help to gain more knowledge of surface adsorption processes if it is possible to create the same surface potential as within the ECL cell mimicking the anodic ECL potential. It is conceivable that scanning electrochemical microscopy can shed some light on influences of electrochemical surface processes and kinetics while luminescence lifetime measurements¹⁶ (complex instrumentation for ECL¹⁷) can serve to better understand the chemiluminescent contribution to the ECL process.

The findings on surfactant effects can, besides for all different cases where the surfactants are required by the employed assay - be beneficial in situations where they are normally not needed but can create additional rewarding effects. Exemplary, surfactants can be present e.g. in paper based sensor designs combined with electrodes¹⁸ which is especially interesting for ECL applications. Here, issues like paper-wicking and hydrophobicity are crucial and can be mediated by surfactant addition.¹⁹ It is to note here, that surfactants can also cause problems in paper based microfluidics and that a different material and fabrication strategy can avoid these.²⁰ Also, selectivity enhancement with electrochemical detection on paper has been mediated by surfactant action.²¹ This is just one possible scenario where the insights of surfactant

action on luminol ECL can be beneficial. With a perspective of upcoming diagnostics developments however, paper-based platforms also with ECL detection (e.g. for cost effective Alzheimer detection) represent an important area of interest.²²

In general, the yet untapped potential of luminol ECL in commercial applications is likely to be exploited in a foreseeable timeframe as recent projects towards development of POC-ECL devices indicate.^{23,24} Fang et al. have here recently highlighted the relevance of luminol ECL detection in the area of clinical diagnosis.²⁵ This suggests an uprising role of ECL as detection technique and also the persistent and increasing importance of the classical ECL luminophores, luminol and $[\text{Ru}(\text{bpy})_3]^{2+}$ for sensitive bioassays in diagnostic and many more commercial applications. Signal enhancement strategies are here well appreciated and can enlarge the imaginable application window. While combinations of signal enhancement tools like e.g. a cost-effective, improved ECL probe together with liposomes and finally surfactant-mediated amplification can reach impressive sensitivities, further strategies can be exploited. Reduced sample volumes via liquid handling in miniaturized systems together with e.g. magnetic bead based approaches can be envisioned to further tune the capabilities of the here presented ECL detection strategies.²⁶ While ultra-low sensitivities might also not be needed in all cases, the ECL technique can still play out its advantages with respect to easy and cost effective miniaturization while providing selectivity (vs. pristine electrochemical detection) and lowest noise levels.

LSG electrodes showed in this work a good adaptability to versatile ECL detection in the process of microfluidic design developments. Besides their ability to be easily patterned and just “printed”, their porous nature can supposedly bear further advantages. Kado et al. found an ECL enhancing effect for $[\text{Ru}(\text{bpy})_3]^{2+}$ -ECL with nanoporous electrodes.²⁷ To adapt this effect towards functionality with LSG electrodes can be a beneficial chance. Alternatively, porous carbon or ceramic carbon electrode materials allowed the creation of a “solid-state alike” electrode by immobilization of $[\text{Ru}(\text{bpy})_3]^{2+}$ -species inside a matrix.^{28,29} Despite the used Nafion material in the immobilization processes proved to be difficult in this work, such an approach seems interesting. Finally, the process of laser-scribing carbon electrodes (similar to LSG) on paper again offers further possible applications.³⁰

A combination of luminol and $[\text{Ru}(\text{bpy})_3]^{2+}$ ECL in a multi-detection setup provides another toolset to upscale sensor capabilities with two similar but - regarding emission - clearly separated probes, that adhere mostly to the same constraints. Thus, either for single solution approaches or for multi-detection setups with both ECL probes in separated zones, a distinct emission wavelength can be beneficial. That is, if e.g. a camera, or CCD chips or diodes are used where both detection events are covered under a single capturing area, thus resolving both emission events clearly without an increase of noise.

All this illustrates how the here presented strategies and findings for ECL as detection method in modern biosensing provide a multitude of possibilities over many different application fields. After all, luminol and $[\text{Ru}(\text{bpy})_3]^{2+}$ as classical ECL probes, demonstrate by means of their performance and versatility that they adhere to the current benchmarks in biosensing and are best options also for practical and commercial scenarios.

References

- (1) Griesche, C. *Development of surface modified liposomes and dendrimers for signal amplification*. Master thesis, Regensburg, **2017**.
- (2) Jimenez-Ruiz, A.; Grueso, E.; Perez-Tejeda, P. Electrogenerated chemiluminescence reactions between the $[\text{Ru}(\text{bpy})_3]^{2+}$ complex and PAMAM GX.0 dendrimers in an aqueous medium. *J. Inorg. Biochem.* **2015**, *151*, 18-25. doi: 10.1016/j.jinorgbio.2015.06.021.
- (3) Marzari, G.; Cappellari, M. V.; Morales, G. M.; Fungo, F. Electrochemiluminescent detection of glyphosate using electrodes modified with self-assembled monolayers. *Anal. Methods* **2017**, *9*, 2452-2457. doi: 10.1039/c7ay00506g.
- (4) Otto, D. P.; de Villiers, M. M. Poly(amidoamine) Dendrimers as a Pharmaceutical Excipient. Are We There yet? *J. Pharm. Sci.* **2018**, *107*, 75-83. doi: 10.1016/j.xphs.2017.10.011.
- (5) Wang, B.; Sun, Y.; Davis, T. P.; Ke, P. C.; Wu, Y.; Ding, F. Understanding Effects of PAMAM Dendrimer Size and Surface Chemistry on Serum Protein Binding with Discrete Molecular Dynamics Simulations. *ACS Sustainable Chem. Eng.* **2018**, *6*, 11704-11715. doi: 10.1021/acssuschemeng.8b01959.

- (6) DeFever, R. S.; Sarupria, S. Association of small aromatic molecules with PAMAM dendrimers. *Phys. Chem. Chem. Phys.* **2015**, *17*, 29548-29557. doi: 10.1039/c5cp03717d.
- (7) Mayer, M. *Luminol and ruthenium electrochemiluminescence for a dual ECL detection approach*. Master thesis, Regensburg, **2015**.
- (8) Alshaer, W.; Hillaireau, H.; Vergnaud, J.; Ismail, S.; Fattal, E. Functionalizing Liposomes with anti-CD44 Aptamer for Selective Targeting of Cancer Cells. *Bioconjugate Chem.* **2015**, *26*, 1307-1313. doi: 10.1021/bc5004313.
- (9) Reulen, S. W. A.; Brusselaars, W. W. T.; Langereis, S.; Mulder, W. J. M.; Breurken, M.; Merckx, M. Protein-Liposome Conjugates Using Cysteine-Lipids And Native Chemical Ligation. *Bioconjugate Chem.* **2007**, *18*, 590-596. doi: 10.1021/bc0602782.
- (10) Rink, S. *Development and Characterization of a New Chemiluminescent Probe for Bioanalytical Applications*. Master thesis, Regensburg, **2018**.
- (11) Brundrett, R. B.; White, E. H. Synthesis and chemiluminescence of derivatives of luminol and isoluminol. *J. Am. Chem. Soc.* **1974**, *96*, 7497-7502. doi: 10.1021/ja00831a018.
- (12) Wilson, R.; Akhavan-Tafti, H.; DeSilva, R.; Schaap, A. P. Comparison between acridan ester, luminol, and ruthenium chelate electrochemiluminescence. *Electroanalysis* **2001**, *13*, 1083-1092. doi: 10.1002/1521-4109(200109)13:13<1083::AID-ELAN1083>3.0.CO;2-D.
- (13) Hermanson, G. T., *Bioconjugate Techniques*. (Elsevier, Amsterdam, Boston, Heidelberg, **2013**). doi: 10.1016/C2009-0-64240-9.
- (14) Chen, X.; Wo, F.; Jin, Y.; Tan, J.; Lai, Y.; Wu, J. Drug-Porous Silicon Dual Luminescent System for Monitoring and Inhibition of Wound Infection. *ACS nano* **2017**, *11*, 7938-7949. doi: 10.1021/acsnano.7b02471.
- (15) Latus, A.; Noël, J.-M.; Volanschi, E.; Lagrost, C.; Hapiot, P. Scanning Electrochemical Microscopy Studies of Glutathione-Modified Surfaces. An Erasable and Sensitive-to-Reactive Oxygen Species Surface. *Langmuir* **2011**, *27*, 11206-11211. doi: 10.1021/la2020034.
- (16) Suomi, J.; Håkansson, M.; Jiang, Q.; Kotiranta, M.; Helin, M.; Niskanen, A. J.; Kulmala, S. Time-resolved detection of electrochemiluminescence of luminol. *Anal. Chim. Acta* **2005**, *541*, 165-167. doi: 10.1016/j.aca.2004.12.058.
- (17) Kankare, J.; Fäldén, K.; Kulmala, S.; Haapakka, K. Cathodically induced time-resolved lanthanide(III) electroluminescence at stationary aluminium disc electrodes. *Anal. Chim. Acta* **1992**, *256*, 17-28. doi: 10.1016/0003-2670(92)85320-6.
- (18) Tortorich, P. R.; Shamkhalichenar, H.; Choi, J.-W. Inkjet-Printed and Paper-Based Electrochemical Sensors. *Appl. Sci.* **2018**, *8*. doi: 10.3390/app8020288.
- (19) Chen, H.; Cogswell, J.; Anagnostopoulos, C.; Faghri, M. A fluidic diode, valves, and a sequential-loading circuit fabricated on layered paper. *Lab Chip* **2012**, *12*, 2909-2913. doi: 10.1039/c2lc20970e.

- (20) Shin, H. J.; Park, J.; Park, J.-K. Organic Solvent and Surfactant Resistant Paper-Fluidic Devices Fabricated by One-Step Embossing of Nonwoven Polypropylene Sheet. *Micromachines* **2017**, *8*. doi: 10.3390/mi8010030.
- (21) Aneesh, K.; Berchmans, S. Highly selective sensing of dopamine using carbon nanotube ink doped with anionic surfactant modified disposable paper electrode. *J. Solid State Electrochem.* **2017**, *21*, 1263-1271. doi: 10.1007/s10008-016-3482-2.
- (22) Liu, H. X.; Zhou, X. M.; Shen, Q.; Xing, D. Paper-based electrochemiluminescence sensor for highly sensitive detection of amyloid-beta oligomerization: Toward potential diagnosis of Alzheimer's disease. *Theranostics* **2018**, *8*, 2289-2299. doi: 10.7150/thno.23483.
- (23) Labmaster Oy, "Labmaster LUCIA™ -Labmaster LUCIA™ is a point-of-care (POC) platform based on patented CECL technology.", can be found under <https://www.labmaster.fi/index.php?cat=3&lang=en&project=>, **2018**.
- (24) Chen, X.-Y.; Zheng, R.-J.; Ren, L.-Q.; Sun, J.-J. Determination of ultra-trace catecholamines based on hot electron-induced cathodic electrochemiluminescence at a naturally oxide-covered tantalum electrode. *RSC Advances* **2016**, *6*, 16495-16499. doi: 10.1039/c5ra26201a.
- (25) Fang, C.; Li, H.; Yan, J.; Guo, H.; Yifeng, T. Progress of the Electrochemiluminescence Biosensing Strategy for Clinical Diagnosis with Luminol as the Sensing Probe. *ChemElectroChem* **2017**, *4*, 1587-1593. doi: 10.1002/celec.201700465.
- (26) Tekin, H. C.; Gijs, M. A. M. Ultrasensitive protein detection: a case for microfluidic magnetic bead-based assays. *Lab Chip* **2013**, *13*, 4711-4739. doi: 10.1039/c3lc50477h.
- (27) Takashi, K.; Masatoshi, T.; Seiichi, O.; Wataru, T.; Keiichi, K.; Shuji, H. Enhanced Electrochemiluminescence by Use of Nanoporous TiO₂ Electrodes: Electrochemiluminescence Devices Operated with Alternating Current. *Jpn. J. Appl. Phys.* **2005**, *44*, 8161.
- (28) Xu, Y.; Lv, Z.; Xia, Y.; Han, Y.; Lou, B.; Wang, E. Highly porous magnetite/graphene nanocomposites for a solid-state electrochemiluminescence sensor on paper-based chips. *Anal. Bioanal. Chem.* **2013**, *405*, 3549-3558. doi: 10.1007/s00216-012-6510-9.
- (29) Shi, L.; Liu, X.; Li, H.; Xu, G. Electrochemiluminescent Detection Based on Solid-Phase Extraction at Tris(2,2'-bipyridyl)ruthenium(II)-Modified Ceramic Carbon Electrode. *Anal. Chem.* **2006**, *78*, 7330-7334. doi: 10.1021/ac060767v.
- (30) de Araujo, W. R.; Frasson, C. M. R.; Ameku, W. A.; Silva, J. R.; Angnes, L.; Paixão, T. R. L. C. Single-Step Reagentless Laser Scribing Fabrication of Electrochemical Paper-Based Analytical Devices. *Angew. Chem. Int. Ed.* **2017**, *56*, 15113-15117. doi: 10.1002/anie.201708527.

Curriculum Vitae

Persönliche Daten

Michael Mayer | Westerndorfer Straße 22 | 83071 Stephanskirchen | michael.mayer@ur.de

Geburtsdatum: 16.09.1988 | Geburtsort: Rosenheim | Staatsangehörigkeit: Deutsch

Ausbildung

03/2015 – 11/2018	Promotionsstudium, Chemie – Universität Regensburg Dissertation: "Signal Enhancement Strategies in Classical Electrochemiluminescence Techniques for Modern Biosensing" Institut für Analytische Chemie, Chemo- und Biosensorik (Prof. Antje J. Bäumner)
10/2012 - 01/2015	Master of Science, Chemie – Universität Regensburg Masterarbeit: "Luminol and ruthenium electrochemiluminescence for a dual ECL detection approach" Institut für Analytische Chemie, Chemo- und Biosensorik (Prof. Antje J. Bäumner)
10/2009 - 09/2012	Bachelor of Science, Chemie – Universität Regensburg Bachelorarbeit: "Synthesis of α -substituted chalcones from modified precursors" Institut für Organische Chemie (Dr. Sabine Amslinger)
07/2009 - 09/2009	Ausbildung zum Rettungssanitäter – Rettungsdienstschule München
10/2008 - 06/2009	Zivildienst im Rettungsdienst - Bayerisches Rotes Kreuz, Rosenheim
09/1999 – 06/2008	Allgemeine Hochschulreife – Finsterwalder Gymnasium Rosenheim
09/1995-07/1999	Grundschule Schlossberg

Forschungstätigkeit

2015-2018

Wissenschaftlicher Mitarbeiter – Doktorand, Universität Regensburg

Untersuchung von dendrimer-basierten, liposomalen, surfactant-basierten und mikrofluidischen Signalverbesserungsstrategien in der Elektrochemilumineszenzdetektion (ECL) für die ECL Moleküle Luminol und $[\text{Ru}(\text{bpy})_3]^{2+}$ und Anwendung dieser Systeme in bioanalytischen Nachweismethoden.

2014

Wissenschaftlicher Mitarbeiter – Masterand, Universität Regensburg

Charakterisierung und Optimierung der Elektrochemilumineszenzsysteme Luminol und $[\text{Ru}(\text{bpy})_3]^{2+}$ für eine duale-Anwendung in einem geteiltem Detektionssystem.

Sonstige Qualifikationen

1. „PolyNano - Bringing lab-on-chip systems closer to the market“, summer school an der DTU Nanotech, Kopenhagen, Dänemark, 2018.
2. “Polymer Chemistry: from physical basics to microencapsulation and fiber applications, modules I and II ” – Kurs
Prof. Margret Frey, Universität Regensburg, 2017.
3. „Qualitätsmanagement in der Analytischen Chemie“ – Kurs
Dr. Robert Schupfner & Dr. Michael Schäferling, 2015.

Presentations

Oral Presentations

2017	BBMEC 12 , Rome, Italy
2017	First European/ 10th German BioSensor Symposium , Potsdam, Germany
2016	10th Interdisciplinary PhD student Seminar , Berlin, Germany

Poster Presentations

2016	Gordon Research Seminar & Conference , Newport, RI, USA
2015	BBMEC 11 , Regensburg, Germany
2015	ANAKON , Graz, Austria
2015	9th German BioSensor Symposium , Munich, Germany

Publications

1. **M. Mayer** and A. J. Baeumner
“ABC Spotlight on Analytics 4.0” *Anal. Bioanal. Chem.*, **2018**, 410, 5095-5097,
doi: 10.1007/s00216-018-1191-7.

2. **M. Mayer**⁺, S. Takegami⁺, M. Neumeier, S. Rink, A. Jacobi von Wangelin, S. Schulte, M. Vollmer, A. G. Griesbeck, A. Duerkop, A. J. Baeumner
“Electrochemiluminescence Bioassays with a Water-Soluble Luminol Derivative Can Outperform Fluorescence Assays”, *Angew. Chem. Int. Ed.* **2017**, 57, 408-411,
doi: 10.1002/anie.201708630.

3. S. Chandra, **M. Mayer** A.J. Baeumner
“PAMAM dendrimers: A multifunctional nanomaterial for ECL biosensors”, *Talanta*, **2017**, 168, 126-129, doi: 10.1016/j.talanta.2017.03.016.

4. S. Kirschbaum-Harriman, **M. Mayer**, A. Duerkop, T. Hirsch, A. J. Baeumner
“Signal enhancement and low oxidation potentials for miniaturized ECL biosensors via N-butyl-diethanolamine”, *Analyst*, **2017**, 142, 2469-2474, doi: 10.1039/C7AN00261K.

⁺ indicates equal contribution.

Eidesstattliche Erklärung

Ich erkläre hiermit an Eides statt, dass ich die vorliegende Arbeit ohne unzulässige Hilfe Dritter und ohne Benutzung anderer als der angegebenen Hilfsmittel angefertigt habe; die aus anderen Quellen direkt oder indirekt übernommenen Daten und Konzepte sind unter Angabe des Literaturzitats gekennzeichnet.

Weitere Personen waren an der inhaltlich-materiellen Herstellung der vorliegenden Arbeit nicht beteiligt. Insbesondere habe ich hierfür nicht die entgeltliche Hilfe eines Promotionsberaters oder anderer Personen in Anspruch genommen. Niemand hat von mir weder unmittelbar noch mittelbar geldwerte Leistungen für Arbeiten erhalten, die im Zusammenhang mit dem Inhalt der vorgelegten Dissertation stehen.

Die Arbeit wurde bisher weder im In- noch im Ausland in gleicher oder ähnlicher Form einer anderen Prüfungsbehörde vorgelegt.

Ort, Datum

Unterschrift